

การสังเคราะห์และสมบัติเรืองแสงของเดนดริติกพอลิอิลิกโพรไลด์ฟลูออโรฟอร์



นาย นคร เนียมนนท์

ศูนย์วิทยทรัพยากร
จุฬาลงกรณ์มหาวิทยาลัย

วิทยานิพนธ์นี้เป็นส่วนหนึ่งของการศึกษาตามหลักสูตรปริญญาวิทยาศาสตรดุษฎีบัณฑิต

สาขาวิชาเคมี ภาควิชาเคมี

คณะวิทยาศาสตร์ จุฬาลงกรณ์มหาวิทยาลัย

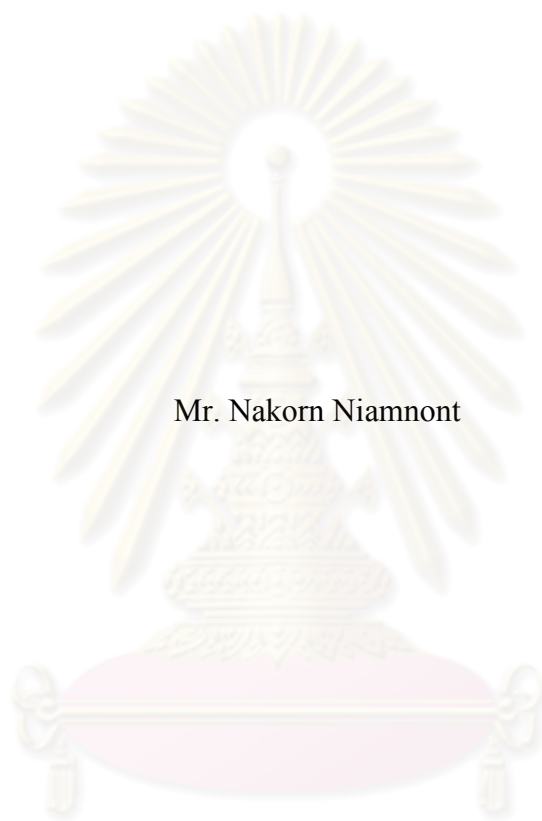
ปีการศึกษา 2553

ลิขสิทธิ์ของจุฬาลงกรณ์มหาวิทยาลัย



4 9 7 2 3 3 2 1 2 3

SYNTHESIS AND FLUORESCENT PROPERTIES OF DENDRITIC
POLYELECTROLYTE FLUOROPHORES



Mr. Nakorn Niamnont

ศูนย์วิทยทรัพยากร
จุฬาลงกรณ์มหาวิทยาลัย
A Dissertation Submitted in Partial Fulfillment of the Requirements
for the Degree of Doctor of Philosophy Program in Chemistry

Department of Chemistry

Faculty of Science


Chulalongkorn University

Academic Year 2010

Copyright of Chulalongkorn University

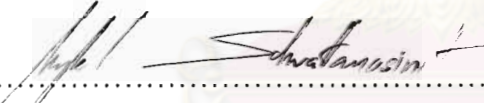
Thesis Title SYNTHESIS AND FLUORESCENT PROPERTIES OF
DENDRITIC POLYELECTROLYTE FLUOROPHORES
By Mr. Nakorn Niamnont
Field of Study Chemistry
Thesis Advisor Associate Professor Mongkol Sukwattanasinitt, Ph.D.
Thesis Co-Advisor Assistant Professor Paitoon Rashatasakhon, Ph.D.

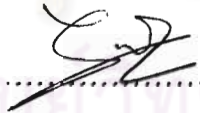
Accepted by the Faculty of Science, Chulalongkorn University in Partial
Fulfillment of the Requirements for the Doctoral Degree


..... Dean of the Faculty of Science
(Professor Supot Hannongbua, Dr.rer.nat.)

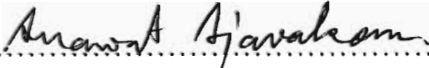
THESIS COMMITTEE


..... Chairman
(Associate Professor Sirirat Kokpol, Ph.D.)

..... Thesis Advisor
(Associate Professor Mongkol Sukwattanasinitt, Ph.D.)

..... Thesis Co-Advisor
(Assistant Professor Paitoon Rashatasakhon, Ph.D.)

..... Examiner
(Professor Thawatchai Tuntulani, Ph.D.)

..... Examiner
(Anawat Ajavakom, Ph.D.)

..... External Examiner
(Assistant Professor Radchada Bunttem, Ph.D.)

นคร เนียมมนท์ : การสังเคราะห์และสมบัติเรืองแสงของเดนดริติกพอลิอิเล็กโทรไลต์ฟลูออโรฟออร์. (SYNTHESIS AND FLUORESCENT PROPERTIES OF DENDRITIC POLYELECTROLYTE FLUOROPHORES) อ.ที่ปรึกษาวิทยานิพนธ์หลัก: รศ.ดร.มงคล สุขวัฒนาศินิทธิ, อ.ที่ปรึกษาวิทยานิพนธ์ร่วม: ผศ.ดร.ไพฑูรย์ รัชตะสาคร, 137 หน้า.

สารเรืองแสงที่มีคุณสมบัติละลายน้ำได้ประกอบด้วยหน่วยเรืองแสงหลายหน่วยเป็นสิ่งที่น่าสนใจสำหรับการวิเคราะห์สารเคมีและการวินิจฉัยโรคที่ต้องการความไวสูง โดยสารเรืองแสงที่สามารถควบคุมหน่วยเรืองแสงได้นั้น จะแสดงกลไกการเปลี่ยนแปลงสัญญาณการเรืองแสงได้เป็นอย่างดีและสามารถทำการทดลองตรวจสอบซ้ำได้ ดังนั้นในวิทยานิพนธ์ฉบับนี้จึงได้สังเคราะห์ชุดของสารเรืองแสงเดนดริติกที่มีประจุหลากหลาย(ประจุ $6C^-$, $3C^-$, $2C^-N^0$, C^-2N^0 , $2C^-N^+$, $2C^0N^+$, C^02N^+ , $3N^+$, และ $6N^+$) ซึ่งประกอบด้วยจำนวนที่แน่นอนของหน่วยเรืองแสงสายกิ่งของพาราฟีนิลีนเอทาโนลีน (PPE) และคาร์บอกซิเลทประจุลบหรือแอมโมเนียมประจุบวกที่หมู่พื้นผิวด้วยปฏิกิริยาควบไซโนกาซิรา ผลการศึกษาพบว่าเดนดริเมอร์ประจุลบชั้นที่หนึ่ง $6C^-$ แสดงการระงับสัญญาณการเรืองแสงได้อย่างเลือกจำเพาะกับไอออนของปรอทประจุสองบวกโดยมีค่าคงที่ของการระงับการเรืองแสง (K_{sv}) เท่ากับ $33,700 M^{-1}$ ในสารละลายที่มีสารลดแรงตึงผิวไตรตอนเอ็กซ์-100 นอกจากนี้สารเรืองแสงทั้งเก้าชนิดได้ถูกประกอบเป็นชุดทดสอบแบบแถว (array) ในการวิเคราะห์ไฮโปรตีน โดยใช้วิธีวิเคราะห์องค์ประกอบหลัก (PCA) และวิธีวิเคราะห์แบบจำแนก (FDA) ผลการวิเคราะห์พบว่า ความยาวคลื่นที่เหมาะสมที่สุดสำหรับการตรวจจับมีค่า 500 นาโนเมตรและลดจำนวนสารเรืองแสงลงจากเก้าชนิดเหลือเพียงสองชนิด (C^02N^+ และ $3C^-$) ซึ่งได้ความถูกต้องของการแยก 100% นอกจากนี้ ผลการศึกษายังแสดงให้เห็นว่า การใช้เซลล์ลูโลสอะซิเตทนาโนไฟเบอร์แบบไฟฟ้าสถิตที่เติม $3C^-$ เพื่อตรวจวัดไฮโปรตีนที่มีโลหะเป็นองค์ประกอบ พบว่าการเรืองแสงของนาโนไฟเบอร์ลดลงเมื่อเติมฮีโมโกลบิน และมีค่าคงที่ของการระงับการเรืองแสงเท่ากับ $1.7 \times 10^6 M^{-1}$ กล่าวโดยสรุป ผลการวิจัยในวิทยานิพนธ์ฉบับนี้ได้ค้นพบสารเรืองแสงชนิดใหม่ที่ น่าสนใจสำหรับประยุกต์เป็นวัสดุการตรวจวัดในระบบน้ำ

ภาควิชา.....เคมี.....
สาขาวิชา.....เคมี.....
ปีการศึกษา.....2553.....

ลายมือชื่อนิสิต นคร เนียมมนท์
ลายมือชื่อ อ.ที่ปรึกษาวิทยานิพนธ์หลัก [Signature]
ลายมือชื่อ อ.ที่ปรึกษาวิทยานิพนธ์ร่วม [Signature]

4972332123 : MAJOR CHEMISTRY

KEYWORDS : DENDRIMERS / FLUORESCENCE / ARRAY SENSOR

NAKORN NIAMNONT: SYNTHESIS AND FLUORESCENT PROPERTIES OF DENDRITIC POLYELECTROLYTE FLUOROPHORES. THESIS ADVISOR: ASSOC. PROF. MONGKOL SUKWATTASINITT, Ph.D., THESIS CO-ADVISOR: ASST. PROF. PAITON RASHATASAKHON, Ph.D., 137 pp.

Water soluble fluorophores containing multiple fluorogenic moieties are of interests for chemical analysis and highly sensitive medical diagnosis. The fluorophores with controllable numbers of fluorogenic units can provide good mechanistic understanding and experimental reproducibility. In this thesis, a series of nine variously charged dendritic fluorophores (charges: $6C^-$, $3C^-$, $2C^0N^0$, C^02N^0 , $2C^0N^+$, $2C^0N^+$, C^02N^+ , $3N^+$, and $6N^+$) composed of exact numbers of the paraphenyleneethynylene (PPE) fluorogenic branches and anionic carboxylate or cationic ammonium peripheral groups are synthesized via Sonogashira coupling. The first generation anionic dendrimer, $6C^-$ exhibits a highly selective fluorescence quenching by Hg^{2+} ions with quenching efficiency K_{sv} of $33,700 M^{-1}$ in the presence of Triton X-100 surfactant. The nine fluorophores are assembled into an array for protein analysis. Using principal component analysis (PCA) and factorial discriminant analysis (FDA), the optimum detection wavelength is located at 500 nm and the number of sensing elements is reduced from nine to two (C^02N^+ and $3C^-$) with 100% discriminating accuracy. The cellulose nanofiber mats doped with $3C^-$ fluorophore are fabricated by electrospinning technique. The mats can be applied as a reusable solid-state fluorescent sensing device for metalloproteins such as hemoglobin which shows high K_{sv} of $1.7 \times 10^6 M^{-1}$. The findings in this thesis work have established a new interesting class of fluorophores useful for sensing applications in aqueous media.

Department : Chemistry
 Field of Study : Chemistry
 Academic Year : 2010

Student's Signature Nakorn Niamnont.
 Advisor's Signature Mongkol Sukwattasinitt
 Co-Advisor's Signature Paiton Rashatasakhon

ACKNOWLEDGEMENTS

I would like to express my sincere gratitude to my advisor, Associate Professor Mongkol Sukwattanasinitt, Ph.D., my Co-Advisor Assistant Professor Paitoon Rashatasakhon, Ph.D., Anawat Ajavakom, Ph.D., Sumrit Wacharasindhu, Ph.D., and Gamolwan Tumcharern, Ph.D. for their invaluable guidance, excellent and kind supervision, and helpful suggestion throughout this research. This thesis research would not be completed without their advice and guidance.

I am also greatly grateful to Prof. Dr. Quan Jason Cheng at Department of Chemistry, University of California Riverside, Riverside, California, USA, and Prof. Dr. Jay S. Siegel at Department of Chemistry, University of Zurich, Zurich, Switzerland for giving me a good opportunity to join their group for six months. I also would like to thank my friends at Riverside and Zurich for wonderful and fun time during I was there as a visiting student at Riverside and Zurich.

My appreciation is also given to Associate Professor Sirirat Kokpol, Ph.D., Professor Thawatchai Tuntulani, Ph.D., and Anawat Ajavakom, Ph.D. thesis defense committee, for their kind attention, valuable suggestion and recommendations. I would like to thank Assistant Professor Radchada Buntam, Ph.D., thesis defense committee from Silpakorn University for suggestions.

Furthermore, I gratefully thank to my friends for their genuine, Miss Radeemada, Miss Warathip, Mr Thirawat, and everyone in MS-group for spirit, smile, good wish and their helps in everything.

I would like to thank The Development and Promotion of Science and Technology Talents Project (DPST) Scholarship by Institute for the Promotion of Teaching Science and Technology (IPST), the 90th Anniversary of Chulalongkorn University Fund (Ratchada-phiseksomphot Endowment Fund), and Center for Petroleum, Petrochemicals, and Advanced Materials (PPAM) for the financial support of this work.

Finally, I would like to express thankfulness to my family for their love, care, encouragement and support throughout my study.

CONTENTS

	Page
ABSTRACT (THAI)	iv
ABSTRACT (ENGLISH)	v
ACKNOWLEDGEMENTS	vi
CONTENTS	vii
LIST OF TABLES	x
LIST OF FIGURES	xi
LIST OF SCHEMES	xviii
LIST OF ABBREVIATIONS	xix
CHAPTER	
I INTRODUCTION	1
1.1 Overview.....	1
1.2 Molecular structures of some conjugated fluorophores.....	1
1.3 Fluorescence spectra.....	4
1.4 Fluorescence quenching.....	4
1.5 Optical sensor application of conjugated polyelectrolytes.....	6
1.6 Fluorescent sensors based on small molecules.....	13
1.7 Objectives of this research.....	21
II EXPERIMENTAL	22
2.1 Chemicals and materials	22
2.2 Analytical instruments.....	23
2.3 Synthesis of dendritic fluorophores.....	24
2.3.1 Preparation of 4,4',4''-triiodotriphenylamine	24
2.3.2 Preparation of TMS2I	24
2.3.3 Preparation of methyl 4-((trimethylsilyl)ethynyl)benzoate	25
2.3.4 Preparation of 4-iodo- <i>N,N</i> -dimethylaniline.....	25
2.3.5 Preparation of <i>N,N</i> -dimethyl-4-((trimethylsilyl)ethynyl) -aniline.....	26

CHAPTER	Page
2.3.6 Preparation of methyl 4-ethynylbenzoate.....	26
2.3.7 Preparation of 4-ethynyl- <i>N,N</i> -dimethylaniline.....	27
2.3.8 Preparation of TMS2C⁰	27
2.3.9 Preparation of E2C⁰	28
2.3.10 Preparation of I2N⁰	29
2.3.11 Preparation of TMS2N⁰	29
2.3.12 Preparation of E2N⁰	30
2.3.13 Preparation of 3C⁰	30
2.3.14 Preparation of 3N⁰	31
2.3.15 Preparation of 3C⁻	32
2.3.16 Preparation of 3N⁺	32
2.3.17 Preparation of 6C⁰	33
2.3.18 Preparation of 6N⁰	33
2.3.19 Preparation of 6C⁻	34
2.3.20 Preparation of 6N⁺	35
2.3.21 Preparation of 2IC⁰, I2C⁰ and 3C⁰	35
2.3.22 Preparation of C⁰2N⁰	36
2.3.23 Preparation of 2C⁰N⁰	37
2.3.24 Preparation of 2C⁻N⁰	38
2.3.25 Preparation of C⁻2N⁰	38
2.3.26 Preparation of 2C⁻N⁺	39
2.3.27 Preparation of 2C⁰N⁺	40
2.3.28 Preparation of C⁰2N⁺	40
2.4 Photophysical property study.....	41
2.4.1 UV-visible spectroscopy.....	41
2.4.2 Fluorescence spectroscopy.....	41
2.4.3 Fluorescence quantum yields.....	41
2.5 Fluorescent sensor study.....	42
2.5.1 Metal ion sensor.....	42
2.5.2 Proteins array sensor.....	42
2.6 Dendritic fluorophore incorporated nanofibers for metallo- protein detection.....	43

CHAPTER	Page
III RESULTS AND DISCUSSION	45
3.1 Synthesis and characterization of zeroth and first generation of dendritic fluorophores (3C⁻ , 6C⁻ , 3N⁺ and 6N⁺).....	45
3.2 Synthesis and characterization of variously charged dendritic fluorophores (2C⁻N⁰ , C⁻2N⁰ , 2C⁻N⁺ , 2C⁰N⁺ , and C⁰2N⁺).....	48
3.3 Photophysical property study.....	53
3.4 Surfactant enhancement of 3C⁻ , 3N⁺ , and 6C⁻	55
3.5 Metal ion sensor.....	56
3.6 Proteins array sensor.....	59
3.7 Nanofibers doped with dendritic fluorophores for protein sensor.....	67
IV CONCLUSION	73
REFERENCES	75
APPENDIX A	82
APPENDIX B	121
VITAE	137



 ศูนย์วิทยทรัพยากร
 จุฬาลงกรณ์มหาวิทยาลัย

LIST OF TABLES

Table		Page
3.1	Photophysical properties of the dendritic fluorophores.....	53
3.2	Photophysical properties of $3C^-$, $3N^+$, and $6C^-$ in 50 mM phosphate buffer (pH 8.0) without and with Triton X-100.....	56
3.3	Variance contribution of the first two PCs and classification accuracy obtained from PCA and FDA on the fluorescent intensities (ΔI) measured at various wavelengths.....	64



ศูนย์วิทยทรัพยากร
จุฬาลงกรณ์มหาวิทยาลัย

LIST OF FIGURES

Figure		Page
1.1	Molecular structures of some common conjugated polymers (CPs)	2
1.2	Molecular structures of some common CPEs	2
1.3	Examples of PPEs with different structural modifications.....	3
1.4	Simple Jablonski diagram illustrating fluorescent processes	4
1.5	Mechanism of fluorescence quenching. A) Dynamic quenching. B) Static quenching.....	5
1.6	Proposed mechanism for detection of avidin using CPE via the avidin-biotin binding mechanism.....	8
1.7	Molecular structures of PPV-SO ₃ ⁻ and variously charged of viologen quenchers.....	8
1.8	Structure of carboxylated PPE 8 and pictures taken under a hand-held UV light to show the fluorescence under different situations: A) 8 -papain complex ([8] = 5 μM, [papain] = 5 μM). B) All 10 metal ions added to 8 -papain complex ([each metal] = 0.4 mM). C) Same as B without Hg ²⁺	9
1.9	Qualitative interpretation of the Hg ²⁺ -induced agglutination of the 8 -papain complex. A) PPE 8 alone. B) Electrostatic complex of 8 and papain. C) The addition of Hg ²⁺ to 8 -papain complex leads to its precipitation by cross-linking of the papain molecules through Hg ²⁺	10
1.10	Detection of spermine, spermidine and putrescine using PPE <i>via</i> aggregation induced quenching mechanism	10
1.11	Molecular structures of CPEs	11
1.12	Molecular structures of some CPEs (8 , 15-18).....	11
1.13	Molecular structures of some CPEs (8 , 15 , 17-20).....	12
1.14	Molecular structure of 21 (left) and relative emission at 420 nm as a function of the ratio of (EtO) ₃ PO to the 1:1 metal/ligand complexes [21 ·MX ⁿ] (0.025 mM, M=Eu ³⁺ , La ³⁺ , and Zn ²⁺) in CHCl ₃ /CH ₃ CN (9:1, v/v)	13
1.15	Molecular structure of 22 (left) and proposed binding modes of 22 with Cd ²⁺ or Pb ²⁺ (right).....	14

Figure	Page	
1.16	Molecular structure of 23 (left) and comparison of the K_{SV} values obtained from SV plots for the series quenching by MV^+ and HV^+ in MeOH (right).....	15
1.17	Molecular structure of 24a-d and pictures of 24b and 24d in the presence of Ag^+ (14 eq)	15
1.18	Proposed of Ba^{2+} sensing mechanism of 25	16
1.19	Molecular structure of 26a-e	16
1.20	Molecular structure of 27a-h	17
1.21	Molecular structure of 28a-c	17
1.22	Molecular structure of 29 and proposed cysteine sensing mechanism	18
1.23	Molecular structure of 30a (left) and picture of 30a in the presence of cysteine which is converted into 30b (right).....	19
1.24	Molecular structure of 31 (left) and showing picture of 31 in the presence of cysteine (right).....	20
1.25	The target molecules.....	21
3.1	1H -NMR (400 MHz) of 2IC⁰ , C⁰2N⁰ , C⁻2N⁰ and C⁰2N⁺	50
3.2	1H -NMR (400 MHz) of I2C⁰ , C⁰2N⁰ , 2C⁻N⁰ and 2C⁰N⁺	51
3.3	MALDI-TOF-MS of 2IC⁰ , I2C⁰ , 2C⁰N⁰ , and C⁰2N⁰	52
3.4	MALDI-TOF-MS of MALDI-TOF-MS of 2C⁻N⁰ , C⁻2N⁰ , 2C⁰N⁺ , C⁰2N⁺ , and 2C⁻N⁺	52
3.5	Normalized absorption spectra of nine fluorophores (10 μ M) in phosphate buffer pH 8.0.....	54
3.6	Emission spectra of nine fluorophores (10.0 μ M) in phosphate buffer pH 8.0. Expanded emission spectra of six fluorophores.....	54
3.7	Normalized emission spectra of 3C⁻ , 3N⁺ , and 6C⁻ (10^{-7} M) in the absences and present of Triton X-100 (500 μ M) in 50 mM phosphate buffered pH 8.0.....	55
3.8	Emission spectra of the solutions of 3C⁻ , 3N⁺ , and 6C⁻ (10 μ M) upon the addition of metal ions (40 μ M): without Triton X-100 for (a) 3C⁻ , (b) 3N⁺ , and (c) 6C⁻ ; with 0.1 mM Triton X-100 for (d) 3C⁻ (1 μ M), (e) 3N⁺ (0.1 μ M), and (f) 6C⁻ (0.1 μ M).....	57

Figure	Page
3.9 Stern-volmer plots for fluorescence quenching of $6C^-$ (0.1 μ M) with and without of Triton X-100 (0.1 mM).....	58
3.10 Emission spectra of $6C^-$ (0.1 μ M) upon the addition of Hg^{2+} (40 μ M) and EDTA (100 μ M).....	59
3.11 Photographic image of the fluorophore solutions (10 μ M) in phosphate buffer saline (10 mM, pH 7.4) in the presence and absence of BSA ($A_{280} = 0.1, 2.1 \mu$ M) under black light.....	60
3.12 Cropped photographic images of the fluorophore solutions (2.0 μ M) in phosphate buffer saline (10 mM, pH 7.4) upon addition of each protein ($A_{280} = 0.1$) under black light.....	61
3.13 Histogram plot of logarithmic values of relative intensity (I/I_0) at 460 nm ($\lambda_{ex} = 375$ nm) of fluorophore solutions (0.20 μ M) in phosphate buffer saline (10 mM, pH 7.4) upon addition of each protein ($A_{280} = 0.01$).....	62
3.14 PCA score plot of ΔI measured at 460 nm obtained from the data set of 5 fluorophores x 8 protein samples x 9 replicates.....	63
3.15 PCA score plot of ΔI measured at 500 nm obtained from the data set of 5 fluorophores x 8 protein samples x 9 replicates.....	64
3.16 PCA loading plot of ΔI measured at 500 nm obtained from the data set of 5 fluorophores x 8 protein samples x 9 replicates.....	65
3.17 PCA score plot of ΔI measured at 500 nm obtained from the data set of the reduced array sensors composing of (a) $3C^-$ and C^02N^+ , and (b) $3C^-$ and $3N^+$	66
3.18 SEM image of electrospun $3C^-$ -doped deacetylated cellulose fibers (17% CA/0.1% AFD dissolved in 8:1 acetone/water). Inset is a zoomed-in image of the fiber.....	67
3.19 Fluorescence emission spectra of the $3C^-$ -functionalized nanofibers in response to varied concentrations of (A) Cyt C, (B) Hgb, and (C) BSA ($\lambda_{Ex}/\lambda_{Em} = 370/475$ nm).....	69

Figure	Page
3.20 Stern–Volmer plots of the nanofibers for cyt c (■) and Hgb (•). Inset: Analyte-dependent pattern for 200 nM of bovine metalloproteins (Cyt C, Hgb) and nonmetalloprotein (BSA) in PBS buffer solution (pH 7.4).....	70
3.21 Confocal fluorescence images of the electrospun nanofibers before (left) and after (right) incubation in a 10 μM cyt c solution for 15 min.....	71
3.22 Repeated switching of normalized fluorescence emission of the nanofibers for 5 cycles of 25 μM cyt c of quenching/regeneration process.	72
A.1 ¹ H NMR of TI₃ in CDCl ₃	83
A.2 ¹³ C NMR of TI₃ in CDCl ₃	83
A.3 ¹ H NMR of TMS2I in CDCl ₃	84
A.4 ¹³ C NMR of TMS2I in CDCl ₃	84
A.5 ¹ H NMR of Methyl 4-((trimethylsilyl)ethynyl)benzoate in CDCl ₃ ..	85
A.6 ¹³ C NMR of Methyl 4-((trimethylsilyl)ethynyl)benzoate in CDCl ₃ ..	85
A.7 ¹ H NMR of 4-iodo- <i>N,N</i> -dimethylaniline in CDCl ₃	86
A.8 ¹³ C NMR of 4-iodo- <i>N,N</i> -dimethylaniline in CDCl ₃	86
A.9 ¹ H NMR of <i>N,N</i> -dimethyl-4-((trimethylsilyl)ethynyl)aniline in CDCl ₃	87
A.10 ¹³ C NMR of <i>N,N</i> -dimethyl-4-((trimethylsilyl)ethynyl)aniline in CDCl ₃	87
A.11 ¹ H NMR of Methyl 4-ethynylbenzoate in CDCl ₃	88
A.12 ¹³ C NMR of Methyl 4-ethynylbenzoate in CDCl ₃	88
A.13 ¹ H NMR of 4-ethynyl- <i>N,N</i> -dimethylaniline in CDCl ₃	89
A.14 ¹³ C NMR of 4-ethynyl- <i>N,N</i> -dimethylaniline in CDCl ₃	89
A.15 ¹ H NMR of TMS2C⁰ in CDCl ₃	90
A.16 ¹³ C NMR of TMS2C⁰ in CDCl ₃	90
A.17 ¹ H NMR of E2C⁰ in CDCl ₃	91
A.18 ¹³ C NMR of E2C⁰ in CDCl ₃	91
A.19 ¹ H NMR of I2N⁰ in CDCl ₃	92

Figure		Page
A.20	^{13}C NMR of $\mathbf{I2N^0}$ in CDCl_3	92
A.21	^1H NMR of $\mathbf{TMS2N^0}$ in CDCl_3	93
A.22	^{13}C NMR of $\mathbf{TMS2N^0}$ in CDCl_3	93
A.23	^1H NMR of $\mathbf{E2N^0}$ in CDCl_3	94
A.24	^{13}C NMR of $\mathbf{E2N^0}$ in CDCl_3	94
A.25	^1H NMR of $\mathbf{3C^0}$ in CDCl_3	95
A.26	^{13}C NMR of $\mathbf{3C^0}$ in CDCl_3	95
A.27	MALDI-TOF-MS of $\mathbf{3C^0}$	96
A.28	^1H NMR of $\mathbf{3N^0}$ in CDCl_3	96
A.29	^{13}C NMR of $\mathbf{3N^0}$ in CDCl_3	97
A.30	MALDI-TOF-MS of $\mathbf{3N^0}$	97
A.31	^1H NMR of $\mathbf{3C^-}$ in DMSO-d_6	98
A.32	^{13}C NMR of $\mathbf{3C^-}$ in DMSO-d_6	98
A.33	MALDI-TOF-MS of $\mathbf{3C^-}$	99
A.34	^1H NMR of $\mathbf{3N^+}$ in CD_3CN	99
A.35	^{13}C NMR of $\mathbf{3N^+}$ in CD_3CN	100
A.36	MALDI-TOF-MS of $\mathbf{3N^+}$	100
A.37	^1H NMR of $\mathbf{6C^0}$ in CDCl_3	101
A.38	^{13}C NMR of $\mathbf{6C^0}$ in CDCl_3	101
A.39	MALDI-TOF-MS of $\mathbf{6C^0}$	102
A.40	^1H NMR of $\mathbf{6N^0}$ in CDCl_3	102
A.41	^{13}C NMR of $\mathbf{6N^0}$ in CDCl_3	103
A.42	MALDI-TOF-MS of $\mathbf{6N^0}$	103
A.43	^1H NMR of $\mathbf{6C^-}$ in DMSO-d_6	104
A.44	^{13}C NMR of $\mathbf{6C^-}$ in DMSO-d_6	104
A.45	MALDI-TOF-MS of $\mathbf{6C^-}$	105
A.46	^1H NMR of $\mathbf{6N^+}$ in CD_3CN	105
A.47	^{13}C NMR of $\mathbf{6C^-}$ in CD_3CN	106
A.48	MALDI-TOF-MS of CD_3CN	106
A.49	^1H NMR of $\mathbf{2IC^0}$ in CDCl_3	107
A.50	^{13}C NMR of $\mathbf{2IC^0}$ in CDCl_3	107

Figure	Page
A.51 ^1H NMR of $\mathbf{I2C^0}$ in CDCl_3	108
A.52 ^{13}C NMR of $\mathbf{I2C^0}$ in CDCl_3	108
A.53 ^1H NMR of $\mathbf{C^02N^0}$ in CDCl_3	109
A.54 ^{13}C NMR of $\mathbf{C^02N^0}$ in CDCl_3	109
A.55 ^1H NMR of $\mathbf{2C^0N^0}$ in CDCl_3	110
A.56 ^{13}C NMR of $\mathbf{2C^0N^0}$ in CDCl_3	110
A.57 ^1H NMR of $\mathbf{2C^+N^0}$ in DMSO-d ₆	111
A.58 ^{13}C NMR of $\mathbf{2C^+N^0}$ in DMSO-d ₆	111
A.59 ^1H NMR of $\mathbf{2C^+N^+}$ in CD_3CN	112
A.60 ^{13}C NMR of $\mathbf{2C^+N^+}$ in CD_3CN	112
A.61 ^1H NMR of $\mathbf{2C^0N^+}$ in Acetone-d ₆	113
A.62 ^{13}C NMR of $\mathbf{2C^0N^+}$ in Acetone-d ₆	113
A.63 ^1H -NMR (400 MHz) of $\mathbf{C^02N^+}$ in CD_3CN	114
A.64 ^{13}C -NMR (100 MHz) of $\mathbf{C^02N^+}$ in CD_3CN	114
A.65 Emission spectra of fluorophore solutions: a) $\mathbf{3C^-}$ (1 μM) b) $\mathbf{3N^+}$ (0.1 μM) c) $\mathbf{6C^-}$ (0.1 μM) in the presence of increasing concentration of triton X-100. $\Delta\lambda_{\text{max}}$ plots with the concentration of triton X-100..	115
A.66 I_0/I plots of $\mathbf{6C^-}$ (0.1 μM) with the addition of Hg^{2+} (40 μM) in the presence of various concentration of Triton X-100.....	116
A.67 Emission spectra of (a) $\mathbf{3C^-}$ (0.2 μM) (b) $\mathbf{C^02N^+}$ (0.2 μM) (c) $\mathbf{3N^+}$ (0.2 μM) upon addition of various concentrations of BSA in 10 mM PBS buffer pH 7.4.....	117
A.68 PCA score plot of ΔI measured at 430 nm obtained from the data set of 5 fluorophores x 8 protein samples x 9 replicates.....	118
A.69 PCA score plot of ΔI measured at 490 nm obtained from the data set of 5 fluorophores x 8 protein samples x 9 replicates.....	118
A.70 PCA score plot of ΔI measured at 510 nm obtained from the data set of 5 fluorophores x 8 protein samples x 9 replicates.....	119
A.71 PCA score plot of ΔI measured at 520 nm obtained from the data set of 5 fluorophores x 8 protein samples x 9 replicates.....	119

Figure		Page
A.72	FT-IR spectra of cellulose acetate (CA) and cellulose fibrous materials (top, before deacetylation; bottom, after deacetylation). The characteristic adsorption peaks attributed to the vibrations of the acetate group at 1745($\nu_{C=O}$), 1375(ν_{C-CH_3}), and 1235 cm^{-1} (ν_{C-O-C}) disappeared after deacetylation of CA.....	120



LIST OF SCHEMES

Scheme		Page
2.1	Schematic illustration of the electrospinning setup, encapsulation of the fluorescent dendrimer, and deacetylation process used in this study.....	43
3.1	Synthesis of peripheral groups	45
3.2	Synthesis of 3C⁻	46
3.3	Synthesis of 6C⁻	46
3.4	Synthesis of E2N⁰	47
3.5	Synthesis of 3N⁺	47
3.6	Synthesis of 6N⁺	48
3.7	Synthetic route to variously charged dendritic fluorophores.....	49


 ศูนย์วิจัยทรัพยากร
 จุฬาลงกรณ์มหาวิทยาลัย

LIST OF ABBREVIATIONS

Ar	aromatic
calcd	calculated
^{13}C NMR	carbon-13 nuclear magnetic resonance
CDCl_3	deuterated chloroform
$\text{DMSO-}d_6$	deuterated dimethyl sulfoxide
DMSO	dimethylsulfoxide
d	doublet (NMR)
dd	doublet of doublet (NMR)
ESIMS	electrospray ionization mass spectrometry
equiv	equivalent (s)
FT-IR	fourier transform infrared spectroscopy
g	gram (s)
^1H NMR	proton nuclear magnetic resonance
Hz	Hertz
HRMS	high resolution mass spectrum
h	hour (s)
IR	infrared
J	coupling constant
mg	milligram (s)
mL	milliliter (s)
mmol	millimole (s)
m/z	mass per charge
m	multiplet (NMR)
M.W.	molecular weight
M	molar
MHz	megaHertz
rt	room temperature
s	singlet (NMR)
THF	tetrahydrofuran

TLC	thin layer chromatography
UV	ultraviolet
δ	chemical shift
$^{\circ}\text{C}$	degree Celsius
μL	microliter (s)
μM	micromolar (s)
Φ	quantum yield
% yield	percentage yield



ศูนย์วิทยทรัพยากร
จุฬาลงกรณ์มหาวิทยาลัย

CHAPTER I

INTRODUCTION

1.1 Overview

Phenyleneethynylene is an important class of π -conjugated molecules currently applied as fluorescent transducers in various optical sensing systems. Critical features spurring interest in and usefulness of this class of compounds include their structural rigidity allowing more predictable geometry, high fluorescence quantum efficiency and efficient syntheses. During the past decade, a number of crucial developments of both small and polymeric phenyleneethynylene conjugated systems have been witnessed, mostly containing para-phenyleneethynylene moieties, into more sensitive and selective sensors for wider applications. This thesis focuses mainly on the synthesis, photophysical investigations and sensing applications of novel dendritic phenyleneethynylenes by incorporation of appropriate interfacial groups as sensing probes for specific or selective chemical and biological sensors.

1.2 Molecular structures of some conjugated fluorophores.

Attention in chemical and bio-sensing systems relies upon rapid and high selectivity. The methods have been progressively improved using redox [1], chromogenic [2], or fluorogenic [3] changes as the detection signals. Fluorescence based methodologies have attracted much interest due to their intrinsic sensitivity and selectivity [4]. Considerable efforts have been devoted to the design of fluorescent compounds to be used as transducers. Conjugated polymers (CPs) have emerged as one of the most important classes of transduction materials. They transform a chemical signal to easily measurable electrical or optical events. CPs with delocalized π -electron systems has attracted an overpowering interest due to their versatile optical and electrical properties [5]. **Figure 1.1** shows structures of a variety of CPs commonly investigated, including polythiophene (1) [6], polypyrrole (2) [7], polyfluorene (3) [8], poly(para-phenylene vinylene) (4) [9], and poly(para-phenylene ethynylene) (5) [10]. The CPs are prepared *via* a palladium-catalyzed cross-coupling polymerization offer the benefits of mild reaction conditions, wide functional group, and solvent compatibility [11]. The delocalized electronic structure of CPs enables

them to exhibit efficient absorption and strong emission, and produce amplified signal changes upon interacting with various analytes.

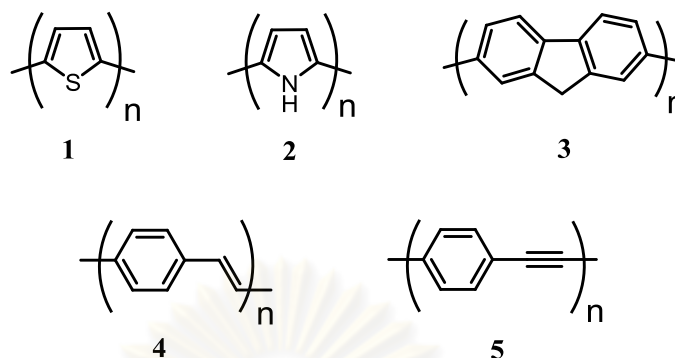


Figure 1.1. Molecular structures of some common conjugated polymers (CPs).

Conjugated polymeric polyelectrolytes (CPEs) are conjugated polymers containing multiple charges which make them water soluble [Figure 1.2]. Polyelectrolytes can either be cationic or anionic and commonly used ionic side groups including sulfonate ($-\text{SO}_3^-$), phosphonate ($-\text{PO}_3^{2-}$), carboxylate ($-\text{CO}_2^-$), and alkyl ammonium ($-\text{NR}_3^+$); polymers that are zwitterionic called polyampholytes [4, 11, 12]. This interesting class of polymers has been an area of intense research for the past few decades for applications in optical sensors [13]. The most CPE-based sensor approaches developed based on electrostatic interaction between the probes and the target ionic species, such as metal ions, anions, DNA, proteins, virus bacteria and cancer cells [4].

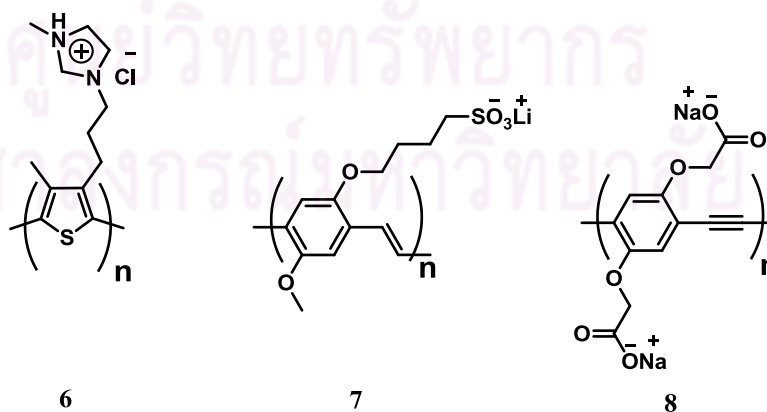


Figure 1.2. Molecular structures of some common CPEs.

Poly(para-phenyleneethynylene)s (PPEs) are representative poly(arylene-ethynylene) (PAE) in the CP family having benzene rings as the aromatic groups connecting *via* triple bonds with 180° bond angle between the phenyl carbon and sp^1 carbon [14]. Compared with its PPV analogues, the first group of CP used in fluorescence-based sensors for biological targets [15], PPEs [16] have more predictable geometry and exhibit higher quantum yield. Due to their optimal photophysical characteristics, PPEs have been explored as an important class of CPs for sensing and served as potential transducers [17, 18]. As a representative class of PAEs, PPEs have been well studied and applied to many sensory systems, including methyl viologen salt sensor [19], TNT sensors [20], and metal ion sensors [21]. The PPEs are not only feature superior photostability compared to other CPEs, such as PPVs, but they also demonstrate different electronic and optical properties from parent molecules upon structural modifications. The main chains of PAEs have three isomers: ortho-, meta- and para-, defined by their different connectivity via the acetylenic groups. Different aromatic building blocks can also be introduced into the conjugated backbone to engineer the electronic properties (**Figure 1.3**) [22]. Also, variable side chains can be introduced to modify the polymer structures and their supramolecular interactions. All these strategies are meant to make the PPEs amphiphilic, water-soluble, highly fluorescent, and able to interact with targets.

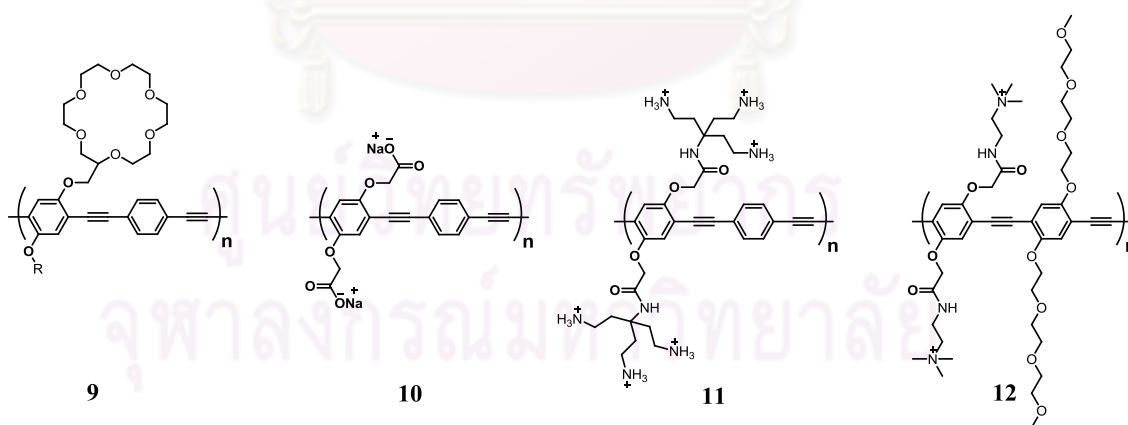


Figure 1.3. Examples of PPEs with different structural modifications.

1.3 Fluorescence spectra

The fluorescent processes that occur between the absorption and emission of light are usually described by the Jablonski diagram [23]. Jablonski diagrams are used in a variety of forms, to illustrate various molecular processes that can occur in excited states. A simplified Jablonski diagram shown in **Figure 1.4** illustrates that upon absorption of photons, a fluorophore is excited to singlet excited electronic states (S_1 or S_2) and form an excited fluorophore. The fluorescence signal is observed when F^* relaxes to ground singlet electronic state (S_0) via photon emission. The time required to complete this whole process takes nano-second.

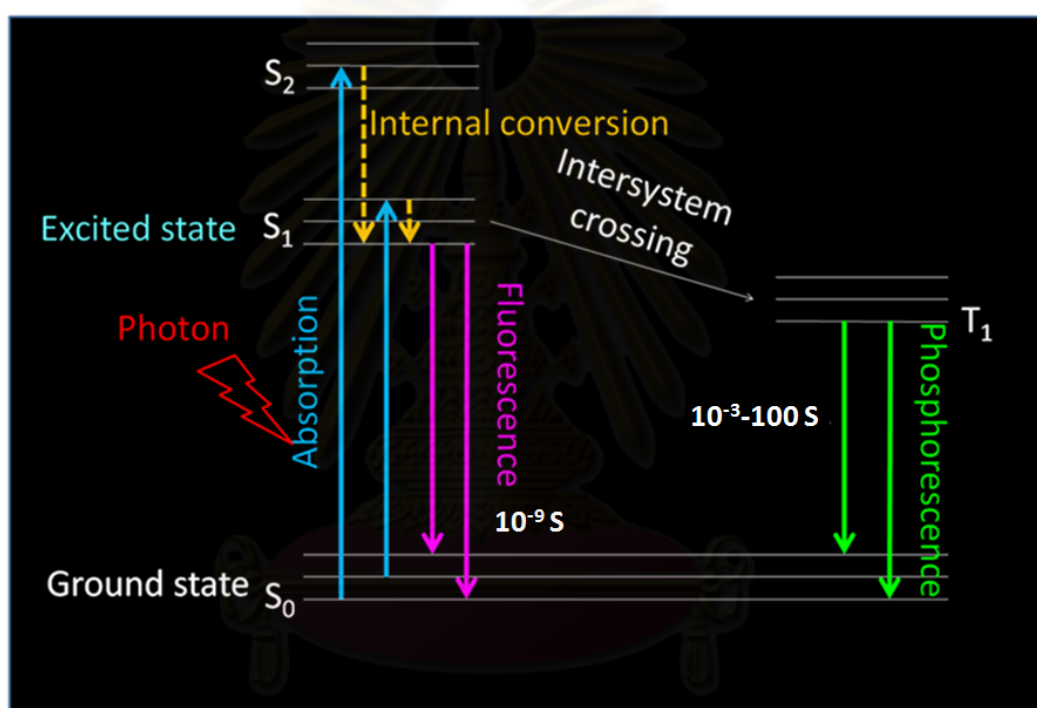


Figure 1.4. Simple Jablonski diagram illustrating fluorescent processes.

1.4 Fluorescence quenching

Generally, fluorescence quenching has two main different mechanisms, dynamic quenching and static quenching [23]. Dynamic quenching, also called collisional quenching, is controlled by the diffusion rate of the fluorophore and quencher. As shown in **Figure 1.5A**, dynamic quenching occurs when the F^* is deactivated upon a diffusive encounter of Q and return to S_0 without emission of a photon, while Q is not chemically altered in the process. **Figure 1.5B** illustrates the static quenching which happens as a result of stable non-fluorescent complex ($F \cdot Q$)

formation between the F and Q. When this complex absorbs light, it immediately returns to the ground state without emitting fluorescence. The static quenching occurs in the ground state and its efficiency is related to the association constant (K_a) for F·Q complexation.

There are several ways to distinguish these two mechanisms. First, the fluorescence lifetime decay in static quenching does not change, because the fluorescence occurs from the uncomplexed fluorophore, which remains the same during the quenching process. However, the lifetime in dynamic quenching decreases in proportion to the intensity. Second, static quenching decreases at higher temperature due to dissociation of weakly bound complexes formed in the quenching process, while dynamic quenching increases at higher temperature due to faster diffusion and collision. However, it is important to realize that the dynamic and static processes are concurrently present in many systems.

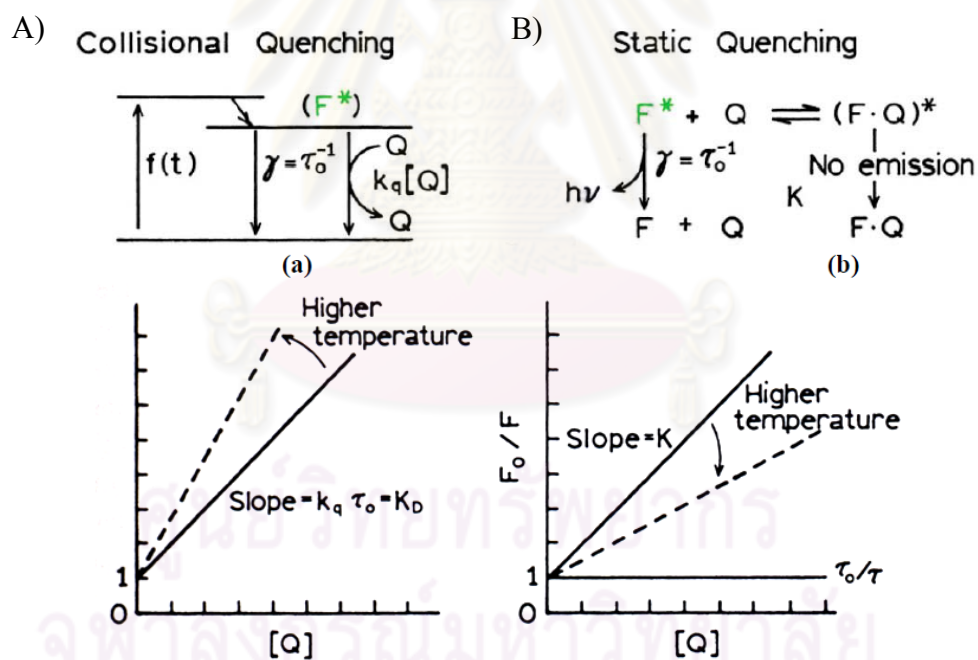


Figure 1.5. Mechanism of fluorescence quenching. A) Dynamic quenching. B) Static quenching.

Stern-Volmer Equation

Both dynamic quenching and static quenching are described by Stern-Volmer (SV) equation which is given by

$$\frac{I_0}{I} = 1 + K_{SV}[Q]$$

where I_0 and I are the fluorescence intensity observed in the absence and presence of quencher, respectively, $[Q]$ is the quencher concentration, and K_{SV} is the SV quenching. A linear relationship of I_0/I with $[Q]$ may indicate either a dynamic or static quenching process. The moderate to large binding constants give rise to Stern-Volmer constants (K_{SV}) that exceed the rate achievable at the diffusion limit, and hence, static quenching can be inferred. Another method to determine if the quenching process is dynamic or static is to determine the dependence of the lifetime on the quencher concentration, $[Q]$.

The dynamic quenching shortens the lifetime of the fluorophore according to the equation shown below where k_q is the bimolecular rate constant of fluorescence quenching, τ_0 is the lifetime without added quencher, and τ is the lifetime upon addition quencher at molar concentration of $[Q]$. For pure dynamic quenching k_q must be smaller than the diffusion limit k_d which can be determined from Stoke-Einstein equation; $k_d = 8RT/3\eta$ where R is the universal gas constant, T is the absolute temperature and η is the solution viscosity.

$$\tau_0/\tau = (1 + k_q\tau_0[Q])$$

In the case of static quenching, a fluorophore bound to a quencher is in a dark non-emissive state. The unbound fluorophores exhibit their same lifetimes, and τ is thus independent to $[Q]$ giving constant τ_0/τ at 1.

1.5 Optical sensor application of conjugated polyelectrolytes (CPE)

Over the past decade, CPEs have been studied extensively as optical sensors for various analytes [4], including small ions or biomolecules i.e. proteins and nucleic

acids. The unique structural and optical properties of CPEs provide several advantages over the routine sensor methods. First, the multiple-charged structure of CPEs affords the high water solubility which is essential for carrying out biological assays in aqueous media. Second, the CPE-based optical sensors afford a homogeneous approach which is less labor intensive and less time consuming compared with heterogeneous assay such as enzyme-linked immunosorbent assay (ELISA). As a result, the CPE-based assay is simpler, faster, and readily adapted to a fluorescence-based high-throughput screening (HTS) format [24]. Third, and most importantly, signal amplification is achieved based on sensitive and collective response of CPEs to external stimuli including a very small amount of quenchers (amplified quenching effect) and minor changes in aggregation or conformation. Therefore, the CPE-based optical sensors show superior sensitivity with typical detection limits in nanomolar [25] or even in zeptomolar concentration range [26].

CPE-based optical sensors have been realized in two detection modes, colorimetric and fluorometric. Colorimetric detection is based on a change in absorption wavelength of CPEs; while the fluorometric assay affords inherent high sensitivity as well as versatility in detection of various signals, which include the changes in intensity, wavelength and lifetime. In most of the CPE-based sensors that have been developed, the fluorescence can be either enhanced to give a turn-on signal or quenched to give a turn-off signal upon direct or indirect interaction with targets. Both the turn-on and turn-off approaches are realized by three mechanisms, i.e. photoinduced electron transfer (PeT) mechanism, photoinduced energy transfer (PET) via fluorescence resonance energy transfer (FRET) and conformational change mechanism [27]. It is important to point out that these three mechanisms are not exclusive. It is some already developed CPE-based sensors utilize more than one or even all of them in one assay.

In 1999, Chen et al. [15] published the first example of a CPE-based biosensor based on this mechanism. As shown in **Figure 1.6**, a biotin-functionalized viologen quencher serves as the QTL complex and it quenches the fluorescence of PPV-SO₃⁻ (7) probably via photo-induced electron transfer (PeT). Addition of avidin into the solution of the polymer and quencher results in a fluorescence turn-on response. The quenching to unquenching signal change was proposed to be attributed to the binding of the biotin-functionalized viologen by avidin, thus producing a sterically large avidin-bound quencher and preventing the close association of the quencher with the

polymer. However, further studies by Bazan et al. on the same polymer, quencher and avidin systems have indicated that the increase of the fluorescence is at least partially due to the non-specific interaction between the cationic avidin and anionic polymer that shields the polymer from the quencher [28].

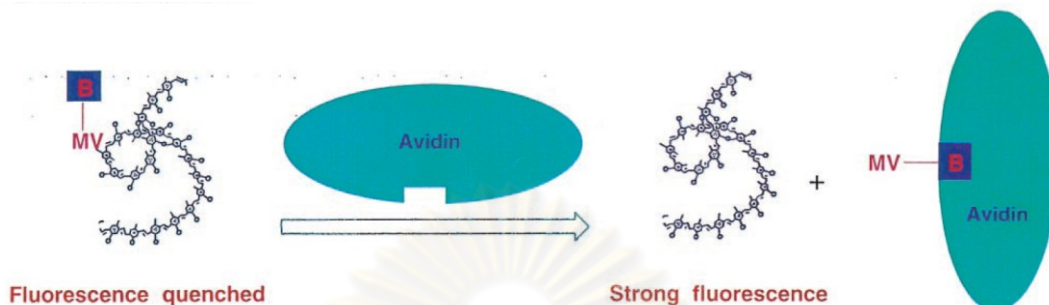


Figure 1.6. Proposed mechanism for detection of avidin using CPE via the avidin-biotin binding mechanism.

In 2001, Wang et al. [29] also examined the amplified quenching behavior of PPV-SO₃⁻ by a series of methyl viologen that has varied charge (0, +1, +2, and +4). They found that the fluorescent quenching increased when charge of methyl viologen was increased. The highest of K_{sv} is $2.2 \times 10^7 \text{ M}^{-1}$ in the presence of +4 methyl viologen. This work also found that the K_{sv} depended on the ionic strength of the solution. They have suggested that the quenching mechanism is a static quenching [Figure 1.7].

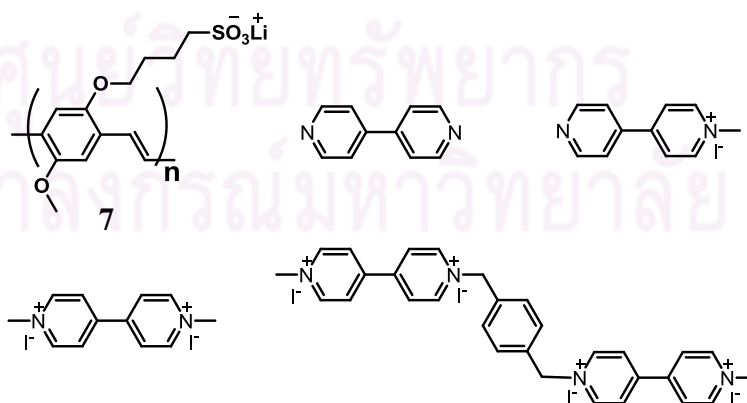


Figure 1.7. Molecular structures of PPV-SO₃⁻ and increased charged of viologen quenchers.

In 2005, Bunz et al. [30] reported a sensitive and selective lead(II) ion (Pb^{2+}) sensor which was based on the heavy metal induced fluorescence quenching of a carboxylated PPE **8** (**Figure 1.8**). The high sensitivity of this sensor was attributed to the combination of multivalent effect between **8** and Hg^{2+} , as well as the exciton migration (amplified quenching effect) along the polymer chain. More recently, the same group employed the same polymer and developed selective sensor for mercury(II) ion (Hg^{2+}) [31]. The assay was based on a formation of an electrostatic complex between **8** and papain, a cationic cysteine-rich protease. As shown in Figure 1.8, the **8**-papain complex displays selective fluorescence quenching response only to Hg^{2+} over 9 other control metal ions (i.e., Zn^{2+} , Cd^{2+} , Pb^{2+} , Fe^{2+} , Ni^{2+} , Co^{2+} , Cu^{2+} , Ca^{2+} and Mg^{2+}). The authors proposed an agglutination mechanism to explain this selectivity as shown in **Figure 1.9**. Papain with free thiol groups is known to bind Hg^{2+} . In the **8**-papain complex, the protein chains are strongly cross-linked by the anionic polymer, forming a supramolecular structure which is more sensitive towards agglutination than either **8** or papain alone. As a result, a weak emissive precipitation and a non-fluorescent solution were observed after adding Hg^{2+} to the **8**-papain complex solution.

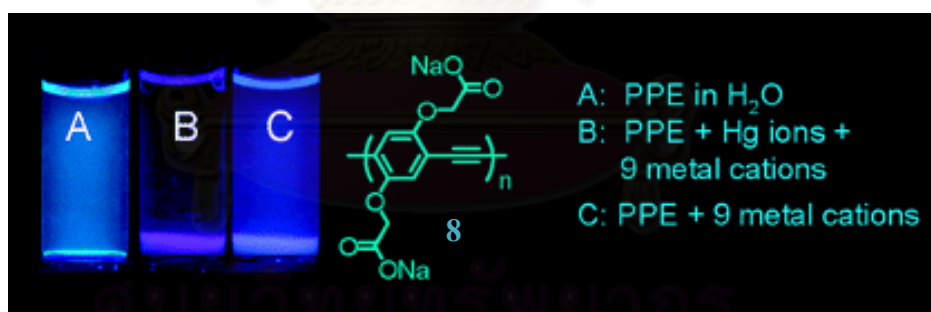


Figure 1.8. Structure of carboxylated PPE **8** and pictures taken under a hand-held UV light to show the fluorescence under different situations: A) **8**-papain complex ($[\mathbf{8}] = 5 \mu\text{M}$, $[\text{papain}] = 5 \mu\text{M}$). B) All 10 metal ions added to **8**-papain complex ($[\text{metal ion}] = 0.4 \text{ mM}$). C) All ions except Hg^{2+} add to **8**.

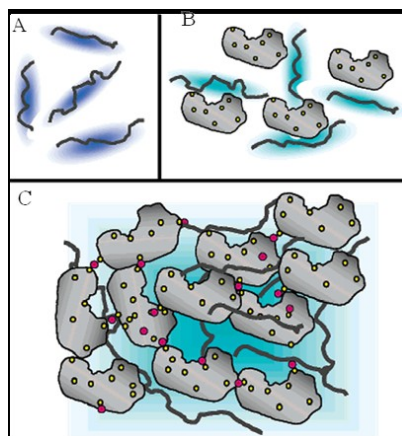


Figure 1.9. Qualitative interpretation of the Hg^{2+} -induced agglutination of the **8**-papain complex. A) PPE **8** alone. B) Electrostatic complex of **8** and papain. C) The addition of Hg^{2+} to **8**-papain complex leads to its precipitation by cross-linking of the papain molecules through Hg^{2+} .

In 2007, Satrijo et al. [32] studied derivatives of (*p*-phenyleneethynylene) polymer (**13**) that can be applied widely in the analysis of spermine, spermidine and putrescine. These compounds cannot quench the polymers directly but there have electrostatic interaction between spermine, spermidine, and putrescine with polymers. There are indicated significant spermine, spermidine, and putrescine induced self quenching of the polymers. The fluorescent intensity of **13** decreased and red shifts [Figure 1.10].

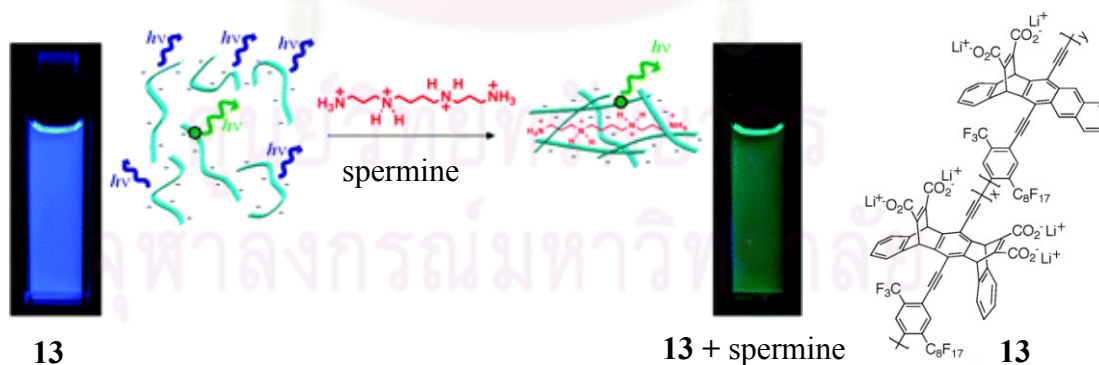


Figure 1.10. Detection of spermine, spermidine and putrescine using PPE **13** via π - π stacking quenching mechanism.

In 2005, Kim et al. [33] studied the changes in fluorescent properties of polymer **14** with various proteins. In the presence of bovine serum albumin (BSA),

the fluorescent signal increases but histone (His) induced the fluorescence quenching. BSA was proposed to behave like a surfactant interacting and preventing collisional self quenching of the polymer while the quenching by His. It was due to indicate significant His induced π - π stacking of **14**. Then, the fluorescent intensity of **14** decreased [Figure 1.11].

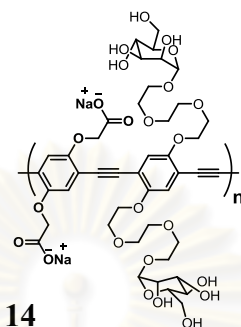


Figure 1.11. Molecular structures of CPEs.

In 2007, Miranda et al. [34] have demonstrated that a PPE-based sensor array can effectively detect and identify proteins. Benefiting from their high fluorescence sensitivity as well as inherent amplification effects, this array of six conjugated polyelectrolytes displays an unprecedented discrimination ability of 17 protein analytes. Further experiments are, however, required to demonstrate the robustness of the system, as cross-reactive arrays being still prone to errors. In particular, the array must be tested with complex mixtures of proteins for their ability to detect species at very low concentrations in the presence of large amounts of potentially interfering species [Figure 1.12].

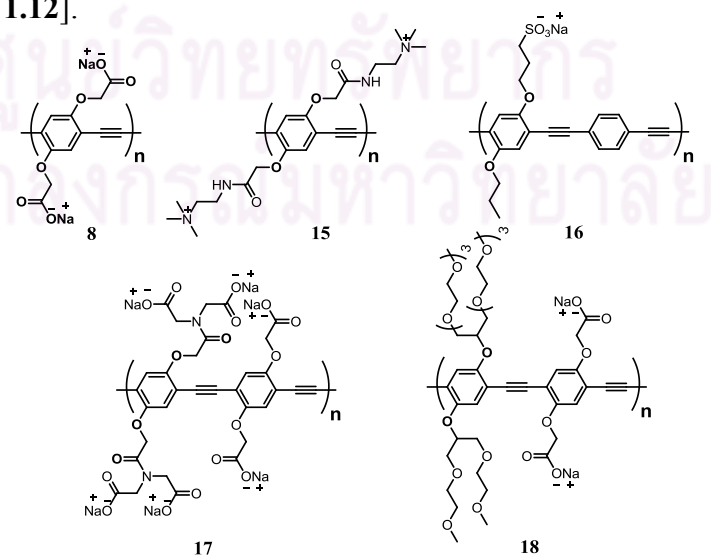


Figure 1.12. Molecular structures of some CPEs (**8**, **15-18**).

In 2010, Bajaj et al. [35] have developed a conjugated fluorescent polymer-based sensor array using PPE polymers and demonstrated its utility in cell sensing. Using this sensor array, they were able to distinguish between several cancer cell types as well as between isogenic healthy, cancerous, and metastatic cells that possess the same genetic background. Taken together, these studies provide an effective sensor for differentiating cell types as well as a potential direction in the creation of polymer-based imaging agents and delivery vehicles based on differential cell interactions. Thus, nose-based polymer sensor arrays represent a new method for diagnostic, biophysical, and surface science processes involving cell surface [Figure 1.13].

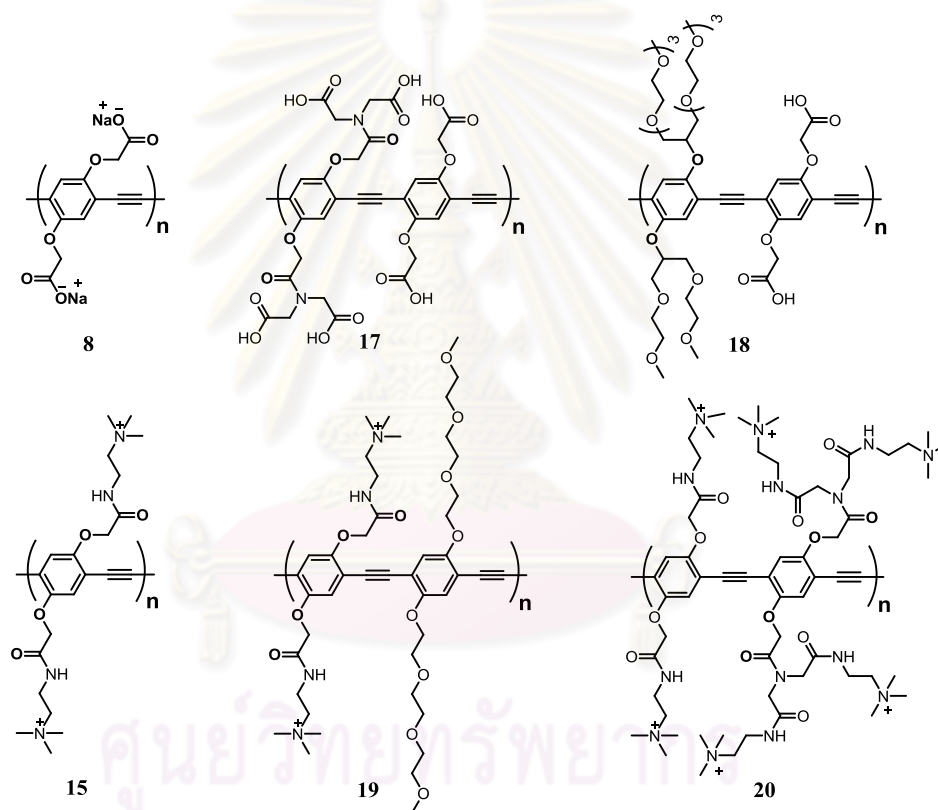


Figure 1.13. Molecular structures of some CPEs (8, 15, 17-20).

As witnessed from the literature works described above, linear CPEs have shown promisingly high sensitivity in the sensor application due to water solubility and amplified quenching effect via efficient intramolecular energy transfer along their conjugated backbone. There are a number of fluorescent CPEs exhibiting very high sensitivity to oppositely charged molecular quenchers anticipated to quench fluorescent signal by either electron or energy transfer processes. It is important to

understand the basic process, mechanisms and expression of fluorescence quenching. Both electron and energy transfer processes are expected to increase with the distance between the fluorophores and analytes thus the decreased quenching ability. However, linear CPEs have some drawbacks to be applied as analytical agents. The nature of condensation polymerization used for synthesizing these linear polymers generally provided wide molecular weight distribution of which batch-to-batch reproducibility is virtually out of question. Unpredictable secondary structures of linear polymeric chains in aqueous media also add another complication to understand the transducing properties. It is thus of interest to explore if a polycationic fluorophore can be defined molecular size and charges. Some other research works thus focus on design and study of small fluorescent conjugated molecules for sensor applications as described below.

1.6 Fluorescent sensors based on small molecules

In 2006, Knapton et al. [36] developed metallo-supramolecular materials (**21**) as a modular Eu^{3+} , La^{3+} , and Zn^{2+} sensory system that utilizes a multimetal/multiligand-based approach as a function of the ratio of $(\text{EtO})_3\text{PO}$ to the 1:1 metal/ligand complexes $[\mathbf{21} \cdot \text{MX}_n]$ in $\text{CHCl}_3/\text{CH}_3\text{CN}$ [Figure 1.14]. The judicious design of fluorescent ligands and the careful selection of metal/ligand combinations allowed them to create a very simple system for selective detection of aliphatic organophosphates with good sensitivity. By tailoring the nature of the metal–ligand interactions, it should be possible to further enhance the sensitivity of these systems on the one hand and tailor their selectivity towards different analytes on the other.

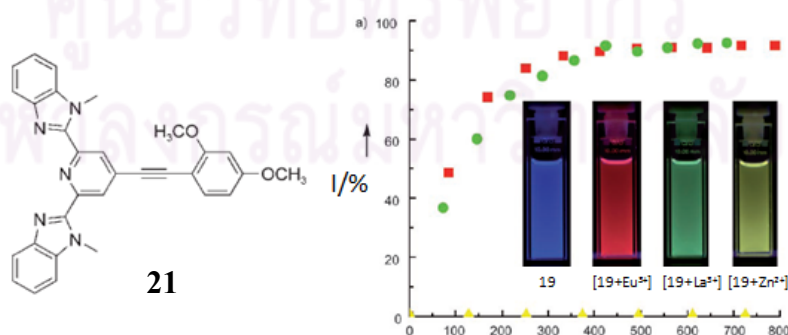


Figure 1.14. Molecular structure of **21** (left) and relative emission at 420 nm as a function of the ratio of $(\text{EtO})_3\text{PO}$ to the 1:1 metal/ligand complexes $[\mathbf{21} \cdot \text{MX}_n]$ (0.025 mM, $\text{M}=\text{Eu}^{3+}$, La^{3+} , and Zn^{2+}) in $\text{CHCl}_3/\text{CH}_3\text{CN}$ (9:1, v/v).

In 2008, Ha-Thi et al. [37] synthesized a series of phenylethynyl phosphane oxide derivatives (**22**) bearing two or four fluorescent arms starting from simple materials [Figure 1.15]. **22** show the large Stokes shift and the unresolved vibronic structure of the fluorescence spectra also suggest the formation of an intramolecular charge transfer. Addition of a heavy metal cation such as Cd^{2+} induces a bathochromic shift of the absorption and emission spectra due to an enhancement of the electron-withdrawing character of the complexed phosphane oxide group. High stability constants ($\log K_{21} = 6.6-6.9$) were observed upon complexation with Pb^{2+} , and Cd^{2+} ions in $\text{CH}_3\text{CN}/\text{CHCl}_3$ (8:2). This compound is therefore of great interest as first prototypical biphotonic sensors for Cd^{2+} cations, and hold much promise for the development of devices for the detection of toxic heavy metals in water and effluents.

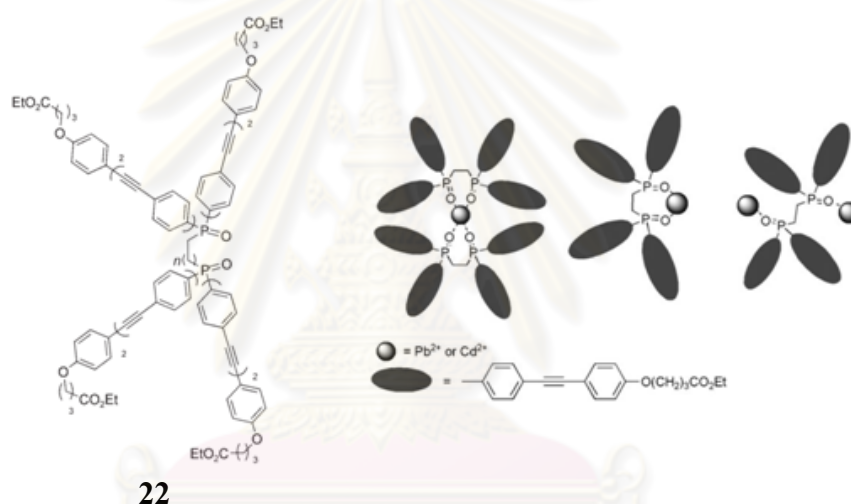


Figure 1.15. Molecular structure of phosphane oxide **22** (left) and proposed binding modes of **22** with Cd^{2+} or Pb^{2+} (right).

In 2008, Zhao et al. [38] studied the quenching of PPE (**23**) in methanol with monovalent quencher ions (MV^+ and HV^+), it is possible to discern the relationship between the amplified quenching effect and polymer chain length [Figure 1.16]. The most significant result is the observation that for short PPE chain lengths the amplification factor systematically increases, saturating at a value of ~ 50 DP ($K_{\text{sv}} = 1.4 \times 10^5 \text{ M}^{-1}$ at 436 nm). This discovery is consistent with earlier studies and suggests that in poly(phenyleneethynylene) the singlet exciton is able to transfer upto ~ 80 repeat units during its lifetime from interchain exciton diffusion within CPE aggregates.

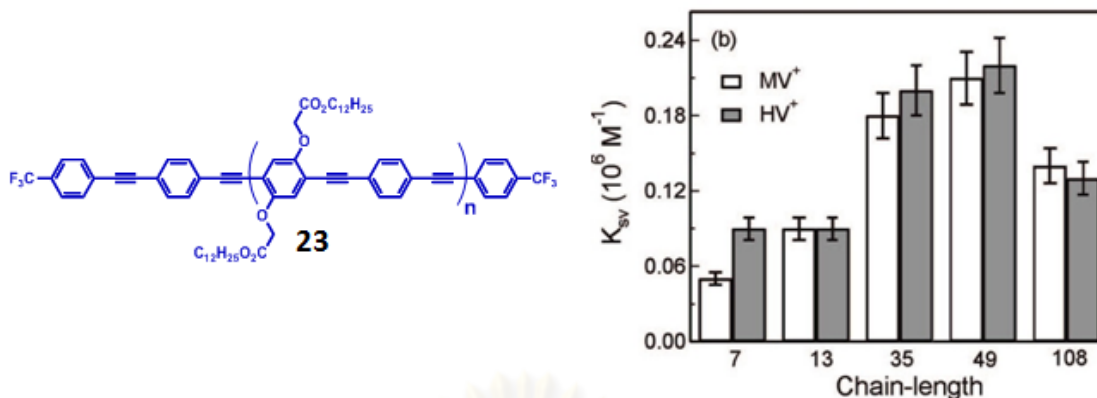


Figure 1.16. Molecular structure of **23** (left) and comparison of the K_{SV} values obtained from SV plots for the series quenching by MV^+ and HV^+ in MeOH (right).

In 2008, Zhou et al. [39] reported a new class of two-dimensional, π -conjugated, skewed H-shaped co-oligomers of phenylene vinylene and phenylene ethynylene (**24a-d**, termed H-mers) were synthesized using Sonogashira coupling and Wittig-Horner reactions as the key steps [Figure 1.17]. The photophysical properties of the H-mers were investigated by UV-vis absorption, fluorescence spectroscopic techniques. The spectral titration outcomes for **24b** and **24d** with TFA and AgOTf signify their fluorescence sensing function.

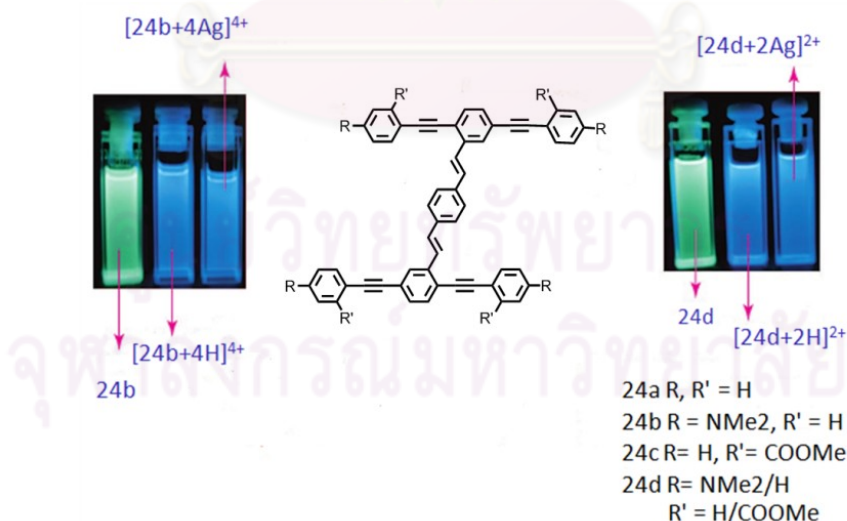


Figure 1.17. Molecular structure of **24a-d** and pictures of **24b** and **24d** in the presence of Ag^+ (14 eq).

In 2010, Shao et al. [40] synthesized a new type of fluorescence chemosensor **25** based on a biscrown-annulated TTFAQ receptor and two anthracene fluorophores [Figure 1.18]. Compound **25** exhibited fluorescence sensing capability to various metal ions, with a particularly high sensitivity for large alkaline earth metal cations like Ba^{2+} due to the formation of the 1:2 complex.

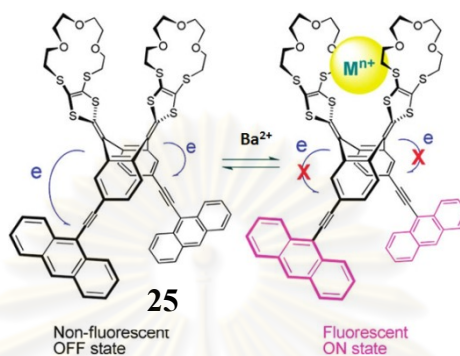


Figure 1.18. Proposed of Ba^{2+} sensing mechanism of **25**.

In 2010, Mangalum et al. [41] synthesized a series of easily-prepared materials **26a-e** derivatized with bis(dimethylamino) ligating units. Several chromophore subunits of contemporary interest have been incorporated into these molecules, including phenyleneethynylene and fluorene moieties [Figure 1.19]. Cross-conjugated cruciforms, a class of materials of escalating importance in chemical sensing, have also been examined. All of these molecules show a photoluminescence response to Zn^{2+} or Cu^{2+} over other common metal ions screened in THF, although these two ions could not be differentiated from one another showing similar I/I_0 values of 0.42-8.6 and 0.84-9.2, respectively. This simple strategy should yield materials capable of commercially viable ratiometric shifts in emission turn-on magnitudes.

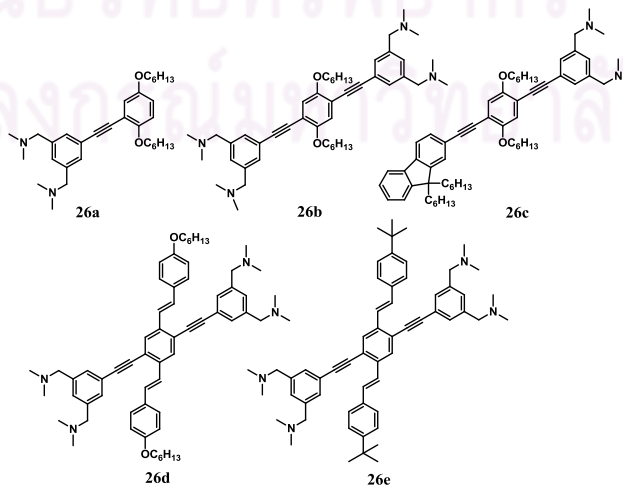


Figure 1.19. Molecular structure of **26a-e**.

In 2009, Zhao et al. [42] synthesized a series of 1,4-bis(arylethynyl)-2,5-diborylbenzenes **27a-h** containing various *p*-substituents on the terminal benzene rings and investigated the substituent effects on their absorption and fluorescence properties [Figure 1.20]. In addition, most of these synthesized derivatives showed enhanced fluorescence in the solid state compared to solution. These findings imply that diborylphenylene unit is a very effective and useful core skeleton to prevent fluorescence quenching in the solid state. They also investigated the fluorescence fluoride ion sensing ability of the most emissive **27a** and demonstrated the intense fluorescence properties irrespective of the turn on modes. The binding constant of **27a** with F^- was determined to be $1.25 \times 10^5 \text{ M}^{-1}$ in THF.

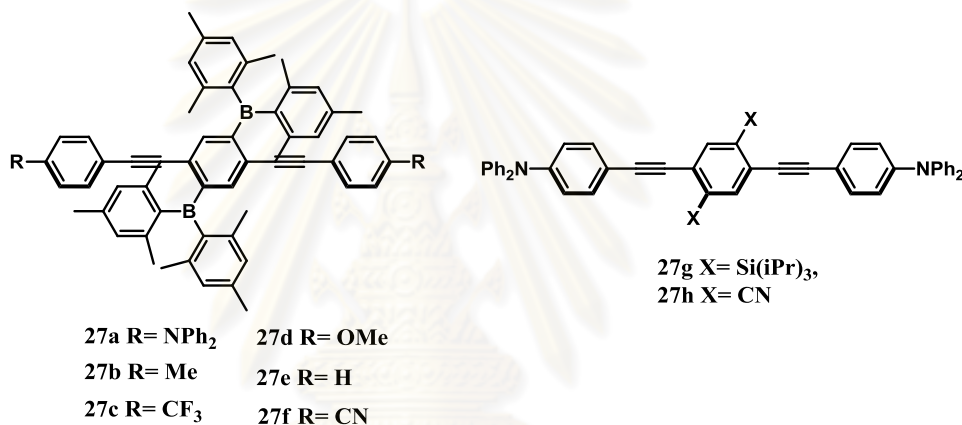


Figure 1.20. Molecular structure of **27a-h**.

In 2010, Swinburne et al. [43] designed conformational fluorescent switch anion receptors **28a-c** based on an induced fit binding approach. The addition of chloride ion results in a planarization of the chromophore and hence an increase in the energy trap by the non-emissive dark state. This results in a significant increase in the fluorescence emission from the receptor. The chloride ion binding constants for the receptors determined in $CHCl_3/DMSO$ (70:30) solution showed $\log \beta$ as 2.557, 1.831, and <1 , respectively [Figure 1.21].

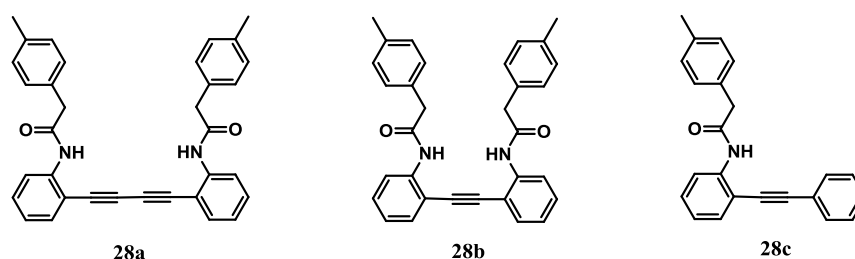


Figure 1.21. Molecular structure of **28a-c**.

In 2009, Acharya et al. [44] immobilized a monolayer of 10-formylanthracenyl-terminated *p*-phenylene ethynylene derivative **29** on glass surface via an alkyl chain linker. The modified glass surface showed significant ratiometric fluorescent response with cysteine. The enhanced intensity was significant for cysteine concentrations ranging from 0.1 to 10 mM, and resulted in a 3-fold total enhancement of the fluorescence quantum yield, with the 450 nm band being the major contributor. On the practical side, this phenomenon can provide a useful platform to increase optical gain in fluorescent chemodetection [Figure 1.22].

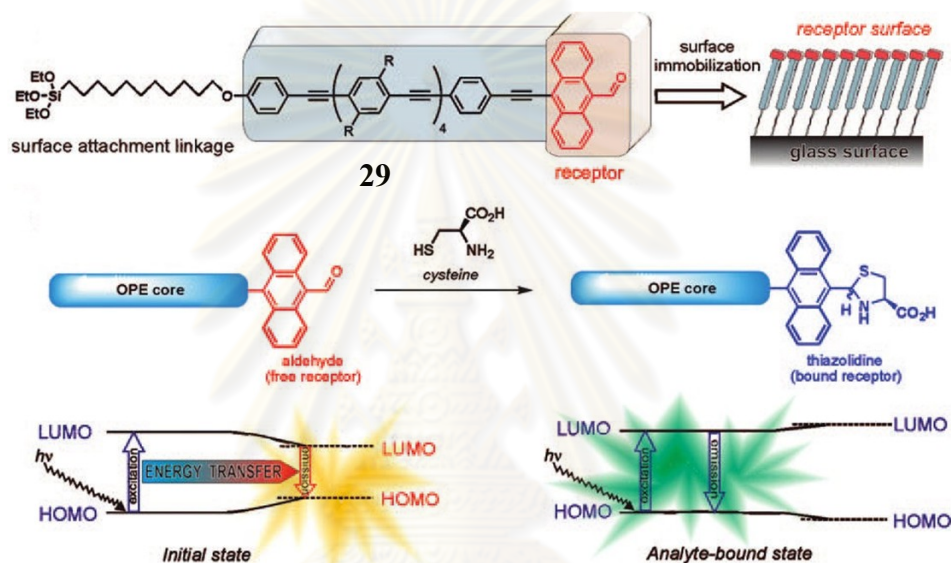


Figure 1.22. Molecular structure of **29** and proposed cysteine sensing mechanism.

In 2009, Ji et al. [45] synthesized 1, 8- and 1, 6-bis(phenylethynyl) pyrenes **30a-b** with different intramolecular charge transfer (ICT) feature and studied the ICT effect on the photophysical properties. Phenylethynylated pyrene derived fluorescent thiol probes with 2, 4-dinitrobenzenesulfonyl amide structure were designed to show fluorescence OFF-ON switching effect in the presence of thiol. The TDDFT calculations predict lowest-lying dark states of S1 for the probes, induced by ICT effect (electron transfer from fluorophore to 2, 4-dinitrobenzenesulfonyl unit). This dark state infers the probe is nonfluorescent. Cleavage of the 2,4-dinitrobenzenesulfonyl unit by thiol releases the free fluorophore (the ICT effect is terminated), for which the lowest-lying excited state S1 is no longer a dark state, therefore the product will potentially be fluorescent. The probes were successfully used for bioimaging of thiols in living cells. This investigation is the successful application of new

fluorophores and molecular probes with predetermined photophysical properties in biosensor application [Figure 1.23].

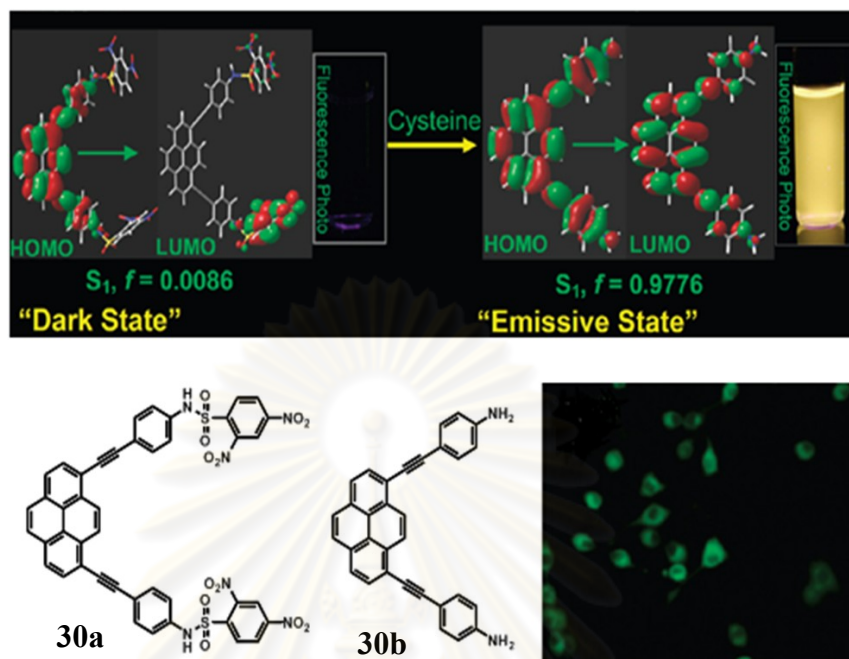


Figure 1.23. Molecular structure of **30a** (left) and picture of **30a** in the presence of cysteine which is converted into **30b** (right).

In 2009 Zhang [46] et al. designed a dendritic fluorescent probe **31** exhibiting strong two-photon absorption and efficient sensing due to ICT presence/absence before and after reaction with Cys/Hcy in DMSO. Upon binding to Cys/Hcy, the probe exhibited both turn-on fluorescence and large peak shift (165 nm) due to the ICT switch off. This is the first report that exhibits both greatly enhanced emission intensity and large peak shift. The potential reactivity of aldehyde toward other nucleophiles, this work should be a general guideline for the design of novel multisignal one- and two-photon turn-on probes, based on ICT switch on/off, with various sensing applications [Figure 1.24].

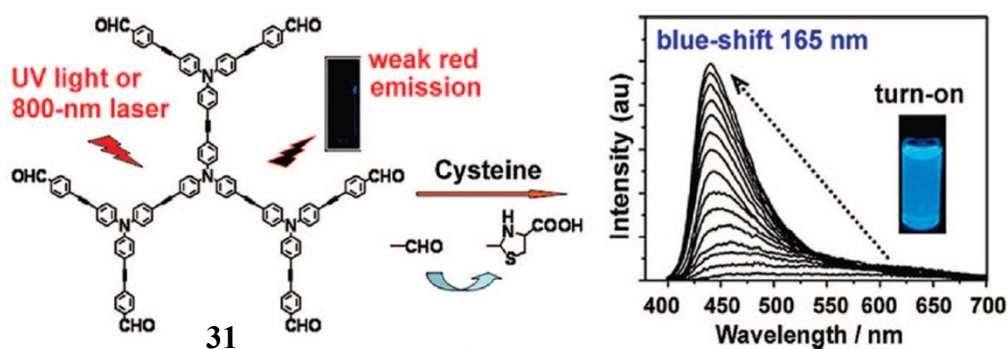


Figure 1.24. Molecular structure of **31** (left) and showing picture of **31** in the presence of cysteine (right).

In comparison with CPEs, small fluorescent molecules offer better defined structures and conformation that lead to greater understanding of the sensing mechanism. Therefore, a dendrimer obtained from controlled stepwise synthesis should provide an opportunity to study a combined amplification effect of the polymers with a well defined structure of small molecules and will be the focus of this thesis work.

ศูนย์วิทยทรัพยากร
จุฬาลงกรณ์มหาวิทยาลัย

1.7 Objectives of this research

The aim of this work focuses on the synthesis of water soluble dendritic fluorophores composed of phenyleneethynylene repeating units and anionic carboxylate or cationic ammonium peripheral groups (**Figure 25**) and study of photophysical properties of these compounds. The application of these new fluorophores as metal ion and protein sensors in aqueous media will also be explored.

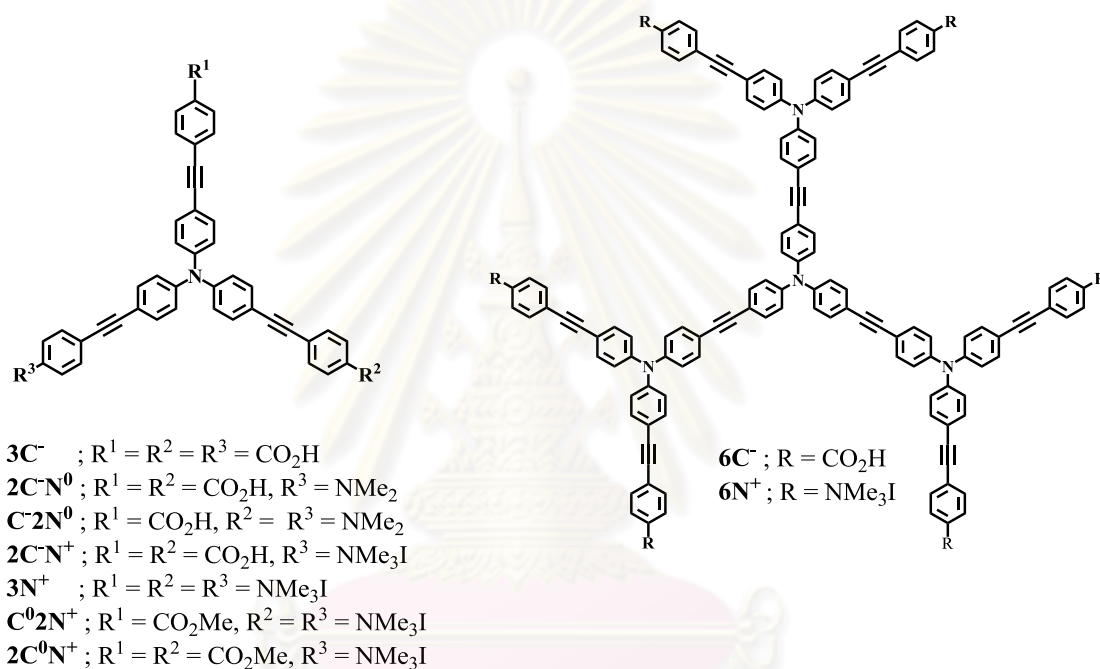


Figure 1.25 The target molecules.

ศูนย์วิทยทรัพยากร
จุฬาลงกรณ์มหาวิทยาลัย

CHAPTER II

EXPERIMENTAL

2.1 Chemicals and materials

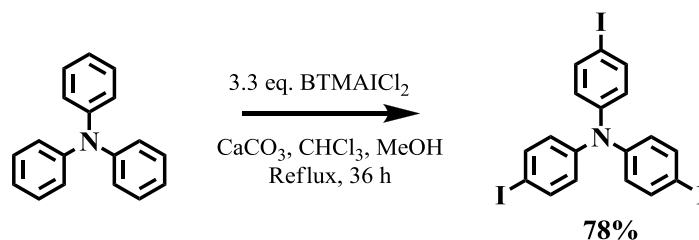
N,N-dimethylaniline, trimethylsilylacetylene, bis(triphenylphosphine)palladium(II)dichloride ($\text{PdCl}_2(\text{PPh}_3)_2$), sodium thiosulfate, benzyltrimethylammonium chloride, potassium hydroxide, potassium carbonate, calcium carbonate, and bovine serum albumin (BSA) were purchased from Fluka (Switzerland). Triphenylamine, iodine monochloride, copper (I) iodide, 1, 8-diazabicyclo [5.4.0] undec-7-ene (DBU), 4-iodobenzoic acid and quinine sulfate were purchased from Aldrich. Concanavalin A (ConA, from Jack bean), cytochrome C (CytC, from equine heart), histone (His, from calf thymus, type III-S), human serum albumin (HSA), lysozyme (Lys, from chicken egg white), myoglobin (Myo, from equine heart) and papain (Pap, from papaya latex) were purchased from Sigma and used without further purification. All other reagents were non-selectively purchased from Sigma-Aldrich, Fluka or Merck (Germany). For most reactions, solvents such as dichloromethane and acetonitrile were reagent grade stored over molecular sieves. In anhydrous reactions, solvents such as THF and toluene were dried and distilled before use according to the standard procedures. All column chromatography were operated using Merck silica gel 60 (70-230 mesh). Thin layer chromatography (TLC) was performed on silica gel plates (Merck F₂₄₅). Solvents used for extraction and chromatography such as dichloromethane, hexane, ethyl acetate and methanol were commercial grade and distilled before use while diethyl ether and chloroform were reagent grade. Milli-Q water was used in all experiments unless specified otherwise. The most reactions were carried out under positive pressure of N₂ filled in rubber balloons.

2.2 Analytical instruments

The melting points of all products were acquired from a melting point apparatus (Electrothermal 9100, Fisher Scientific, USA). Elemental (C, H, N) analyses were performed on a PE 2400 series II analyzer (Perkin-Elmer, USA). Mass spectra were recorded on a Microflex MALDI-TOF mass spectrometer (Bruker Daltonics) using doubly recrystallized α -cyano-4-hydroxy cinnamic acid (CCA) as a matrix. The HRMS spectra were measured on an electrospray ionization mass spectrometer (microTOF, Bruker Daltonics). Fourier transform infrared spectra were acquired on Nicolet 6700 FT-IR spectrometer equipped with a mercury-cadmium telluride (MCT) detector (Nicolet, USA). $^1\text{H-NMR}$ and $^{13}\text{C-NMR}$ spectra were acquired from sample solution in CDCl_3 , acetone- d_6 , CD_3CN , CD_3OD and $\text{DMSO-}d_6$ on Varian Mercury NMR spectrometer (Varian, USA) at 400 MHz and 100 MHz, respectively. The UV-visible absorption spectra were obtained from a Varian Cary 50 UV-Vis spectrophotometer (Varian, USA) and the fluorescence emission spectra were recorded on a Varian Cary Eclipse spectrofluorometer (Varian, USA).

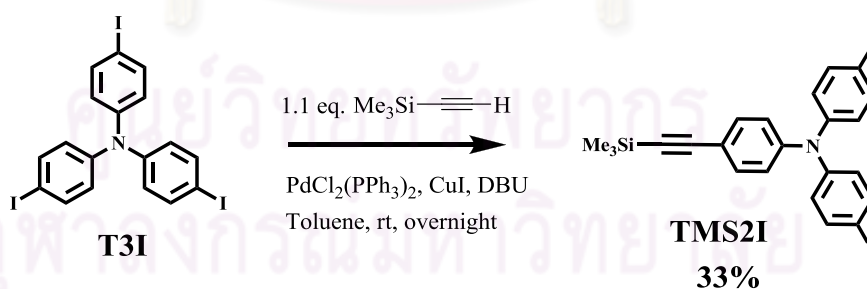
2.3 Synthesis of dendritic fluorophores

2.3.1 Preparation of 4, 4', 4''-triiodotriphenylamine.



A mixture of triphenylamine (7.36 g, 30 mmol) in chloroform (100 mL) and methanol (50 mL) was added with BTMAICl₂ (34.47 g, 99 mmol) and CaCO₃ (18 g, 180 mmol). The reaction mixture was allowed to reflux for 72 h and 20% Na₂S₂O₃ solution was then added to the mixture until the mixture became light yellow. The mixture was filtered and the filtrate was extracted with dichloromethane (3 × 50 mL). The combined organic phase was washed with water (2 × 100 mL) and dried over anhydrous MgSO₄. The solution was concentrated and the residue was reprecipitated in methanol from dichloromethane solution. Triiodotriphenylamine (**T3I**) was obtained (14.59 g, 78%) as a white solid: mp; 182-184°C; ¹H NMR (CDCl₃, 400 MHz): δ (ppm) 7.53 (d, *J* = 7.5 Hz, 6H), 6.80 (d, *J* = 7.5 Hz, 6H); ¹³C NMR (CDCl₃, 100 MHz): δ (ppm) 146.6, 138.5, 126.1, 88.7; MALDI-TOF *m/z* Calcd. for C₁₈H₁₂I₃N, 622.810 Found: 622.561.

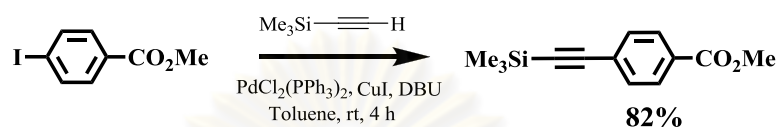
2.3.2 Preparation of TMSI₂.



A mixture of **T3I** (2.0 g, 3.2 mmol), PdCl₂(PPh₃)₂ (0.11 g, 0.16 mmol), CuI (30 mg, 0.16 mmol) and trimethylsilyl acetylene (0.34 g, 3.5 mmol) in toluene (10 mL) was added with DBU (1 mL) and the mixture was stirred at room temperature for 24 h. The mixture was filtered and the solid residue was washed with toluene (3 × 15 mL). The filtrate was evaporated and the residue was eluted through a silica gel column by hexane to afford **TMSI₂** as a light yellow oil (0.57 g, 33% yield). ¹H NMR

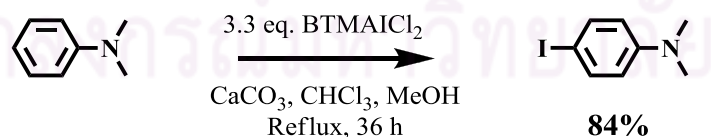
(CDCl₃, 400 MHz): δ (ppm) 7.53 (d, J = 6.8 Hz, 4H), 7.33 (d, J = 8.8 Hz, 2H), 6.94 (d, J = 8.8 Hz, 2H), 6.81 (d, J = 6.8 Hz, 4H), 0.23 (s, 9H); ¹³C NMR (CDCl₃, 100 MHz): δ (ppm) 46.5, 138.4, 133.2, 126.3, 123.1, 117.5, 140.6, 93.9, 86.7, 0.01; MALDI-TOF m/z Calcd for C₂₃H₂₁I₂NSi, 592.953 Found: 593.247.

2.3.3 Preparation of Methyl 4-((trimethylsilyl)ethynyl)benzoate.



A mixture of methyl 4-iodobenzoate (2.00 g, 7.6 mmol), PdCl₂(PPh₃)₂ (0.27 g, 0.4 mmol), CuI (0.07g, 0.38 mmol) and trimethylsilylacetylene (0.83 g, 8.4 mmol) in toluene (10 mL) was added with DBU (1 mL) and the mixture was stirred at room temperature for 24 h. The reaction mixture was then filtered and the solid was washed with toluene (3 × 15 ml). The filtrate was evaporated and the residue was eluted through a silica gel column by gradient solvents starting from pure hexane to dichloromethane/hexane (1/4) as an eluent to afford Methyl 4-((trimethylsilyl)ethynyl)benzoate as a white solid (1.45 g, 82% yield). mp: 108-110°C; ¹H NMR (CDCl₃, 400 MHz): δ (ppm) 7.99 (d, J = 8.4 Hz, 2H), 7.55 (d, J = 8.4 Hz, 2H), 3.92 (s, 3H), 0.23 (s, 9H); ¹³C NMR (CDCl₃, 100 MHz): δ (ppm) 166.7, 132.0, 129.8, 129.5, 127.9, 104.2, 97.9, 52.4, 0.01; MALDI-TOF m/z Calcd for C₁₃H₁₆O₂Si, 232.092 Found: 233.425.

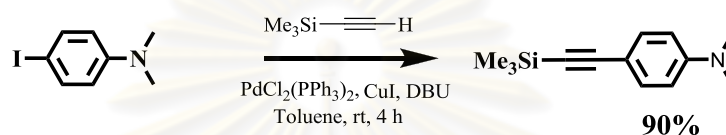
2.3.4 Preparation of 4-iodo-*N,N*-dimethylaniline.



A mixture of *N,N*-dimethylaniline (6.0 g, 50 mmol) in chloroform (100 mL) and methanol (50 mL) was added with BTMAICl₂ (18.08 g, 52 mmol) and CaCO₃ (16.45 g, 0.15 mmol). After the reaction mixture was refluxed for 36 h, 20% Na₂S₂O₃ solution was added to the mixture until the mixture became light yellow. The mixture was filtered and the filtrate was extracted with dichloromethane (3 × 50 mL). The

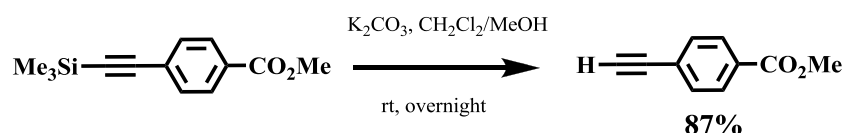
combined organic phase was washed with water (2×100 mL) and dried over anhydrous MgSO_4 . The solution was concentrated and the residue was reprecipitated in methanol from dichloromethane solution. 4-Iodo-*N,N*-dimethylaniline was obtained as a purple solid (10.37 g, 84%): mp ; 91-93°C; ^1H NMR (CDCl_3 , 400 MHz): δ (ppm) 7.46 (d, $J = 5.6$ Hz, 2H), 6.49 (d, $J = 5.6$ Hz, 2H), 2.92 (s, 6H); ^{13}C NMR (CDCl_3 , 100 MHz): δ (ppm) 137.5, 114.7, 40.4.

2.3.5 Preparation of *N,N*-dimethyl-4-((trimethylsilyl)ethynyl)aniline.



A mixture of 4-iodo-*N,N*-dimethylaniline (2.51 g, 10 mmol), $\text{PdCl}_2(\text{PPh}_3)_2$ (0.35 g, 0.5 mmol), CuI (0.08 g, 0.5 mmol) and trimethylsilylacetylene (1.08 g, 11 mmol) in toluene (10 ml) was added with DBU (1 mL) and the mixture was stirred at room temperature for 4 h. The reaction mixture was then filtered and the solid was washed with toluene (3×15 ml). The filtrate was evaporated and the residue was eluted through a silica gel column by gradient solvents starting from pure hexane to dichloromethane/hexane (1/3) as an eluent to afford *N,N*-dimethyl-4-((trimethylsilyl)ethynyl)aniline as a yellow solid (2.17 g, 90% yield). mp: 88-89°C; ^1H NMR (CDCl_3 , 400 MHz): δ (ppm) 7.11(d, $J = 7.2$ Hz, 2H), 6.35 (d, $J = 7.2$ Hz, 2H), 2.72 (s, 6H), 0.01 (s, 9H); ^{13}C NMR (CDCl_3 , 100 MHz): δ (ppm) 149.9, 132.9, 111.3, 109.6, 106.3, 90.9, 39.9, 0.01.

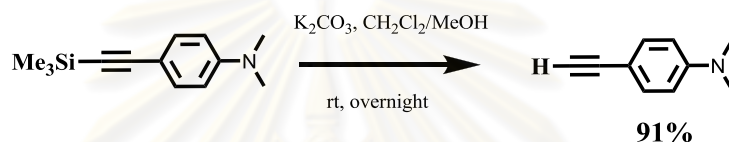
2.3.6 Preparation of methyl 4-ethynylbenzoate.



A mixture of methyl 4-((trimethylsilyl)ethynyl)benzoate (1.00 g, 4.3 mmol) and K_2CO_3 (0.059 g, 0.43 mmol) in dichloromethane (15 mL) and methanol (15 mL) was stirred at room temperature for 24 h. The organic layer was separated and the aqueous

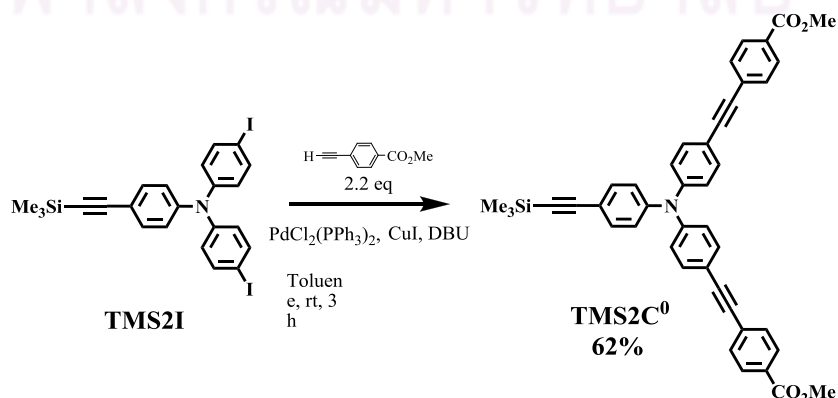
phase was extracted with dichloromethane (2 x 50 mL) and was then dried over anhydrous MgSO_4 . The solvent was evaporated and the residue was eluted through a silica gel column by gradient solvents starting from pure hexane to dichloromethane/hexane (1/4) as an eluent to afford Methyl 4-ethynylbenzoate as a white solid (0.60 g, 87% yield). mp: 103-105°C. ^1H NMR (CDCl_3 , 400 MHz): δ (ppm) 7.98 (d, $J = 8.4$ Hz, 2H), 7.55 (d, $J = 8.4$ Hz, 2H), 3.92 (s, 3H); ^{13}C NMR (CDCl_3 , 100 MHz): δ (ppm) 166.3, 132.0, 130.1, 129.4, 126.7, 82.8, 80.1, 52.2; 90-92°C; MS m/z Calcd for $\text{C}_{10}\text{H}_8\text{O}_2$, 160.052 Found: 161.035.

2.3.7 Preparation of 4-ethynyl-*N,N*-dimethylaniline.



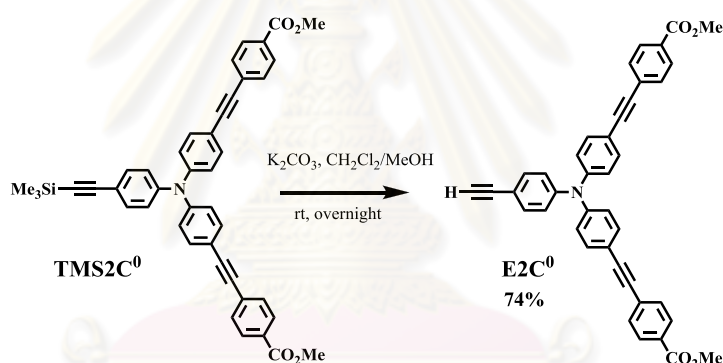
A mixture of *N,N*-dimethyl-4-((trimethylsilyl)ethynyl)aniline (1.00 g, 4.6 mmol) and K_2CO_3 (0.059 g, 0.43 mmol) in dichloromethane (15 mL) and methanol (15 mL) was stirred at room temperature for 12 h. Next addition of water, the organic layer was separated and the aqueous phase was extracted with dichloromethane (2 x 50 mL) and was then dried over anhydrous MgSO_4 . The filtrate was evaporated and the residue was eluted through a silica gel column by gradient solvents starting from pure hexane to dichloromethane/hexane (1/3) as an eluent to afford 4-ethynyl-*N,N*-dimethylaniline as a brown-yellow solid (0.60 g, 91 % yield). mp: 67-69°C. ^1H NMR (CDCl_3 , 400 MHz): δ (ppm) 7.37 (d, $J = 8.8$ Hz, 2H), 6.62 (d, $J = 8.8$ Hz, 2H), 2.07 (s, 7H); ^{13}C NMR (CDCl_3 , 100 MHz): δ (ppm) 150.4, 133.2, 111.7, 108.7, 84.9, 74.9, 40.

2.3.8 Preparation of TMS2C⁰.



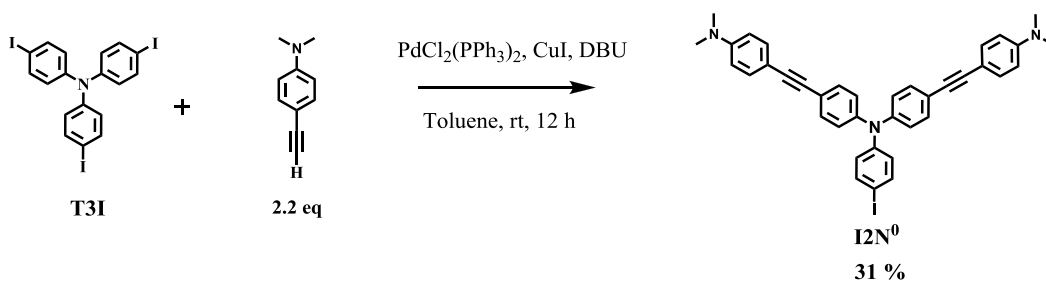
A mixture of **TMS2I** (0.41 g, 0.69 mmol), PdCl₂(PPh₃)₂ (49 mg, 0.07 mmol), CuI (14 mg, 0.07 mmol), Methyl 4-ethynylbenzoate (2.43 g, 1.52 mmol) in toluene (10 ml) was added with DBU (1 ml) and the mixture was stirred at room temperature for 3 h. The mixture was filtered and the filtrate was evaporated. The residue was eluted through a silica gel column by gradient solvents starting from pure hexane to dichloromethane/hexane (2/1) as an eluent to afford **TMS2C⁰** as a yellow solid (0.28 g, 62% yield). mp: 120-122°C; ¹H NMR (CDCl₃, 400 MHz): δ (ppm) 8.02 (d, *J* = 8.0 Hz, 4H), 7.57 (d, *J* = 8.0 Hz, 4H), 7.44 (d, *J* = 8.4 Hz, 4H), 7.39 (d, *J* = 8.4 Hz, 2H), 7.06 (d, *J* = 8.4 Hz, 2H), 7.04 (d, *J* = 8.4 Hz, 2H), 3.93 (s, 6H), 0.23 (s, 9H); ¹³C NMR (CDCl₃, 100 MHz): δ (ppm) 0.01; MALDI-TOF *m/z* Calcd for C₄₃H₃₅NO₄Si, 657.234 Found: 656.908.

2.3.9 Preparation of **E2C⁰**.



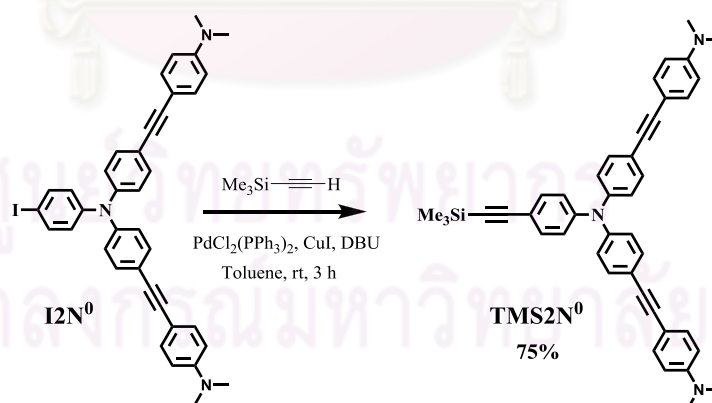
A mixture of **TMS2C⁰** (0.20 g, 0.34 mmol) and K₂CO₃ (42 mg, 0.034 mmol) in dichloromethane (15 mL) and methanol (15 mL) was stirred at room temperature for 24 h. The organic layer was separated and the aqueous phase was extracted with dichloromethane (2 x 50 mL) and was then dried over anhydrous MgSO₄. The solvent was evaporated and the residue was eluted through a silica gel column by gradient solvents starting from pure hexane to dichloromethane/hexane (2/1) as an eluent to afford **E2C⁰** as a yellow solid (0.15 g, 74% yield). mp: 193-195°C; ¹H NMR (CDCl₃, 400 MHz): δ (ppm) 8.01 (d, *J* = 8.0 Hz, 4H), 7.57 (d, *J* = 8.0 Hz, 4H), 7.44 (d, *J* = 8.4 Hz, 4H), 7.41 (d, *J* = 8.4 Hz, 2H), 7.07 (d, *J* = 8.4 Hz, 2H), 7.04 (d, *J* = 8.4 Hz, 2H), 3.93 (s, 6H), 0.23 (s, 9H); ¹³C NMR (CDCl₃, 100 MHz): δ (ppm) 166.6, 147.0, 138.4, 133.0, 129.5, 129.3, 128.1, 124.1, 124.0, 117.4, 117.1, 92.3, 88.7, 83.4, 52.2; MALDI-TOF *m/z* Calcd for C₄₀H₂₇NO₄, 585.194 Found: 584.804.

2.3.10 Preparation of **I2N⁰**.



A mixture of **T3I** (1.0 g, 0.80 mmol), PdCl₂(PPh₃)₂ (20 mg, 0.03 mmol), CuI (6 mg, 0.03 mmol), 4-ethynyl-*N,N*-dimethylaniline (0.26 g, 1.8 mmol) in toluene (240 ml) was added to DBU (1 ml) and the mixture was stirred at rt for 12 h. The combined filtrate was evaporated and the residue was eluted through a silica gel column by gradient solvents from pure hexane to CH₂Cl₂/hexane (3/1) as an eluent to obtain **I2N⁰** as a brown solid (0.33 g, 31% yield). mp: 206-209 °C. ¹H NMR (CDCl₃, 400 MHz): δ (ppm) 7.54 (d, *J* = 8.5 Hz, 2H), 7.36-7.39 (m, 4H), 7.01 (d, *J* = 8.5 Hz, 4H), 6.68 (d, *J* = 8.5 Hz, 2H), 6.65 (d, *J* = 8.5 Hz, 4H), 3.00 (s, 12H). ¹³C NMR (CDCl₃, 100 MHz): δ (ppm) 149.9, 146.8, 146.0, 138.4, 132.8, 126.3, 123.8, 123.7, 118.7, 111.8, 110.1, 90.4, 87.1, 86.2, 40.3. MALDI-TOF *m/z* Calcd for C₃₈H₃₂I₃N₃, 657.164; Found: 656.610.

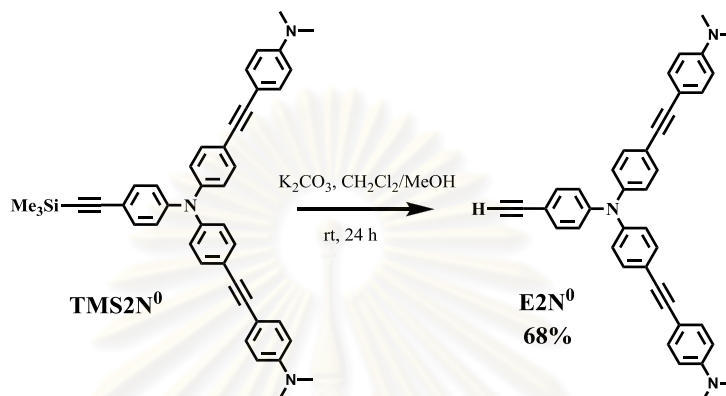
2.3.11 Preparation of **TMS2N⁰**.



A mixture of **I2N⁰** (0.2 g, 0.30 mmol), PdCl₂(PPh₃)₂ (2 mg, 0.003 mmol), CuI (2 mg, 0.01 mmol), trimethylsilyl acetylene (39 mg, 0.40 mmol) in toluene (10 ml) was added to DBU (1 mL) and the reaction was stirred at rt for 3 h. The mixture was filtered and the solid washed with toluene (3 x 15 ml). The combined filtrate was evaporated and the residue was eluted through a silica gel column by hexane to obtain **TMS2N⁰** as a light yellow oil (0.14 g, 75% yield). mp: 116-119 °C. ¹H NMR (CDCl₃, 400 MHz): δ (ppm) 7.16-7.09 (m, 10H), 6.76

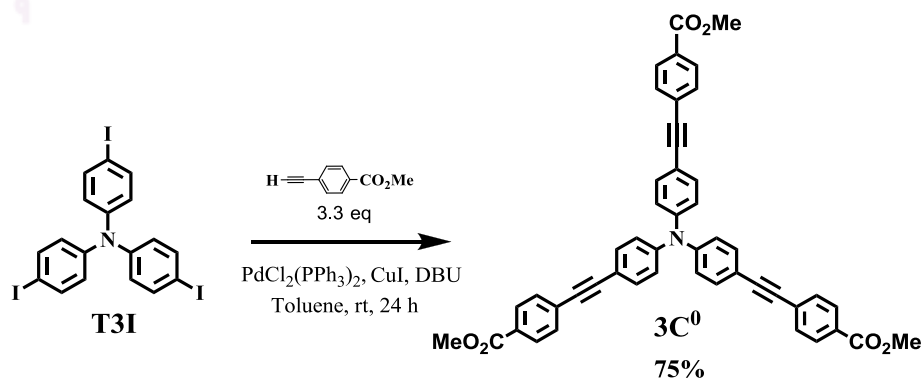
(d, $J = 8.5$ Hz, 6H), 6.40 (d, $J = 8.5$ Hz, 4H), 2.73 (s, 12H), 0.01 (s, 9H). ^{13}C NMR (CDCl_3 , 100 MHz): δ (ppm) 149.9, 147.1, 145.9, 133.0, 132.6, 132.6, 132.3, 124.1, 123.3, 118.8, 117.1, 111.8, 110.1, 105.0, 93.6, 90.4, 87.1, 40.2, 0.01. MALDI-TOF m/z Calcd for $\text{C}_{43}\text{H}_{41}\text{N}_3\text{Si}$: 627.307; Found: 626.814.

2.3.12 Preparation of E2N^0 .



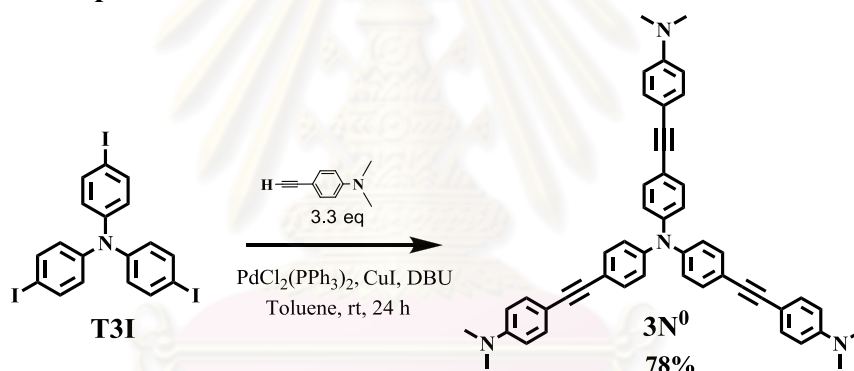
A mixture of TMS2N^0 (0.10 g, 0.16 mmol) and K_2CO_3 (42 mg, 0.034 mmol) in CH_2Cl_2 (15 mL) and methanol (15 mL) was stirred at rt for 24 h. The organic layer was separated and the aqueous layer was extracted with CH_2Cl_2 (2 x 50 mL) and was then dried over anhydrous MgSO_4 . The combined filtrate was evaporated and the residue was eluted through a silica gel column by gradient solvents from pure hexane to CH_2Cl_2 /hexane (2/1) as an eluent to afford E2N^0 as a yellow solid (60 mg, 68% yield). mp: 135-138 °C. ^1H NMR (CDCl_3 , 400 MHz): δ (ppm) 7.39 (d, $J = 8.5$ Hz, 10H), 7.04 (d, $J = 8.5$ Hz, 6H), 6.66 (d, $J = 8.5$ Hz, 4H), 2.99 (s, 13H). ^{13}C NMR (CDCl_3 , 100 MHz): δ (ppm) 150.0, 147.4, 145.9, 133.2, 132.6, 132.4, 124.2, 123.4, 123.3, 119.0, 115.9, 111.8, 110.1, 90.5, 87.1, 83.7, 40.3. MALDI-TOF m/z Calcd for $\text{C}_{40}\text{H}_{33}\text{N}_3$: 555.267; Found: 554.969.

2.3.13 Preparation of 3C^0 .



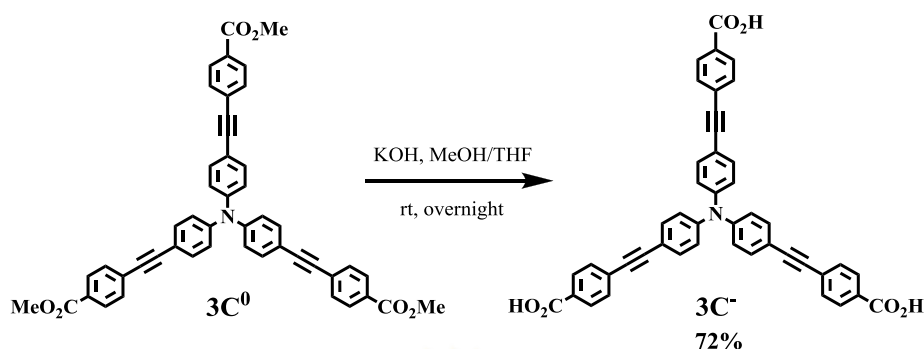
A mixture of Ti_3 (0.30 g, 0.48 mmol), $\text{PdCl}_2(\text{PPh}_3)_2$ (55 mg, 0.080 mmol), CuI (15 mg, 0.080 mmol), **methyl 4-ethynylbenzoate** (0.25 g, 1.6 mmol) in toluene (10 ml) was added with DBU (1 mL) and the mixture was stirred at room temperature for 24 h. The mixture was filtered and the filtrate was evaporated. The residue was eluted through a silica gel column by gradient solvents starting from pure hexane to dichloromethane/hexane (2/1) as an eluent to afford **3C⁰** as a yellow solid (0.80 g, 75% yield). mp: 242-244°C; ^1H NMR (CDCl_3 , 400 MHz): δ (ppm) 8.00 (d, $J = 8.4$ Hz, 6H), 7.56 (d, $J = 8.4$ Hz, 6H), 7.45 (d, $J = 8.4$ Hz, 6H), 7.08 (d, $J = 8.4$ Hz, 6H); ^{13}C NMR (CDCl_3 , 100 MHz): δ (ppm) 166.5, 146.9, 133.0, 131.4, 129.5, 129.3, 128.0, 124.1, 117.5, 92.3, 88.7, 52.2; MALDI-TOF m/z Calcd for $\text{C}_{48}\text{H}_{33}\text{NO}_6$, 719.231 Found: 719.802.

2.3.14 Preparation of **3N⁰**.



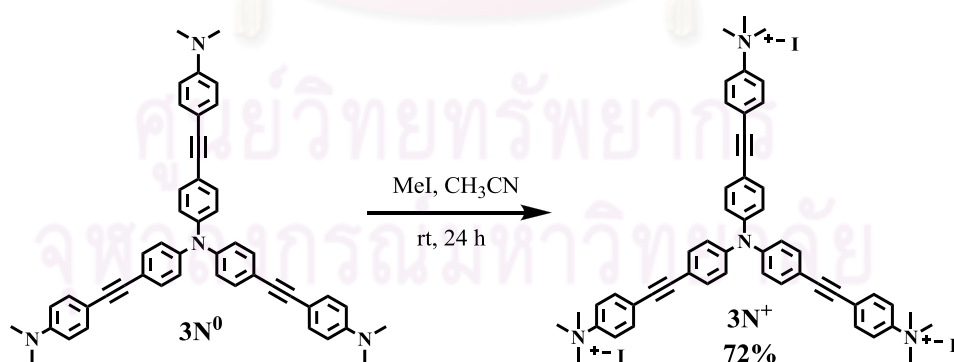
A mixture of **T3I** (0.30 g, 0.48 mmol), $\text{PdCl}_2(\text{PPh}_3)_2$ (55 mg, 0.080 mmol), CuI (15 mg, 0.080 mmol), 4-ethynyl-*N,N*-dimethylaniline (0.25 g, 1.6 mmol) in toluene (10 ml) was added DBU (1 mL) and the mixture was stirred at room temperature for 24 h. After the combined filtrate was evaporated and the residue was eluted through a silica gel column by gradient solvents from pure hexane to methylene chloride/hexane (2/3) as an eluent to afford **3N⁰** as a yellow solid (0.25 g, 78% yield). mp: 284-286°C; ^1H NMR (CDCl_3 , 400 MHz) δ (ppm) 7.39(d, $J = 8.8$ Hz, 6H), 7.38(d, $J = 8.8$ Hz, 6H), 7.04 (d, $J = 8.8$ Hz, 6H), 6.66 (d, $J = 8.8$ Hz, 6H), 2.99 (s, 18 Hz); ^{13}C NMR (CDCl_3 , 100 MHz) δ (ppm) 150.0, 146.2, 132.6, 132.4, 123.9, 118.6, 111.8, 110.2, 90.3, 87.2, 40.3; MALDI-TOF m/z Calcd for $\text{C}_{48}\text{H}_{42}\text{N}_4$, 674.341 Found: 674.845.

2.3.15 Preparation of $3C^-$.



A mixture of $3C^0$ (0.50 g, 0.69 mmol) in THF (15 mL) and methanol (15 mL) was added with saturated KOH aqueous solution (0.5 mL) and the mixture was stirred at room temperature. After 24 h the solution was evaporated and the residue was dissolved in water (30 mL). Ice (~50 g) was then added to the aqueous solution, acidified and kept in a refrigerator for 1 h. The product was filtered to afford $3C^-$ as a yellow solid (0.34 g, 72% yield). mp. $>350^\circ\text{C}$ decompose; ^1H NMR (DMSO- d_6 , 400 MHz): δ (ppm) 13.13(broad, 3H), 7.95 (d, $J = 8.4$ Hz, 6H), 7.63 (d, $J = 8.4$ Hz, 6H), 7.55 (d, $J = 8.4$ Hz, 6H), 7.10 (d, $J = 8.4$ Hz, 6H); ^{13}C NMR (DMSO- d_6 , 100 MHz): δ (ppm) 166.4, 146.7, 133.9, 131.8, 130.0, 126.4, 124.3, 117.4, 92.2, 88.7; MALDI-TOF m/z Calcd for $\text{C}_{45}\text{H}_{27}\text{NO}_6$, 677.184 Found: 677.776. Anal. Calcd for $\text{C}_{45}\text{H}_{27}\text{NO}_6$: C, 79.75; H, 4.02; N, 2.07. Found: C, 79.45; H, 4.22; N, 2.12.

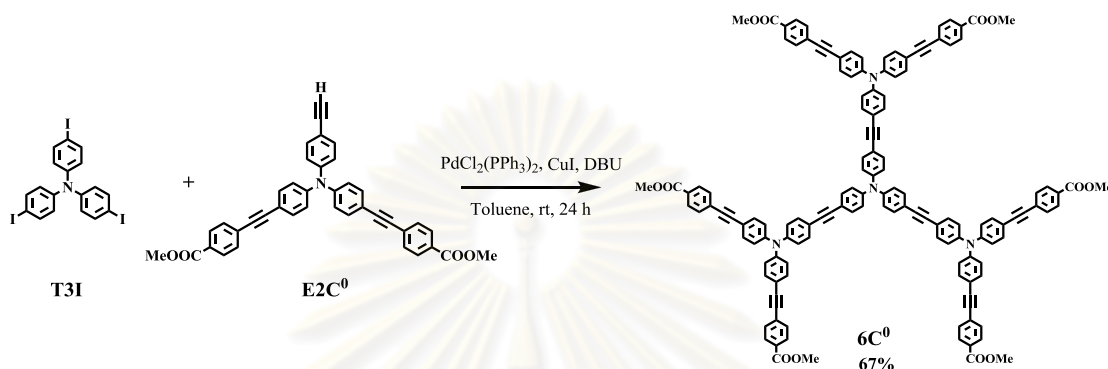
2.3.16 Preparation of $3N^+$.



A mixture of $3N^0$ (0.20 g, 0.69 mmol) in CH_3CN (15 mL) was added CH_3I (0.5 mL) and the mixture was stirred at 70°C in seal tube. After 24 h the solution was evaporated to afford $3N^+$ as a yellow solid (0.34 g, 72% yield). mp: $>350^\circ\text{C}$ decompose; ^1H NMR (CD_3CN , 400 MHz) δ (ppm) 7.88 (d, $J = 8.0$ Hz, 6H), 7.76 (d, $J = 8.4$ Hz,

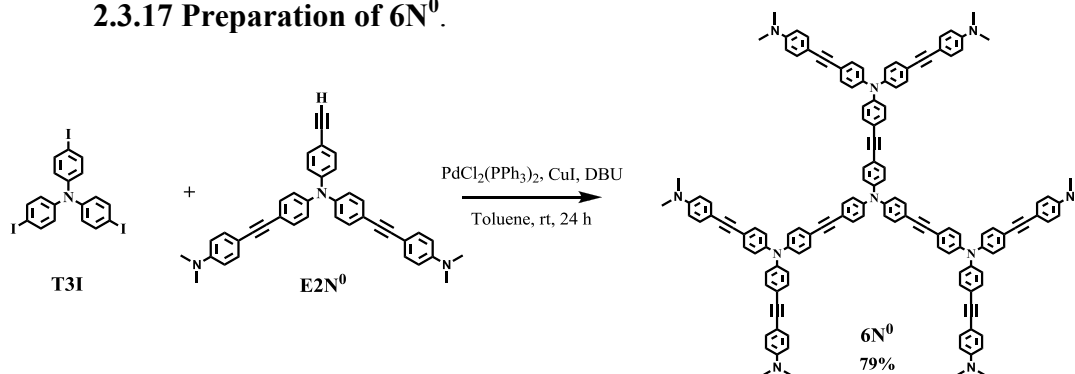
6H), 7.53 (d, $J = 8.4$ Hz, 6H), 7.15 (d, $J = 8.0$ Hz, 6H); ^{13}C NMR (CD_3CN , 100 MHz) δ (ppm) 147.5, 146.3, 133.3, 133.1, 125.8, 124.5, 121.0, 91.9, 87.0, 57.3; MS-ES $^+$ m/z Calcd for $\text{C}_{51}\text{H}_{51}\text{I}_3\text{N}_4$, 719.691 Found: 240.004 $[\text{M}]^{3+}$. Anal. Calcd for $\text{C}_{51}\text{H}_{51}\text{I}_3\text{N}_4$: C, 55.65; H, 4.67; N, 5.09 Found: C, 54.49; H, 4.95; N, 4.97.

2.3.18 Preparation of 6C^0 .



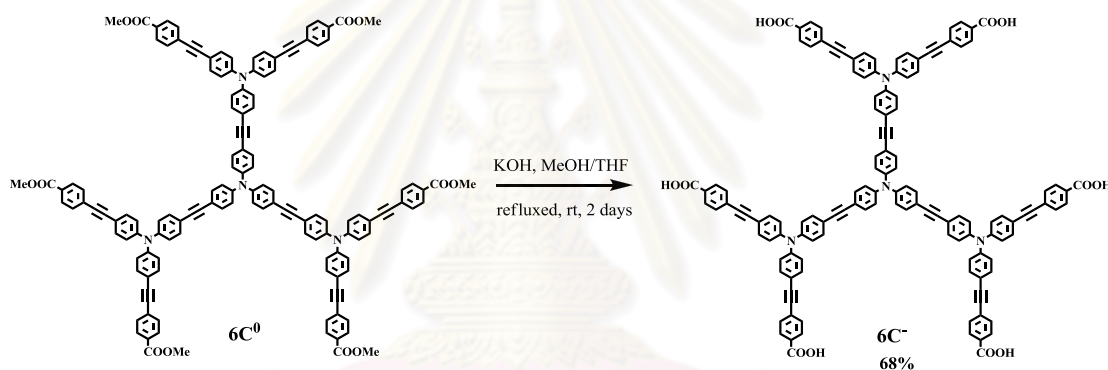
A mixture of **T3I** (20 mg, 0.032 mmol), $\text{PdCl}_2(\text{PPh}_3)_2$ (5 mg, 0.007 mmol), CuI (2 mg, 0.001 mmol), **E2C⁰** (0.11 g, 0.18 mmol) in toluene (10 mL) was added with DBU (0.1 mL) and the mixture was stirred at room temperature for 24 h. The reaction mixture was filtered and the filtrate was evaporated. The residue was eluted through a silica gel column by gradient solvents starting from pure hexane to dichloromethane/hexane (3/1) as an eluent to afford **6C⁰** as a yellow solid (43 mg, 67% yield). mp: 198-200°C; ^1H NMR (CDCl_3 , 400 MHz): δ (ppm) 8.01 (d, $J = 8.0$ Hz, 12H), 7.56 (d, $J = 8.0$ Hz, 12H), 7.45 (d, $J = 8.4$ Hz, 24H), 7.09 (d, $J = 8.4$ Hz, 24H), 3.93 (s, 18H); ^{13}C NMR (CDCl_3 , 100 MHz): δ (ppm) 166.6, 147.0, 146.6, 146.3, 133.0, 132.8, 132.7, 131.4, 129.5, 129.3, 128.1, 124.4, 124.0, 123.9, 118.5, 118.0, 117.3, 92.4, 89.1, 88.7, 52.2; MALDI-TOF m/z Calcd for $\text{C}_{138}\text{H}_{90}\text{N}_4\text{O}_{12}$, 1996.211 Found: 1997.537. Anal. Calcd for $\text{C}_{138}\text{H}_{90}\text{N}_4\text{O}_{12}$: C, 83.03; H, 4.54; N, 2.81. Found: C, 81.28; H, 4.53; N, 2.66.

2.3.17 Preparation of 6N^0 .



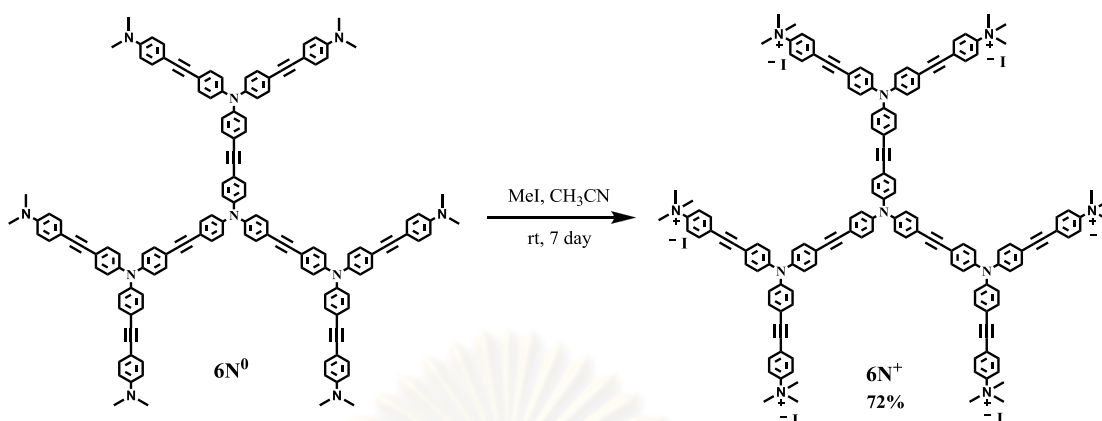
A mixture of **T3I** (22 mg, 0.035 mmol), PdCl₂(PPh₃)₂ (5 mg, 0.07 mmol), CuI (2 mg, 0.07 mmol), **E2N⁰** (0.11 g, 0.18 mmol) in toluene (10 mL) was added to DBU (0.1 mL) and the mixture was stirred at rt for 24 h. The combined filtrate was evaporated and the residue was eluted through a silica gel column by gradient solvents from pure hexane to CH₂Cl₂ as an eluent to afford **6N⁰** as a yellow solid (52 mg, 79% yield). mp: 216-218 °C. ¹H NMR (CDCl₃, 400 MHz): δ (ppm) 7.40 (*d*, *J* = 8.5 Hz, 36H), 7.06 (*d*, *J* = 8.5 Hz, 24H), 6.65 (*d*, *J* = 8.5 Hz, 12H), 2.99 (*s*, 36H). ¹³C NMR (CDCl₃, 100 MHz): δ (ppm) 149.9, 146.8, 146.5, 146.0, 132.9, 132.7, 132.4, 124.1, 123.6, 118.8, 118.1, 117.5, 111.9, 111.8, 110.2, 90.4, 89.3, 88.9, 87.1, 40.2. MALDI-TOF *m/z* Calcd for C₁₃₈H₁₀₈N₁₀: 1904.876; Found: 1906.071.

2.3.19 Preparation of **6C⁻**.



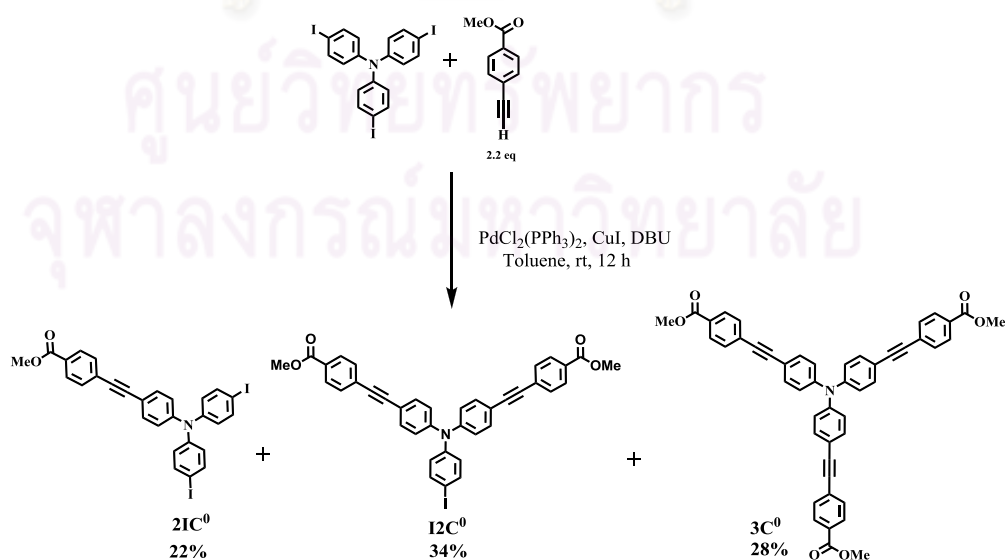
A mixture of **6C⁰** (40 mg, 0.02 mmol), Saturated KOH aqueous solution (0.1 mL) in THF (10 mL), methanol (10 mL) and water (10 mL) was refluxed with stirring for 2 days. The solution was evaporated and the residue was dissolved in water (15 mL). Ice was added to the aqueous solution, acidified and kept in a refrigerator for 1 h. The product was filtered to afford **6C⁻** as a yellow solid (26 mg, 68% yield). mp, >350 °C decompose; ¹H NMR (DMSO-d₆, 400 MHz): δ (ppm) 7.92(*d*, *J* = 7.4 Hz, 12H), 7.59 (*d*, *J* = 7.4 Hz, 12H), 7.51-7.45 (*m*, 24 H), 7.02 (*s*, 24H); ¹³C NMR (DMSO-d₆, 100 MHz): δ (ppm) 167.1, 147.0, 146.5, 146.3, 133.5, 133.4, 133.1, 131.7, 130.8, 129.9, 127.1, 124.25, 118.0, 116.9, 92.4, 92.3, 89.5, 88.9; MALDI-TOF *m/z* Calcd. for C₁₃₂H₇₈N₄O₁₂, for 1910.562 Found: 1911.357. Anal. Calcd for C₁₃₈H₉₀N₄O₁₂·10H₂O: C, 75.78; H, 4.72; N, 2.68. Found C, 74.96; H, 4.01; N, 2.68.

2.3.20 Preparation of $6N^+$.



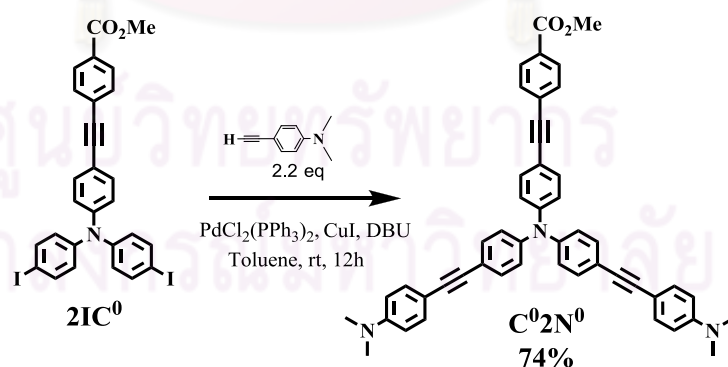
A mixture of $6N^0$ (0.20 g, 0.69 mmol) in CH_3CN (15 mL) was added to CH_3I (0.5 mL) and the mixture was stirred at 70 °C in a sealed tube. After 24 hrs the solution was evaporated to afford $6N^+$ as a yellow solid (0.34 g, 72% yield). mp: > 300 °C (decompose). 1H NMR (CD_3CN , 400 MHz): δ (ppm) 7.80 (d, $J = 8.5$ Hz, 12H), 7.51 (d, $J = 8.5$ Hz, 12H), 7.46 (d, $J = 8.5$ Hz, 12H), 7.13 (d, $J = 8.5$ Hz, 12H), 7.10 (t, $J = 8.5$ Hz, 24H). ^{13}C NMR (CD_3CN , 100 MHz): δ (ppm) 148.5, 134.1, 133.9, 133.7, 126.7, 125.8, 125.3, 125.2, 121.7, 120.4, 87.8, 58.1. MALDI-TOF m/z Calcd for $C_{144}H_{126}N_{10}$: 1995.013; Found: 1920.013 $[M-5CH_3]^+$. HRMS m/z Calcd for $C_{144}H_{126}N_{10}^{6+}$: 332.5017 Found: 332.6498 $[M/6]^{6+}$.

2.3.21 Preparation of $2IC^0$, $12C^0$, and $3C^0$.



To a mixture of **T3I** (5.0 g, 0.80 mmol), PdCl₂(PPh₃)₂ (0.12 g, 0.16 mmol), CuI (20 mg, 0.11 mmol) and methyl 4-ethynylbenzoate (2.88 g, 1.8 mmol) in toluene (40 mL) was added with DBU (2 mL) and the reaction mixture was stirred at room temperature for 12 h. The reaction mixture was filtered and the solvent was evaporated under reduced pressure. The residue was purified by flash chromatography on silica gel using gradient eluents varied from pure hexane to CH₂Cl₂/hexane (2/1). **2IC⁰** was obtained as a brown solid (1.17 g, 22% yield) mp: 169-172 °C. ¹H NMR (CDCl₃, 400 MHz): δ (ppm) 8.01 (d, *J* = 8.5 Hz, 2H), 7.56 (d, *J* = 8.5 Hz, 6H), 7.40 (d, *J* = 8.5 Hz, 2H), 7.01 (d, *J* = 8.5 Hz, 2H), 6.85 (d, *J* = 8.5 Hz, 4H), 3.93 (s, 3H). ¹³C NMR (CDCl₃, 100 MHz): δ (ppm) 166.6, 147.2, 146.5, 138.6, 138.4, 133.0, 131.4, 129.7, 129.3, 128.2, 123.1, 116.9, 92.4, 88.6, 87.1, 52.3. MALDI-TOF *m/z* Calcd for C₂₈H₁₉I₂NO₂, 654.95; Found, 654.58 [M]⁺. **12C⁰** was obtained as a yellow solid (1.88 g, 34% yield), mp: 205-208 °C. ¹H NMR (CDCl₃, 400 MHz): δ (ppm) 8.01 (d, *J* = 8.5 Hz, 4H), 7.58 (t, *J* = 8.5 Hz, 6H), 7.43 (d, *J* = 8.5 Hz, 4H), 7.05 (d, *J* = 8.5 Hz, 4), 6.89 (d, *J* = 8.5 Hz, 2H), 3.93 (s, 6H). ¹³C NMR (CDCl₃, 100 MHz): δ (ppm) 166.9, 147.3, 146.6, 138.9, 133.2, 131.7, 129.8, 129.6, 128.4, 123.9, 117.5, 92.6, 88.9, 87.7, 52.5. MALDI-TOF *m/z* Calcd for C₃₈H₂₆INO₄, 687.09; Found, 686.44 [M]⁺. **3C⁰** was obtained as a yellow solid (1.62 g, 28% yield). The spectroscopic data of compound **3C⁰** were reported previously.

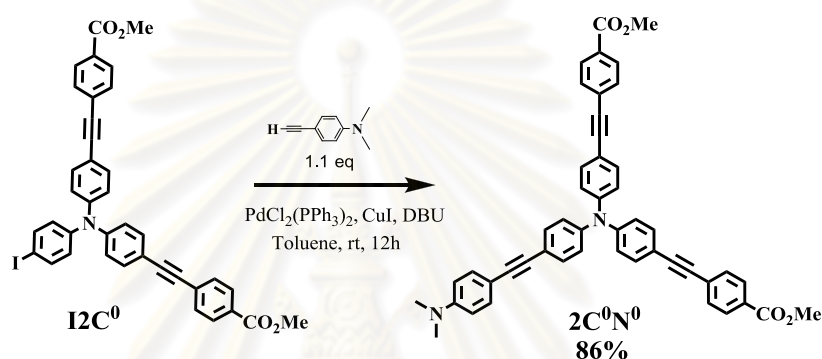
2.3.22 Preparation of C⁰2N⁰.



To a mixture of **2IC⁰** (0.99 g, 1.5 mmol), PdCl₂(PPh₃)₂ (0.10 g, 0.15 mmol), CuI (29 mg, 0.15 mmol), 4-ethynyl-*N,N*-dimethylaniline (0.46 g, 3.17 mmol) in toluene (20 ml) was added with DBU (1 mL) and the mixture was stirred at room temperature for 12 h. The reaction mixture was filtered and the solvent was evaporated under reduced pressure. The residue was purified by flash chromatography on silica gel using gradient eluent ranging from pure hexane to CH₂Cl₂/hexane (3/1). **C⁰2N⁰** was

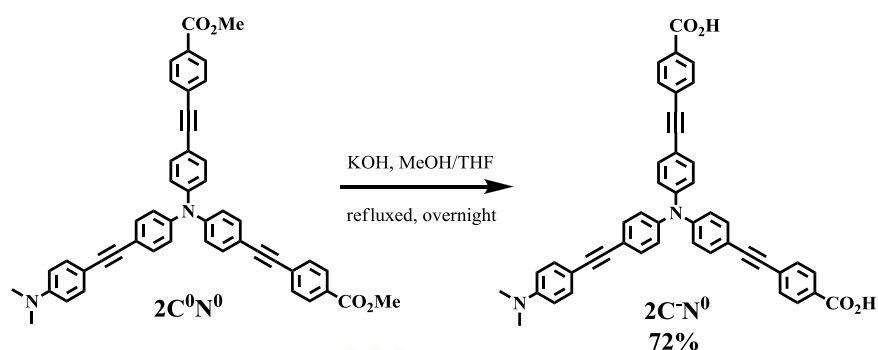
obtained as a yellow solid (0.77 g, 74% yield). mp: 209-211 °C. ^1H NMR (CDCl_3 , 400 MHz): δ (ppm) 8.00 (d, $J = 8.5$ Hz, 2H), 7.55 (d, $J = 8.5$ Hz, 2H), 7.40-7.37 (m, 10H), 7.05 (d, $J = 8.5$ Hz, 6H), 6.65 (d, $J = 8.5$ Hz, 2H), 3.90 (s, 3H), 2.99 (s, 12H). ^{13}C NMR (CDCl_3 , 100 MHz): δ (ppm) 166.6, 147.4, 145.9, 132.9, 132.6, 132.4, 131.3, 129.5, 129.1, 128.3, 128.3, 124.3, 123.2, 119.1, 116.4, 111.8, 110.1, 92.6, 90.5, 88.4, 87.1, 52.2, 40.2. MALDI-TOF m/z Calcd for $\text{C}_{48}\text{H}_{39}\text{N}_3\text{O}_2$: 689.30; Found: 689.19 $[\text{M}]^+$.

2.3.23 Preparation of $2\text{C}^0\text{N}^0$.



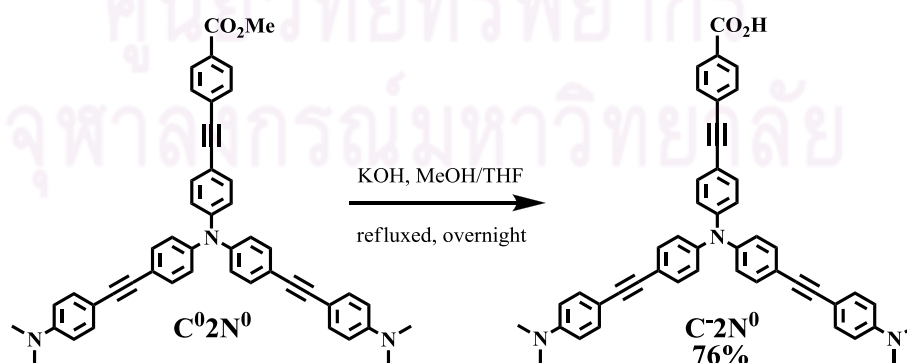
A mixture of 12C^0 (0.51 g, 0.74 mmol), $\text{PdCl}_2(\text{PPh}_3)_2$ (25 mg, 0.04 mmol), CuI (8.0 mg, 0.04 mmol), 4-ethynyl- N,N -dimethylaniline (0.12 g, 0.82 mmol) in toluene (20 mL) was added with DBU (1 mL) and the mixture was stirred at rt for 12 h. The reaction mixture was filtered and the filtrate was evaporated under reduced pressure. The residue was purified by flash chromatography on silica gel using gradient solvents ranging from pure hexane to CH_2Cl_2 /hexane (3/1) as the eluent. $2\text{C}^0\text{N}^0$ was obtained as a yellow solid (0.46 g, 86% yield). mp: 210-213 °C. ^1H NMR (CDCl_3 , 400 MHz): δ (ppm) 8.01(d, $J = 8.5$ Hz, 4H), 7.57 (d, $J = 8.5$ Hz, 4H), 7.45-7.38 (m, 8H), 7.08 (d, $J = 8.5$ Hz, 6H), 6.65 (d, $J = 8.5$ Hz, 2H), 3.93 (s, 6H), 2.99 (s, 6H). ^{13}C NMR (CDCl_3 , 100 MHz): δ (ppm) 166.6, 147.2, 145.6, 132.9, 132.5, 131.4, 129.5, 129.2, 124.7, 123.7, 119.6, 117.0, 92.4, 90.8, 88.5, 86.9, 52.2, 40.2. MALDI-TOF m/z Calcd for $\text{C}_{48}\text{H}_{36}\text{N}_2\text{O}_4$: 704.27; Found: 704.09 $[\text{M}]^+$.

2.3.24 Preparation of $2C^-N^0$.



A mixture of $2C^0N^0$ (200 mg, 0.28 mmol), saturated KOH aqueous solution (0.05 mL) in THF (10 mL), methanol (10 mL) and water (10 mL) was refluxed with stirring for 1 day. The solution was evaporated and the residue was dissolved in water (15 mL). Ice (~20 g) was added to the residue and the mixture was acidified and kept in refrigerator. The product was filtered to afford $2C^-N^0$ as a yellow solid (132 mg, 72% yield). mp: 280 °C (decompose). 1H NMR (DMSO- d_6 , 400 MHz): δ (ppm) 7.96 (d, $J = 8.0$ Hz, 4H), 7.64 (d, $J = 8.0$ Hz, 4H), 7.54 (d, $J = 8.0$ Hz, 4H), 7.46 (d, $J = 8.0$ Hz, 2H), 7.34 (d, $J = 8.5$ Hz, 2H), 7.07 (d, $J = 8.5$ Hz, 6H), 6.71 (d, $J = 8.5$ Hz, 2H), 2.94 (s, 6H). ^{13}C NMR (DMSO- d_6 , 100 MHz): δ (ppm) 166.8, 150.1, 146.9, 145.4, 133.2, 132.6, 132.5, 131.6, 130.4, 129.7, 127.0, 124.9, 123.8, 118.9, 116.4, 112.1, 92.2, 91.0, 88.6, 87.1, 40.3. MALDI-TOF m/z Calcd for $C_{46}H_{32}N_2O_4$: 676.24, Found: 675.66 $[M]^+$. Anal. Calcd for $C_{46}H_{32}N_2O_4$: C 81.64, H 4.77, N 4.14; Found C 81.16, H 4.77, N 4.28.

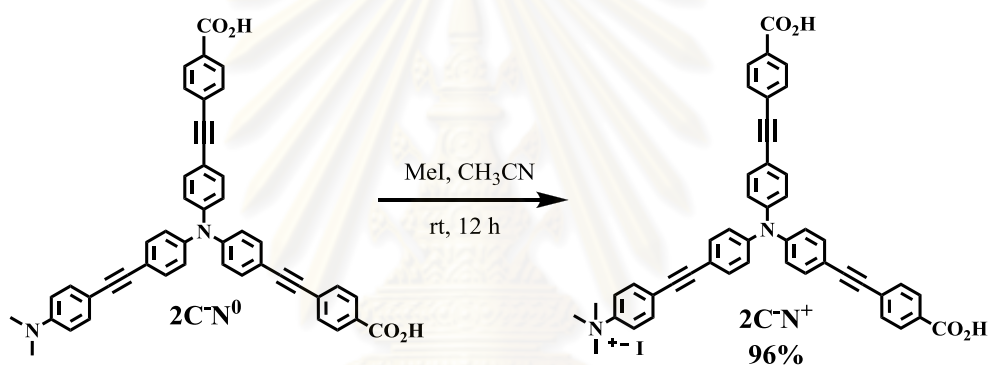
2.3.25 Preparation of C^-2N^0 .



A mixture of C^02N^0 (100 mg, 0.14 mmol), saturated KOH aqueous solution (0.05 mL) in THF (10 mL), methanol (10 mL) and water (10 mL) was refluxed with

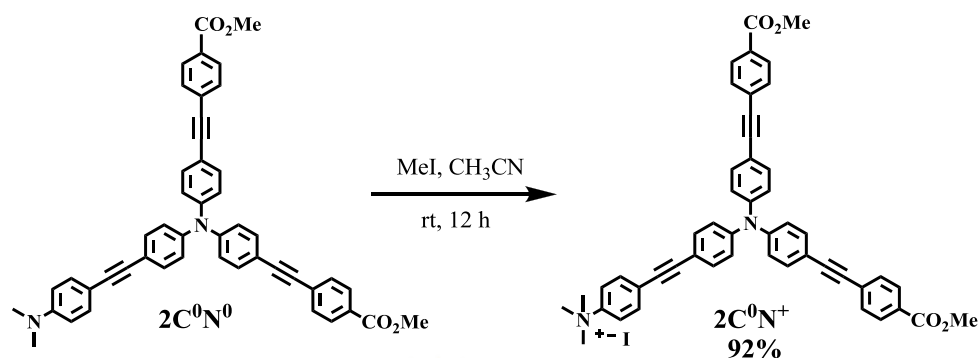
stirring for 2 days. The solution was evaporated and the residue was dissolved in water (15 mL). Approximately 20 g of ice was added to the residue and the mixture was acidified and kept in refrigerator. The product was filtered to afford $2\text{C}^-\text{N}^0$ as a yellow solid (74 mg, 76% yield). mp: 280 °C (decompose). ^1H NMR (DMSO- d_6 , 400 MHz): δ (ppm) 7.83 (d, J = 8.0 Hz, 2H), 7.49 (d, J = 8.0 Hz, 2H), 7.44 (d, J = 8.5 Hz, 4 H), 7.39 (d, J = 8.0 Hz, 2H), 7.33 (d, J = 8.5 Hz, 4H), 7.04 (d, J = 8.0 Hz, 6H), 6.70 (d, J = 8.5 Hz, 4H), 2.94 (s, 12H). ^{13}C NMR (DMSO- d_6 , 100 MHz): δ (ppm) 167.5, 150.0, 146.4, 145.6, 132.3, 130.0, 129.1, 124.1, 123.5, 118.2, 116.8, 111.8, 108.6, 90.6, 87.0, 40.1. MALDI-TOF m/z Calcd for $\text{C}_{47}\text{H}_{37}\text{N}_3\text{O}_2$: 675.29; Found: 675.75 $[\text{M}]^+$. Anal. Calcd for $\text{C}_{47}\text{H}_{37}\text{N}_3\text{O}_2$: C 83.53, H 5.52, N 6.22; Found C 82.41, H 5.28, N 6.32.

2.3.26 Preparation of $2\text{C}^-\text{N}^+$.



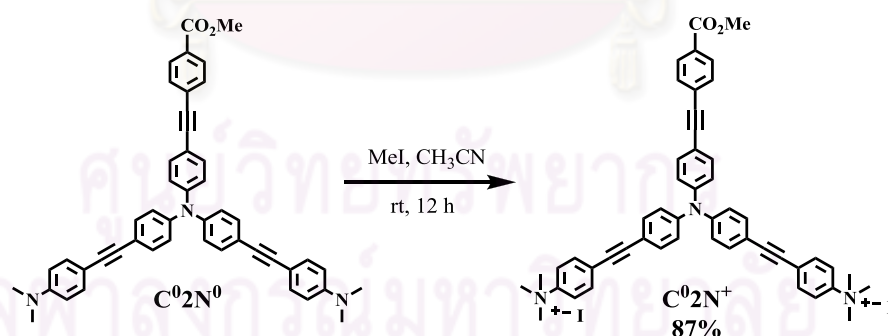
A mixture of $2\text{C}^-\text{N}^0$ (0.10 g, 0.15 mmol) in CH_3CN (15 mL) was added with CH_3I (0.5 mL) and the mixture was stirred at rt in a sealed tube. After 12 h the solution was evaporated to afford $2\text{C}^-\text{N}^+$ as a yellow solid (0.11 g, 95% yield). mp: >300 °C decompose ; ^1H NMR (CD_3CN , 400 MHz): δ (ppm) 8.00 (d, J = 8.5 Hz, 4H), 7.78 (d, J = 8.5 Hz, 2H), 7.74 (d, J = 8.5 Hz, 2H), 7.61 (d, J = 8.5 Hz, 4H), 7.50 (d, J = 8.5 Hz, 6H), 7.13 (d, J = 8.5 Hz, 6H), 3.55(s, 9H). ^{13}C NMR (CD_3CN , 100 MHz): δ (ppm) 166.4, 146.7, 133.9, 131.8, 130.0, 126.4, 124.3, 117.4, 92.2, 88.7. MALDI-TOF m/z Calcd for $\text{C}_{47}\text{H}_{35}\text{IN}_2\text{O}_4$: 691.79; Found: 691.02 $[\text{M}]^+$. Anal. Calcd for $\text{C}_{47}\text{H}_{35}\text{IN}_2\text{O}_4$: C 68.95, H 4.31, N 3.42; Found: C 68.75, H 4.87, N 4.83.

2.3.27 Preparation of $2\text{C}^0\text{N}^+$.



A mixture of $2\text{C}^0\text{N}^0$ (0.10 g, 0.14 mmol) in CH_3CN (15 mL) was added with CH_3I (0.5 mL) and the mixture was stirred at rt in a sealed tube. After 12 hrs the solution was evaporated to afford $2\text{C}^0\text{N}^+$ as a yellow solid (0.11 g, 92% yield). mp: 175-178 °C. ^1H NMR (Acetone- d_6 , 400 MHz): δ (ppm) 8.20 (d, $J = 9.0$ Hz, 2H), 8.03 (d, $J = 8.0$ Hz, 4H), 7.81 (d, $J = 9.0$ Hz, 2H), 7.66 (d, $J = 8.0$ Hz, 4H), 7.56 (d, $J = 8.5$ Hz, 6H), 7.17 (d, $J = 8.5$ Hz, 6H), 3.97 (s, 9H), 3.90 (s, 6H). ^{13}C NMR (Acetone- d_6 , 100 MHz): δ (ppm) 165.7, 147.3, 133.1, 132.9, 131.4, 129.6, 129.5, 127.9, 124.3, 124.2, 121.0, 117.5, 117.0, 92.0, 91.7, 88.3, 86.9, 56.9, 51.6. MALDI-TOF m/z Calcd for $\text{C}_{49}\text{H}_{39}\text{IN}_2\text{O}_4$: 719.29; Found 718.85 $[\text{M}]^+$. Anal. Calcd for $\text{C}_{49}\text{H}_{39}\text{IN}_2\text{O}_4$: C 69.50, H 4.64, N 3.31; Found: C 68.26, H 4.43, N 3.28.

2.3.28 Preparation of C^02N^+ .



A mixture of C^02N^+ (0.10 g, 0.14 mmol) in CH_3CN (15 mL) was added with CH_3I (0.5 mL) and the mixture was stirred at rt in a sealed tube. After 24 hrs the solution was evaporated to afford C^02N^+ as a yellow solid (0.12 g, 87% yield). mp: 182-184 °C. ^1H NMR (CD_3CN , 400 MHz): δ (ppm) 8.02 (d, $J = 8.5$ Hz, 2H), 7.79 (d, $J = 9.0$ Hz, 4H), 7.73 (d, $J = 9.0$ Hz, 4H), 7.62 (d, $J = 8.0$ Hz, 2H), 7.51 (d, $J = 8.5$ Hz, 6H), 7.13 (d, $J = 8.5$ Hz, 6H), 3.88 (s, 3H), 3.56 (s, 18H). ^{13}C NMR (CD_3CN , 100 MHz): δ (ppm) 166.3, 147.6, 147.4, 146.3, 133.3, 131.7, 129.7, 124.7, 124.5, 91.9,

87.0, 57.3. MALDI-TOF m/z Calcd for $C_{50}H_{45}I_2N_3O_2$: 719.35; Found: 704.031[M-CH₃]⁺. Anal. Calcd for $C_{50}H_{45}I_2N_3O_2$: C 61.67, H 4.66, N 4.32; Found: C 62.91, H 4.60, N 4.53.

2.4 Photophysical property study

The stock solutions of 1-10 mM fluorophores diluted to 200 μ M in 50 mM phosphate buffer pH 8.0 or 50 mM phosphate buffer saline pH 7.4 were prepared.

2.4.1 UV-Visible spectroscopy

The UV-Visible absorption spectra of the stock solutions of fluorophores were recorded from 250 nm to 700 nm at ambient temperature.

2.4.2 Fluorescence spectroscopy

The stock solutions of fluorophores were diluted to \sim 0.1 and 1 μ M, respectively, with their respective solvents. The emission spectra of fluorophores were recorded from 390 nm to 700 nm at ambient temperature using an excitation wavelength at 360 to 380 nm, respectively.

2.4.3 Fluorescence quantum yields

The fluorescence quantum yield of fluorophores were performed in phosphate buffer (PB, 50 mM) pH 8.0 by using quinine sulphate ($\Phi_F = 0.54$) in 0.1 M H₂SO₄ as a reference.[47] The UV-Visible absorption spectra of five analytical samples and five reference samples at varied concentrations were recorded. The maximum absorbance of all samples should never exceed 0.1. The fluorescence emission spectra of the same solutions using appropriate excitation wavelengths selected were recorded based on the absorption maximum wavelength (λ_{max}) of each compound. Graphs of integrated fluorescence intensities were plotted against the absorbance at the respective excitation wavelengths. Each plot should be a straight line with 1 interception and gradient m [48].

In addition, the fluorescence quantum yield (Φ_F) was obtained from plotting of integrated fluorescence intensity vs absorbance represented into the following equation:

$$\Phi_X = \Phi_{ST} \left(\frac{Grad_X}{Grad_{ST}} \right) \left(\frac{\eta_X^2}{\eta_{ST}^2} \right)$$

The subscripts Φ_{ST} denote the fluorescence quantum yield of a standard reference which used quinine sulphate in 0.1 M H_2SO_4 ($\Phi = 0.54$) and Φ_X is the fluorescence quantum yield of sample and η is the refractive index of the solvent.

2.5 Fluorescent sensor study

2.5.1 Metal ion sensor

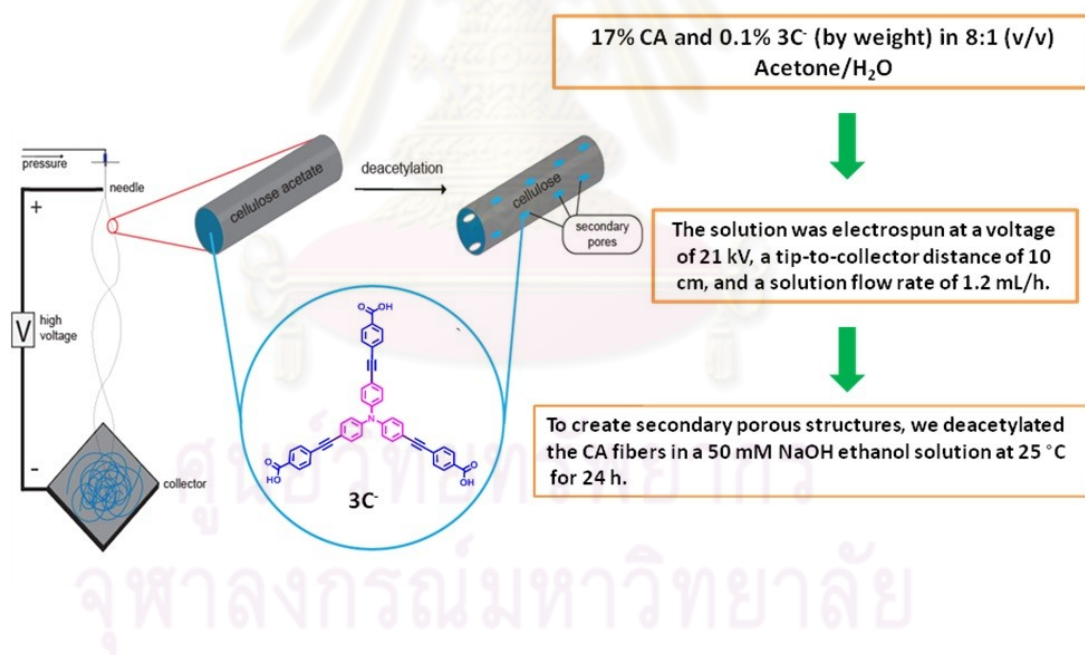
The excitation wavelength was 375 nm and the emission was recorded from 390 to 650 nm. Solutions of $3C^-$, $3N^+$ and $6C^-$ was prepared in 50 mM potassium phosphate buffer (pH= 8.0) using a sonication bath. Concentrations of $3C^-$, $3N^+$ and $6C^-$ were adjusted to 0.20 mM. Metal chloride solutions were prepared in Milli-Q water. Concentrations of all stock metal chloride solutions were adjusted to 0.2 mM and were added with the desired volumes (0-1000 μ L) to the fluorophore solutions. The final volumes of the mixtures were adjusted to 5 mL to afford the final concentration of 10 μ M for the fluorophores and 0-80 μ M for Hg^{2+} .

2.5.2 Proteins array sensor

The excitation wavelength was 375 nm and the emission was recorded from 390 to 600 nm. Solutions of all fluorophores were prepared in 10 mM sodium phosphate buffer saline (PBS) pH= 7.4 using a sonication bath. Concentrations of all fluorophores were adjusted to 5 μ M and used as stock solutions. All protein stock solutions were prepared by dilution with PBS until the absorbance at 280 nm (A_{280}) being 0.4. The protein/fluorophore mixtures were prepared by mixing and PBS dilution to afford the final concentration of fluorophores equal to 0.2 μ M and the protein concentration with Absorbance at $\lambda_{280\text{ nm}} = 0.01$

2.6 Dendritic fluorophore incorporated nanofibers for proteins detection.

All chemicals were of the analytical grade, purchased from Sigma-Aldrich (Milwaukee, WI) and used without further purification, unless otherwise stated. Milli-Q (>18 M Ω) water was used in the preparation of all buffer solutions. Steady-state fluorescence measurements were performed on a HORIBA FluoroLog spectrofluorometer using the excitation at 370 nm. Fluorescence image analysis was performed on a Leica TCS SP2/UV confocal microscope using the excitation at 364 nm. The scanning electron microscope (SEM) used is a Phillips XL30-FEG. Fiber analysis was performed using Fourier transform infrared (FTIR) spectroscopy on a Equinox 55/S FTIR spectrometer with a Bruker A590 microscope. Cellulose acetate (CA) is used as the host matrix in our nanofiber fabrication because of its chemical resistance, thermal stability, low nonspecific absorption, and capacity to be easily functionalized with recognition elements [49].



Scheme 2.1. Schematic illustration of the electrospinning setup, encapsulation of the fluorescent dendrimer, and deacetylation process used in this study.

To further improve the surface area:volume ratio and overall performance a simple deacetylation treatment was used to create specific secondary structures with our electrospun nanofibers. Park and co-workers have demonstrated that secondary

porous structures can be inserted into the backbone of electrospun CA fibers by homogeneous deacetylation treatment of CA to cellulose using a practical processing step while at the same time maintaining the nanofiber's physical properties [50-52]. This deacetylation treatment is used in our work to generate evenly distributed secondary pores throughout the nanofiber backbone of cellulose to improve the sensing performance. A schematic illustration of the electrospinning setup, encapsulation of the fluorescent dendrimer, and deacetylation process is shown in **Scheme 2.1**.

These dendrimers commonly demonstrated low visible fluorescent emission, but 3C⁻ was found to be an exception that gave visibly high fluorescence. The variability of the fluorescent emission among the dendrimers is due to aggregation, which is caused by small differences in the charge distribution among different 3C⁻. The electrospinning solution was prepared by dissolving 17% CA and 0.1% 3C⁻ (by weight) in 8:1 (v/v) Acetone/H₂O, and then placed into a plastic syringe. A high-voltage DC power supply (Glassman High Voltage Inc. Series EH) was connected to a 25-gauge blunt nose needle attached to the syringe containing the electrospinning solution.

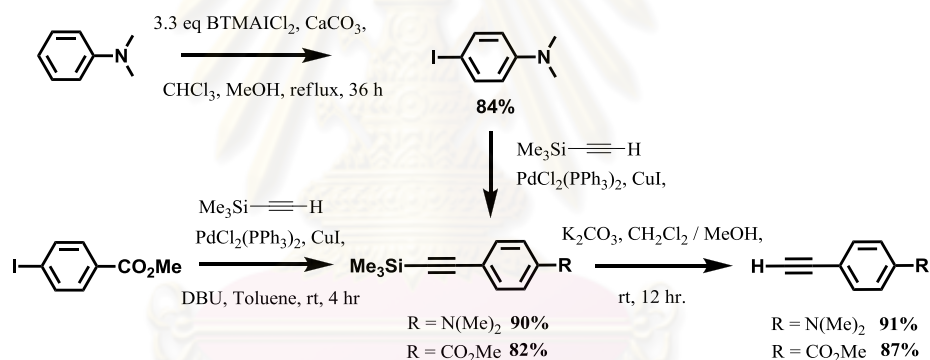
The electrospun fibers were collected on a grounded aluminum plate. The CA/3C⁻ solutions were electrospun at a voltage of 21 kV, a tip-to-collector distance of 10 cm, and a solution flow rate of 1.2 mL/h. All of the electrospinning procedures were carried out at 25 °C with a collection time of approximately 90 s. To create secondary porous structures, we deacetylated the CA fibers in a 50 mM NaOH ethanol solution at 25 °C for 24 h, thoroughly rinsed them with water, and then dried them using N₂. The chemical reaction of CA to cellulose was traced by using FT-IR spectroscopy. The characteristic absorption peaks attributed to the vibrations of the acetate group at 1745(ν CdO), 1375(ν C-CH₃), and 1235 cm⁻¹(ν C-O-C) disappeared after deacetylation of CA. An absorption peak at 3500 cm⁻¹ (ν O-H) was also observed, indicating successful deacetylation. The FT-IR spectrum obtained after deacetylation agreed with that of pure cellulose fibers.

CHAPTER III

RESULTS AND DISCUSSION

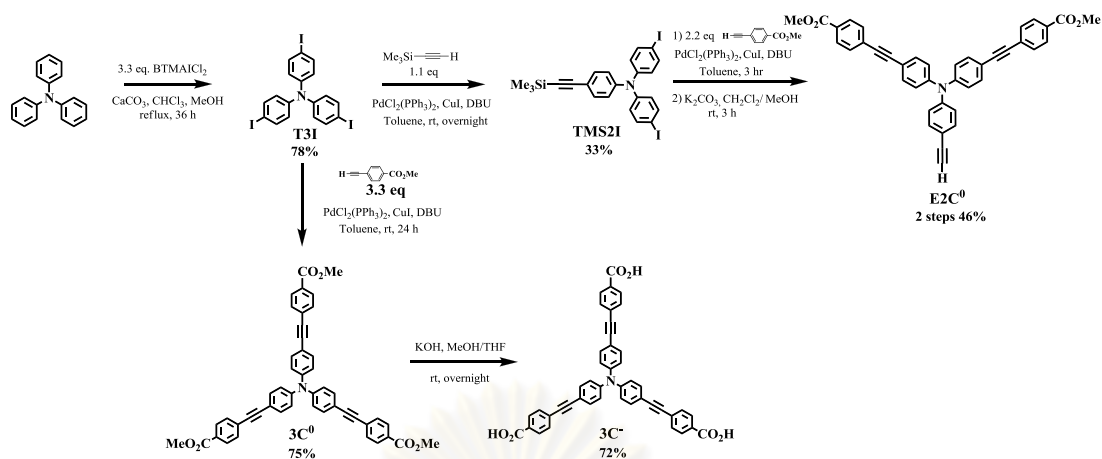
3.1 Synthesis and characterization of zeroth and first generation of dendritic fluorophores ($3C^-$, $6C^-$, $3N^+$ and $6N^+$).

To enhance the water solubility of the dendritic fluorophores, carboxylic acid and quaternary ammonium groups were installed at the peripheral groups of the target molecules. The peripheral building blocks, methyl 4-ethynylbenzoate and *N,N*-dimethyl-4-iodoaniline, were synthesized by the Pd-catalyzed Sonogashira cross-coupling of trimethylsilylacetylene with methyl 4-iodobenzoate or *N,N*-dimethyl-4-iodoaniline followed by a base-catalyzed desilylation (**Scheme 3.1**).



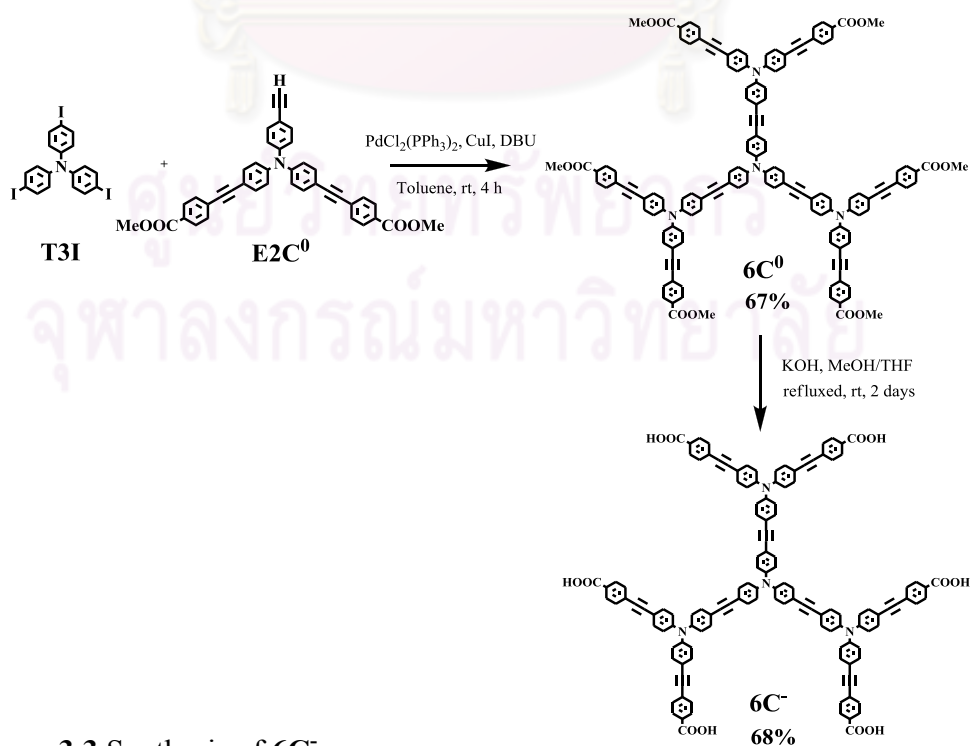
Scheme 3.1 Synthesis of peripheral groups.

The reactive core, 4, 4', 4''-triiodotriphenylamine, was prepared from triple iodination of triphenylamine using benzyltrimethyl-ammonium iododichloride (BTMAICl₂) (**Scheme 3.2**) [53]. With the necessary building blocks in hands, we proceed with the Sonogashira coupling between **T3I** and methyl 4-ethynylbenzoate followed by saponification of $3C^0$ and acidic work-up to afford the zeroth generation ionizable fluorophore $3C^-$.



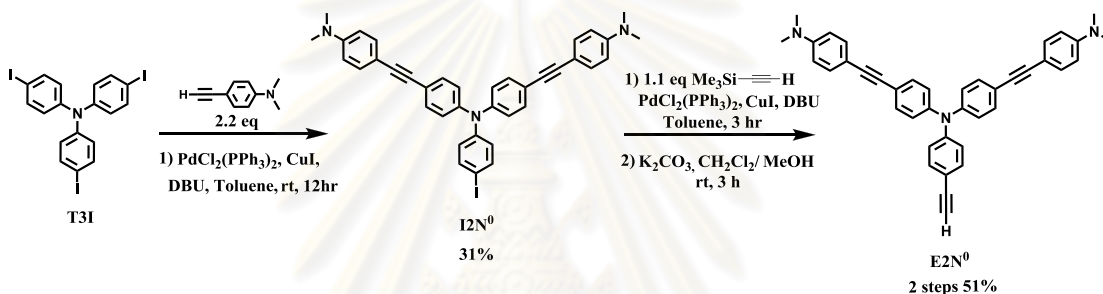
Scheme 3.2 Synthesis of $3C^-$.

Convergent approach was used in the synthesis of the first generation dendritic fluorophore starting from constructing a protected monomer by Sonogashira coupling of the core **T3I** with one equivalent of trimethylsilylacetylene. The coupling of the monomer with methyl 4-ethynylbenzoate followed by base-catalyzed desilylation gave the dendron which was coupled with Tl_3 to afford hexaesters (**6C⁰**). The base-catalyzed hydrolysis of all six methyl ester of **6C⁰** was proven to be very time-consuming taking about 48 h for completion. However, we could eventually obtain the first generation dendritic fluorophore **6C⁻** in satisfactory yield (**Scheme 3.3**).

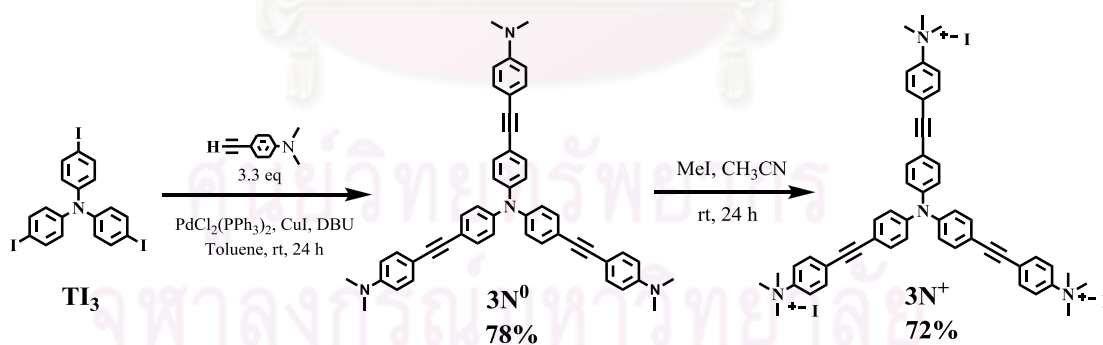


Scheme 3.3 Synthesis of $6C^-$.

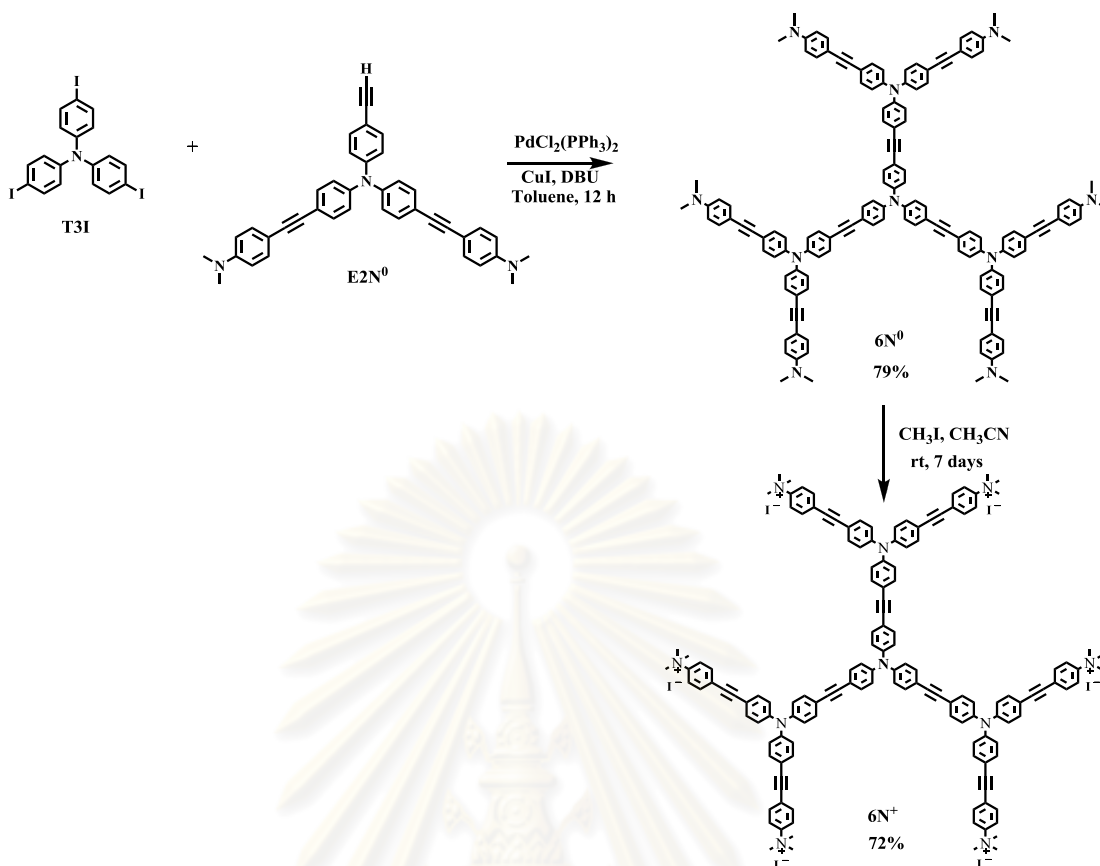
The coupling of **T3I** with 2.2 eq of *N,N*-dimethyl-4-ethynylaniline followed by base-catalyzed desilylation gave the **E2N⁰** (**Scheme 3.4**). The reaction between the *N,N*-dimethyl-4-ethynylaniline and **T3I** gave rise to the **3N⁰**, which was treated with an excess of MeI to provide the polycationic fluorescent compound **3N⁺** (**Figure 3.5**). Compound **6N⁰** was prepared through a convergent synthetic approach in which the final step involved the coupling of **T3I** with 5.5 equiv of the **E2N⁰** whose synthesis was carried out according to the **Scheme 3.6**. The hexacationic dendrimer (**6N⁺**) was derived from an exhaustive methylation of the first generation dimethylamino dendrimer **6N⁰** (**Scheme 3.6**).



Scheme 3.4 Synthesis of **E2N⁰**.



Scheme 3.5 Synthesis of **3N⁺**.

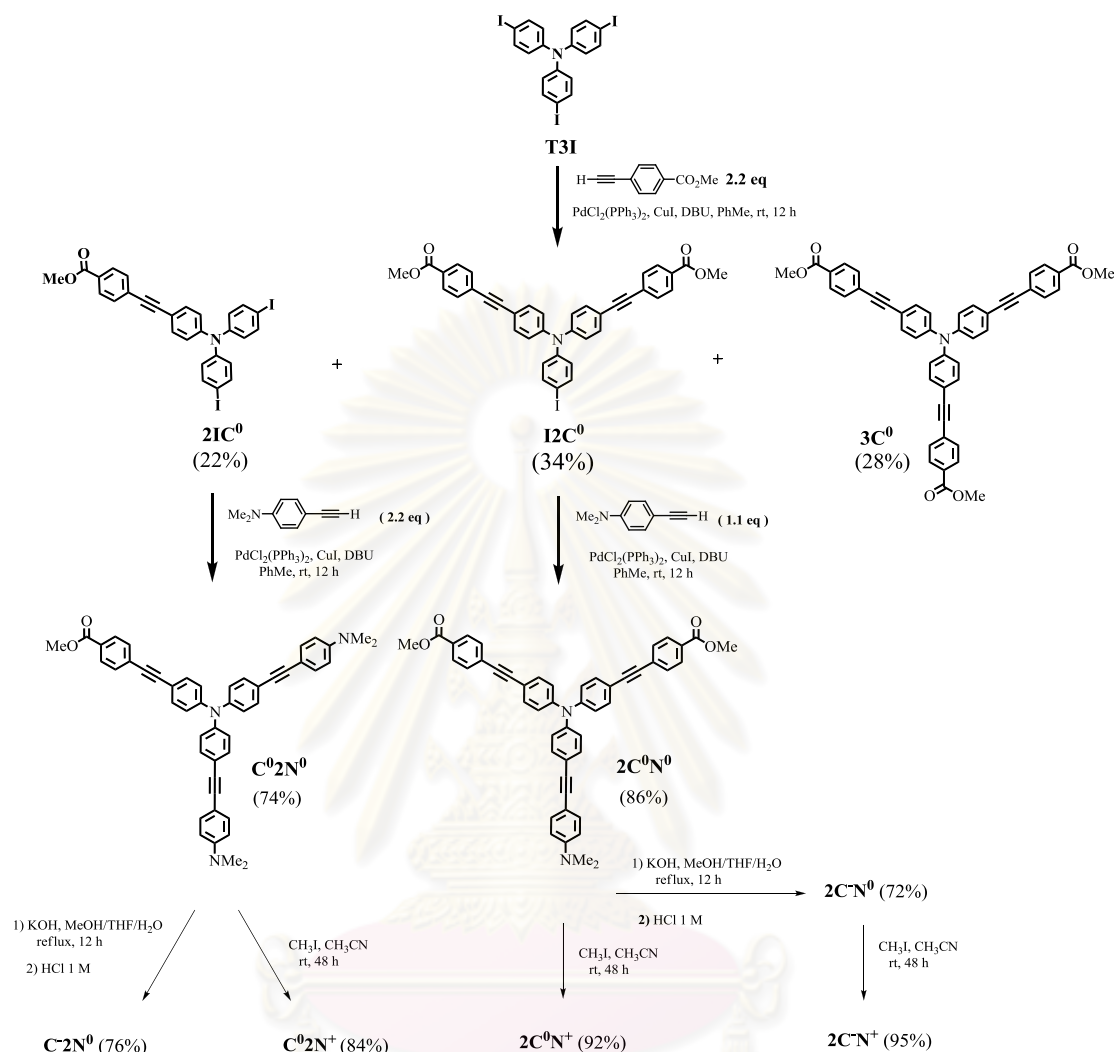


Scheme 3.6 Synthesis of $6N^+$.

3.2 Synthesis and characterization of variously charged dendritic fluorophores ($2C^-N^0$, C^-2N^0 , $2C^-N^+$, $2C^0N^+$, and C^02N^+)

The synthesis of the variously charged dendritic fluorophores began with a statistical Sonogashira coupling between 4,4',4''-triiodotriphenylamine and 2.2 equivalent of methyl-4-ethynylbenzoate (**Scheme 3.6**). The reaction gave a mixture which could be separated and purified by simple silica gel column chromatography to afford the mono-, di-, and triester products in 22%, 34% and 28% yields, respectively, representing the overall yield of 84% (**Scheme 3.7**). Sonogashira coupling of monoester with 2.2 equivalent of *N,N*-dimethyl-4-ethynylaniline afforded C^02N^0 which was hydrolyzed to give the monoanionic compound C^-2N^0 . Using the same synthetic protocol, diesters were coupled with 1.1 equivalent of *N,N*-dimethyl-4-ethynylaniline to give $2C^0N^0$ and the subsequent hydrolysis gave rise to the dianion $2C^-N^0$. Methylation of $2C^0N^0$ and C^02N^0 conveniently produced the di- and monocationic fluorophores C^02N^+ and $2C^0N^+$, respectively. In addition, the zwitterionic compound $2C^-N^+$ was prepared by base-hydrolysis of $2C^0N^+$. All new

compounds were characterized by ^1H NMR spectroscopy, IR spectroscopy, elemental (C, H, N) analysis and high resolution mass spectrometry (HRMS).



Scheme 3.7 Synthetic route to variously charged dendritic fluorophores.

The ^1H NMR spectra of compound **2C⁻N⁰**, **C⁰2N⁰**, **2C⁻N⁺**, **2C⁰N⁺**, and **C⁰2N⁺** are shown in **Figure 3.1-3.2**. All signals can be assigned to all protons in each corresponding structure. Initially, 4,4',4''-triiodotriphenylamine core showed two doublet signals at 6.8 and 7.5 ppm corresponding to its aromatic protons. Then, **T3I** coupling with methyl 4-ethynylbenzoate by using Sonogashira reaction, the mono-ester product showed signals of the methyl ester protons as a singlet at 4.0 ppm and four new doublet signals at 7.2, 7.4, 7.6 (overlapping with the signal of aromatic protons on iodophenyl group at 7.5 ppm) and 8.0 ppm corresponding to the aromatic protons of the newly mounted *p*-substituted benzoate moiety. For **C⁰2N⁰**, a new singlet signal of the methylamine protons appeared at 3.0 ppm and the aromatic

signals appeared as two doublet at 6.7 (4H) and 7.4 ppm (greatly overlapping with other aromatic proton signals). The hydrolysis of C^02N^0 gave C^2N^0 which is insoluble in chloroform and its 1H NMR was obtained from the DMSO-d₆ solution. The spectrum showed that the singlet signal of the methylester protons at 3.9 ppm totally disappeared upon the hydrolysis. The conversion of C^02N^0 to C^02N^+ was achieved by double methylation evidenced by a new singlet signal of the methyl ammonium protons at 3.5 ppm (**Figure 3.4**).

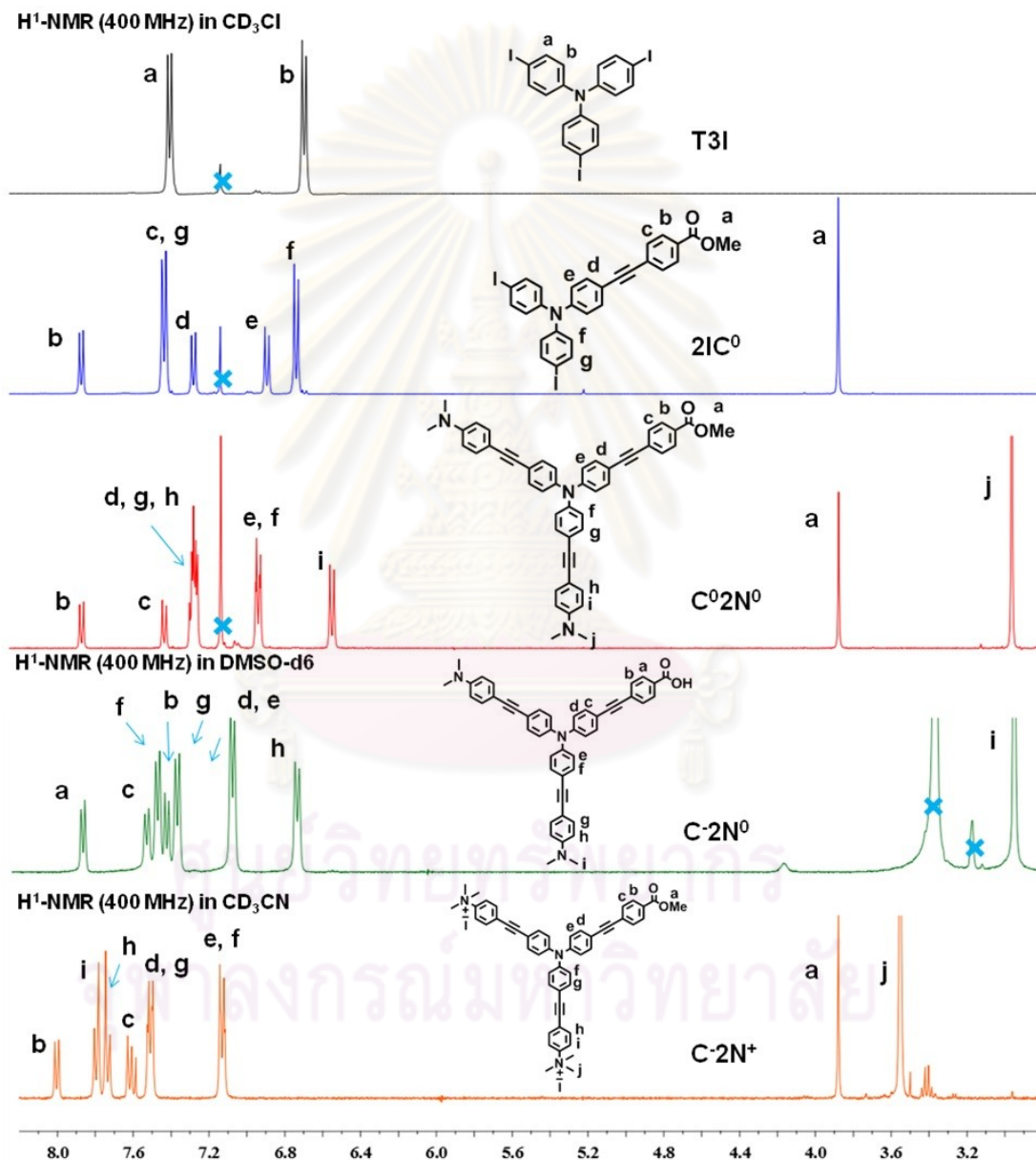


Figure 3.1. 1H -NMR (400 MHz) of $2IC^0$, C^02N^0 , C^2N^0 and C^02N^+ .

The diester product $I2C^0$ showed signals of the methyl ester protons as a singlet at 4.0 ppm and four new doublet signals at 7.2, 7.4, 7.6, and 8.0 ppm corresponding to the

aromatic protons. Upon incorporation of dimethylaniline moiety, $2C^0N^0$ showed new signals of the methylamine protons as a singlet at 3.0 ppm and two doublet signals of aromatic protons at 6.7 (2H) and 7.4 (8H) ppm (**Figure 3.2**). The hydrolysis of $2C^0N^0$ gave $2C^0N^+$ which is insoluble in chloroform and thus its 1H NMR spectrum was obtained from DMSO- d_6 solution. Upon the hydrolysis, the signal of methylester protons at 3.9 ppm disappeared. The successful conversion of $2C^0N^0$ to $2C^0N^+$ by methylation was evidenced by a new singlet signal of the methyl ammonium protons at 3.5 ppm. Again, this cationic compound is insoluble in chloroform that the best 1H NMR was obtained from a CD_3CN solution sample (**Figure 3.3**).

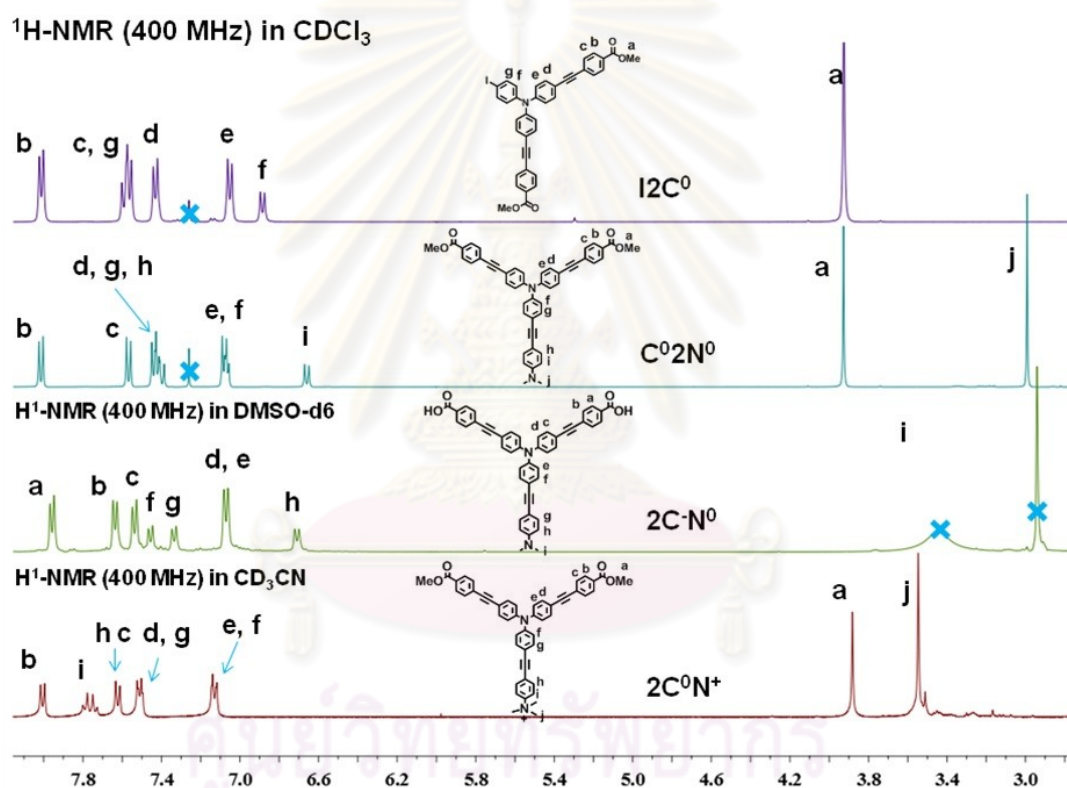


Figure 3.2. 1H -NMR (400 MHz) of I_2C^0 , $C^0_2N^0$, $2C^0N^0$ and $2C^0N^+$.

The structure characterizations of all fluorophores were confirmed by MALDI-TOF-MS that showed the molecular ion peaks corresponding or directly related to their molecular weights (**Figure 3.3** and **3.4**). High resolution MS and elemental analysis results are included in the experimental section at the end of each corresponding synthetic procedure.

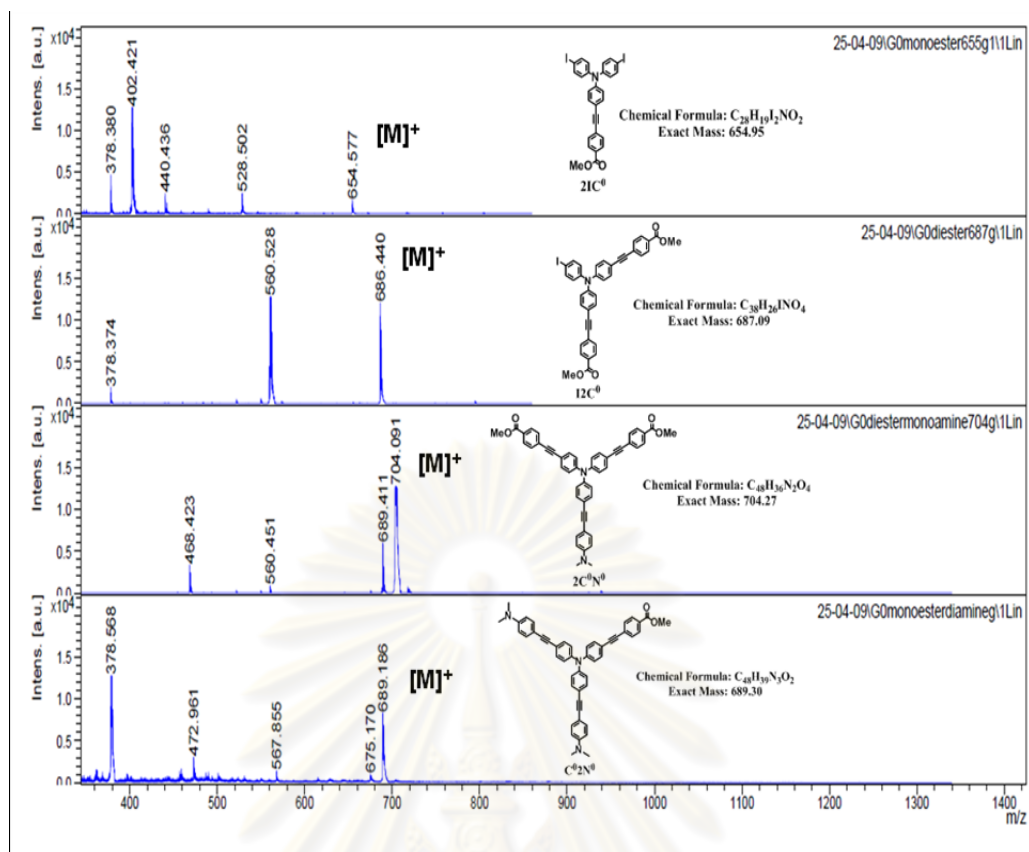


Figure 3.3. MALDI-TOF-MS of 2IC⁰, I₂C⁰, 2C⁰N⁰, and C⁰2N⁰.

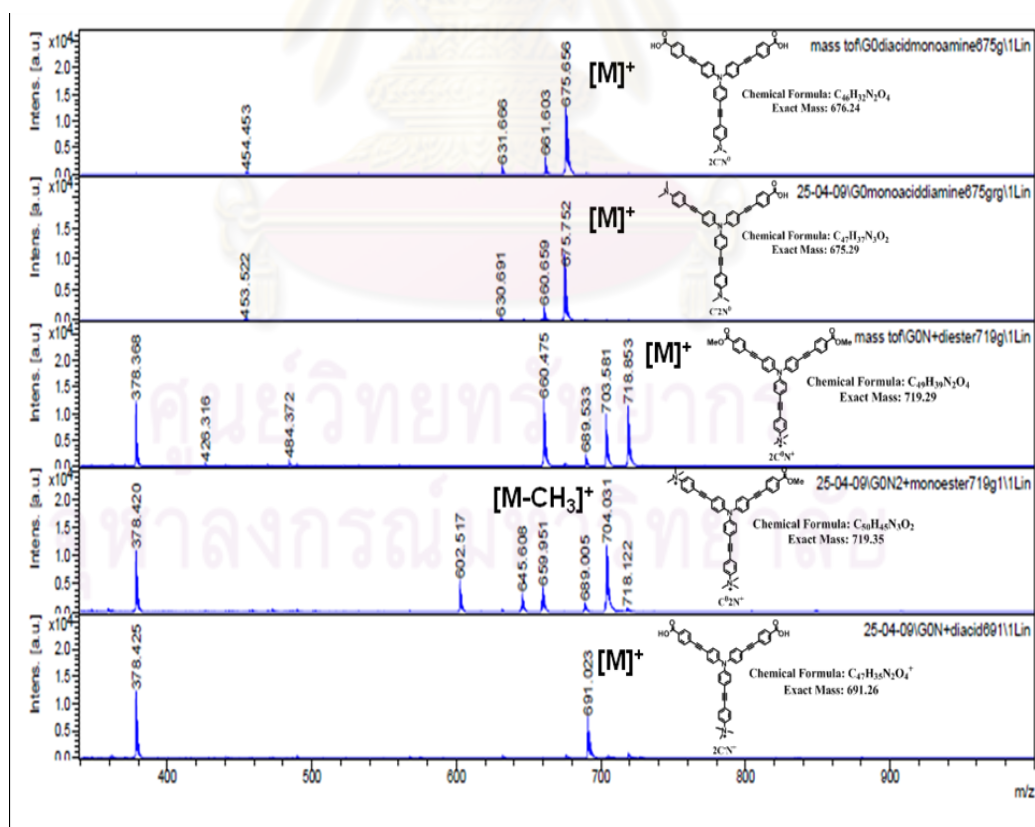


Figure 3.4. MALDI-TOF-MS of 2C⁰N⁺, C₂N⁰, 2C⁰N⁺, C⁰2N⁺, and 2C⁰N⁺.

3.3 Photophysical property study

The photophysical properties of nine fluorophores ($6C^-$, $3C^-$, $3N^+$, $2C^-N^0$, C^-2N^0 , $2C^-N^+$, $2C^0N^+$, C^02N^+ and $6N^+$) were studied. In aqueous solution, they displayed maximum absorption wavelength (λ_{max}) ranging from 368 to 392 nm (Table 3.1). The maximum emission wavelengths of the fluorophores were in the range of 450 to 489 nm. Their fluorescent quantum yields (Φ_F) were relatively low in aqueous media, especially for $2C^-N^0$ and C^-2N^0 which possessed both electron donating amino group and electron withdrawing carboxyl group at their peripheries (Figure 3.5-3.6). The low Φ_F due to intramolecular charge transfer (ICT) between electron donating and electron withdrawing groups has previously been described [55-57].

Table 3.1. Photophysical properties of the dendritic fluorophores.

Compound	Net charge	Absorption		Emission	
		λ_{max} (nm)	$\log \epsilon$ ($M^{-1}cm^{-1}$)	λ_{em} (nm)	$\% \Phi_F^a$
$6C^-$	-6	375	4.8	489	3.7
$3C^-$	-3	374	3.8	454	9.7
$2C^-N^0$	-2	368	4.4	460	0.6
C^-2N^0	-1	385	4.2	450	0.6
$2C^-N^+$	-1	379	4.4	488	2.4
$2C^0N^+$	+1	392	3.8	457	6.1
C^02N^+	+2	377	4.4	489	13.0
$3N^+$	+3	370	4.4	485	14.0
$6N^+$	+6	370	5.2	446	2.9

Quinine sulfate in 0.1 M H_2SO_4 ($\Phi_F = 0.54\%$) was used as the reference.

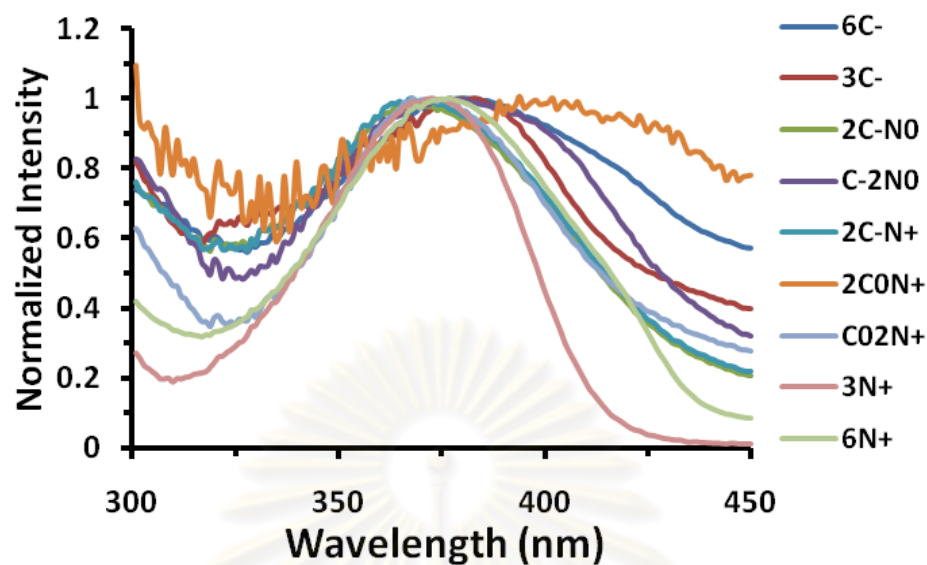


Figure 3.5. Normalized absorption spectra of nine fluorophores (10 μ M) in phosphate buffer pH 8.0.

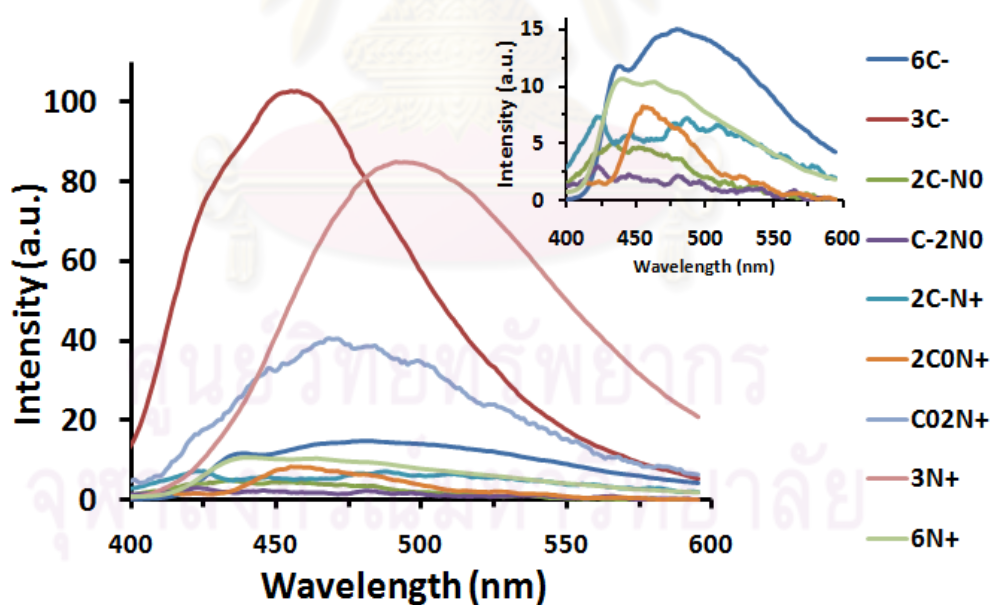


Figure 3.6. Emission spectra of nine fluorophores (10.0 μ M) in phosphate buffer pH 8.0. Expanded emission spectra of six fluorophores.

3.4 Surfactant enhancement of $3C^-$, $3N^+$, and $6C^-$.

In phosphate buffer pH 8.0, compounds $3C^-$, $3N^+$, and $6C^-$ displayed absorption peaks at 374, 370 and 375 nm. Upon the addition of TritonX-100, a nonionic surfactant, the absorption bands were slightly red-shifted to 383, 382 and 379 nm, respectively. The spectral shift behavior was also observed in the emission spectra, but in an opposite direction and a more pronounced fashion. The emission peaks of these compounds were at 454, 489 and 485 nm in the absence of Triton X-100. The surfactant caused the emission bands to blue-shift by 20, 47 and 68 nm, respectively (Figure 3.7). Moreover, the increase in fluorescence quantum yields (Φ_F) strongly agrees with the assumption that Triton X-100 facilitates the intermolecular dissociation of these compounds. The stronger fluorescent signal amplification of $6C^-$ comparing to that of $3C^-$ also suggested that the surfactant dissociation effect is greater for larger fluorophores, likely due to the difference in their initial hydrophobic interactions (Table 3.2).

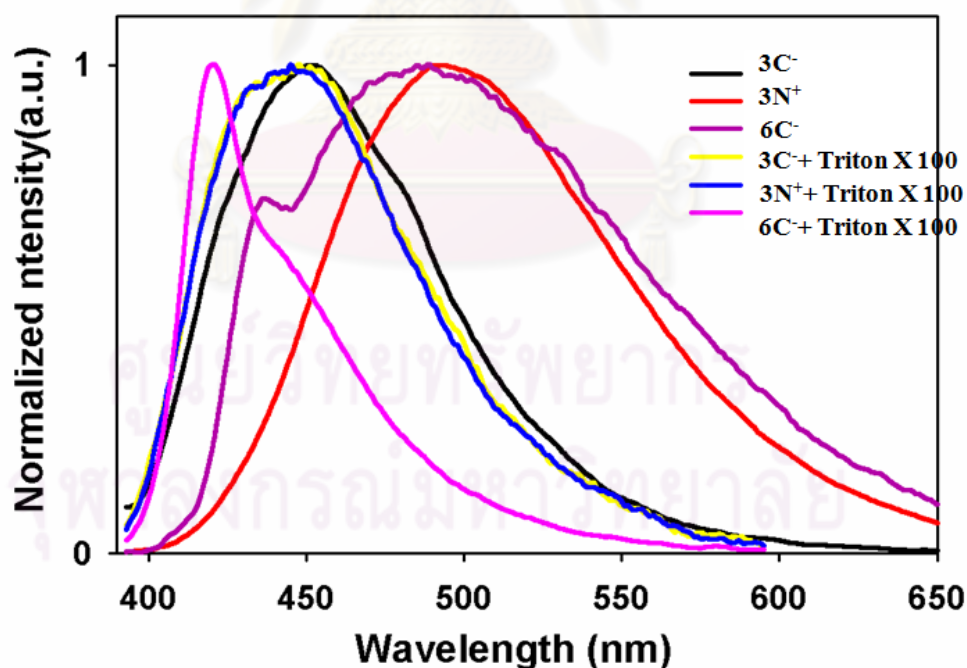


Figure 3.7. Normalized emission spectra of $3C^-$, $3N^+$, and $6C^-$ (10^{-7} M) in the absence and presence of Triton X-100 (500 μ M) in 50 mM phosphate buffer pH 8.0.

Table 3.2. Photophysical properties of **3C⁻**, **3N⁺**, and **6C⁻** in 50 mM phosphate buffer (pH 8.0) without and with Triton X-100.

Without Triton X-100				
Compd.	Absorption		Fluorescence	
	λ_{\max} (nm)	ϵ (M ⁻¹ cm ⁻¹)	λ_{\max} (nm)	Φ
3C⁻	374	5900	454	0.097
3N⁺	370	26823	485	0.14
6C⁻	375	63500	489	0.037
With Triton X-100				
Compd.	Absorption		Fluorescence	
	λ_{\max} (nm)	ϵ (M ⁻¹ cm ⁻¹)	λ_{\max} (nm)	Φ
3C⁻	383	9592	434	0.47
3N⁺	382	21310	438	0.46
3C⁻	379	49820	421	0.65

3.5 Metal ion Sensor.

The fluorogenic responses of **3C⁻**, **3N⁺**, and **6C⁻** into various transition metal ions such as Cr²⁺, Fe²⁺, Co²⁺, Ni²⁺, Cu²⁺, Cd²⁺, Hg²⁺ and Pb²⁺ ions were investigated. In phosphate buffer pH 8, the fluorescence signal of **3C⁻** was slightly quenched by various metal ions and **3N⁺** showed no fluorogenic responses while the fluorescence signal of **6C⁻** was significantly and selectively quenched by only Hg²⁺ (**Figure 3.8a-c**). In the presence of Triton X-100, the fluorescence signal of **3C⁻** could be quenched by all metal ions while the fluorescence signal of **3N⁺** was not affected by any metal ion (**Figure 3.8d and 3.8e**). On the other hand, fluorophore **6C⁻** still exhibited a selective quenching by Hg²⁺ ions (**Figure 3.8f**).

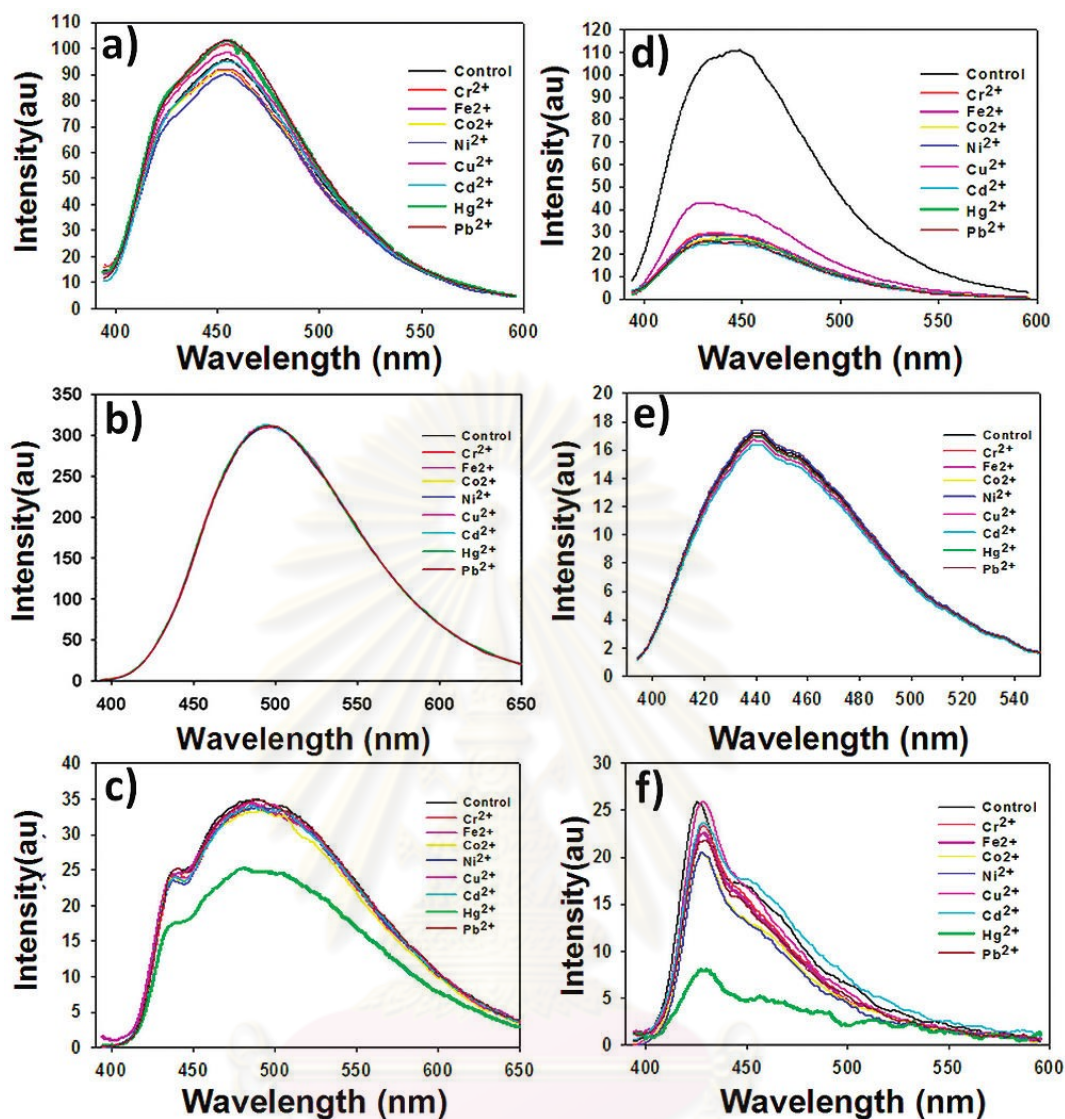


Figure 3.8. Emission spectra of the solutions of $3C^-$, $3N^+$, and $6C^-$ ($10 \mu\text{M}$) upon the addition of metal ions ($40 \mu\text{M}$): without Triton X-100 for (a) $3C^-$, (b) $3N^+$, and (c) $6C^-$; with 0.1 mM Triton X-100 for (d) $3C^-$ ($1 \mu\text{M}$), (e) $3N^+$ ($0.1 \mu\text{M}$), and (f) $6C^-$ ($0.1 \mu\text{M}$).

In order to access a quantitative measurement of fluorescence quenching, Stern-Volmer plots were made from the fluorescence data. Linear relationships between the fluorescence ratio I_0/I and the Hg^{2+} concentration were obtained with the Stern-Volmer constant (K_{sv}) of $33,700 \text{ M}^{-1}$ and $5,800 \text{ M}^{-1}$ for the system with and without Triton X-100. In With Triton X-100, the considerably higher K_{sv} clearly demonstrates that the surfactant can amplify of the selective quenching effect probably by increasing the binding between the fluorophore and Hg^{2+} (**Figure 3.9**). The

nonselective quenching of $3C^-$ suggested that the positively charged metal ions reduce the electrostatic repulsion between the partially dissociated negatively charged fluorophores $3C^-$, resulting in the enhancement of self-quenching. Conversely, the charge repulsion among positively charged fluorophore $3N^+$, having a comparable molecular size to $3C^-$, cannot be reduced by the metal ions and therefore exhibits no enhancement of the self-quenching effect.

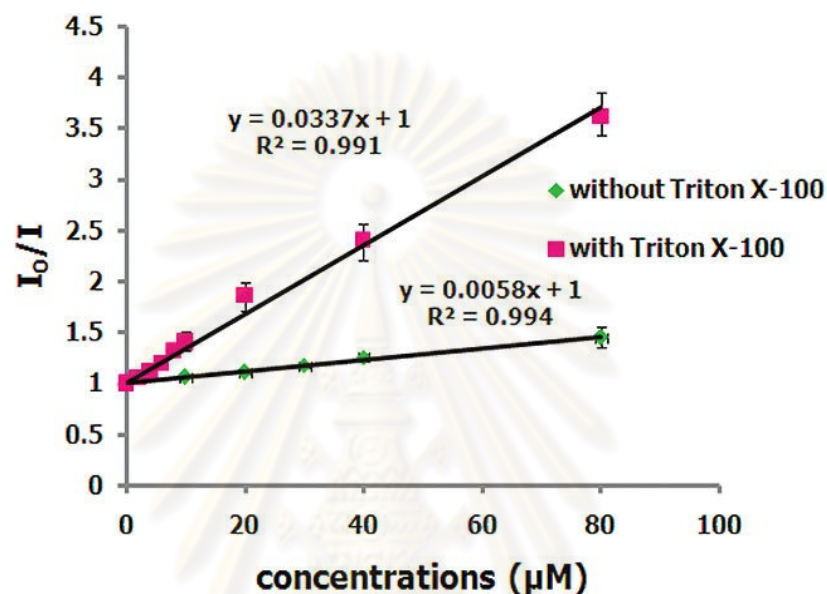


Figure 3.9. Stern-Volmer plots for fluorescence quenching of $6C^-$ ($0.1 \mu\text{M}$) with and without of Triton X-100 (0.1 mM).

The selective fluorescence quenching of $6C^-$ by Hg^{2+} is a little complicated to rationalize. With high selectivity for Hg^{2+} , the common metal ion enhanced associative self-quenching mechanism is unlikely to play the key role. The quenching effect may involve selective formation of $6C^-$ - Hg^{2+} complex at the periphery leading to efficient energy or electron transfer processes between the internal fluorescent units and this complex sites [58-59]. To test if the complexation is reversible, EDTA, a strong chelator, was added. The addition of 2.5 molar equiv of EDTA could restore the fluorescent signal of $6C^-$ to its original level (**Figure 3.10**). The result supports the above hypothesis to some extent.

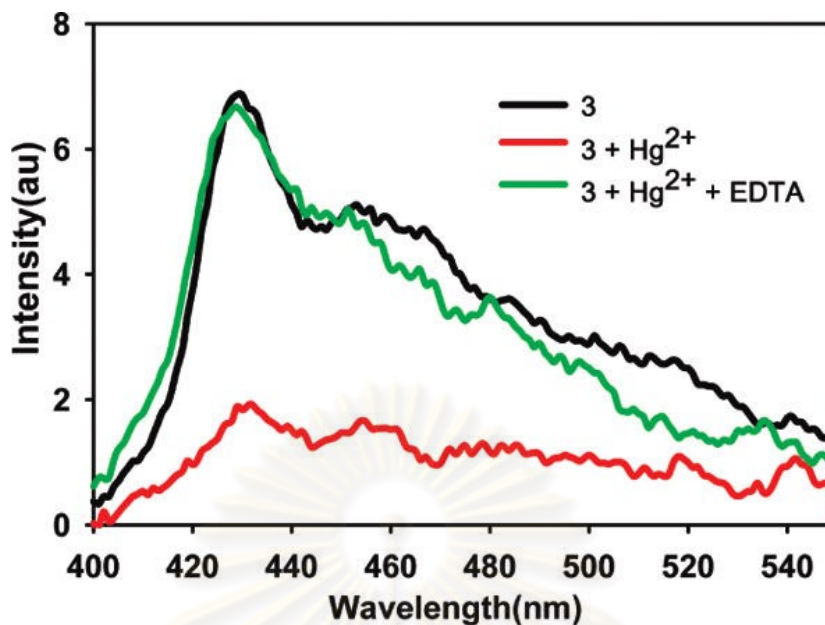


Figure 3.10. Emission spectra of $6C^-$ ($0.1 \mu\text{M}$) upon the addition of Hg^{2+} ($40 \mu\text{M}$) and EDTA ($100 \mu\text{M}$).

3.6 Proteins array sensor.

It has been previously observed that a simple protein such as bovine serum albumin (BSA) can enhance the fluorescence signal of many fluorophores in aqueous media by its surfactant-like property [60-61]. The nine variously charged dendritic fluorophores exhibiting mediocre Φ_F are good candidates for fluorescence enhancement upon protein binding that is useful for protein analysis. To realize the protein sensing potential, BSA was added to a solution of each fluorophore in phosphate buffer saline pH 7.4. The fluorescent intensities of the fluorophores were apparently enhanced differently upon the addition of BSA (**Figure 3.11**), implying diverse interactions between the fluorophores and the protein as anticipated. Various hydrophobic and charged domains of protein surface can generate opulent supramolecular interactions with fluorophores leading to different levels of fluorescent enhancement.

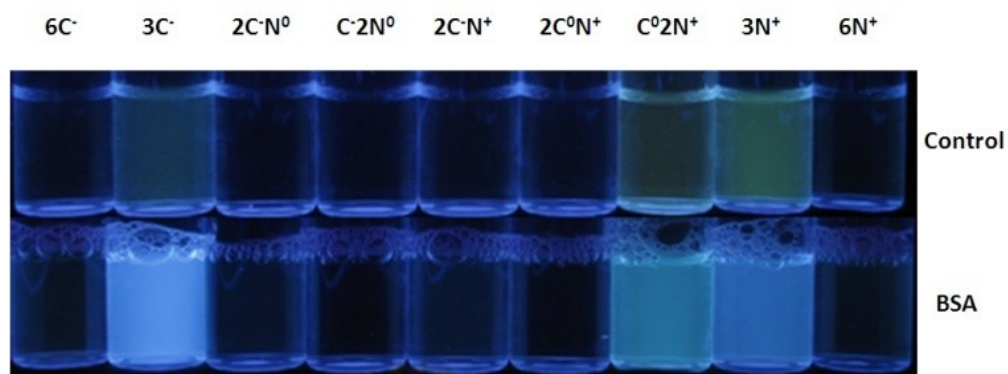


Figure 3.11. Photographic image of the fluorophore solutions (10 μM) in phosphate buffer saline (10 mM, pH 7.4) in the absence and presence of BSA ($A_{280} = 0.1, 2.1 \mu\text{M}$) under black light.

The large increases in fluorescent intensities and blue-shifting of the signals for 3C^- , C^02N^+ , and 3N^+ upon BSA addition indicate significant reduction of the self-quenching process via intermolecular fluorophore dissociation. To investigate the protein dependent fluorogenic responses of the nine fluorophores, a set of eight commercially available proteins were selected for testing based on the variation of isoelectric points (pI) ranging from 4.8 to 10.8 as well as molecular weights ranging from 12.3 to 106 kDa. The selected proteins were Bovine serum albumin (BSA, pI= 4.8, 66.3 kDa), Concanavalin A (ConA, pI = 5.5-8, tetrameric 106 kDa), Cytochrome C (CytC, pI = 10.7, 12.3 kDa), Histone (His, pI = 10.8, 21.5 kDa), Human Serum Albumin (HSA, pI = 5.2, 69.4 kDa), Lysozyme (Lys, pI = 11.0, 14.4 kDa), Myoglobin (Myo, pI = 7.2, 17.0 kDa), and Papain (Pap, pI = 9.6, 23.0 kDa) [34]. Upon the addition of these proteins into solutions of the fluorophores, different fluorogenic response patterns were observed. As shown in **Figure 3.12**, the fluorogenic responses of five fluorophores (3N^+ , C^02N^+ , $2\text{C}^0\text{N}^+$, $2\text{C}^-\text{N}^+$ and 3C^-) are visually detectable whereas the other four (6N^+ , C^-2N^0 , $2\text{C}^-\text{N}^0$ and 6C^-) respond poorly. Owing to their large hydrophobic cores, the insensitivities of 6N^+ and 6C^- may result from strong self associative interaction of the fluorophores which cannot be surmounted by the protein-fluorophore interactions. The observation of relatively lower Φ_{F} of 6N^+ and 6C^- in comparison to their zeroth generation analogs 3N^+ and 3C^- (**Table 3.1**) is another sound evidence for the high tendency of the fluorophore association. For C^-2N^0 and $2\text{C}^-\text{N}^0$, their poor responses may be attributed to the ICT

process, as previously described, in which the protein-induced deaggregation may not influence. The low responsive fluorophores were thus screened out from the array, leaving only five fluorophores for further investigation with fluorescence spectroscopy.

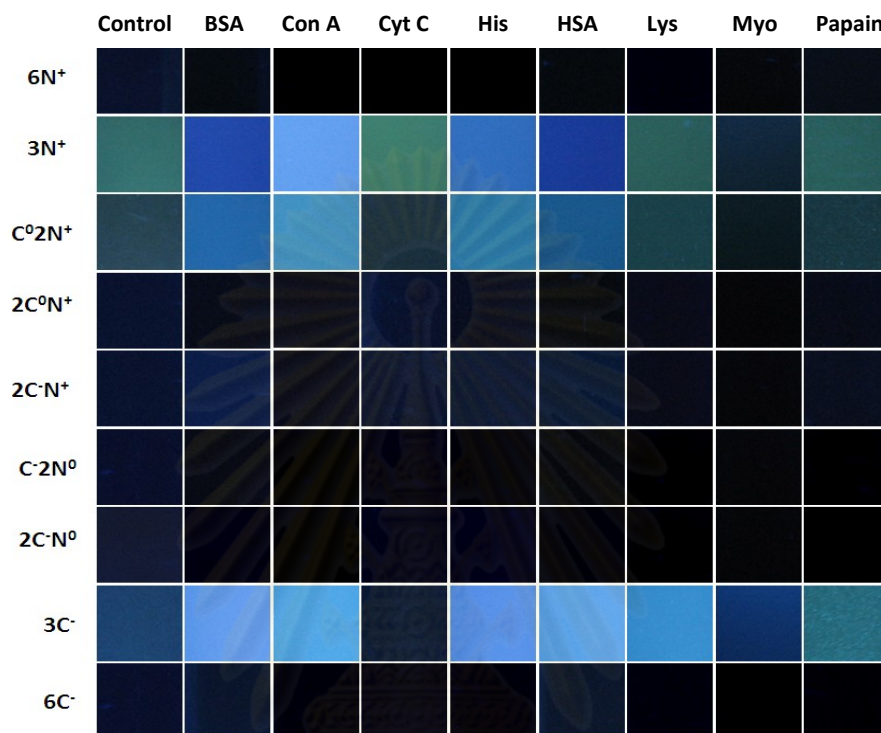


Figure 3.12. Cropped photographic images of the fluorophore solutions (2.0 μM) in phosphate buffer saline (10 mM, pH 7.4) upon addition of each protein ($A_{280} = 0.1$) under black light.

The use of logarithmic values allows a very wide range of data to be concisely and informatively plotted so that the fluorescence quenching (negative values) and enhancement (positive values) can be easily recognized. As shown in **Figure 3.13**, non-metalloproteins such as BSA, HSA, ConA, and His enhance the fluorescence signals of all fluorophores, presumably by protein-induced dissociation mechanism [10]. On the other hands, the metalloproteins containing Fe^{3+} *i.e.* Cyt C and Myo quench most of the fluorescence signals, perhaps by either the electron or energy transfer process.[60-61, 62] Lys and Pap significantly affect only the fluorescent signals of 3C^- and 3N^+ but not the other three fluorophores. Both of these proteins have pI higher than 7.4 (the experimental pH) and therefore they should exist in

cationic forms. These suggest that Lys and Pap interact with the fluorophores mainly via coulombic interaction. The fluorescence enhancement for $3C^-$ is likely to operate by a normal protein-induced dissociation due to a strong electrostatic attraction. For the positively charged fluorophore $3N^+$, the opposite fluorescent response occurs probably as an effect of protein-fluorophore charge repulsion slightly increasing the self-associative quenching.

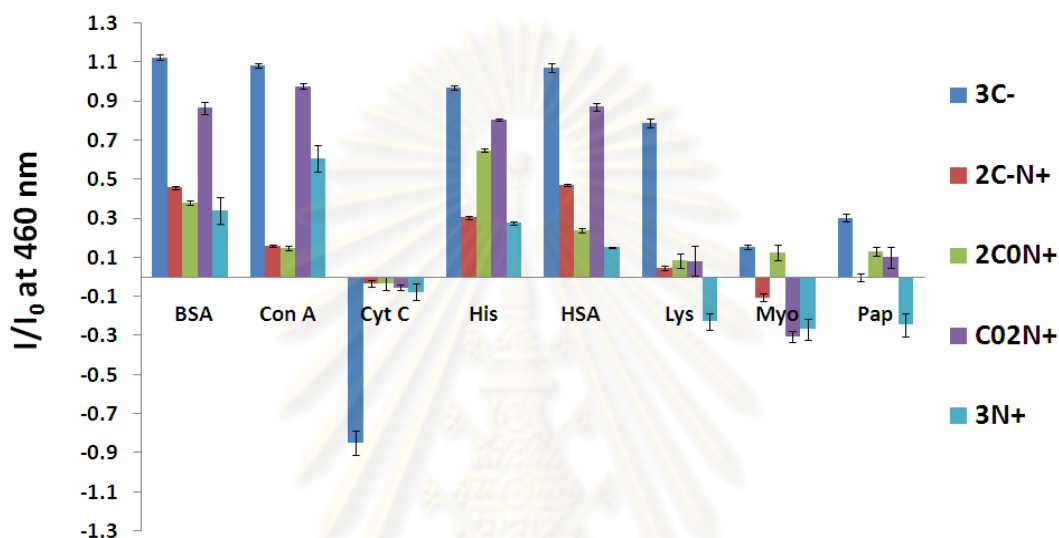


Figure 3.13. Histogram plot of logarithmic values of relative intensity (I/I_0) at 460 nm ($\lambda_{ex} = 375$ nm) of fluorophore solutions ($0.20 \mu\text{M}$) in phosphate buffer saline (10 mM, pH 7.4) upon addition of each protein ($A_{280} = 0.01$).

Although the histogram plot (**Figure 3.13**) already showed differentiable patterns of the fluorogenic responses toward the eight protein analytes. Discrimination of these multi-dimensional data sets (5 fluorophores \times 8 proteins \times 9 replicates) can be further realized by using multivariate statistical analyses. Principal component analysis (PCA) and linear discriminant analysis (LDA) have been successfully used for extracting the maximum useful information from a set of fluorescent data in the discrimination of analytes such as metal ions, anions, amino acids, bacterial cells, and cancer cells [63-69]. In this work, a nonsupervised PCA method was first applied on the data set of fluorescent intensity differences ($\Delta I = I - I_0$) at 460 nm without defining of which replicating data series belong to the same group. The PCA transformed the data set into principle component (PC) scores based on their pattern similarity [70-

71]. The PCA score plot showed roughly eight clusters of the data corresponding to the numbers of the proteins tested (**Figure 3.14**) signifying an encouraging level classification. In the next step, factorial discriminant analysis (FDA), a supervised method [72-74], was applied on the PC scores using a leave-one-out routine to cross-validate the discriminating ability. Based on PCA scores obtained from the fluorescent intensities at various wavelengths ranging from 430 to 520 nm, the FDA results revealed that the data at 500 nm provided the highest classification accuracy of 98.61% (**Table 3.3**). At this wavelength, a total variance of 99.55% can be obtained from the first two PCs in which PC1 and PC2 contributed 96.72% and 2.83%, respectively (**Figure 3.15**).

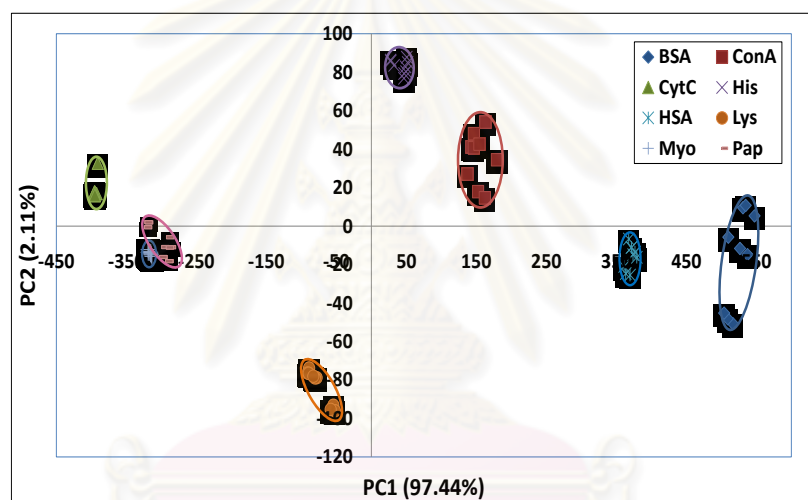


Figure 3.14. PCA score plot of ΔI measured at 460 nm obtained from the data set of 5 fluorophores \times 8 protein samples \times 9 replicates.

Table 3.3. Variance contribution of the first two PCs and classification accuracy obtained from PCA and FDA on the fluorescent intensities (ΔI) measured at various wavelengths.

Wavelength (nm)	PCA			FDA
	PC1	PC2	Sum of CPs	
430	98.49%	1.01%	99.50%	95.83%
460	97.44%	2.11%	99.55%	95.83%
490	96.82%	2.75%	99.57%	95.83%
500	96.72%	2.83%	99.55%	98.61%
510	96.45%	3.07%	99.52%	97.22%
520	96.15%	3.31%	99.46%	98.61%

[a] Classification accuracy for cross-validation.

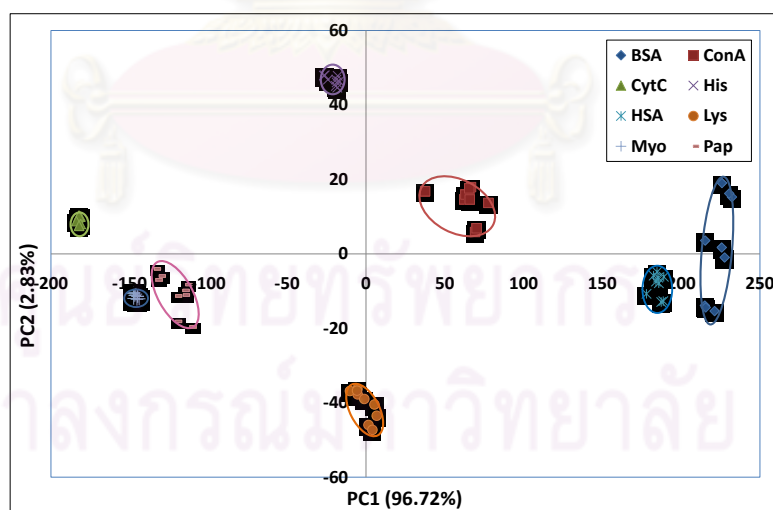


Figure 3.15. PCA score plot of ΔI measured at 500 nm obtained from the data set of 5 fluorophores \times 8 protein samples \times 9 replicates.

Since it is not always the case that every variable sensing elements in the array is significant for the discrimination of the analytes, some of the elements may generate noise or redundancy that can adversely affect the analysis. For practical application of sensor array, it is desirable to work with the lowest numbers of sensing elements that impart satisfactory analysis performance. In our attempt to reduce the sensing elements, PCA loading plot was used to identify the importance of each individual fluorophore toward each PC. The plot obtained from the measurement at 500 nm (**Figure 3.16**) showed that $3C^-$ was the main contributor to PC1 while C^02N^+ was the main contributor to PC2. Consequently, $3C^-$ and C^02N^+ were picked out as the most important sensing elements for this set of proteins.

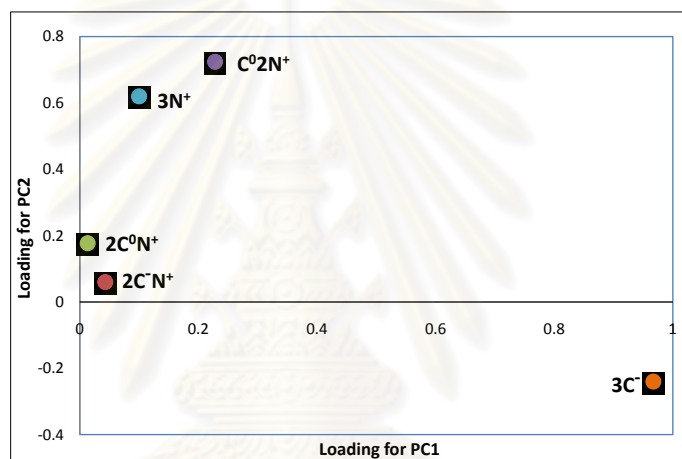


Figure 3.16. PCA loading plot of ΔI measured at 500 nm obtained from the data set of 5 fluorophores \times 8 protein samples \times 9 replicates.

The PCA score plot of the data obtained from these two selected sensing elements ($3C^-$ and C^02N^+) showed that the first two PCs contained 100% of the variance (**Figure 3.17a**). The FDA cross-validation results also revealed 100% classification accuracy for these two sensing elements. In comparison to the five-fluorophore array which provided 99.55% variance for the first two PCs and 98.61% classification accuracy. The results ascertained that this two-fluorophore array displayed a better discriminating ability due to the reduction of non-informative and redundant data. It is also importance to note that this reduced array can even discriminate between the two proteins with closely related structures and properties such as BSA and HSA.

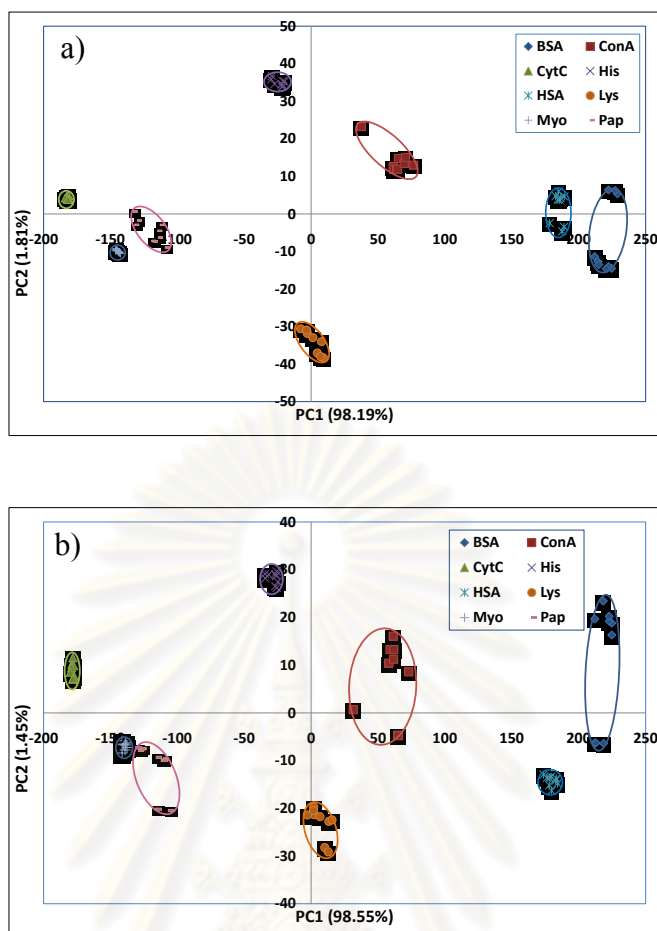


Figure 3.17. PCA score plot of ΔI measured at 500 nm obtained from the data set of the reduced array sensors composing of (a) $3C^-$ and C^02N^+ , and (b) $3C^-$ and $3N^+$.

To prove our proposition for the benefits of charge variation leading to the selection the most suitable sensing elements of $3C^-$ and C^02N^+ , the PCA was also performed on the data obtained from a reduced array comprising $3C^-$ and $3N^+$, which represent usual fluorophores with all negatively or all positively charged groups. Although the first two PCs obtained from $3C^-$ and $3N^+$ model occupied 100% of the total variance, clusters of two out of eight proteins, Myo and Pap, were located awfully close to each other (**Fig 3.17b**). The FDA cross-validation on the PC scores also gave only 97.22% classification accuracy which is lower when comparing to the 100% classification accuracy obtained from the $3C^-/C^02N^+$ array. The results highlighted the benefits of the charge variation in the development of high performance protein sensing arrays.

3.7 Nanofibers doped with dendritic fluorophores for protein detection.

The electrospun fibers were optimally prepared from a solution of cellulose acetate and 3C⁻ (17% and 0.1% w/w) in Acetone/H₂O (8:1 v/v) jetted from a 25-gauge blunt nose needle by a high DC voltage of 21 kV, a tip-to-collector distance of 10 cm, and a solution flow rate of 1.2 mL/h. The doped nanofiber nonwoven mat collected on a grounded aluminum plate exhibited well-defined fibrous morphology without bead formation and good structural stability as shown in the SEM image (**Figure 3.18**). The fibers were continuous, uniform, and had a diameter ranging from approximately 400–2000 nm, similar to those reported by Xiang et al. [75]. The surface area: volume ratio of the electrospun nonwoven film is further magnified by the deacytlation of the cellulose acetate to cellulose to create porosity within the one-dimensional (1D) fibers. This secondary porous structures are assumed to distribute in 3D throughout the nanofiber volumes creating a larger surface area : volume ratio essential for high sensitivity in sensing applications.

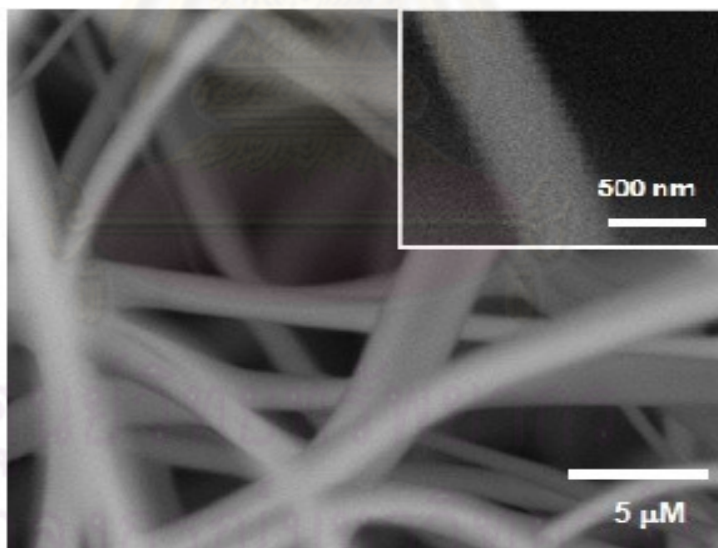


Figure 3.18. SEM image of electrospun 3C⁻-doped deacetylated cellulose fibers (17% CA/0.1% AFD dissolved in 8:1 acetone/water). Inset is a zoomed-in image of the fiber.

The protein sensing properties of the fibers were characterized by monitoring the fluorescence quenching behaviors of cytochrome c (Cyt C), hemoglobin (Hgb), and bovine serum albumin (BSA) as a function of their concentration. All proteins were bovine specific, where cyt c is positively charged (pI 10.2–10.7), Hgb is neutral to slightly negative (pI 7.0–7.4), BSA is negatively charged (pI 4.8–4.9), and $3C^-$ is negatively charged at physiological and experimental pH [60]. The fluorescence intensity decreased proportionally with increase in Cyt C concentration (**Figure 3.19a**). Similar behavior was observed with Hgb (**Figure 3.19b**). The efficient quenching effects of the metalloproteins, cyt c and Hgb, are primarily due to energy transfer of the imbedded fluorescent dendrimer with the protein as both cyt c and Hgb contain metallo-heme portions within the protein. Some of the quenching effect for proteins can be attributed to electron transfer, caused through the electrostatic effects in the binding of the anionic dendrimer to the positive patches of globular proteins. When BSA was used, however, an increase in the fluorescence was observed (**Figure 3.19c**). The slight increase in local fluorescence of the dendritic fluorophore within the high-surface-area of the nanofibers suggested that the negatively charged BSA proteins reduce the π - π stacking of the partially dispersed negatively charged dendritic fluorophores through repulsion forces, resulting in an increase in the fluorescence [76, 77]. It is expected that two main factors contribute to protein detection: (1) the charge distribution density on the proteins surface, and (2) the location of the metalloproteins secondary structure. The intricate nature of the interaction of these two factors should result in protein-dependent signals allowing for good sensing capabilities.

The fluorescence dynamic quenching sensitivity can be quantified through the measurements with the Stern–Volmer equation. The Stern–Volmer analysis of the electrospun sensors for cyt c and Hgb is shown in **Figure 3.20**. At concentrations between 100 nM and 6.4 μ M, a linear relationship between quencher concentration and I_0/I was obtained, showing homogeneous quencher-accessible sites in the electrospun fibers under the experimental conditions. The K_{SV} , sensitivity of the electrospun fibers, was found to be 3.4×10^5 and $1.7 \times 10^6 \text{ M}^{-1}$ for Cyt C and Hgb, respectively.

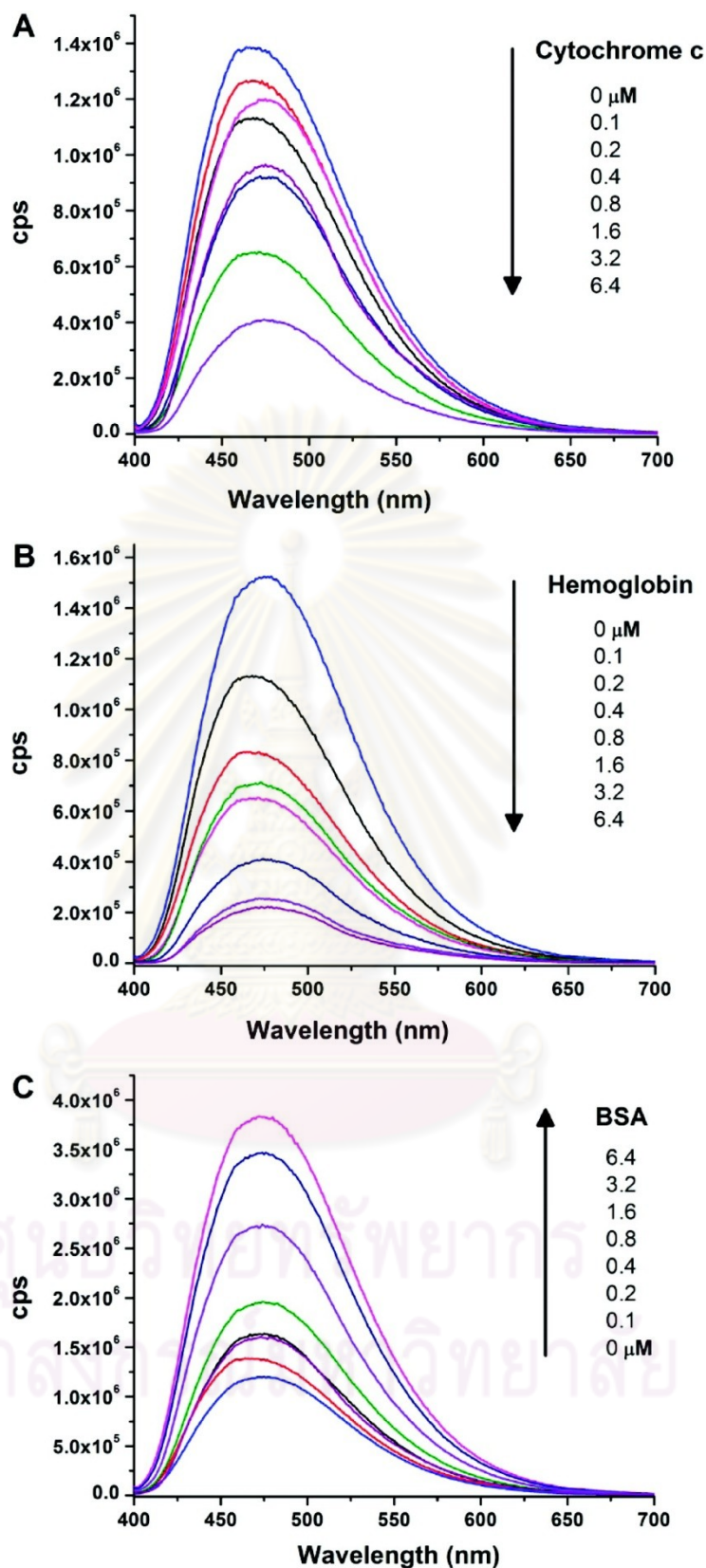


Figure 3.19. Fluorescence emission spectra of the 3C⁻functionalized nanofibers in response to varied concentrations of (A) Cyt C, (B) Hgb, and (C) BSA ($\lambda_{\text{ex}}/\lambda_{\text{em}} = 370/475$ nm.)

While Hgb showed strong quenching signal (large positive $I_0/I -1$), Cyt C and BSA tested under the same experimental conditions demonstrated a small quenching and enhancement (small positive and negative $I_0/I -1$), respectively (**Figure 3.22**). Distinguishable responses for different proteins observed here clearly point to an effective fabrication of solid-state sensors for a specific protein by embedding a selective receptor/transducer into electrospun fibers.

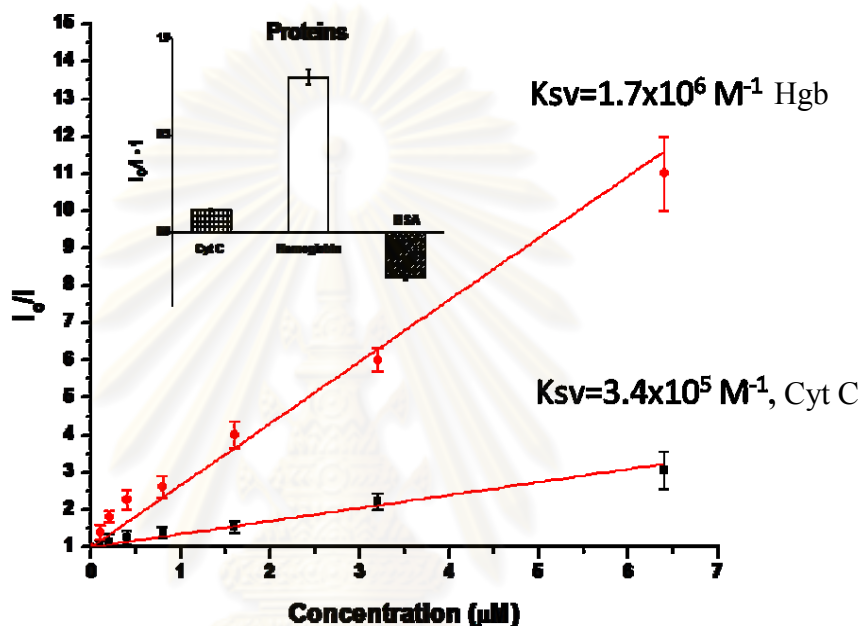


Figure 3.20. Stern–Volmer plots of the nanofibers for Cyt C (■) and Hgb (•). Inset: Analyte-dependent pattern for 200 nM of bovine metalloproteins (cyt c, Hgb) and nonmetalloprotein (BSA) in PBS buffer solution (pH 7.4).

The fluorescence protein detection was further visualized using a high resolution UV confocal microscope. The fluorescence images of the 3C^- doped cellulose nanofibers before and after incubation with 10 μM Cyt C solution for 15 min illustrated the remarkable quenching effect of the nanofiber sensors (**Figure 3.21**). The fluorescence images before the quenching process also indicated the the uniform dispersion of fluorophores throughout the whole length of the cellulose fibers that is beneficial to sensing performance.

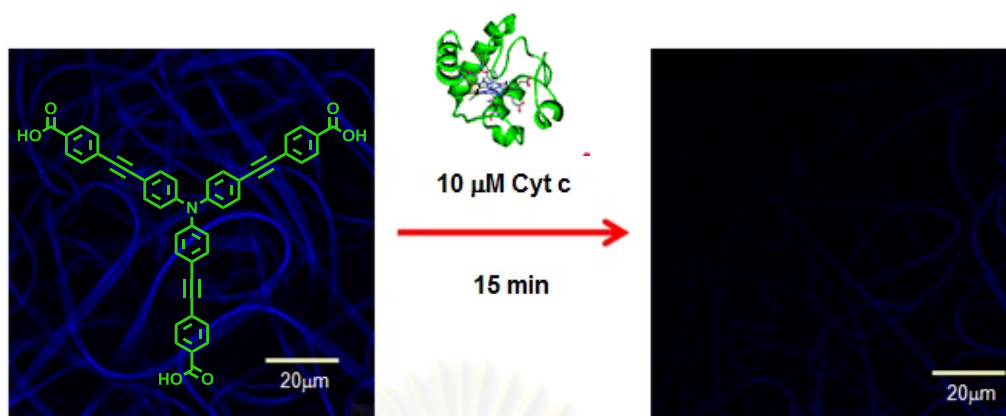


Figure 3.21. Confocal fluorescence images of the electrospun nanofibers before (left) and after (right) incubation in a 10 μM cyt c solution for 15 min.

The reusability, reproducibility, and stability of the nanofiber material were also investigated. To demonstrate the reusability of the sensor, the cellulose nanofibers were immersed in a 25 μM solution of Cyt C for 5 min, and then in a 50 mM NaOH ethanol solution for 15 min followed by rinsing in water and drying in air. The fibers were then reused for sensing the same cyt c solution. In the tested 5 cycles, the nanofibers exhibited less than 15% loss of fluorescence intensity signal (**Figure 3.22**), indicating outstanding reusability. The similar quenching ability of the used nanofibers as the pristine fibers is attributed to the noncovalent nature of the protein-fluorophore interaction, which is largely based on the electrostatic and hydrophobic interaction. In fact, that weak binding events and stripping process do not denature or significantly leach out the fluorophore, which allows for excellent sensing recovery. The reproducibility of the sensor is reflected by low batch-to-batch variation of 5.3% for the cellulose acetate/ 3C^- nanofibers using 3 separate measurements produced on different days. For the stability test, the buffer solutions before and after each experiment were examined, and no leakage of the fluorophore was found

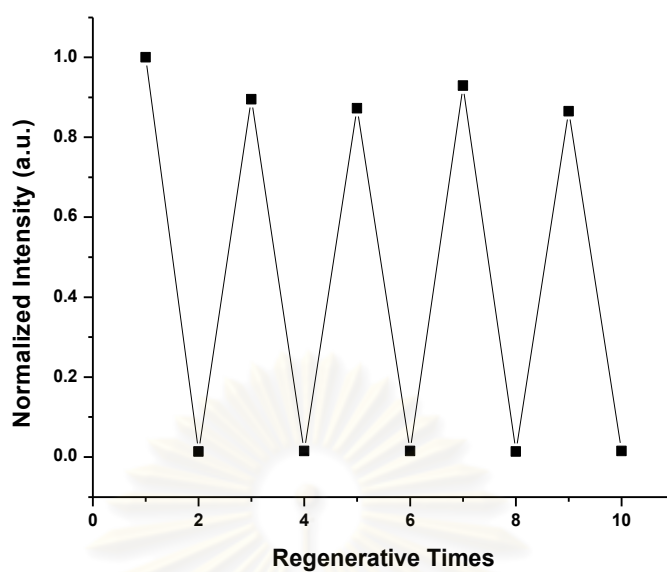


Figure 3.22. Five switching cycles of normalized fluorescence emission of the nanofibers for 25 μM Cyt C of quenching/regeneration process. Quenching time: 15 min, regenerated by immersing into 50 mM NaOH ethanol solution for 5 min, PBS buffered solution (pH 7.4) for 5 min and dried with N_2 gas, $\lambda_{\text{Ex}}/\lambda_{\text{Em}} = 370/475$ nm.

CHAPTER IV

CONCLUSION

In conclusion, a series of phenyleneethynylene dendritic fluorophores containing variously charged peripheral groups were successfully synthesized. These phenyleneethynylene based dendritic molecules with a charge decorated periphery constitute a new intriguing class of fluorophores useful for sensing applications in aqueous media due to their water solubility and wide fluorogenic responses. Investigation of this new class of fluorophores containing exact numbers of fluorogenic units provided insight understanding in the signal responses derived from fluorophore/analyte interactions that led to several successful sensing applications. The fluorescence quantum efficiencies of the fluorophores in water were relatively low, mostly less than 15%, mainly attributed to self associative quenching and internal charge transfer (ICT) process. The quantum efficiencies were considerably enhanced in the presence of a nonionic surfactant such as Triton X-100. In the presence of Triton X-100, the fluorescent signal of the first generation dendrimer containing a carboxylate periphery could be selectively quenched by Hg^{2+} . A wide linear fluorescence quenching response to Hg^{2+} concentration was observed in the range of 2-80 μM (0.4-16 ppm). The fluorophores showed different fluorogenic responses to various proteins depending on the consequence of the fluorophore/protein interaction. Fluorescence enhancement was observed where the interaction caused the reduction of self associative quenching while quenching of was observed where the interaction led to energy or electron transfer non-emissive chromophore. The fluorescence intensities of the fluorophores possessing ICT groups were hardly affected upon protein binding. The wide range of fluorogenic responses of these fluorophores constituted an array of useful data for protein identification. Based on visual observation of fluorogenic responses to the proteins, nine synthetic fluorophores were screened to five to be used as sensing elements. Multivariate statistical analyses, principal component analysis (PCA) and factorial discriminate analysis (FDA), of fluorescence intensity data were systematically used to find the optimum detection wavelength and reduce the array of five fluorophores to two. Eight proteins with wide range of molecular weights and isoelectric points were manifestly

discriminated with 100% accuracy by PCA and FDA based on the fluorescence data from just two charged dendritic fluorophores. Lastly, nanofibers of dendritic fluorophore doped cellulose acetate were developed as a fluorescent protein sensor using electrospinning technique. The selective fluorescence quenching of the fibers was observed for metalloproteins i.e. cytochrom c and hemoglobin probably as a result of energy or electron transfer processes between the embedded fluorescent molecules and the metalloheme portions in the proteins. The quenching effect on the sensor showed good linear dependency with the protein concentration in the range of 0.1-10 μM with a high quenching efficiency, $K_{sv} = 1.7 \times 10^6 \text{ M}^{-1}$ for hemoglobin. The solid-state sensor was reusable by dipping into a 50 mM NaOH ethanol solution to regenerate the fluorescent signal.

For future development along the theme of this work, novel series of fluorescent dendrimers with varieties of peripheral functionalities i.e. salicylaldehyde salicylic dicarboxylic and ammonium should be synthesized and explored for sensing properties. These functionalities are expected to provide greater sensitivity and specificity to other types of analytes. Substituents such as oligo(ethyleneglycol) chains on the phenyl rings are also worth exploring as they should improve water solubility as well as quantum efficiency by reducing self associative quenching. Fabrication of this type of fluorophores into various solid-state platform remains an opening challenge toward the practical applications and commercialization.

ศูนย์วิทยทรัพยากร
จุฬาลงกรณ์มหาวิทยาลัย

REFERENCES

- [1] Caballero, A., et al. Highly selective chromogenic and redox or fluorescent sensors of Hg^{2+} in aqueous environment based on 1, 4-disubstituted azines. *J. Am. Chem. Soc.* (127) 2005: 15666–15667.
- [2] Tang, Y. L., et al. Direct visualization of glucose phosphorylation with a cationic polythiophene. *Adv. Mater.* (20)2008: 703-705.
- [3] McQuade, D. T.; Pullen, A. E.; and Swager, T. M. Conjugated polymer-based chemical sensors. *Chem. Rev.* (100)2000: 2537-2574.
- [4] Thomas, S. W.; Joly, G. D.; and Swager, T. M. Chemical sensors based on amplifying fluorescent conjugated polymers. *Chem. Rev.* (107)2007: 1339-1386.
- [5] Service, R. F. Getting a charge out of plastics. *Science* (290)2000: 425-427.
- [6] Perepichka, I. F.; Perepichka, D. F.; Meng, H.; and Wudl, F. Light-emitting polythiophenes. *Adv. Mater.* (17)2005: 2281-2305.
- [7] Patil, A. O.; Heeger, A. J.; and Wudl, F. Optical properties of conducting polymers. *Chem. Rev.* (88)1988: 183-200.
- [8] Scherf, U.; and List, E. J. W. Semiconducting polyfluorenes towards reliable structure property relationships. *Adv. Mater.* (14)2002: 477-487.
- [9] Kraft, A.; Grimsdale, A. C.; and Holmes, A. B. Electroluminescent Conjugated polymers seeing polymers in a new light. *Angew. Chem. Int. Ed.* (37)1998: 402-428.
- [10] Bunz, U. H. F. Poly(aryleneethynylene)s: syntheses, properties, structures, and applications. *Chem. Rev.* (100)2000: 1605-1644.
- [11] Pinto, M. R.; and Schanze, K. S. Conjugated polyelectrolytes: synthesis and applications. *Synthesis-Stuttgart* 2002: 1293-1309.
- [12] Swager, T. M. The molecular wire approach to sensory signal amplification. *Acc. Chem. Res.* (31)1998: 201-207.
- [13] Sirringhaus, H. Device physics of solution-processed organic field-effect transistors. *Adv. Mater.* (17)2005: 2411-2425.
- [14] Bunz, U. H. F. Poly(aryleneethynylene)s. *Macromol. Rapid Commun.* (30)2009: 772–805.

- [15] Chen, L. H., et al. Highly sensitive biological and chemical sensors based on reversible fluorescence quenching in a conjugated polymer. *Proc. Natl. Acad. Sci. U. S. A.* (96)1999, 12287-12292.
- [16] Weder, C.; Sarwa, C.; Montali, A.; Bastiaansen, G.; and Smith, P. Incorporation of photoluminescent polarizers into liquid crystal displays. *Science* (279)1998: 835-837.
- [17] Tan, C. Y.; Pinto, M. R.; and Schanze, K. S. Photophysics, aggregation and amplified quenching of a water-soluble poly(phenylene ethynylene). *Chem. Commun.* 2002: 446-447.
- [18] Zheng, J.; and Swager, T. M. Poly(arylene ethynylene)s in chemosensing and biosensing. *Adv. Polym. Sci.* (177)2005: 151-179.
- [19] Zhou, Q.; and Swager, T. M. Fluorescent chemosensors based on energy migration in conjugated polymers: The molecular wire approach to increased sensitivity. *J. Am. Chem. Soc.* (117)1995: 12593-12602.
- [20] Long, Y., et al. Electrospun nanofibrous film doped with a conjugated polymer for DNT fluorescence sensor. *Macromolecules* (42)2009: 6501–6509.
- [21] Wang, B.; and Wasielewski, M. R. Design and synthesis of metal ion recognition induced conjugated polymers: an approach to metal ion sensory Materials. *J. Am. Chem. Soc.* (119)1997: 12-21.
- [22] Zheng, J.; and Swager, T. M. In poly(arylene ethynylene)s: from synthesis to application, Springer-Verlag Berlin, Berlin, 2005: 151-179.
- [23] Lakowicz, J. R. Principles of fluorescence spectroscopy; 3rd ed.; John Wiley & Sons, Inc, Kluwer, 2006.
- [24] Hertzberg, R. P.; and Pope, A. J. High-throughput screening: new technology for the 21st century. *Curr. Opin. Chem. Biol.* (4)2000: 445-451.
- [25] Achyuthan, K. E., et al. Fluorescence superquenching of conjugated polyelectrolytes: applications for biosensing and drug discovery. *J. Mater. Chem.* (15)2005: 2648-2656.
- [26] Dore, K., et al. Fluorescent polymeric transducer for the rapid, simple, and specific detection of nucleic acids at the zeptomole level. *J. Am. Chem. Soc.* (126)2004: 4240-4244.

- [27] Tan, C. Y., et al. Amplified quenching of a conjugated polyelectrolyte by cyanine dyes. *J. Am. Chem. Soc.* (126)2004: 13685-13694.
- [28] Dwight, S. J.; Gaylord, B. S.; Hong, J. W.; and Bazan, G. C. Perturbation of fluorescence by nonspecific interactions between anionic poly(phenylenevinylene)s and proteins: implications for biosensors. *J. Am. Chem. Soc.* (126)2004: 16850-16859.
- [29] Wang, D.; Wang, J.; Moses, D.; Bazan, G. C.; and Heeger, A. J. Photoluminescence quenching of conjugated macromolecules by bipyridinium derivatives in aqueous media: charge dependence. *Langmuir* (17)2001: 1262-1266.
- [30] Kim, I.-B.; Dunkhorst, A.; Gilbert, J.; and Bunz, U. H. F. Sensing of lead ions by a carboxylate-substituted PPE: multivalency effects. *Macromolecules* (38)2005: 4560-4562.
- [31] Kim, I.-B.; and Bunz, U. H. F. Modulating the sensory response of a conjugated polymer by proteins: an agglutination assay for mercury ions in water. *J. Am. Chem. Soc.* (128)2006: 2818-2819.
- [32] Satrijo, A.; and Swager, T. M. Anthryl-doped conjugated polyelectrolytes as aggregation-based sensors for nonquenching multicationic analytes. *J. Am. Chem. Soc.* (129)2007: 16020-16028.
- [33] Kim, I.-B.; Dunkhorst, A.; and Bunz, U. H. F. Nonspecific interactions of a carboxylate-substituted PPE with proteins. a cautionary tale for biosensor applications. *Langmuir* (21)2005: 7985-7989.
- [34] Miranda, O. R., et al. Array-based sensing of proteins using conjugated polymers. *J. Am. Chem. Soc.* (129)2007: 9856-9857.
- [35] Bajaj, A., et al. Array-based sensing of normal, cancerous, and metastatic cells using conjugated fluorescent polymers. *J. Am. Chem. Soc.* (132)2010: 1018-1022.
- [36] Knapton, D.; Burnworth, M.; Rowan, S. J.; and Weder, C. Fluorescence organo-metallic sensors for the detection of chemical warfare agent mimics. *Angew. Chem. Int. Ed.* (45)2006: 5825-5829.

- [37] Ha-Thi, M. H., et al. Synthesis, fluorescence, and two-photon absorption of bidentate phosphane oxide derivatives: complexation with Pb^{2+} and Cd^{2+} Cations. *Chem. Eur. J.* (14)2008: 5941–5950.
- [38] Zhao, X.; Jiang, H.; and Schanze, K. S. Polymer chain length dependence of amplified fluorescence quenching in conjugated polyelectrolytes *Macromolecules* (41)2008: 3422-3428.
- [39] Zhou, N.; Wang, Li.; Thompson, D. W.; and Zhao, Y. H-Shaped OPE/OPV oligomers: a new member of 2D-conjugated fluorophore cores. *Org. Lett.* (10)2008: 3001–3004.
- [40] Shao, M.; Dongare, P.; Dawe, L. N. Thompson, D. W.; and Zhao. Y. Biscrown-annulated TTFAQ-dianthracene hybrid: synthesis, structure, and metal ion sensing. *Org. Lett.* (12)2010: 3050–3053.
- [41] Mangalum, A.; Gilliard, R. J.; Hanley, J. M.; Parker, A. M.; and Smith, R. C. Metal ion detection by luminescent 1,3-bis(dimethylaminomethyl) phenyl receptor-modified chromophores and cruciforms. *Org. Biomol. Chem.* (8)2010: 5620–5627.
- [42] Zhao, C-H.; Sakuda, E.; Wakamiya, A.; and Yamaguchi, S. Highly emissive diborylphenylene containing bis(phenylethynyl)benzenes: structure photophysical property correlations and fluoride ion sensing. *Chem. Eur. J.* (15)2009, 15, 10603–10612.
- [43] Swinburne, A.; Paterson, M. J.; Beeby, A.; and Steed, J. W. Fluorescent Twist-on sensing by induced-fit anion stabilisation of a planar chromophore. *Chem. Eur. J.* (16)2010: 2714 – 2718.
- [44] Acharya, J. R.; Zhang, H.; Li, X.; and Nesterov, E. E. Chemically controlled amplified ratiometric fluorescence in surface immobilized end-capped oligo(*p*-phenylene ethynylene)s. *J. Am. Chem. Soc.* (131)2009: 880–881.
- [45] Ji, S., et al. Tuning the intramolecular charge transfer of alkynylpyrenes: effect on photophysical Properties and its application in design of OFF-ON fluorescent thiol probes. *J. Org. Chem.* (74)2009: 4855–4865.
- [46] Zhang, X.; Ren, X.; Xu, Q-H.; Loh, K.P.; and Chen, Z. K. One- and two-photon turn-on fluorescent probe for cysteine and homocysteine with large emission shift. *Org. Lett.* (11)2009: 1257–1260.

- [47] Du, H.; Fuh, R. A.; Li, J.; Corkan, A.; and Lindsey, J. S. Photochem CAD: A computer-aided design and research tool in photochemistry. *Photochem Photobiol.* (68)1998: 141-142.
- [48] Fery-Forgues, S.; and Lavabe, D. Are fluorescence quantum yields so tricky to measure? a demonstration using familiar stationary products. *J. Chem. Educ.* (76)1999: 1260-1264.
- [49] Frey, M. W. Electrospinning cellulose and cellulose derivatives. *Polym. Rev.* (48)2008: 378-391.
- [50] Han, S. O.; Son, W. K.; Youk, J. H.; and Park, W. H. Electrospinning of ultrafine cellulose fibers and fabrication of poly(butylene-succinate) biocompo-sites reinforced by them *J. Appl. Polym. Sci.* (107)2008: 1954-1959.
- [51] Han, S. O.; Youk, J. H.; Min, K. D.; Kang, Y. O.; and Park, W. H. Electrospinning of cellulose acetate nanofibers using a mixed solvent of acetic acid/water: Effects of solvent composition on the fiber diameter. *Mater. Lett.* (62)2008: 759-762.
- [52] Son, W. K.; Youk, J. H.; and Park, W. H. Preparation of ultrafine oxidized cellulose mats via electrospinning. *Biomacromolecules* (5)2004: 197-201.
- [53] Kajigaeshi, S., et al. α -Chlorination of aromatic acetyl derivatives with benzyltrimethylammonium dichloroiodate. *Synthesis* 1988: 545-546.
- [54] Sukwattanasinitt, M. Synthesis and study of conjugated polymers containing di- or triphenylamine. Ph.D. Thesis Iowa State University, Ames, IA 1996.
- [55] Goodson, T. Optical excitations in organic dendrimers investigated by time-resolved and nonlinear optical spectroscopy. *Acc. Chem. Res.* (38)2005: 99-107.
- [56] Terenziani, F.; Painelli, A.; Katan, C.; Charlot, M.; and Blanchard, D. M. Charge instability in quadrupolar chromophores: symmetry breaking and solvatochromism. *J. Am. Chem. Soc.* (128)2006: 15745-15755.

- [57] Zhang, X.; Ren, X.; Xu, Q. H.; Loh, K. P.; and Chen, Z. K. One- and two-photon turn-on fluorescent probe for cysteine and homocysteine with large emission shift. *Org. Lett.* (11)2009, 1257–1260.
- [58] Sandanaraj, B. S.; Demont, R.; Aathimanikandan, S. V.; Savariar, E. N.; and Thayumanavan, S. Selective sensing of metalloproteins from nonselective binding using a fluorogenic amphiphilic Polymer. *J. Am. Chem. Soc.* (128)2006: 10686-10687.
- [59] Jiwanich, S.; Sandanaraj, B. S.; and Thayumanavan, S. Fluorophore-cored dendrimers for patterns in metalloprotein sensing. *Chem. Commun.* 2009: 806-808.
- [60] Kim, I. B.; Dunkhorst, A.; and Bunz, U. H. F. Nonspecific interactions of a carboxylate-substituted PPE with proteins. a cautionary tale for biosensor applications. *Langmuir* (21)2005: 7985–7989.
- [61] Tolosa, J.; and Bunz, U. H. F. Water soluble cruciforms: effect of surfactants on fluorescence. *Chem. Asian J.* (4)2009: 270–276.
- [62] Jiwanich, S.; Sandanaraj, B. S.; and Thayumanavan, S. Fluorophore-cored dendrimers for patterns in metalloprotein sensing. *Chem. Commun.* 2009 806–808.
- [63] Pavlou, A. K., et al. Use of an electronic nose system for diagnoses of urinary tract infections. *Biosens. Bioelectron.* (17)2002: 893–899.
- [64] Wang, Z.; Palacios, M. A.; and Anzenbacher, P. Fluorescence sensor array for metal ion detection based on various coordination chemistries: general performance and potential application *Anal. Chem.* (80)2008: 7451–7459.
- [65] Phillips, R. L.; Miranda, O. R.; You, C. C.; Rotello, V. M.; and Bunz, U. H. F. Rapid and efficient identification of bacteria using gold-nanoparticle poly(para-phenyleneethynylene) constructs. *Angew. Chem., Int. Ed.* (47)2008: 2590–2594.
- [66] De, M., et al. Sensing of proteins in human serum using conjugates of nanoparticles and green fluorescent protein. *Nat. Chem.* (1)2009: 461–465.
- [67] Tan, J.; Wang, H. F.; and Yan, X. P. A fluorescent sensor array based on ion imprinted mesoporous silica. *Biosens. Bioelectron.* (24)2009, 3316–3321.
- [68] Pioggia, G., et al. A composite sensor array impedentiometric electronic tongue: Part II. Discrimination of basic tastes. *Biosens. Bioelectron.* 22(2007), 2624–2628.
- [69] Mottram, T.; Rudnitskaya, A.; Legin, A.; Fitzpatrick, J. L.; and Eckersall, P. D. Evaluation of a novel chemical sensor system to detect clinical mastitis in bovine milk. *Biosens. Bioelectron.* (22)2007, 2689–2693.

- [70] Poulli, K. I.; Mousdis, G. A.; and Georgiou, C. A. Classification of edible and lampante virgin olive oil based on synchronous fluorescence and total luminescence spectroscopy. *Anal. Chim. Acta.* (542)2005: 151–156.
- [71] Dufour, E.; Letort, A.; Laguet, A.; Lebecque, A.; and Serra, J. N. Investigation of variety, typicality and vintage of French and German wines using front-face fluorescence spectroscopy. *Anal. Chim. Acta.* (563)2006: 292–299.
- [72] Sadecka, J.; and Tothova, J. Fluorescence spectroscopy and chemometrics in the food classification - A review. *Czech J. Food Sci.* (25)2007: 159–173.
- [73] Karoui, R.; Dufour, E.; and Baerdemaeker, J. D. Monitoring the molecular changes by front face fluorescence spectroscopy throughout ripening of a semi-hard chees. *Food Chem.* (104)2007: 409–420.
- [74] Karoui, R.; Baerdemaeker, J. D.; and Dufour, E. A comparison and joint use of mid infrared and fluorescence spectroscopic methods for differentiating between manufacturing processes and sampling zones of ripened soft cheeses. *Eur. Food Res. Technol.* (226)2008: 861–870.
- [75] Xiang, C. H.; Frey, M. W.; Taylor, A. G.; and Rebovich, M. E. Selective chemical absorbance in electrospun nonwovens. *J. Appl. Polym. Sci.* (106)2007: 2363-2370.
- [76] Lavigne, J. J.; Broughton, D. L.; Wilson, J. N.; Erdogan, B.; and Bunz, U. H. F. “Surfactochromic” conjugated polymers: surfactant effects on sugar-substituted PPEs. *Macromolecules* (36)2003: 7409-7412.
- [77] Turro, N. J.; Lei, X. G.; Ananthapadmanabhan, K. P.; and Aronson, M. Spectroscopic probe analysis of protein-surfactant interactions: the BSA/SDS system. *Langmuir* (11)1995: 2525-2533.



APPENDIX

ศูนย์วิทยทรัพยากร
จุฬาลงกรณ์มหาวิทยาลัย

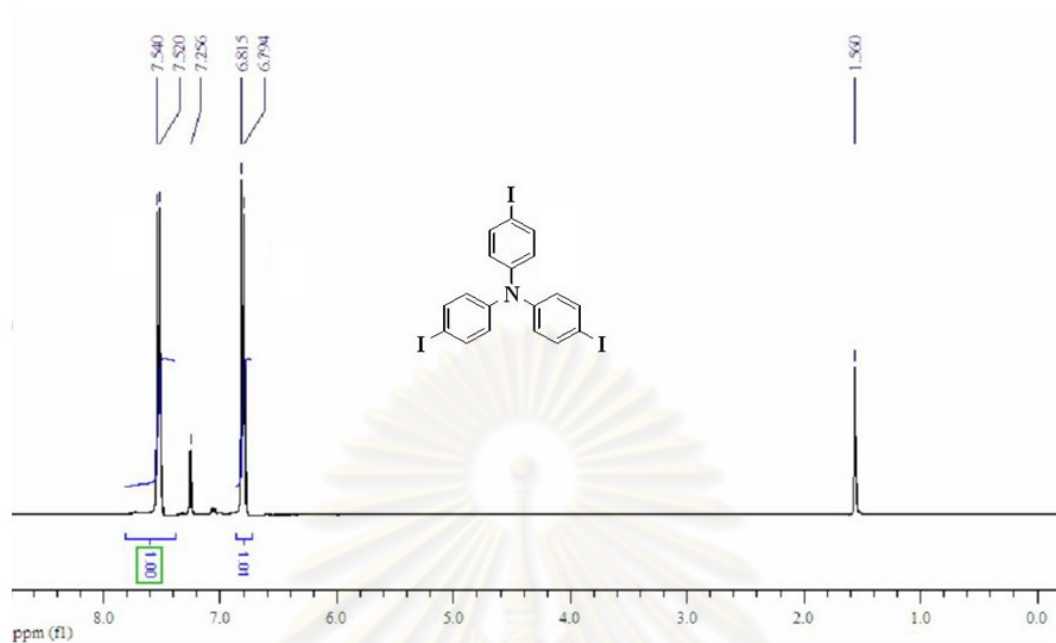


Figure A.1 ^1H NMR of TI_3 in CDCl_3 .

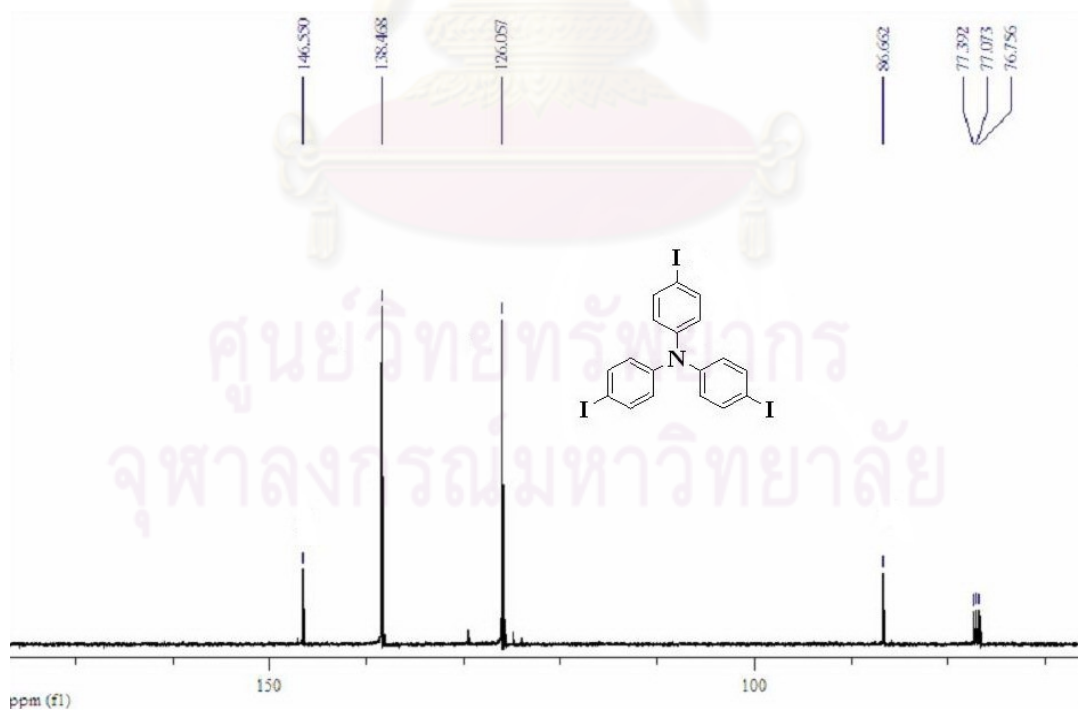


Figure A.2 ^{13}C NMR of TI_3 in CDCl_3 .

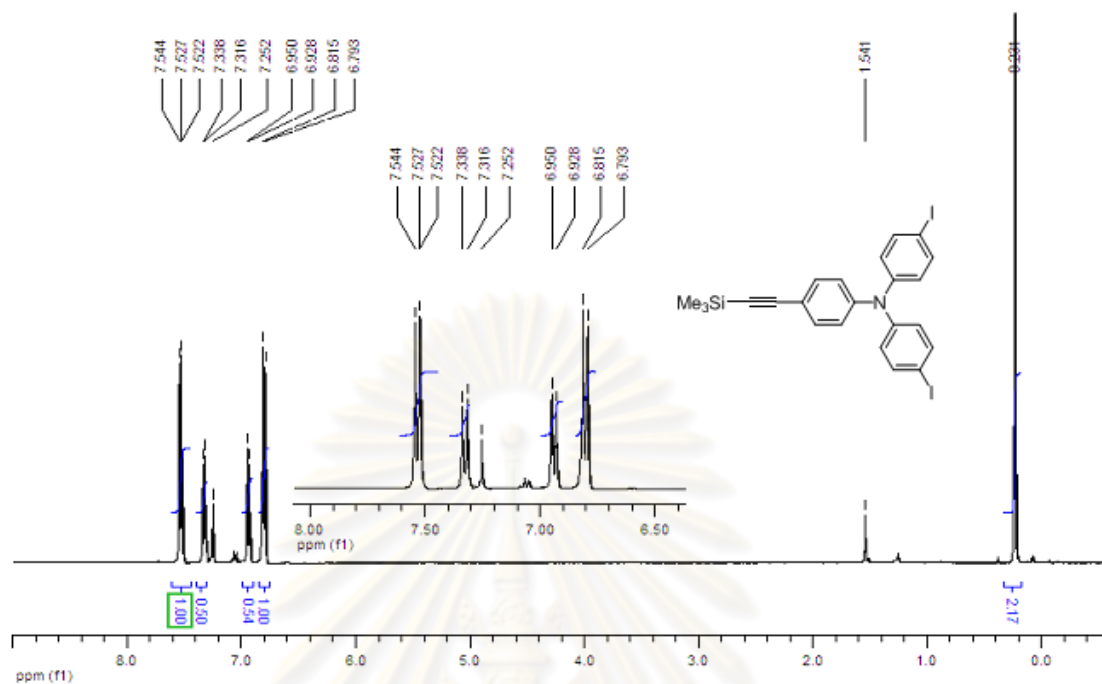


Figure A.3 $^1\text{H NMR}$ of TMS2I in CDCl_3 .

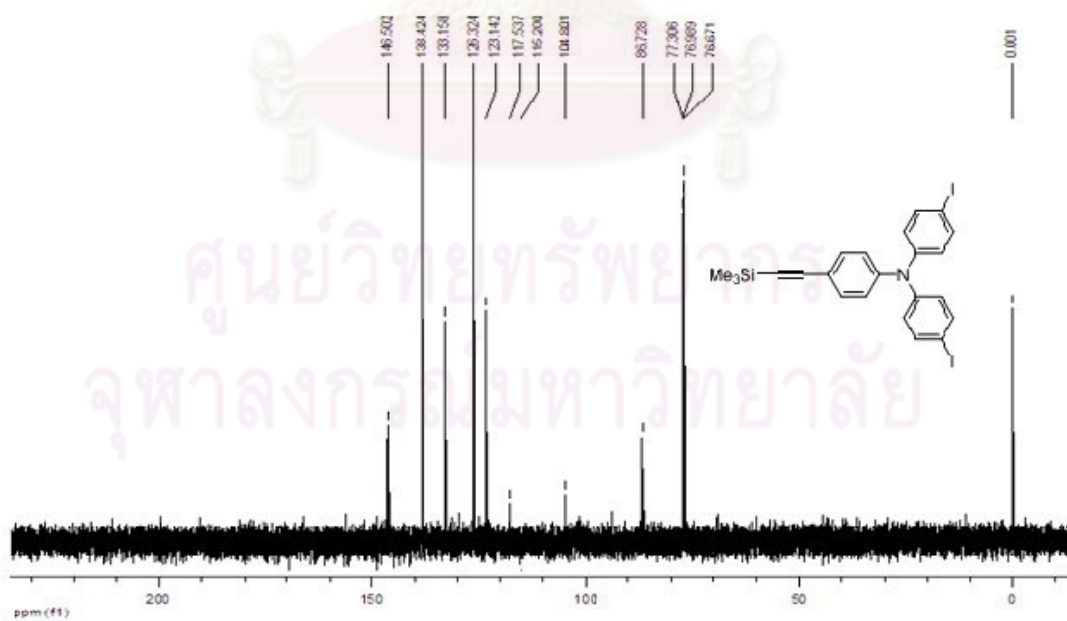


Figure A.4 $^{13}\text{C NMR}$ of TMS2I in CDCl_3 .

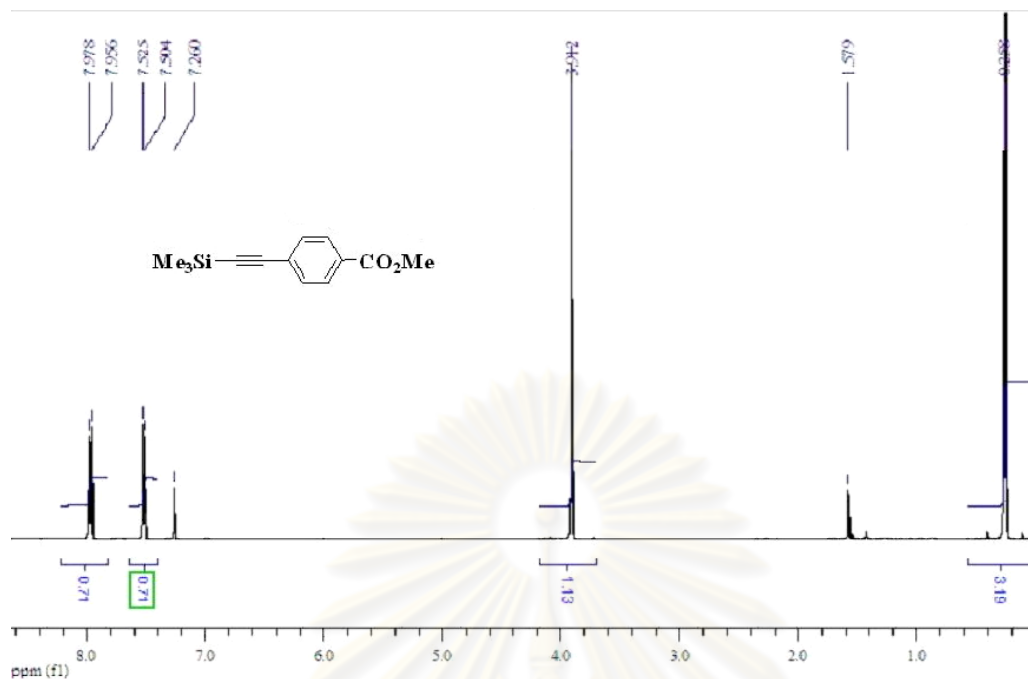


Figure A.5 ¹H NMR of Methyl 4-((trimethylsilyl)ethynyl)benzoate in CDCl₃.

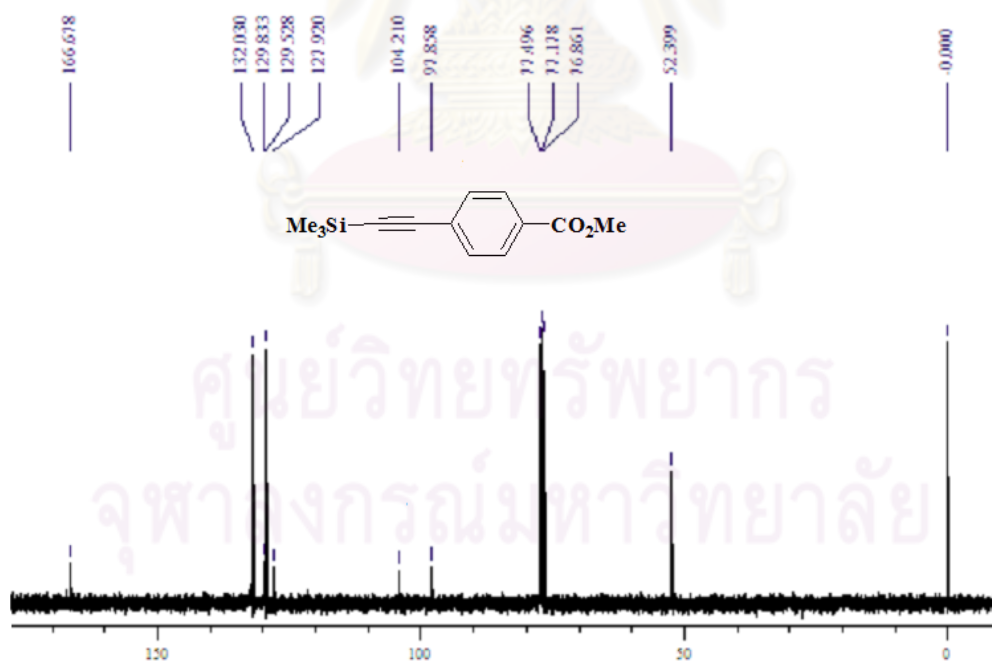


Figure A.6 ¹³C NMR of Methyl 4-((trimethylsilyl)ethynyl)benzoate in CDCl₃.

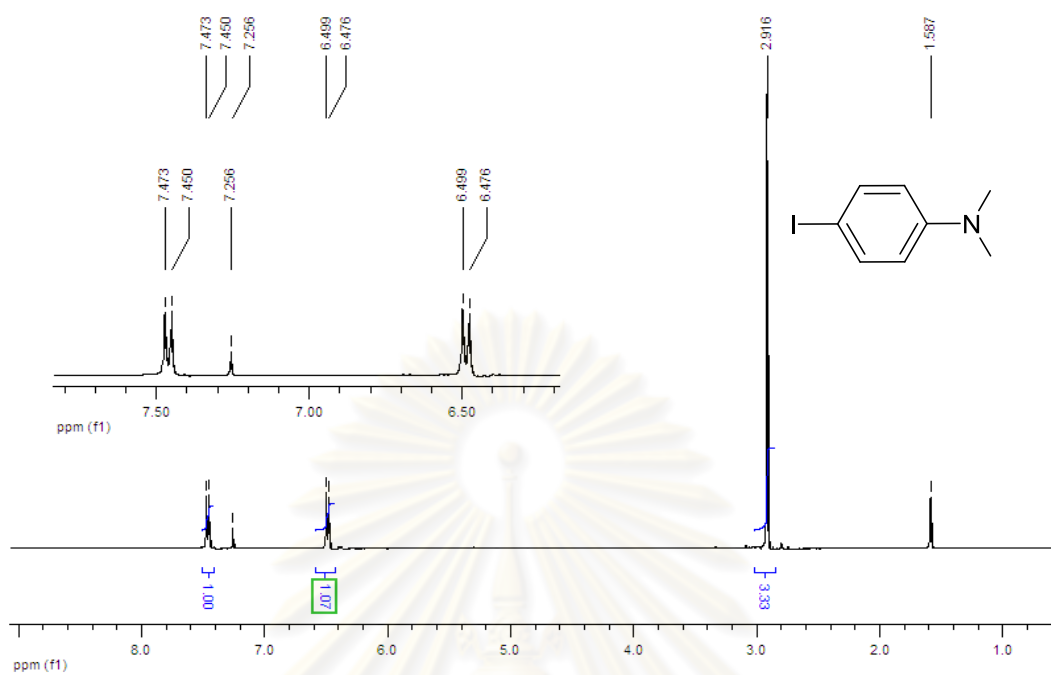


Figure A.7 ¹H NMR of 4-iodo-*N,N*-dimethylaniline in CDCl₃.

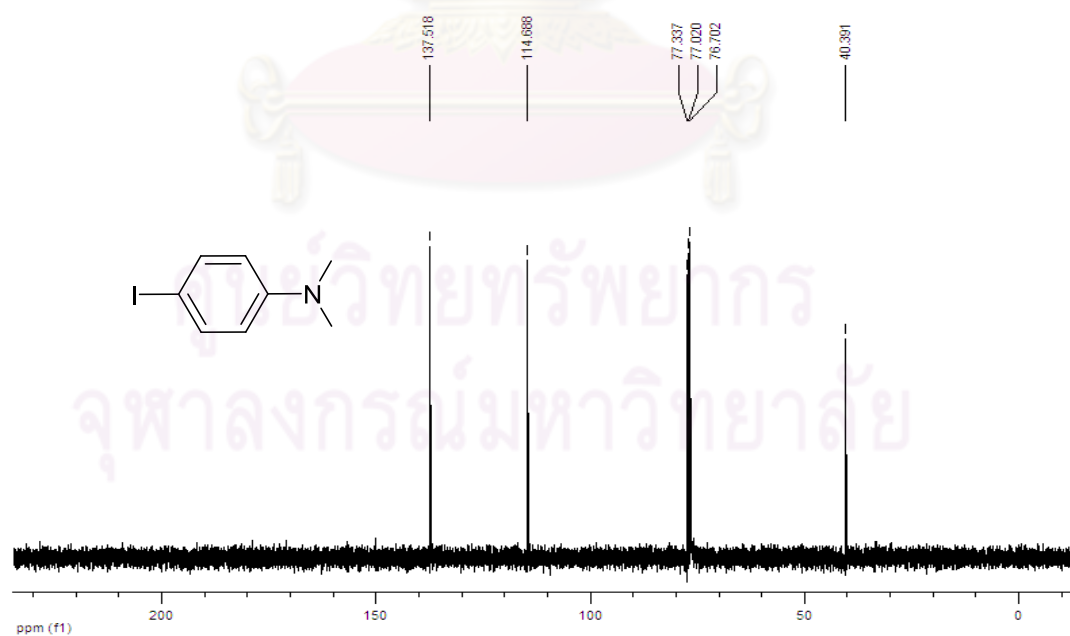


Figure A.8 ¹³C NMR of 4-iodo-*N,N*-dimethylaniline in CDCl₃.

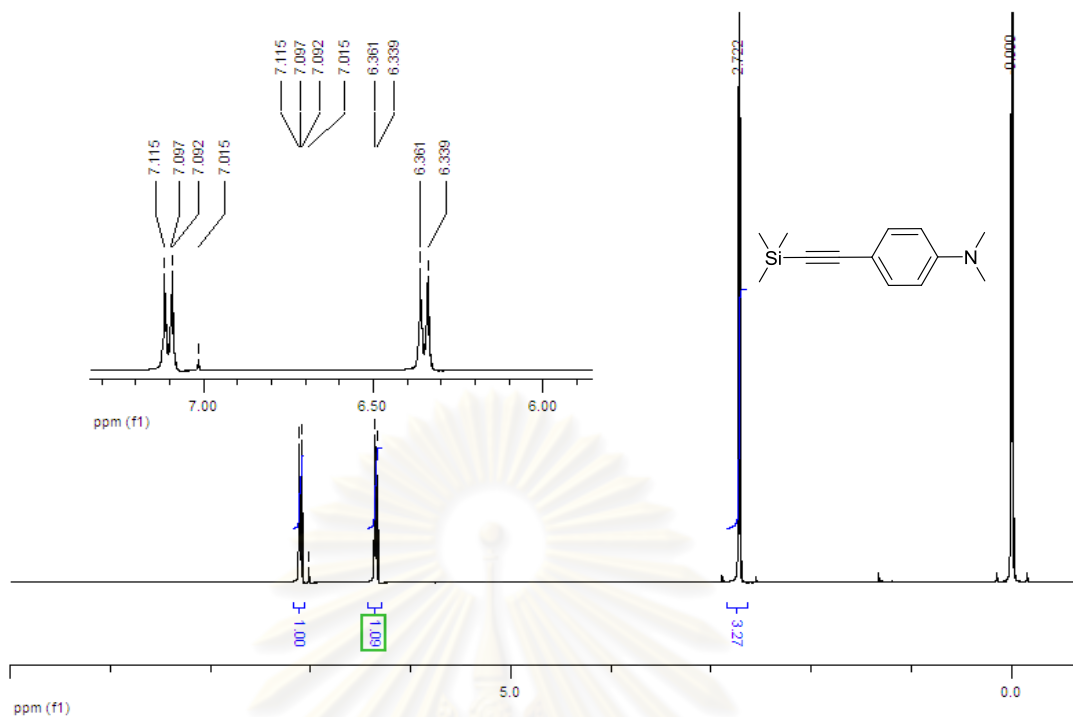


Figure A.9 ¹H NMR of *N,N*-dimethyl-4-((trimethylsilyl)ethynyl)aniline in CDCl₃.

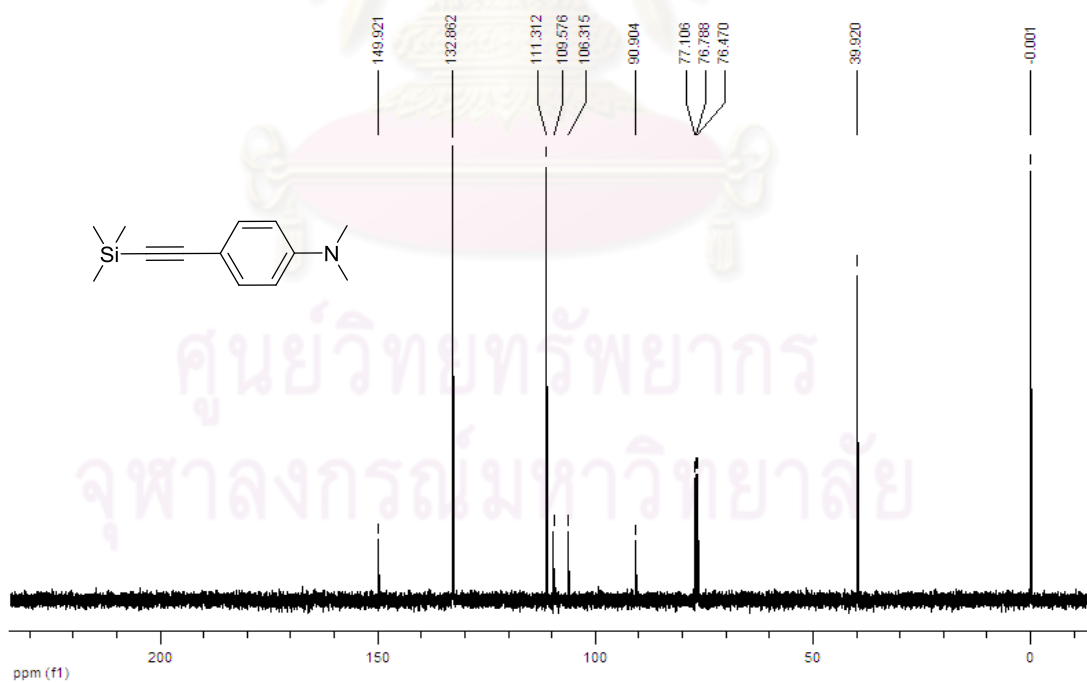


Figure A.10 ¹³C NMR of *N,N*-dimethyl-4-((trimethylsilyl)ethynyl)aniline in CDCl₃.

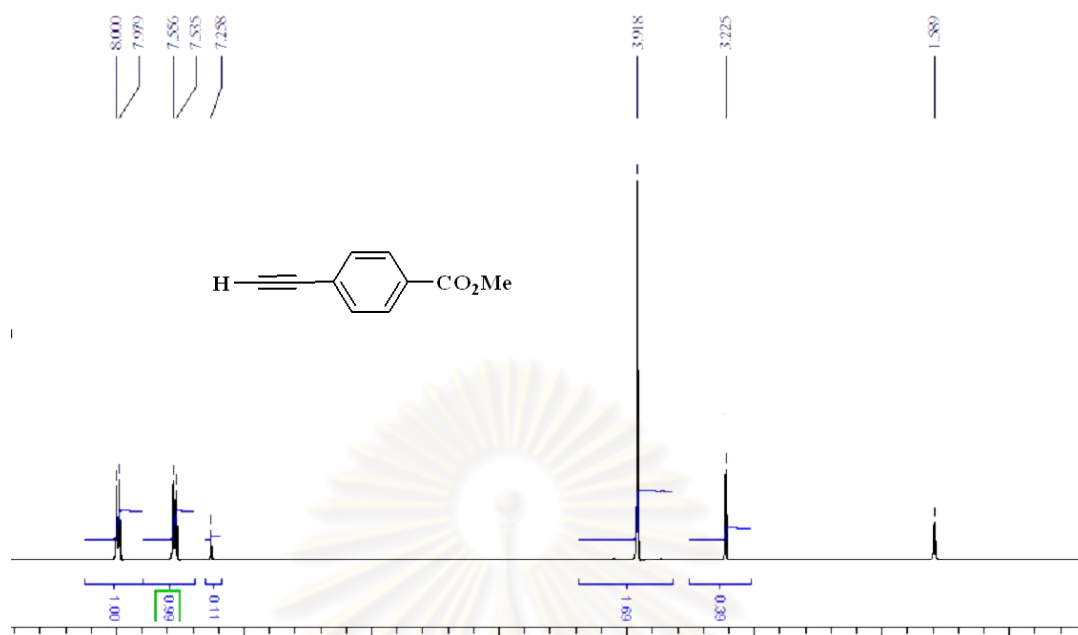


Figure A.11 $^1\text{H NMR}$ of Methyl 4-ethynylbenzoate in CDCl_3 .

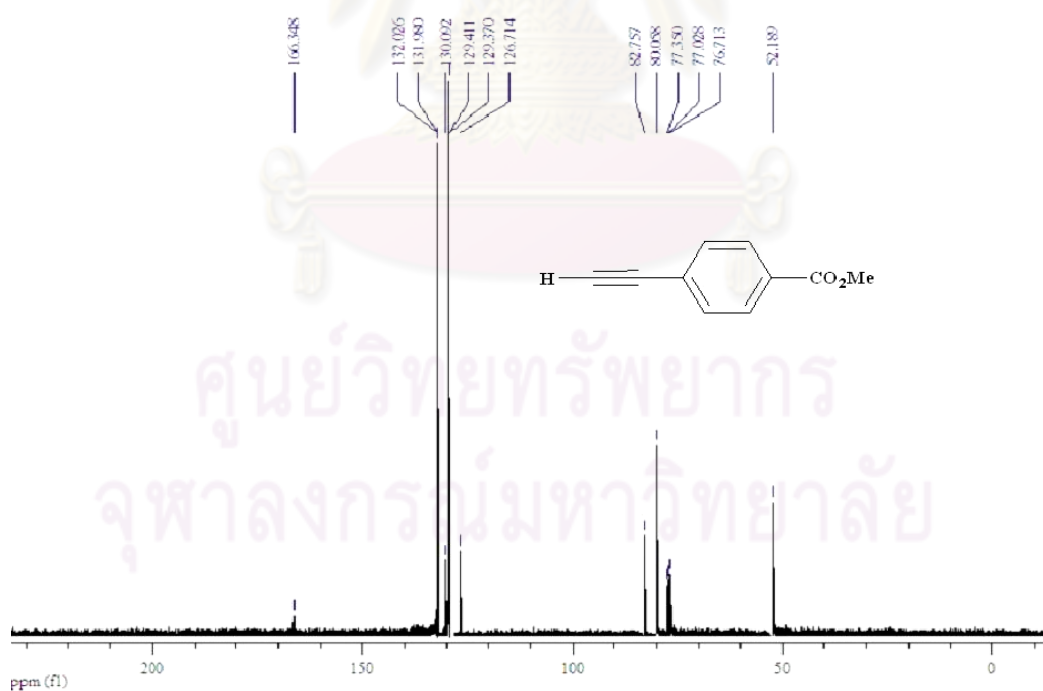


Figure A.12 $^{13}\text{C NMR}$ of Methyl 4-ethynylbenzoate in CDCl_3 .

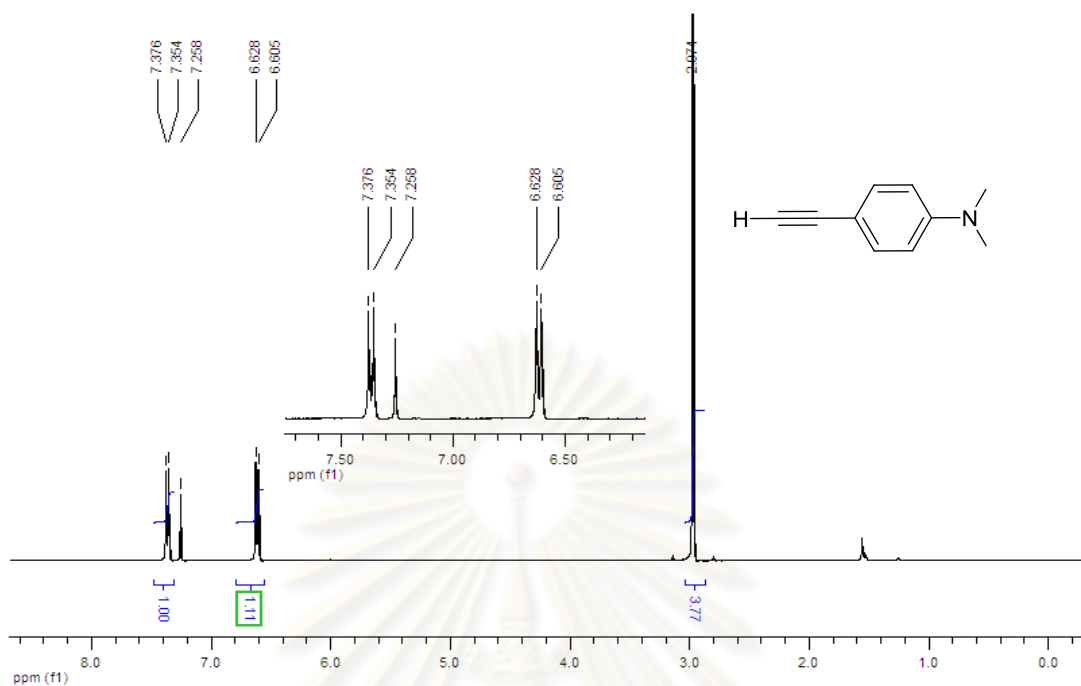


Figure A.13 ^1H NMR of 4-ethynyl-*N,N*-dimethylaniline in CDCl_3 .

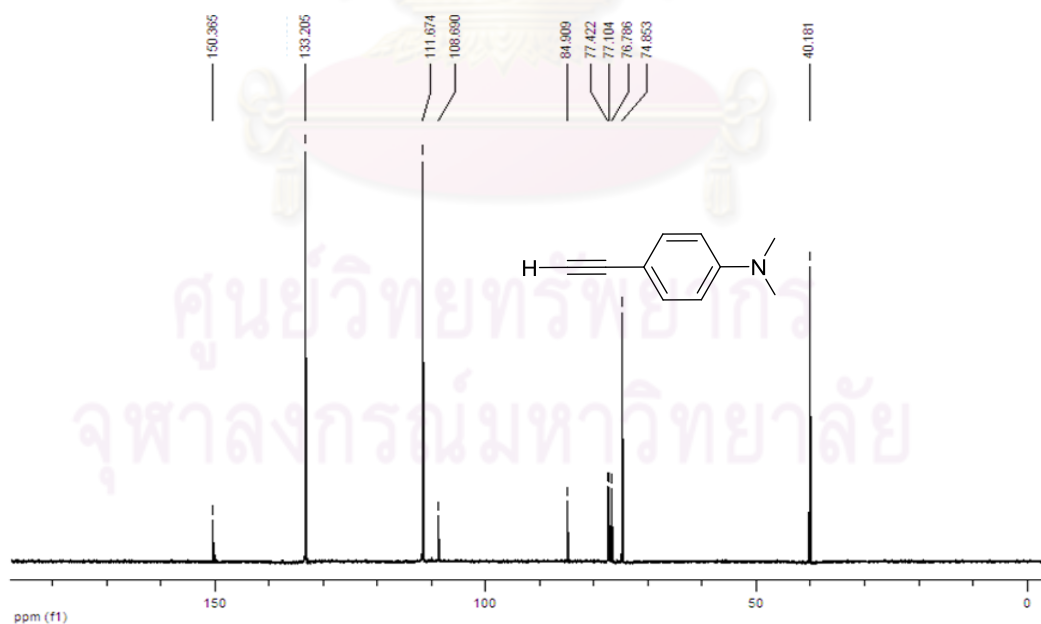


Figure A.14 ^{13}C NMR of 4-ethynyl-*N,N*-dimethylaniline in CDCl_3 .

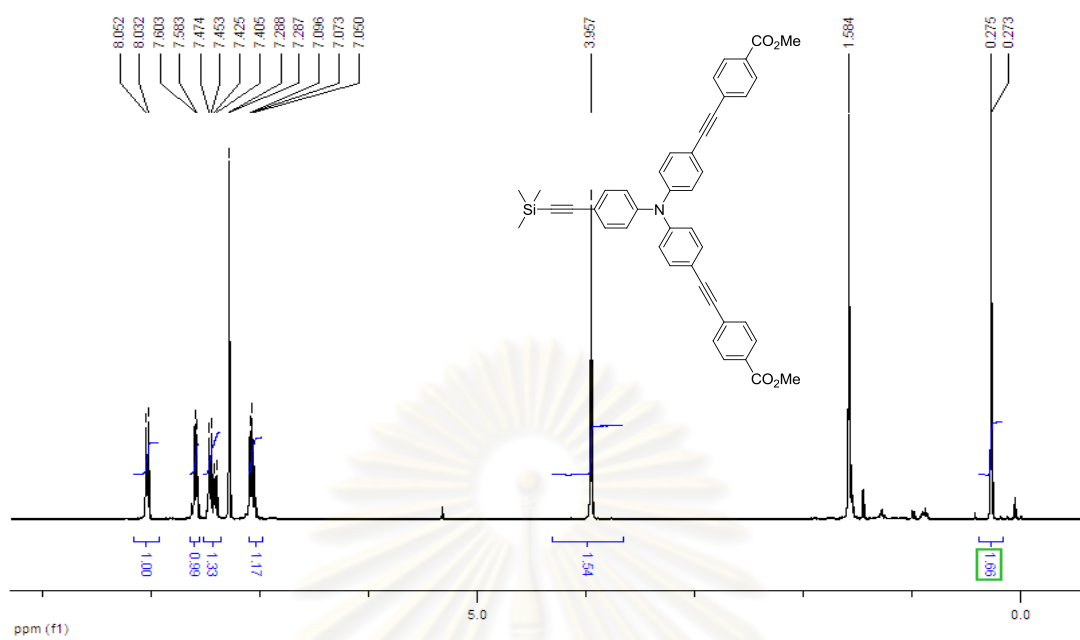


Figure A.15 ¹H NMR of TMS2C⁰ in CDCl₃.

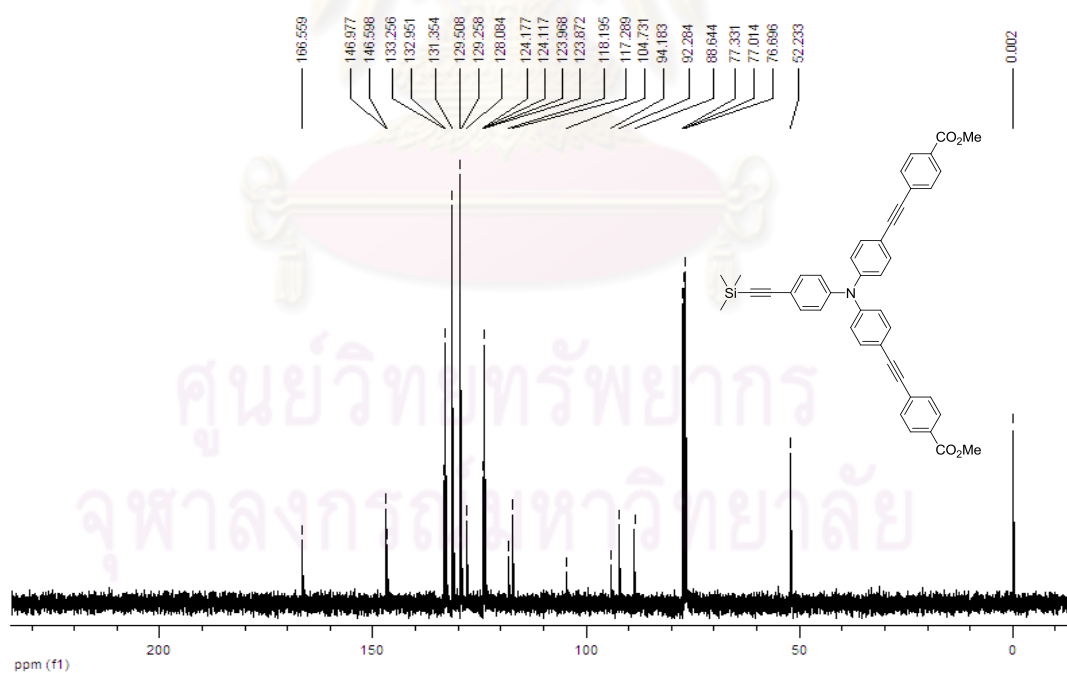


Figure A.16 ¹³C NMR of TMS2C⁰ in CDCl₃.

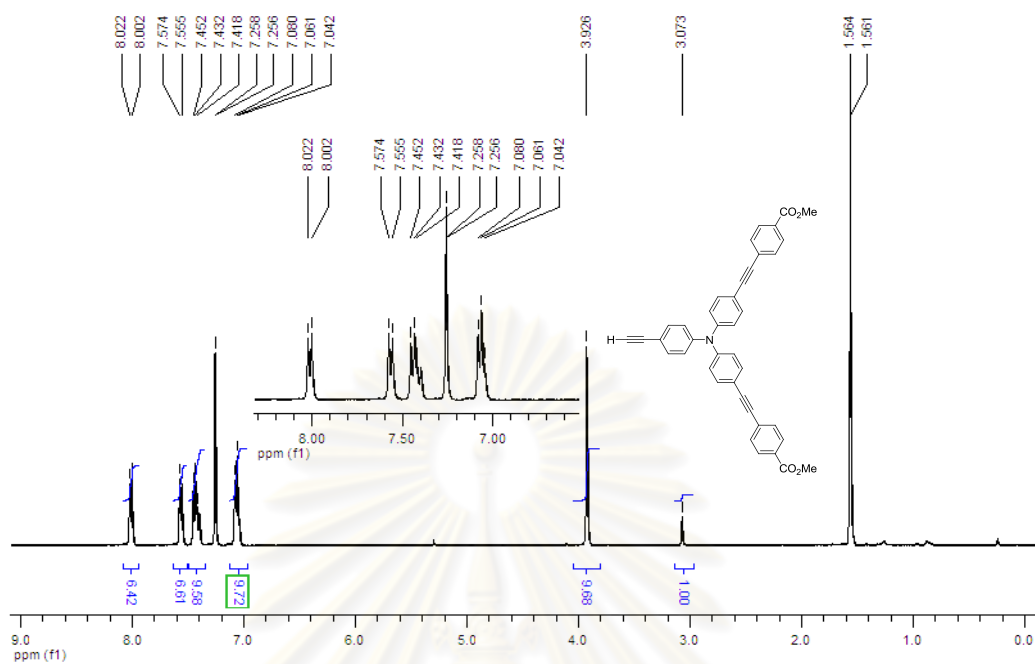


Figure A.17 1H NMR of $E2C^0$ in $CDCl_3$.

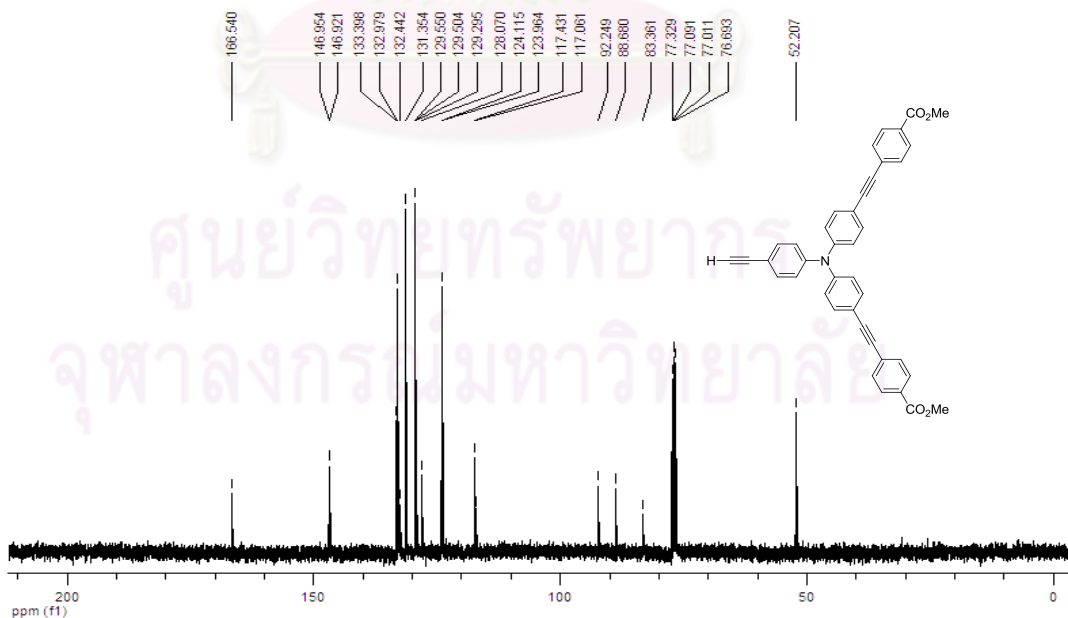


Figure A.18 ^{13}C NMR of $E2C^0$ in $CDCl_3$.

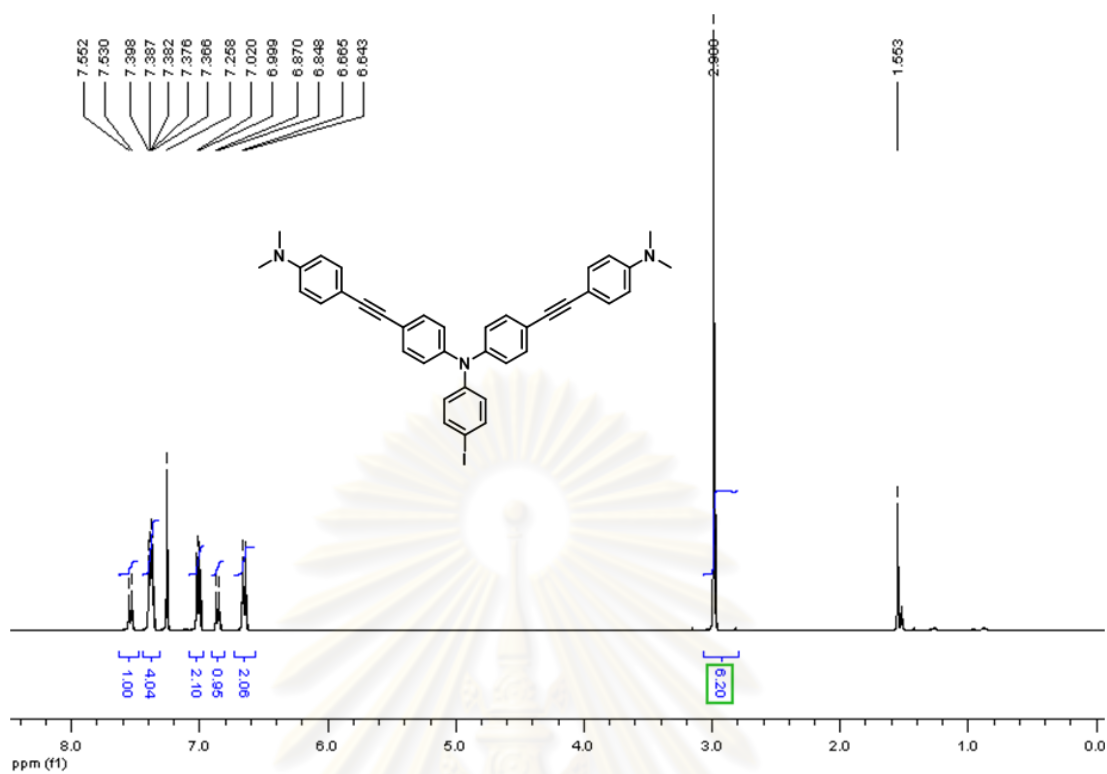


Figure A.19 ^1H NMR of **I2N⁰** in CDCl_3 .

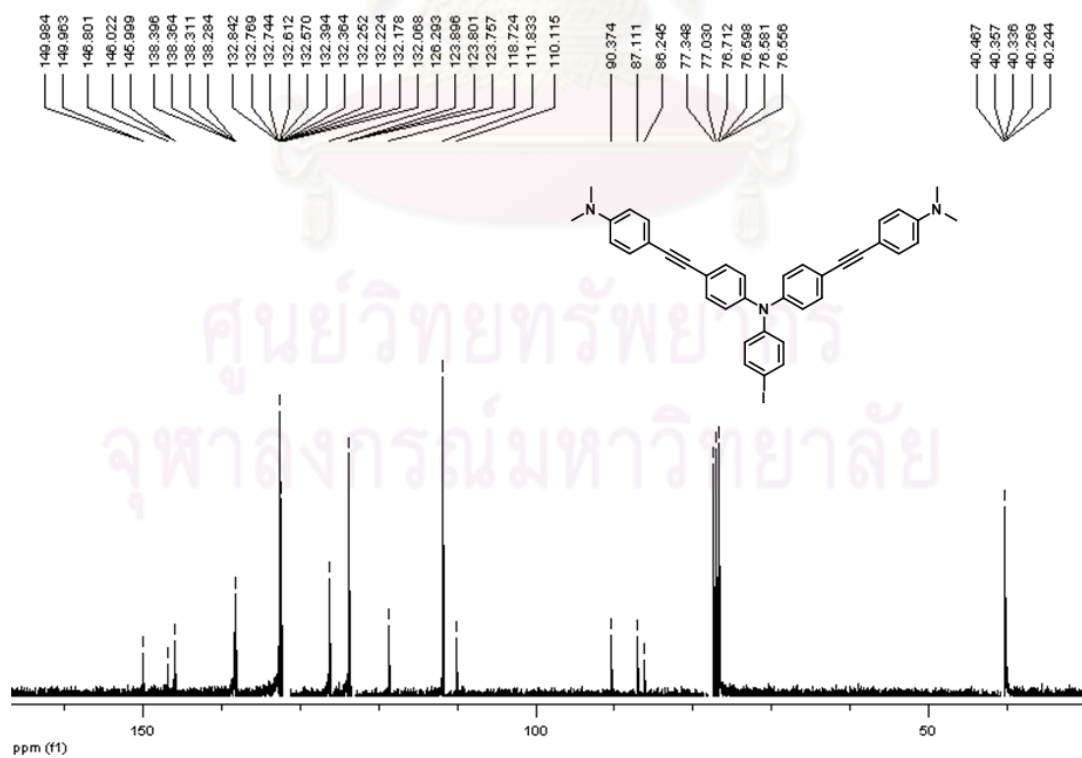


Figure A.20 ^{13}C NMR of **I2N⁰** in CDCl_3 .

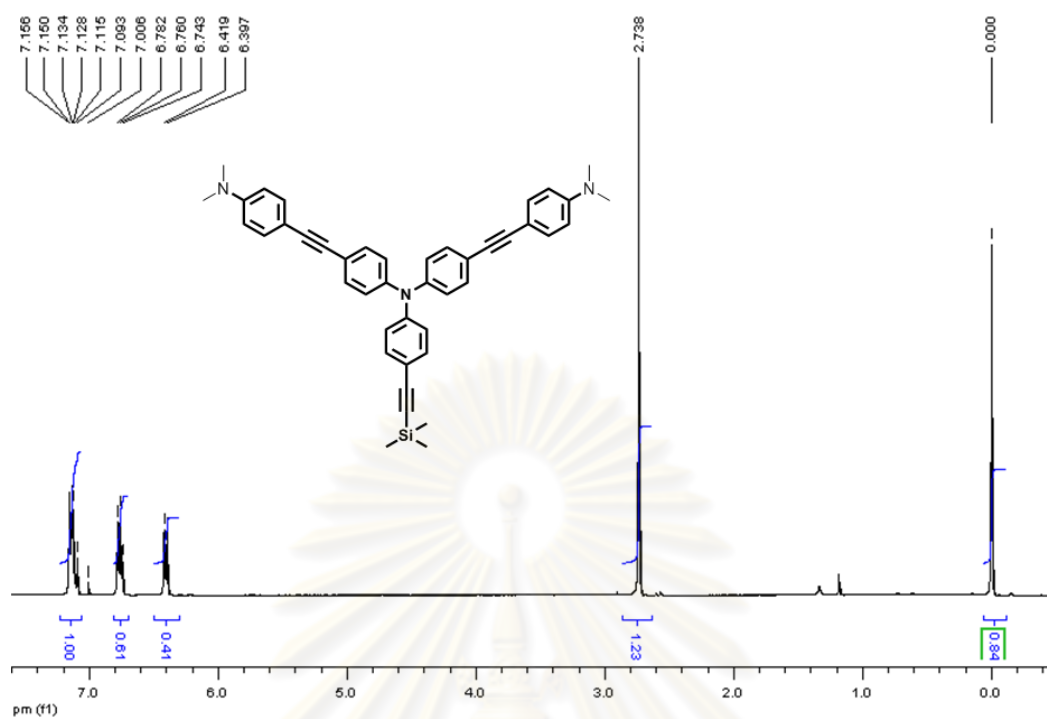


Figure A.21 ^1H NMR of TMS2N⁰ in CDCl₃.

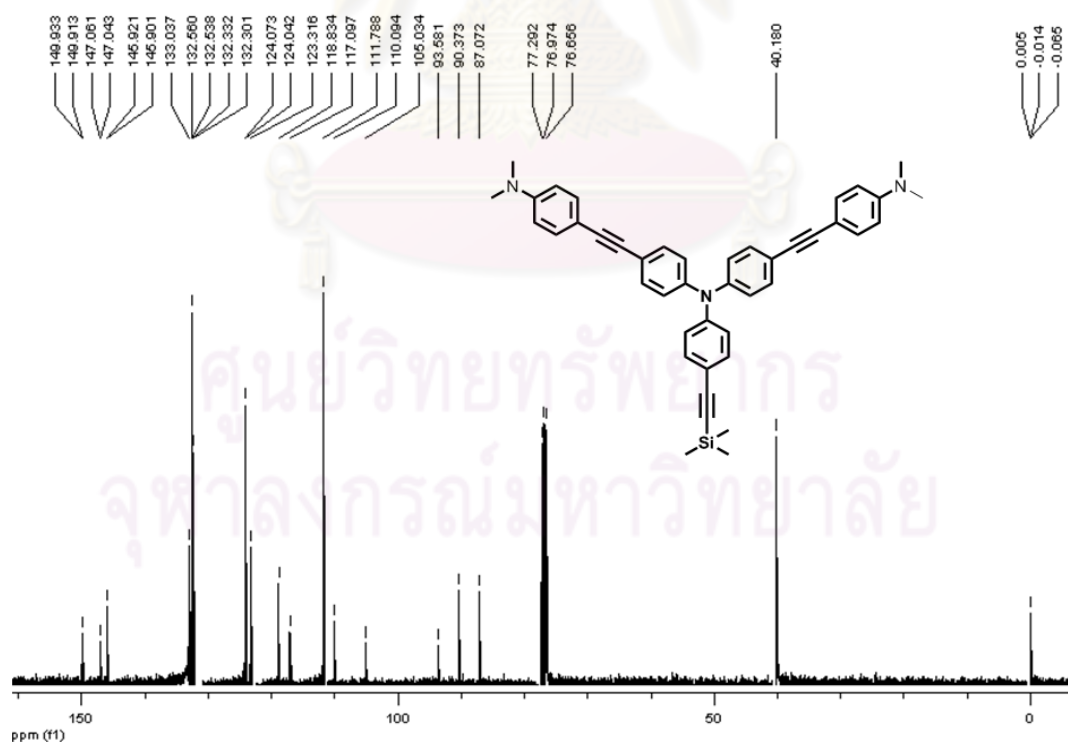


Figure A.22 ^{13}C NMR of TMS2N⁰ in CDCl₃.

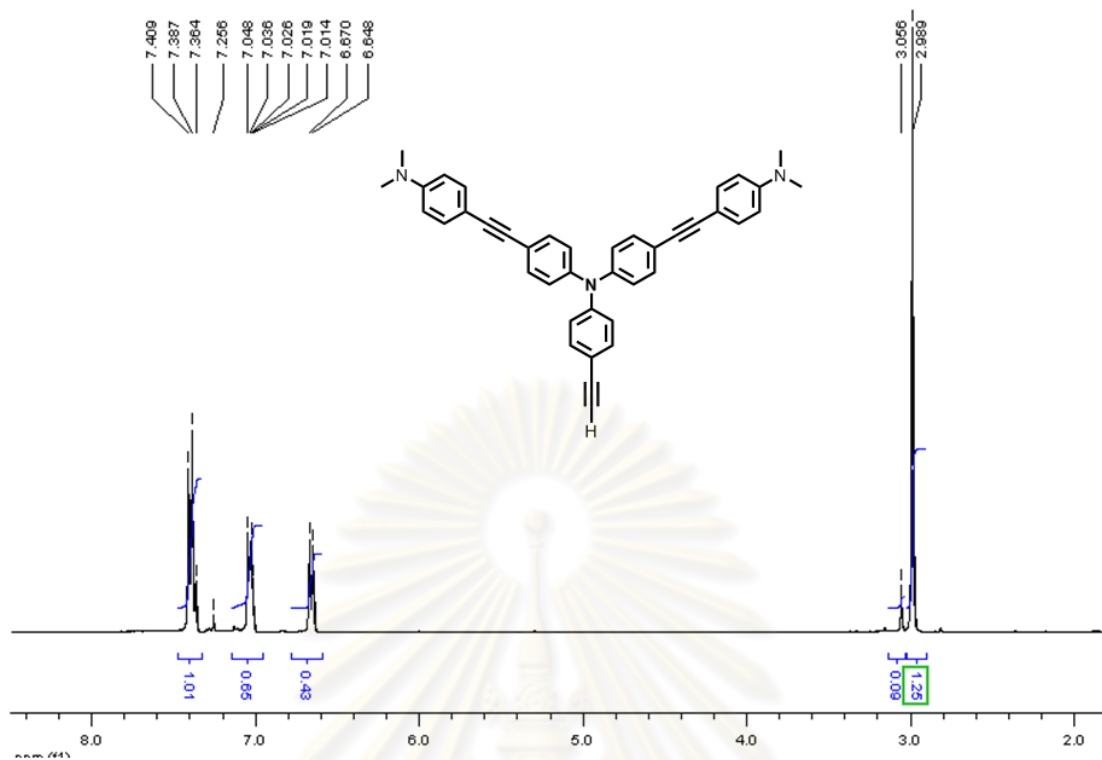


Figure A.23 ^1H NMR of E2N^0 in CDCl_3 .

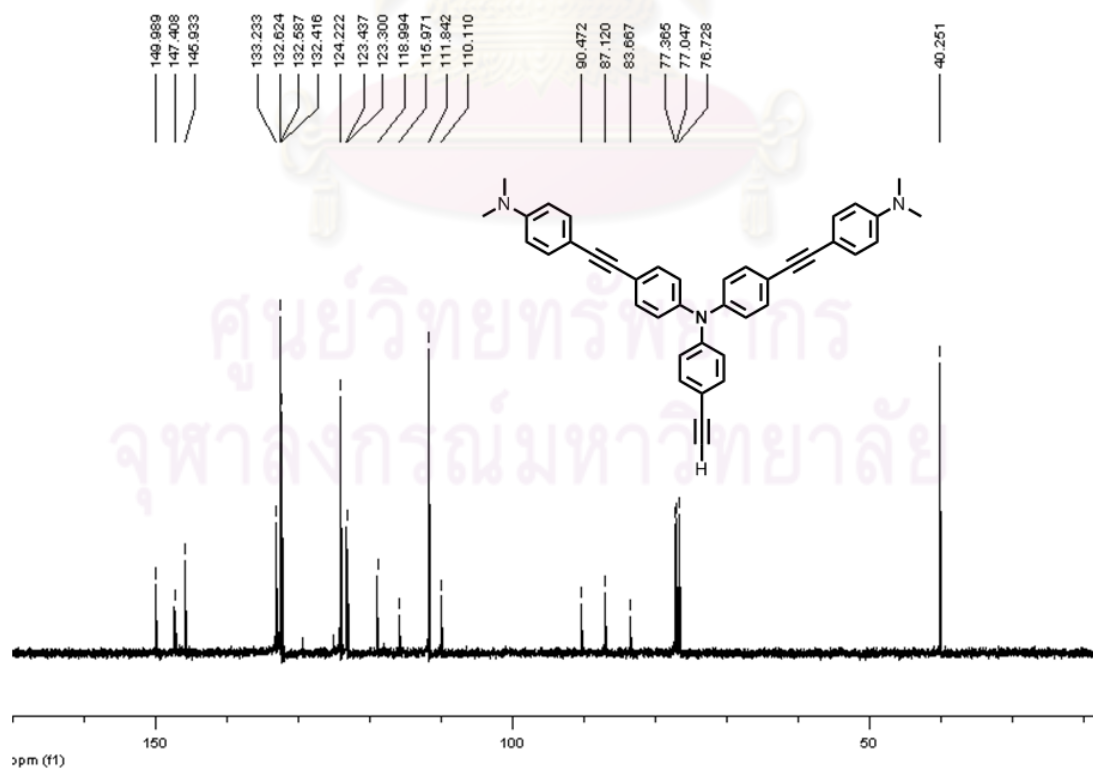


Figure A.24 ^{13}C NMR of TMS2N^0 in CDCl_3 .

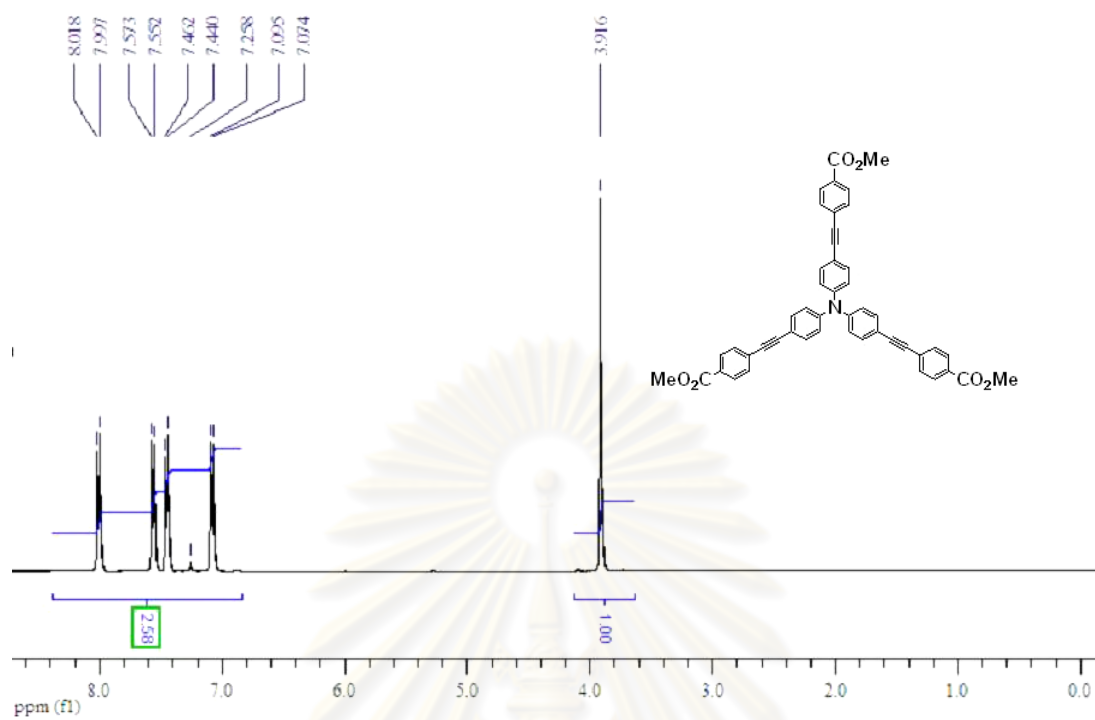


Figure A.25 ¹H NMR of **3C⁰** in CDCl₃.

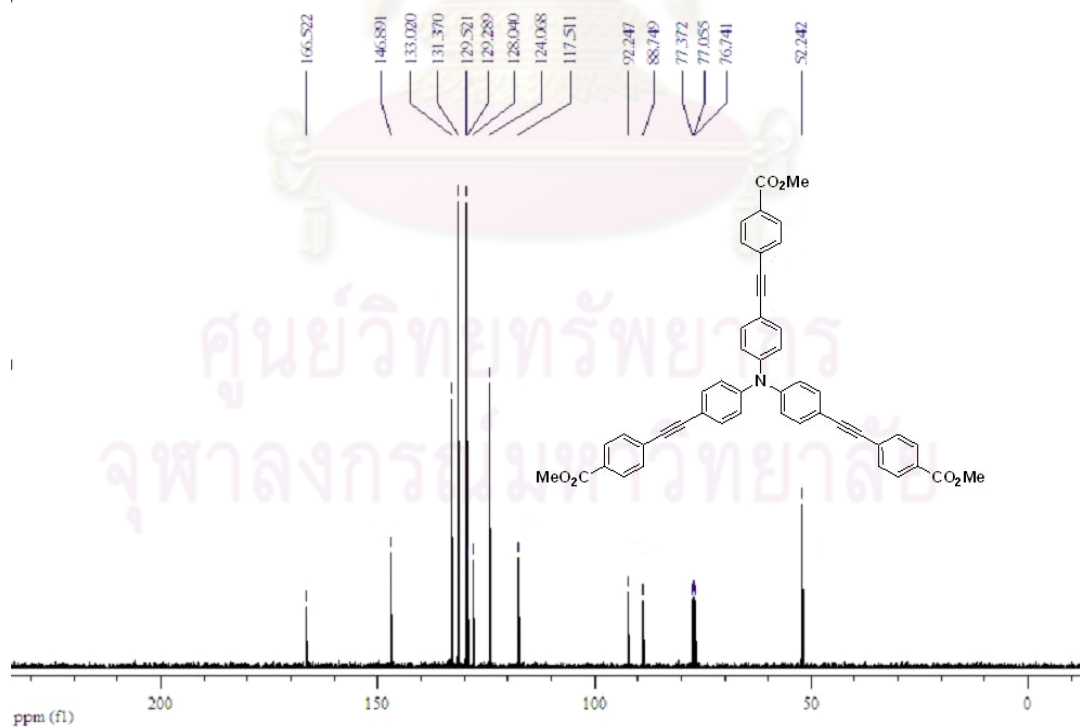


Figure A.26 ¹³C NMR of **3C⁰** in CDCl₃.

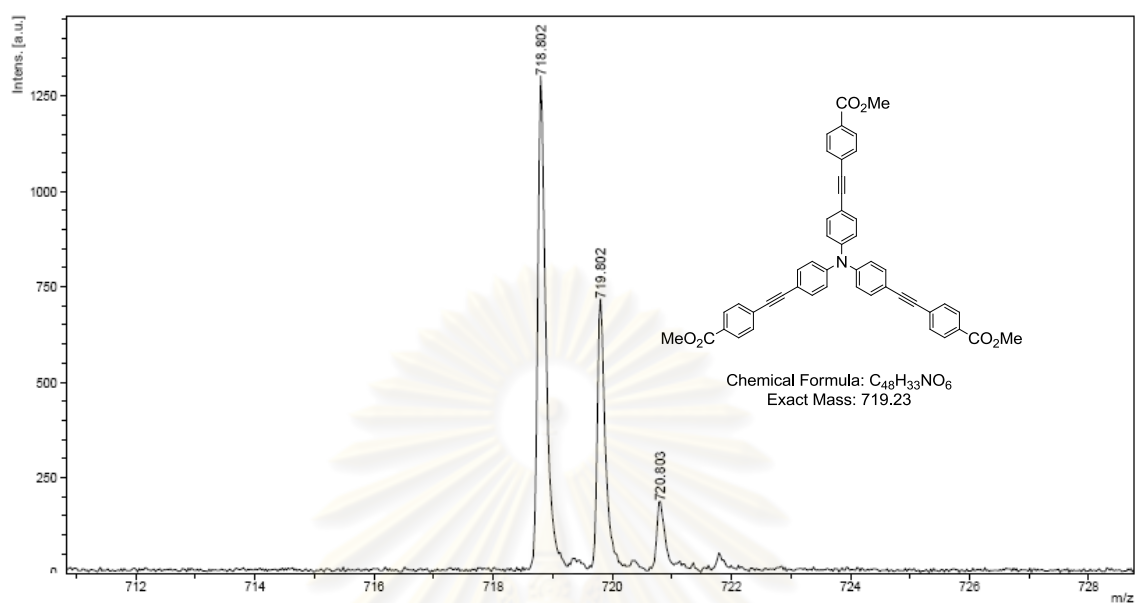


Figure A.27 MALDI-TOF-MS of $3C^0$.

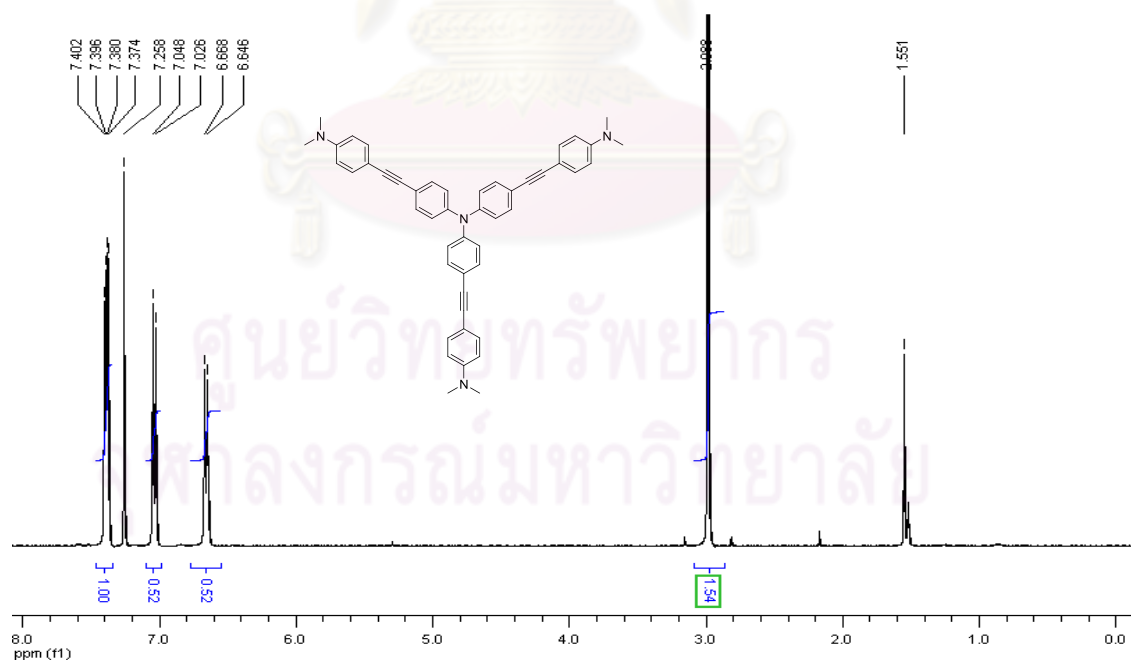


Figure A.28 1H NMR of $3N^0$ in $CDCl_3$.

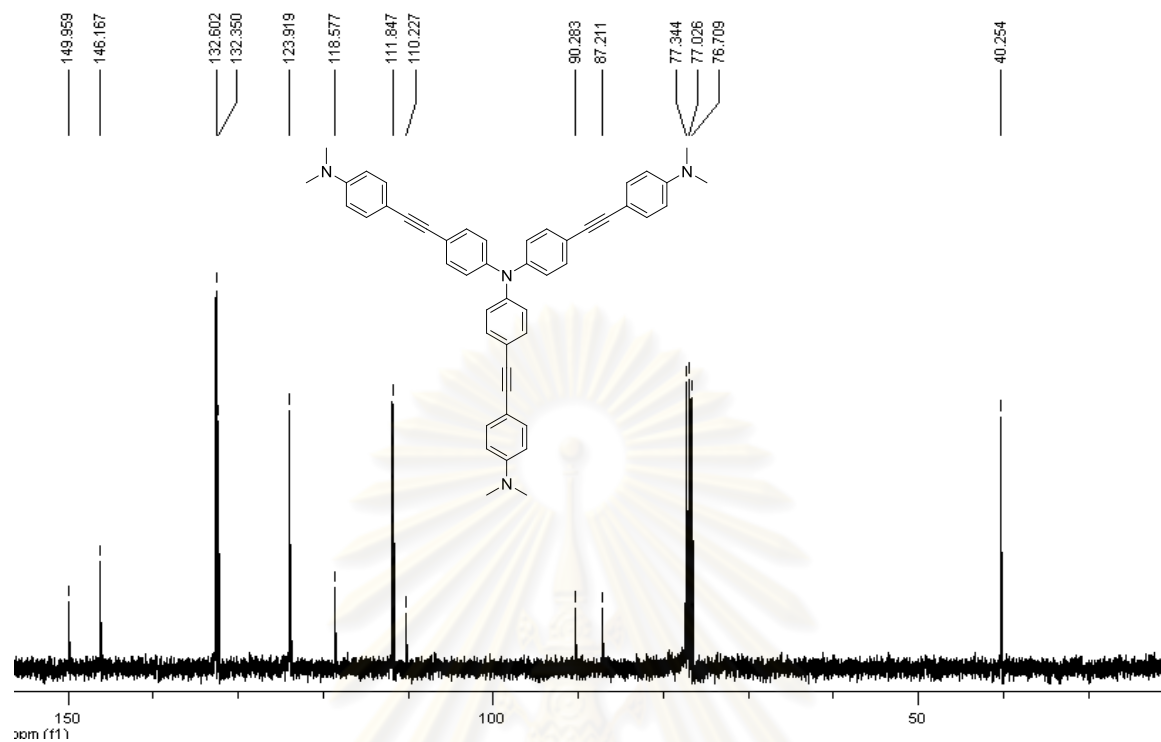


Figure A.29 ^{13}C NMR of $3N^0$ in $CDCl_3$.

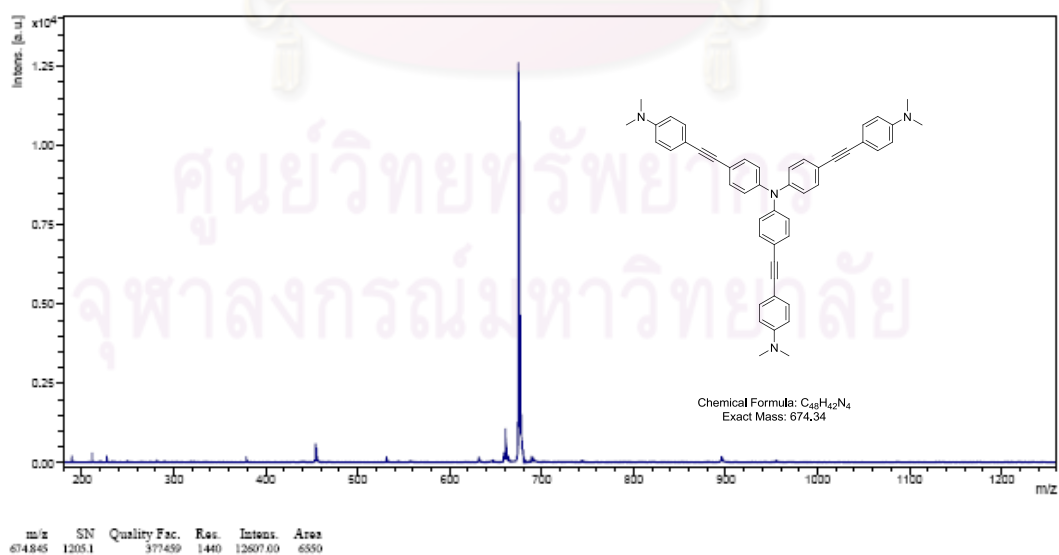


Figure A.30 MALDI-TOF-MS of $3N^0$.

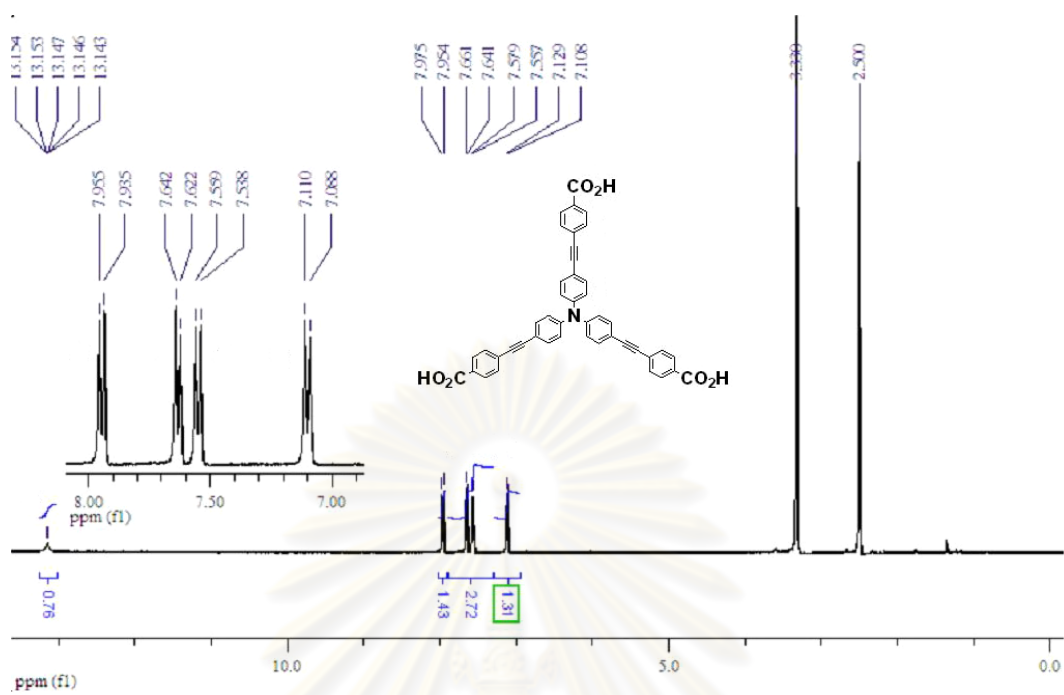


Figure A.31 ^1H NMR of 3C^- in DMSO-d_6 .

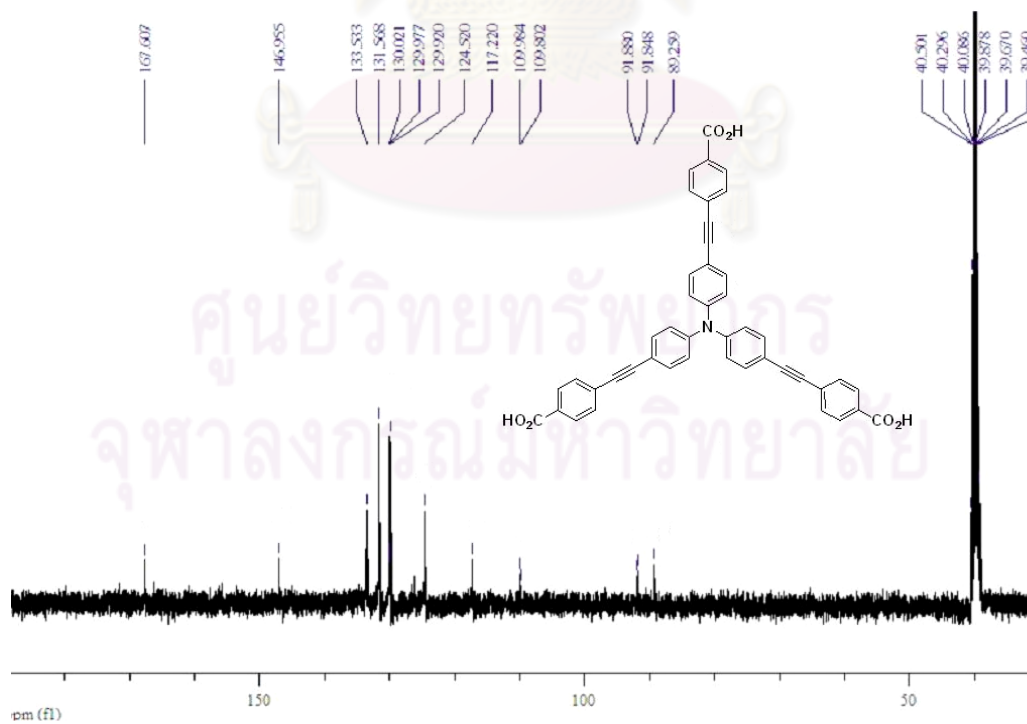


Figure A.32 ^{13}C NMR of 3C^- in DMSO-d_6 .

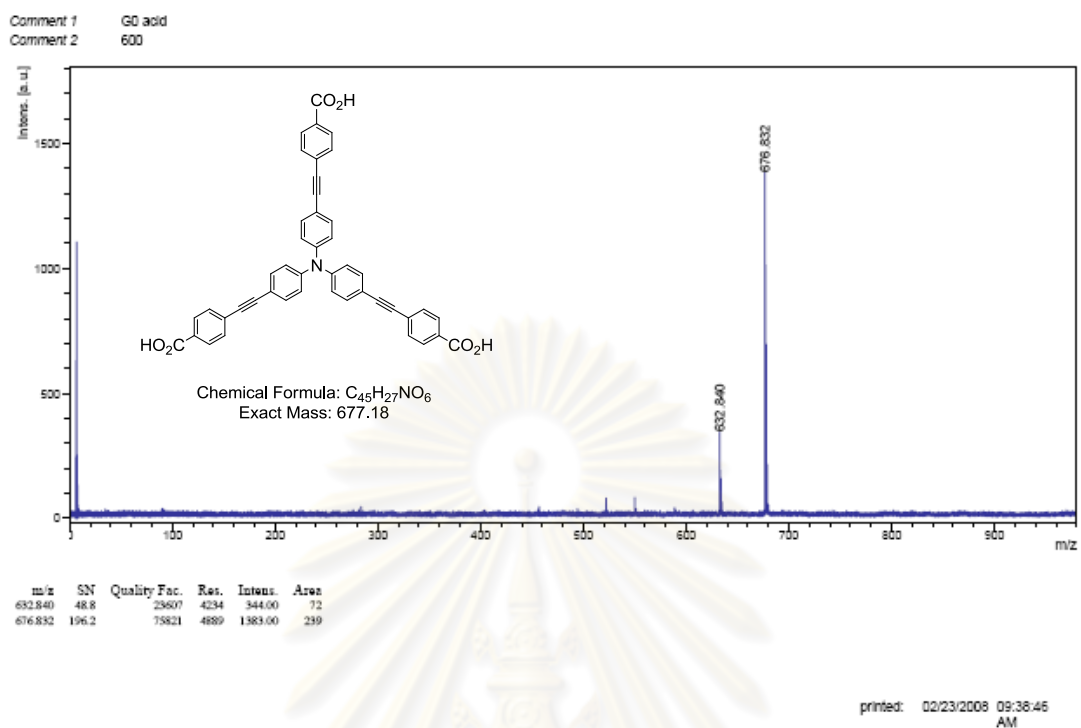


Figure A.33 MALDI-TOF-MS of $3C^-$.

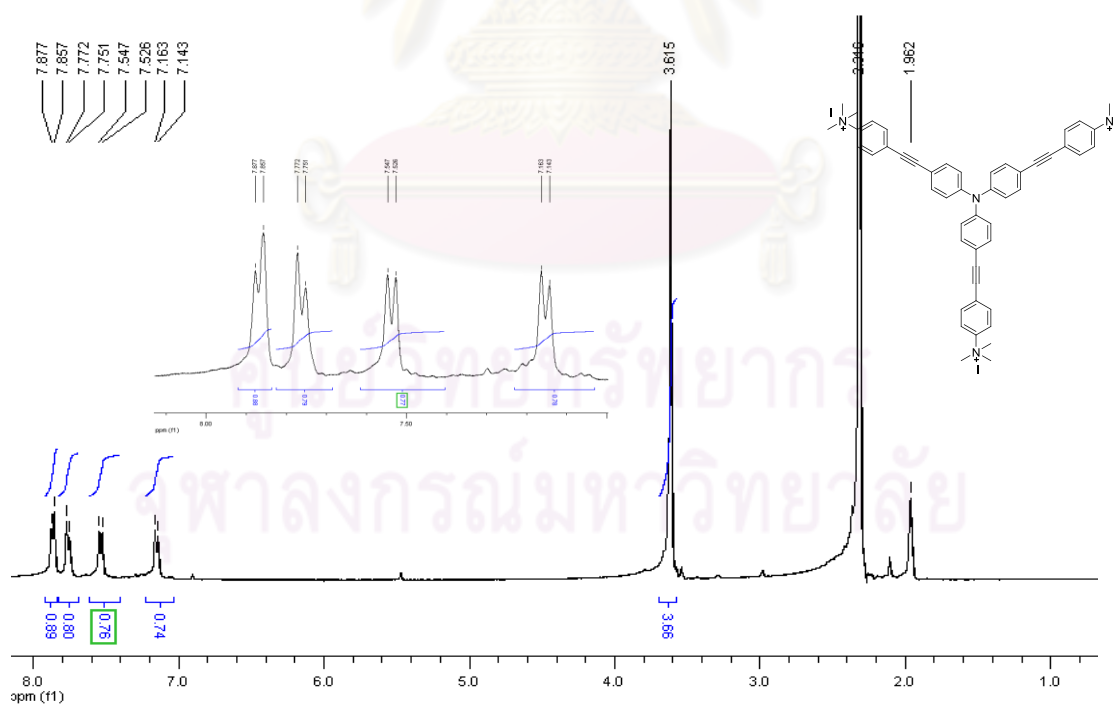


Figure A.34 1H NMR of $3N^+$ in CD_3CN .

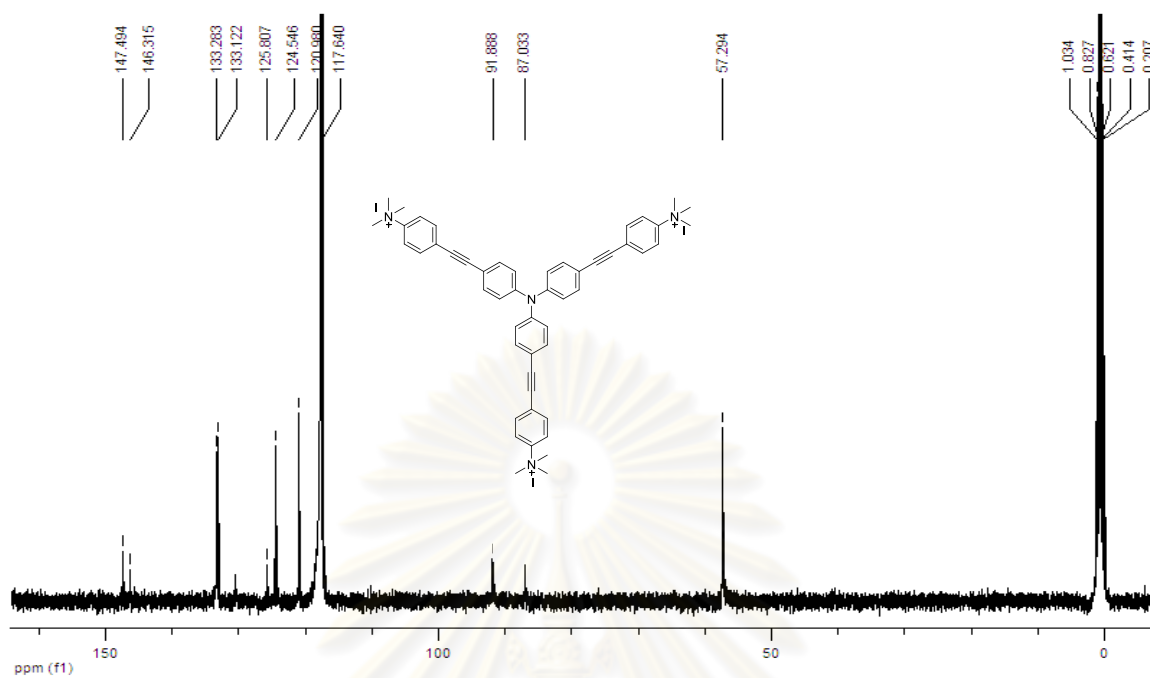


Figure A.35 ^{13}C NMR of 3N^+ in CD_3CN .

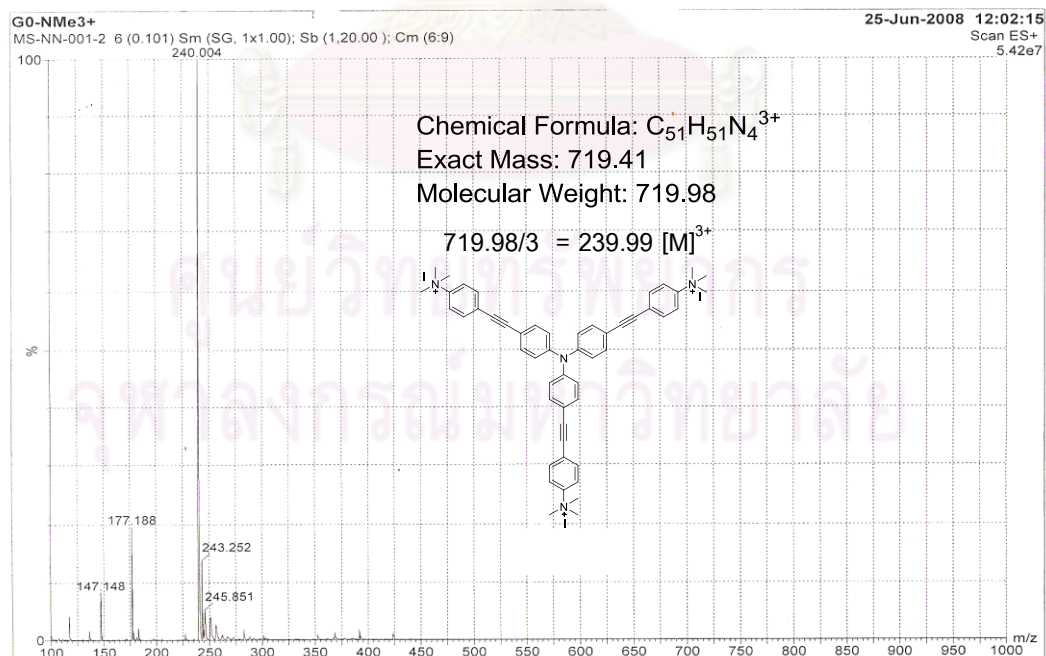


Figure A.36 ESI-MS of 3N^+ .

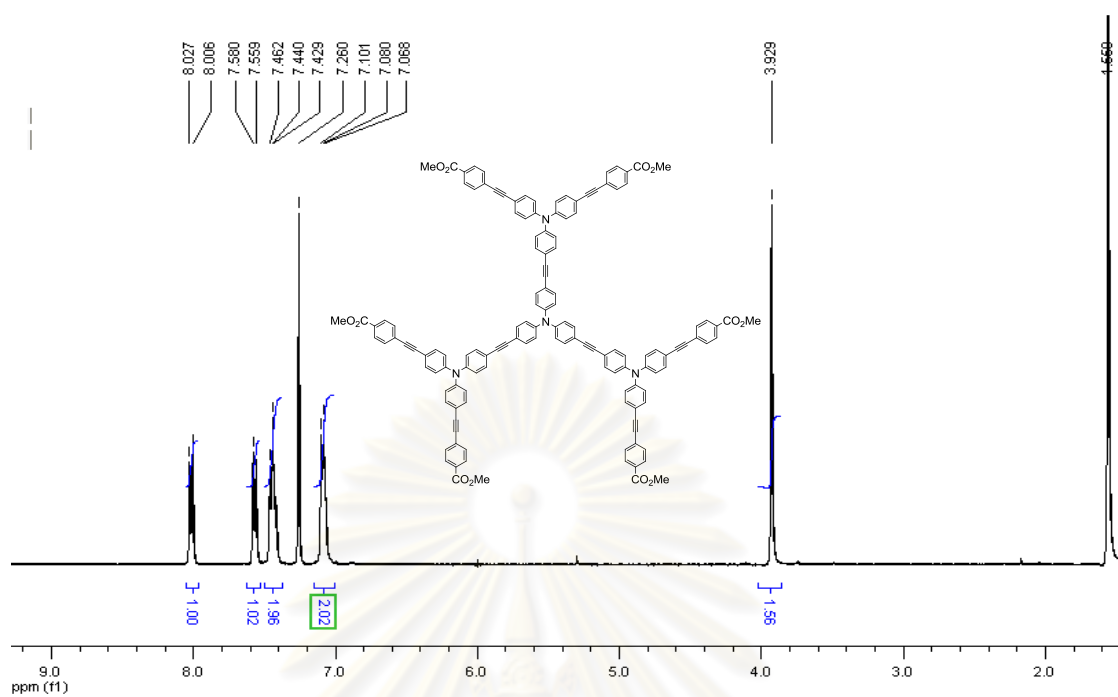


Figure A.37 ¹H NMR of **6C⁰** in CDCl₃.

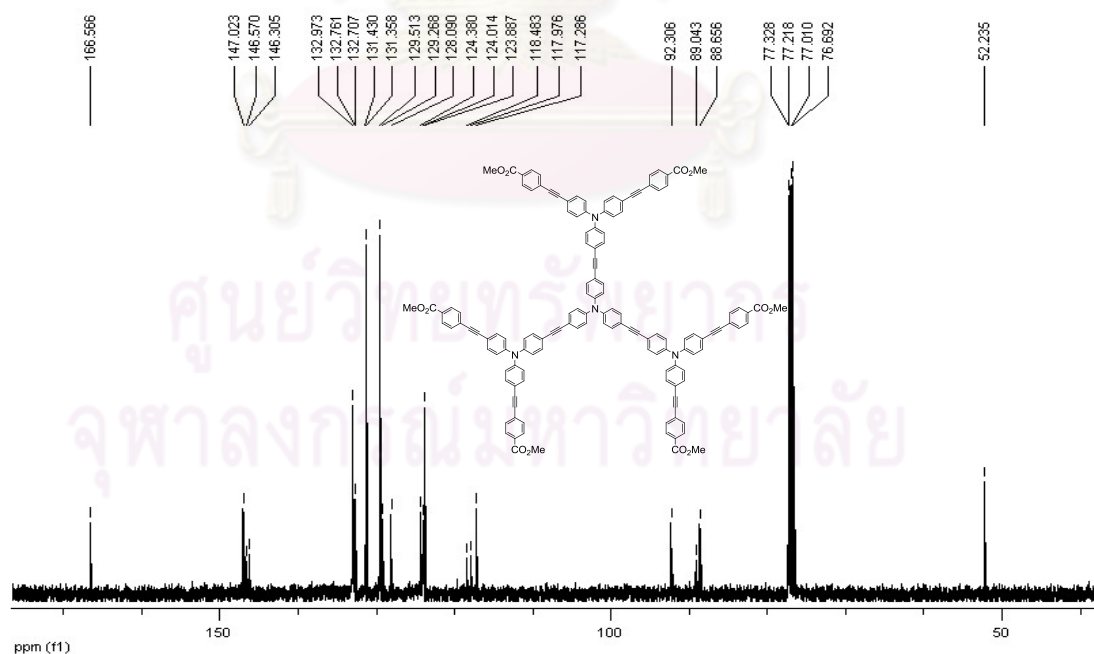


Figure A.38 ¹³C NMR of **6C⁰** in CDCl₃.

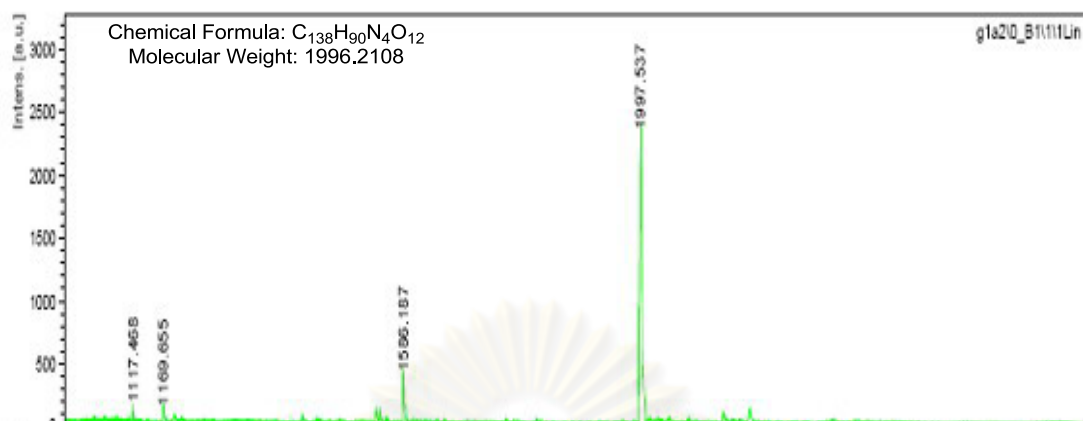


Figure A.39 MALDI-TOF-MS of $6C^0$.

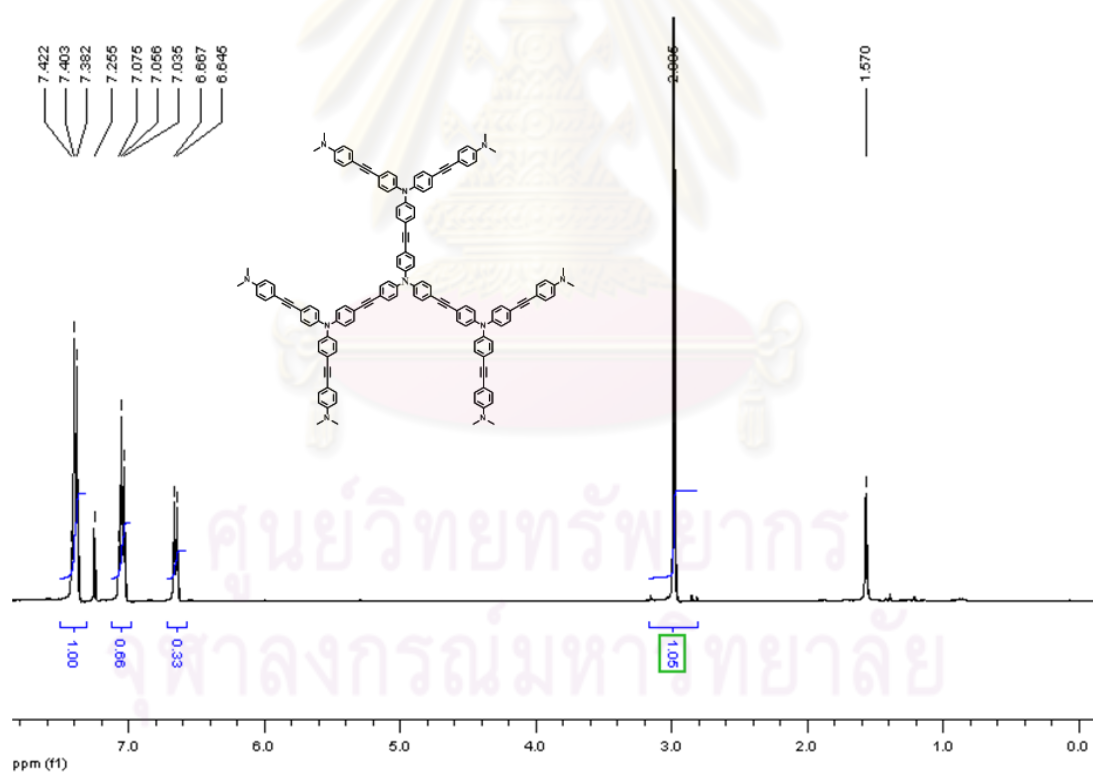


Figure A.40 1H NMR of $6N^0$ in $CDCl_3$.

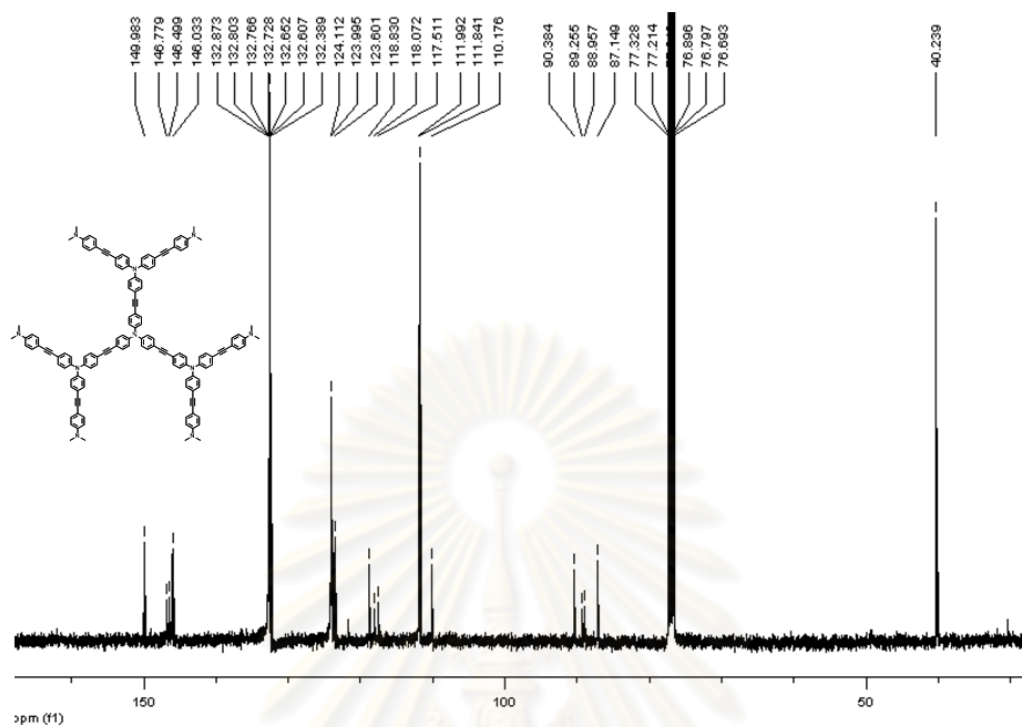


Figure A.41 ^{13}C NMR of 6N⁰ in CDCl_3 .

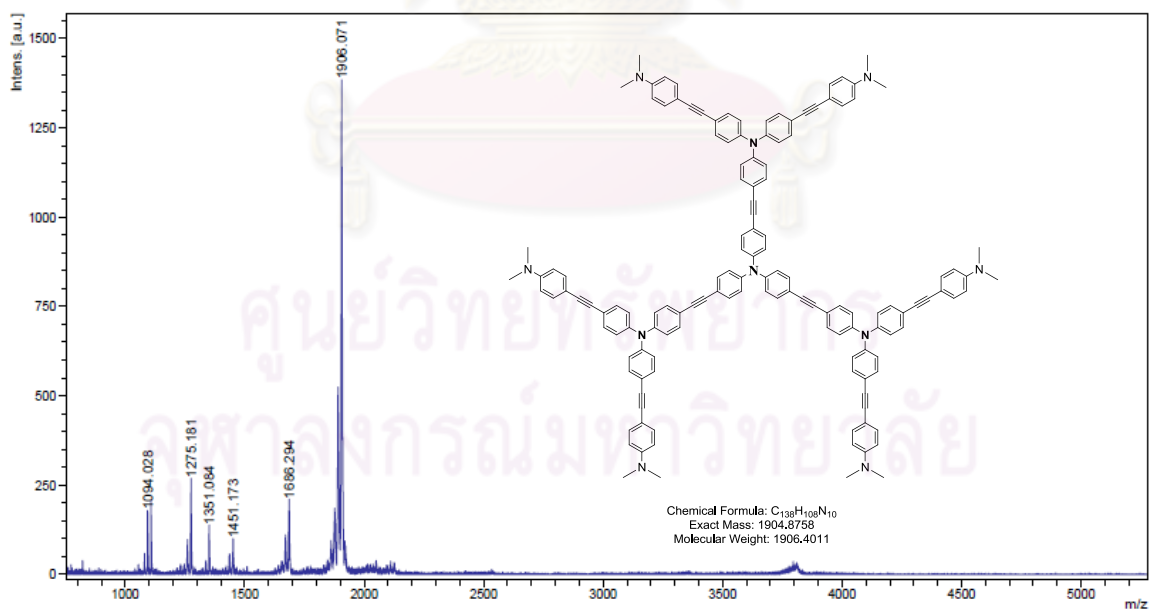


Figure A.42 MALDI-TOF-MS of 6N⁰.

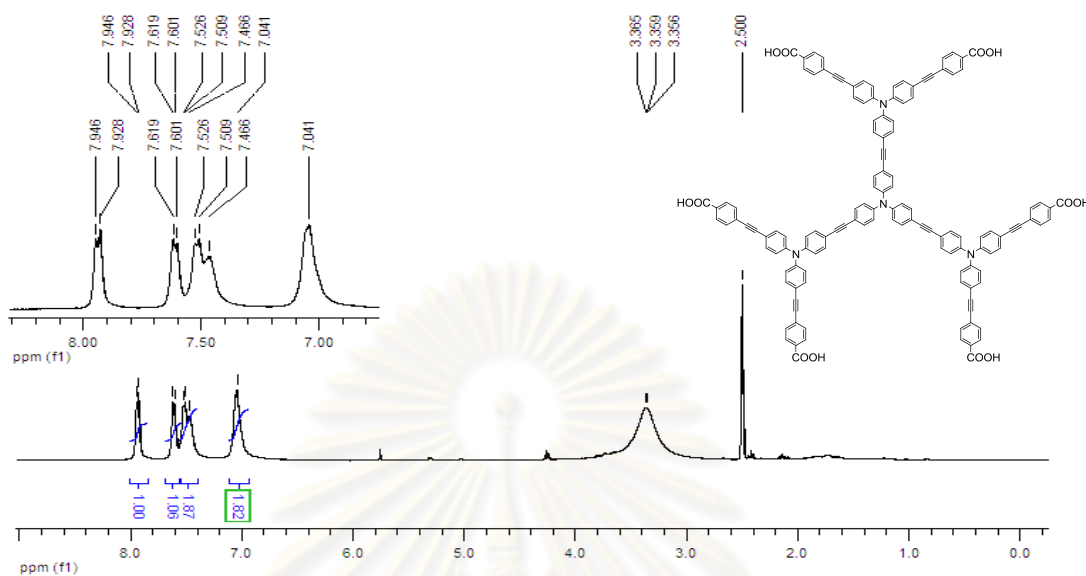


Figure A.43 ^1H NMR of 6C^- in DMSO-d_6 .

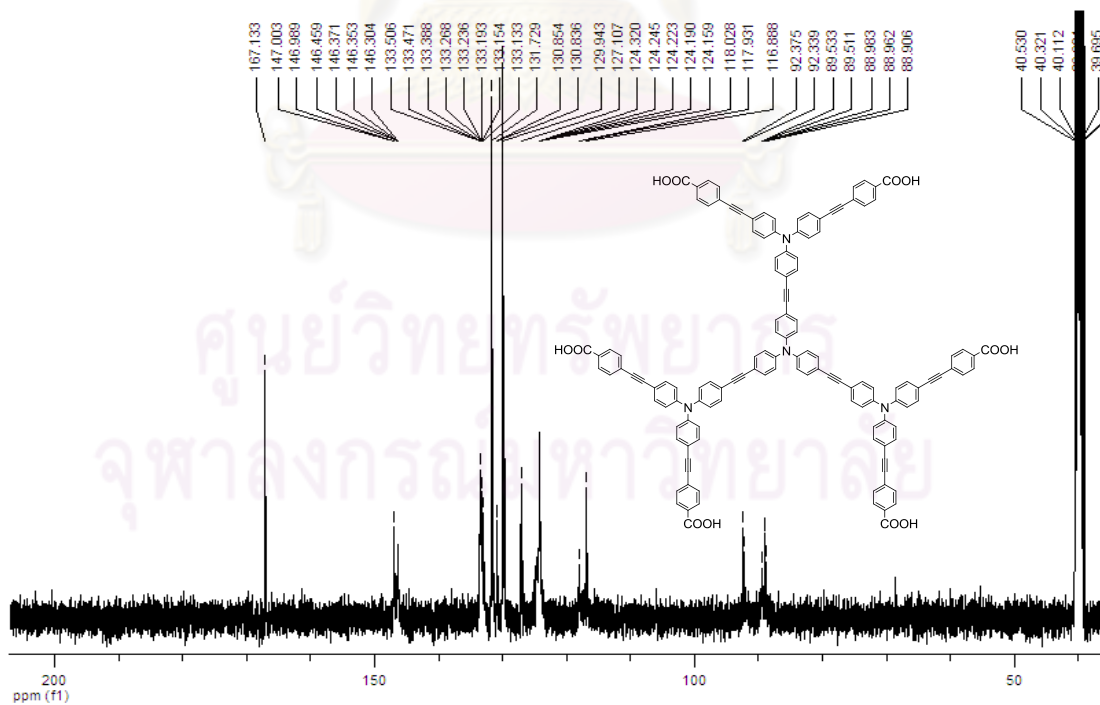


Figure A.44 ^{13}C NMR of 6C^- in DMSO-d_6 .

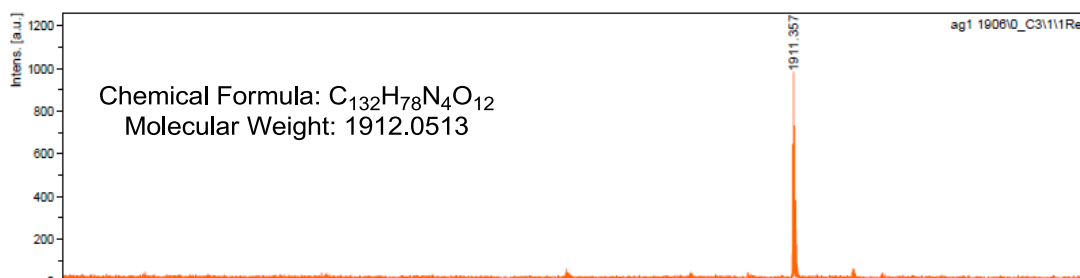


Figure A.45 MALDI-TOF-MS of $6C^-$

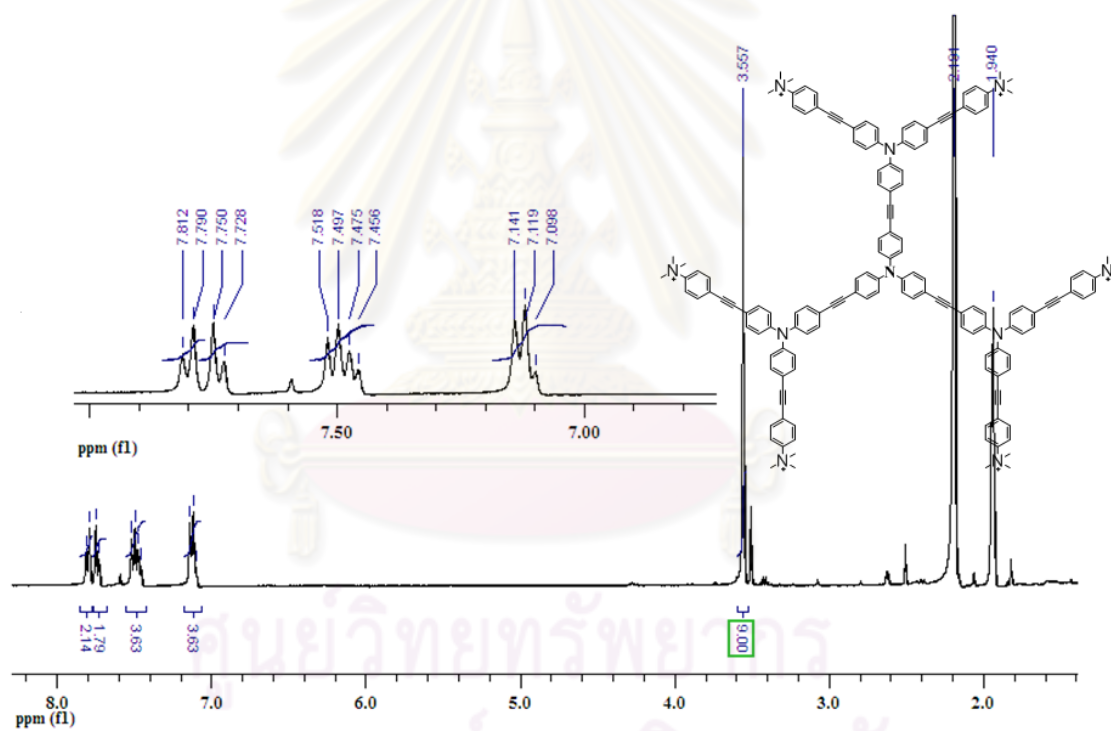


Figure A.46 1H NMR of $6N^+$ in CD_3CN .

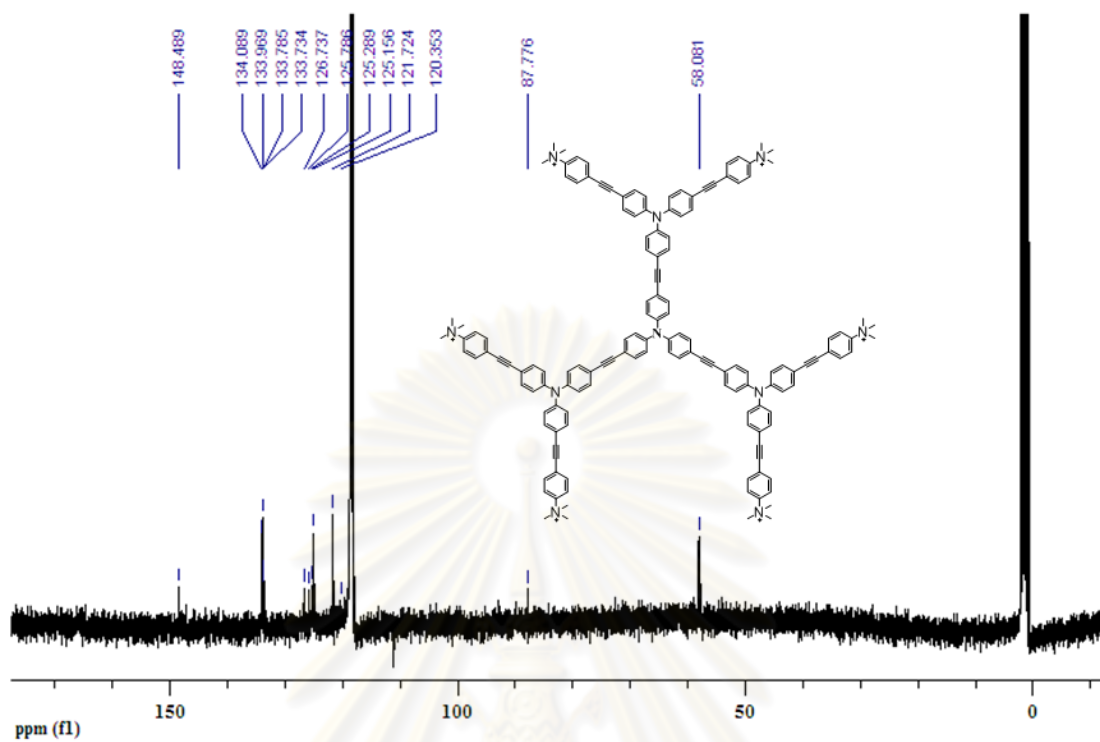


Figure A.47 ^{13}C NMR of 6N^+ in CD_3CN .

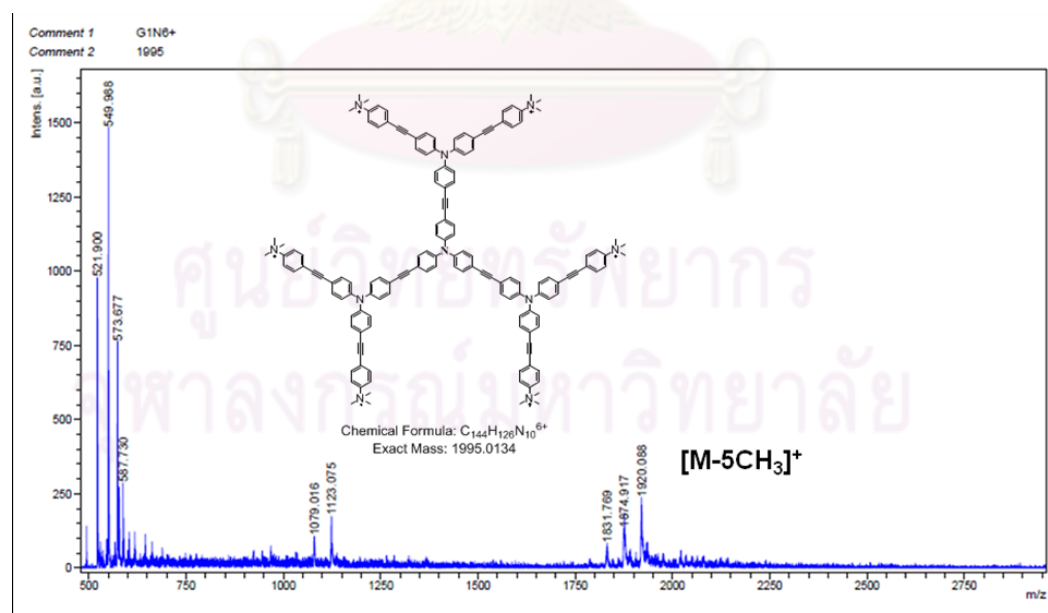


Figure A.48 MALDI-TOF-MS of 6N^+ .

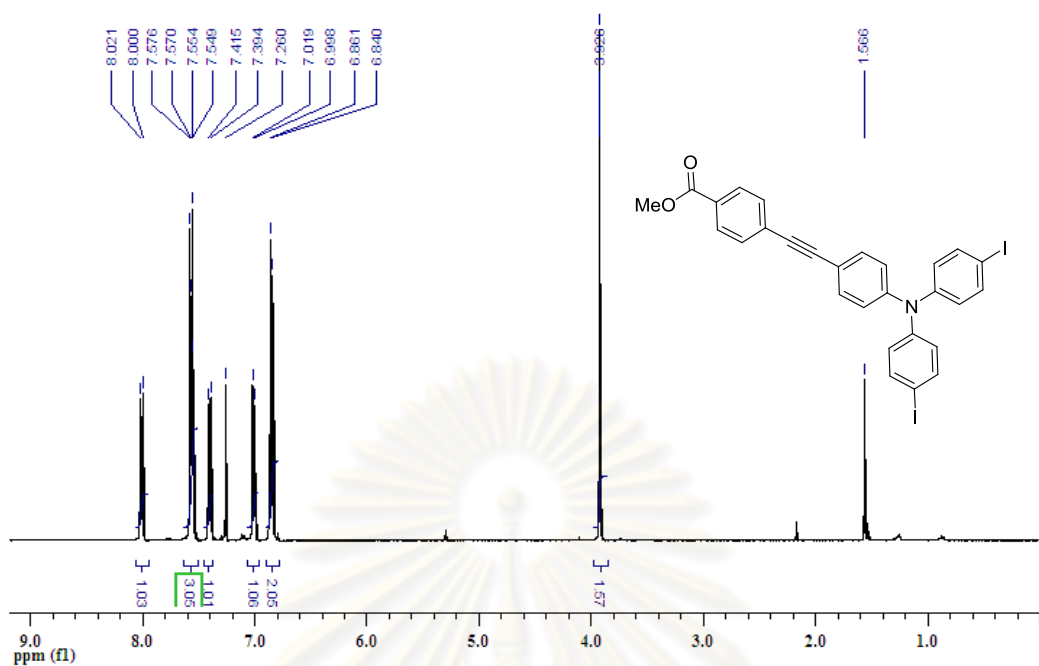


Figure A.49 ¹H NMR of **2IC⁰** in CDCl₃.

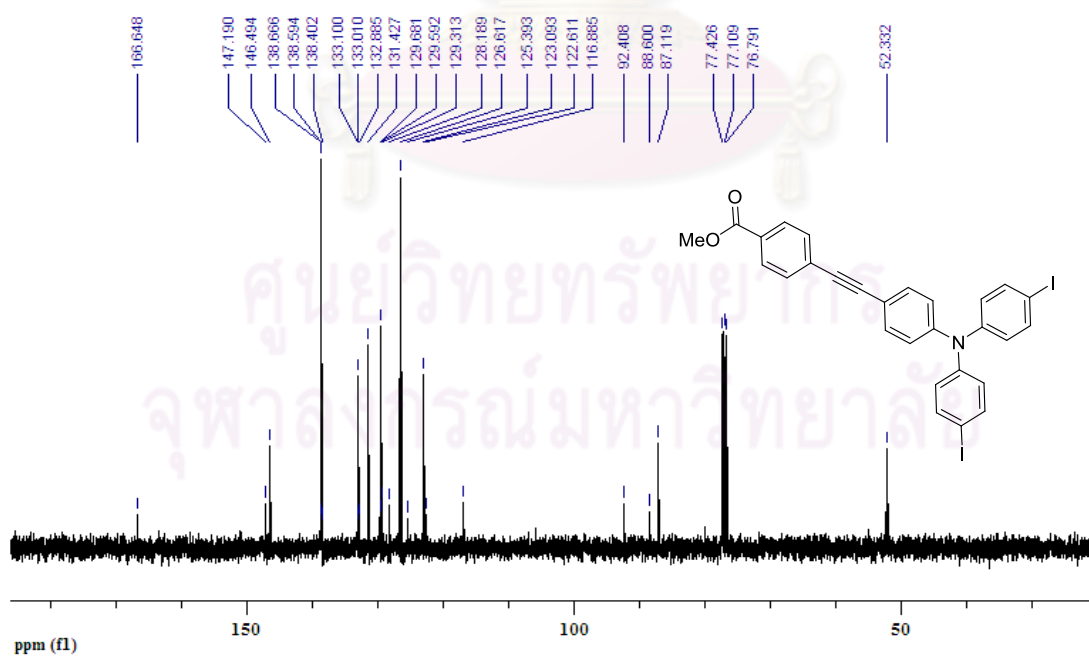


Figure A.50 ¹³C NMR of **2IC⁰** in CDCl₃.

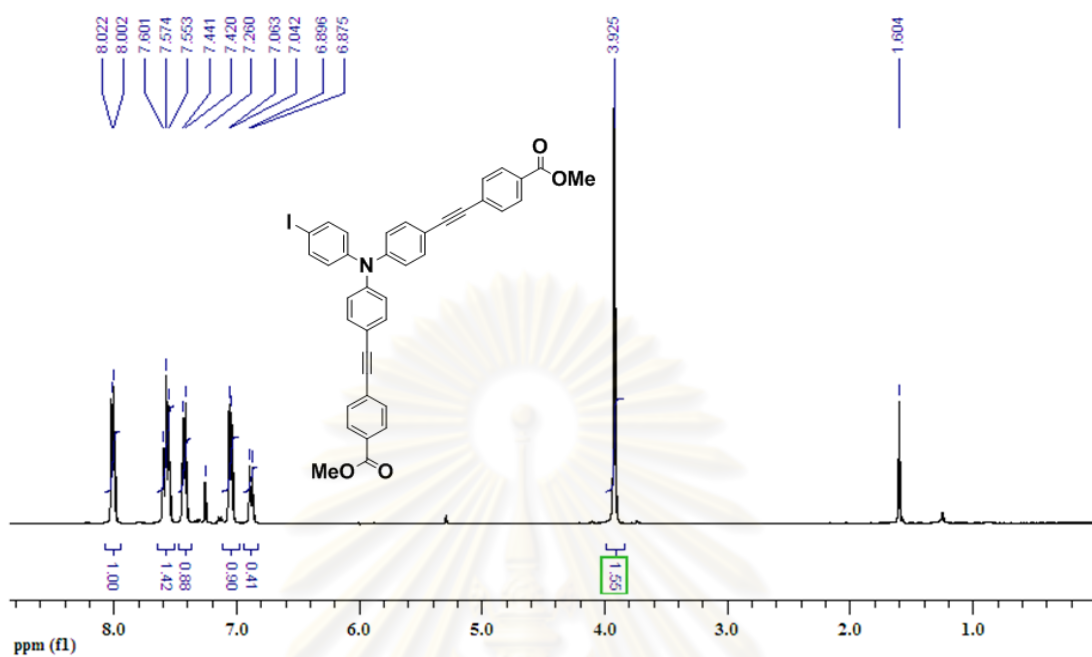


Figure A.51 1H NMR of I_2C^0 in $CDCl_3$.

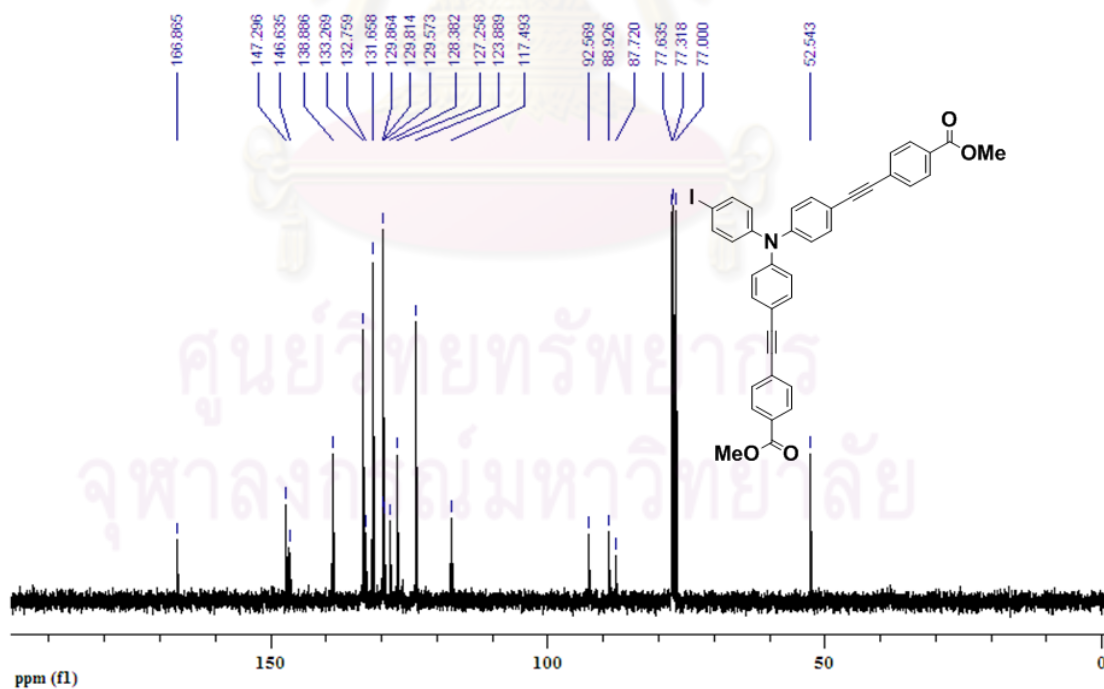


Figure A.52 ^{13}C NMR of I_2C^0 in $CDCl_3$.

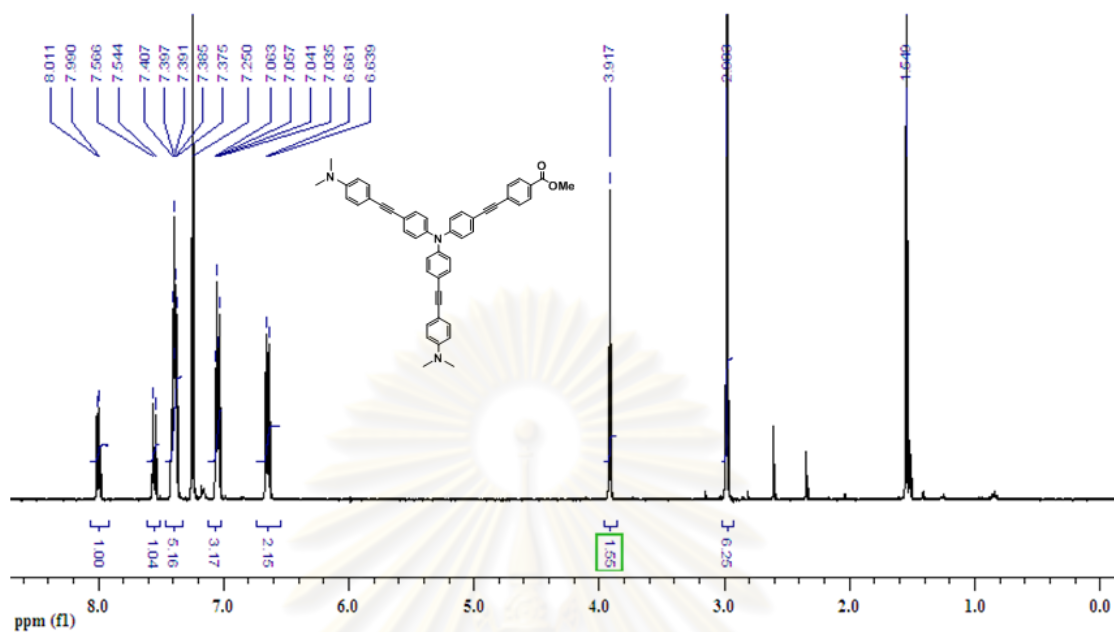


Figure A.53 1H NMR of $C^0_2N^0$ in $CDCl_3$.

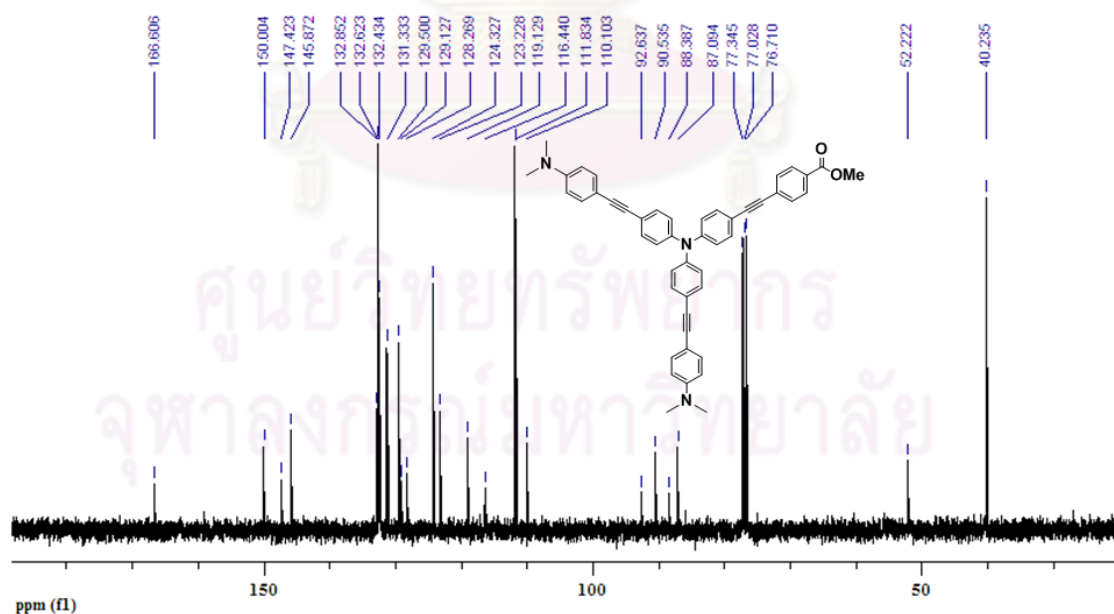


Figure A.54 ^{13}C NMR of $C^0_2N^0$ in $CDCl_3$.

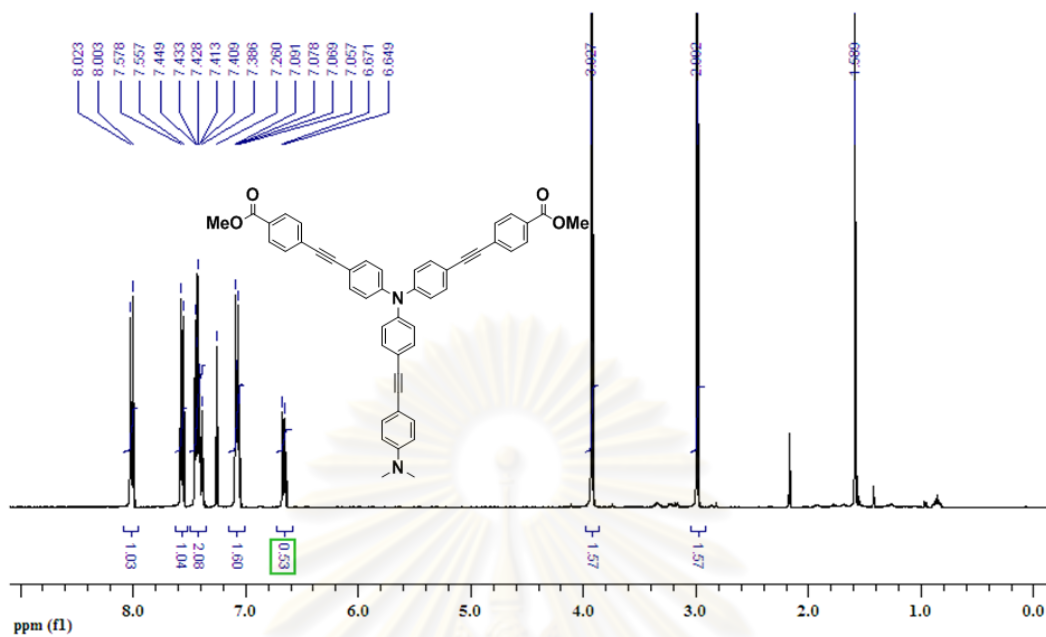


Figure A.55 ^1H NMR of $2\text{C}^0\text{N}^0$ in CDCl_3 .

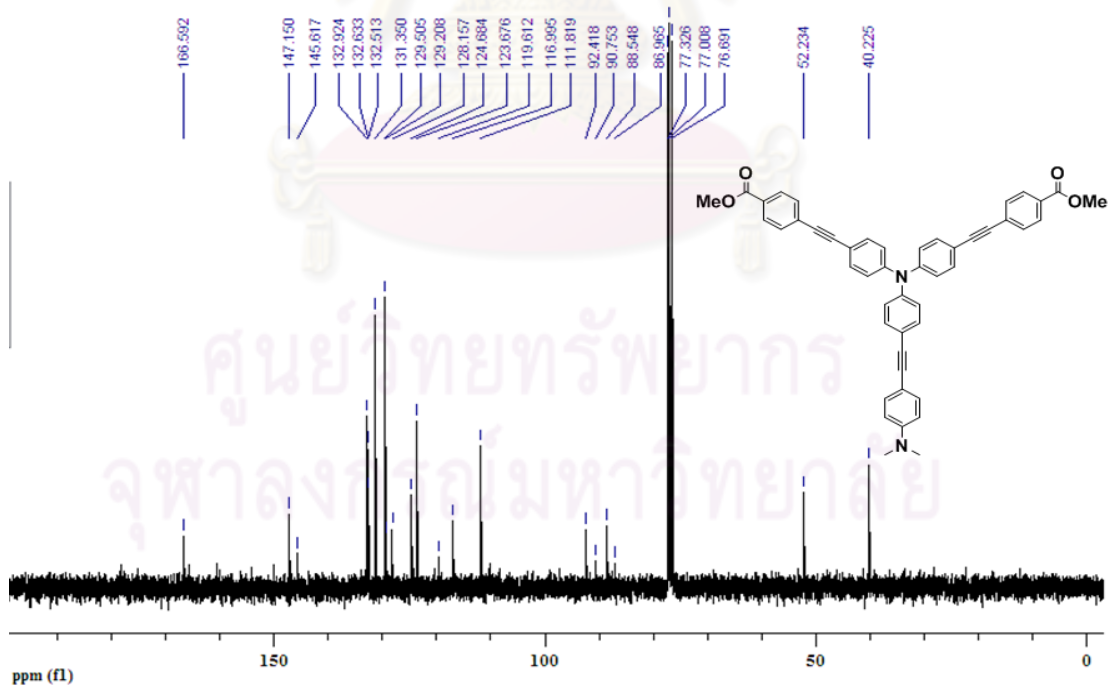


Figure A.56 ^{13}C NMR of $2\text{C}^0\text{N}^0$ in CDCl_3 .

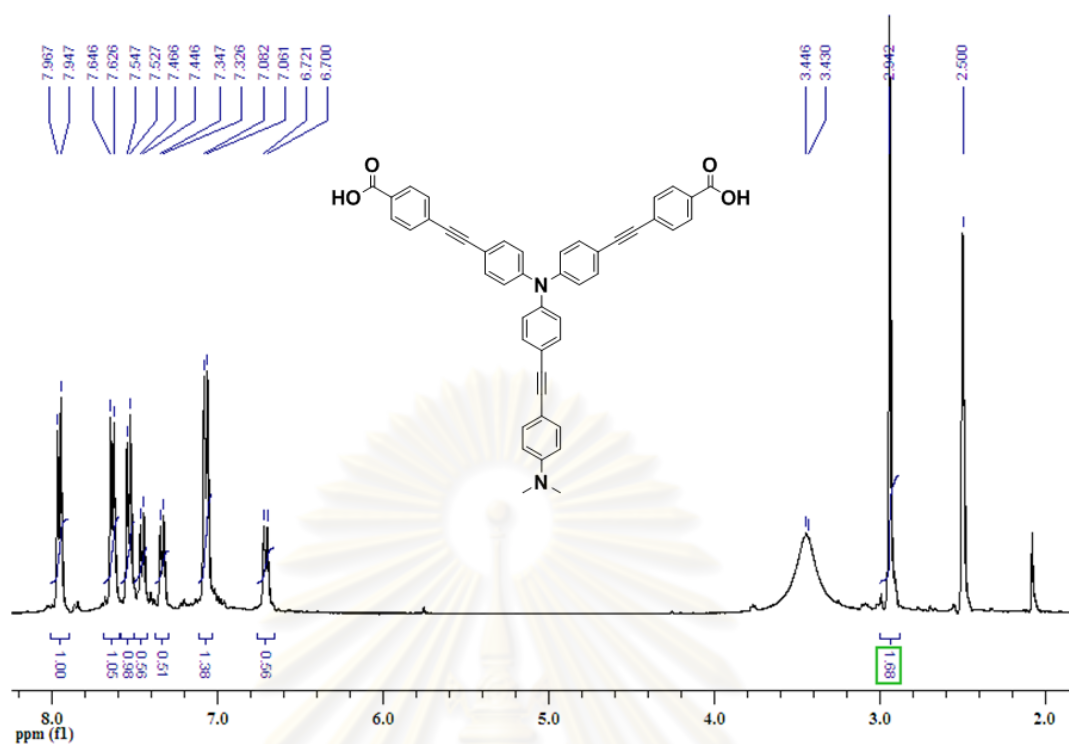


Figure A.57 1H NMR of $2C'N^0$ in $DMSO-d^6$.

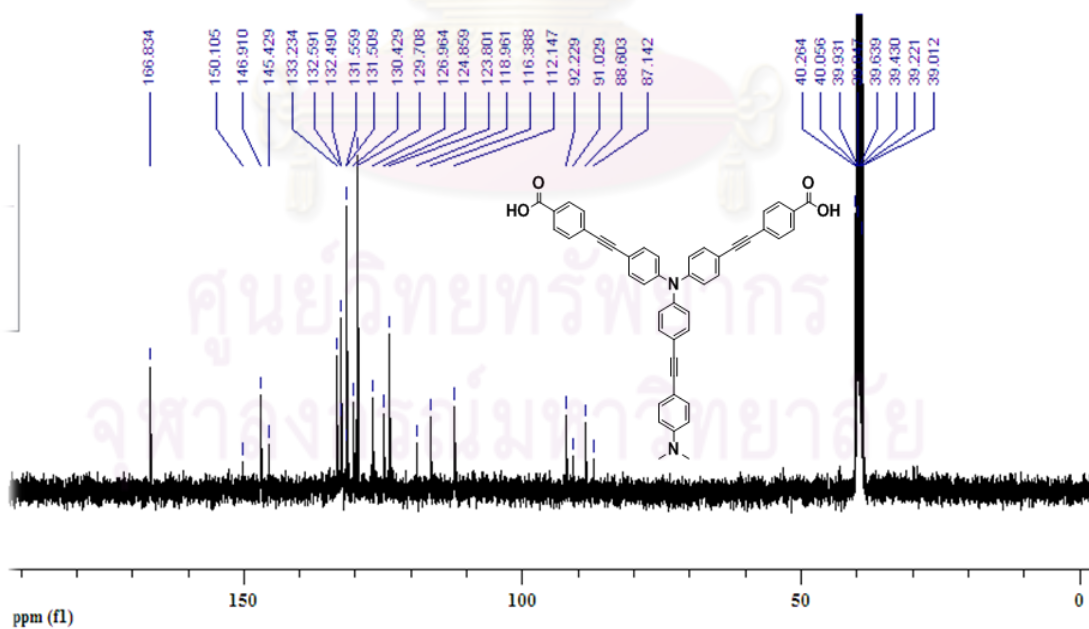


Figure A.58 ^{13}C NMR of $2C'N^0$ in $DMSO-d^6$.

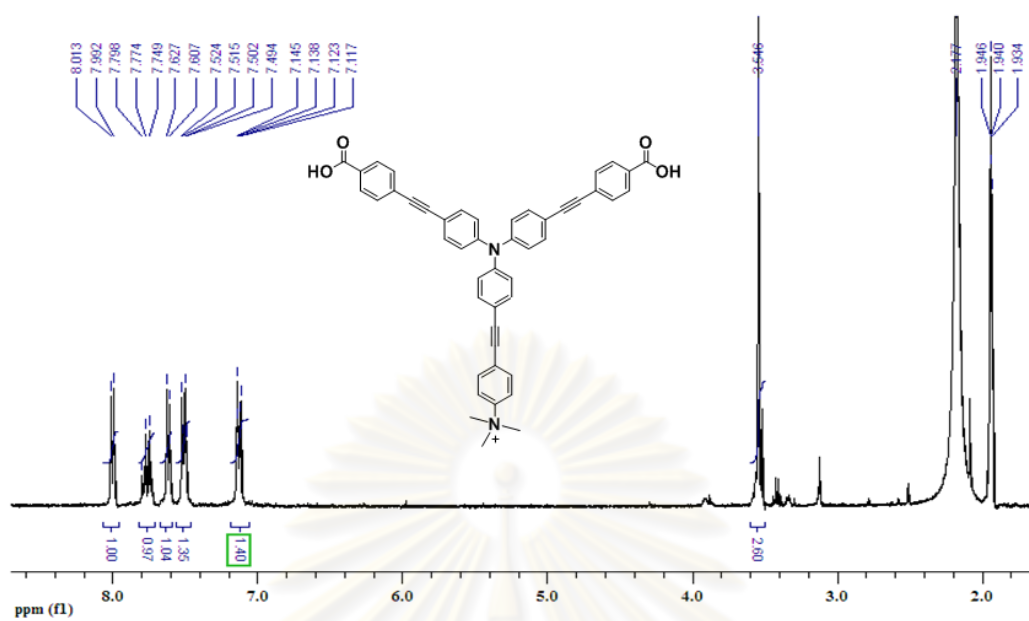


Figure A.59 ^1H NMR of $2\text{C}^+\text{N}^+$ in CD_3CN .

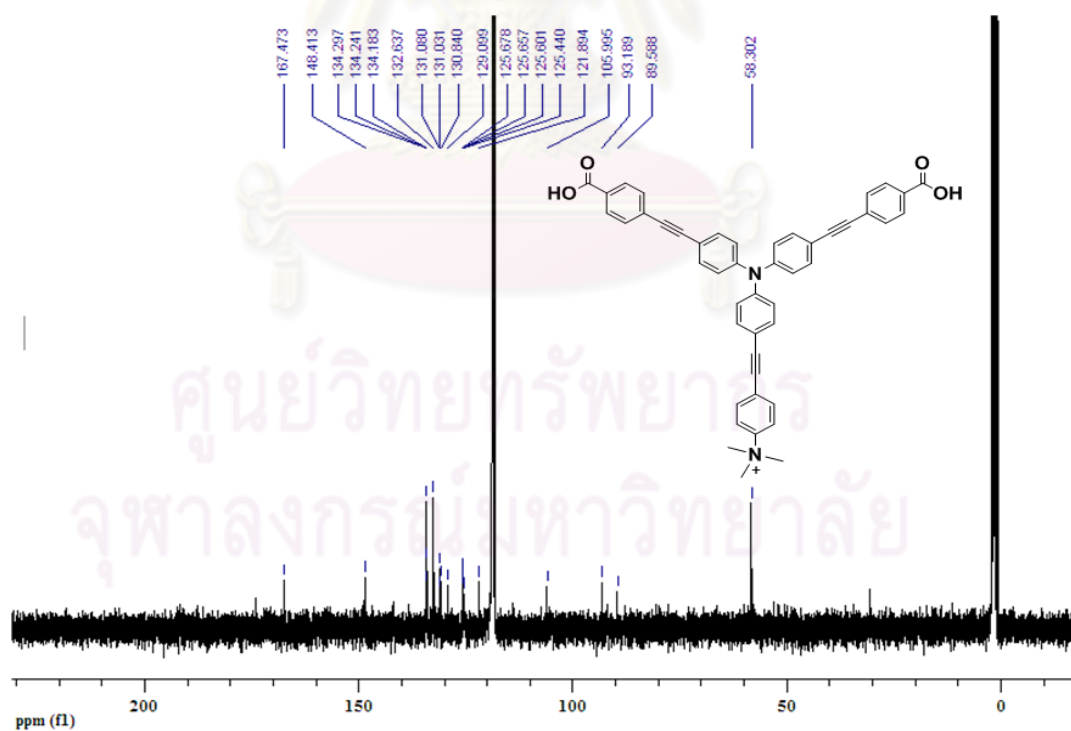


Figure A.60 ^{13}C NMR of $2\text{C}^+\text{N}^+$ in CD_3CN .

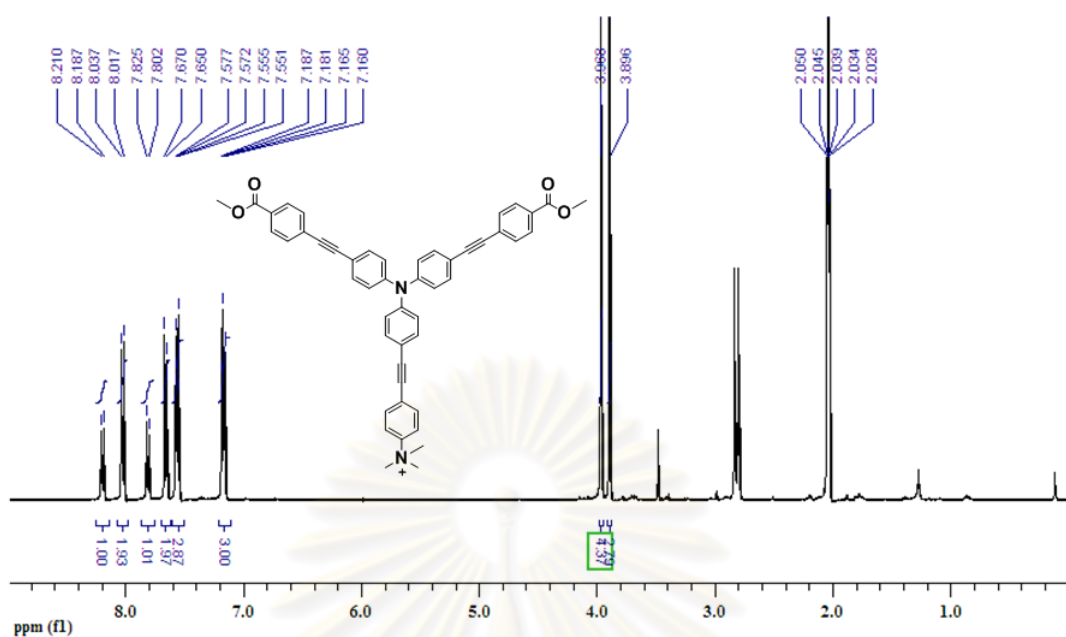


Figure A.61 ^1H NMR of $2\text{C}^0\text{N}^+$ in Acetone- d_6 .

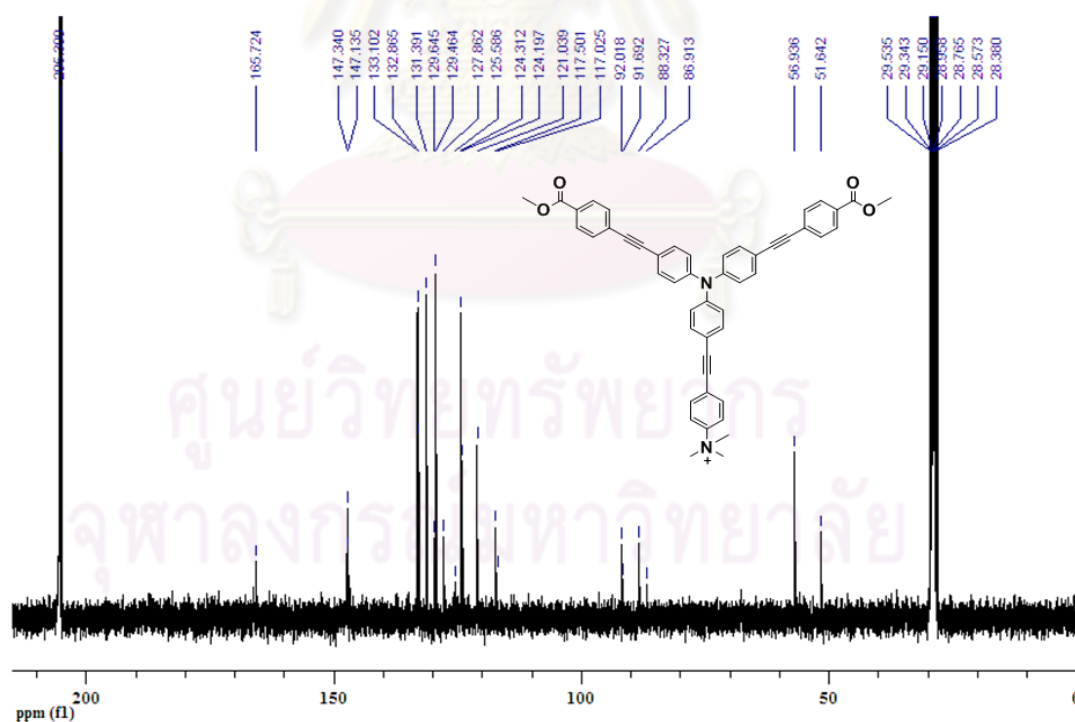


Figure A.62 ^{13}C NMR of $2\text{C}^0\text{N}^+$ in Acetone- d_6 .

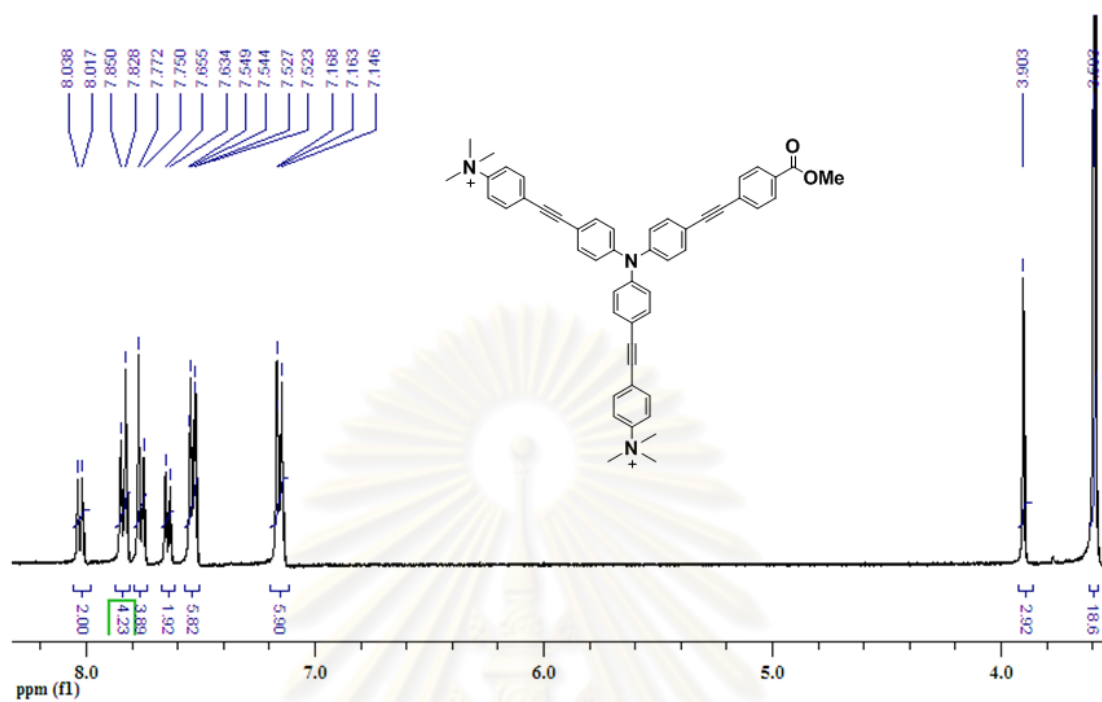


Figure A.63 $^1\text{H-NMR}$ (400 MHz) of $\text{C}^0\text{2N}^+$ in CD_3CN .

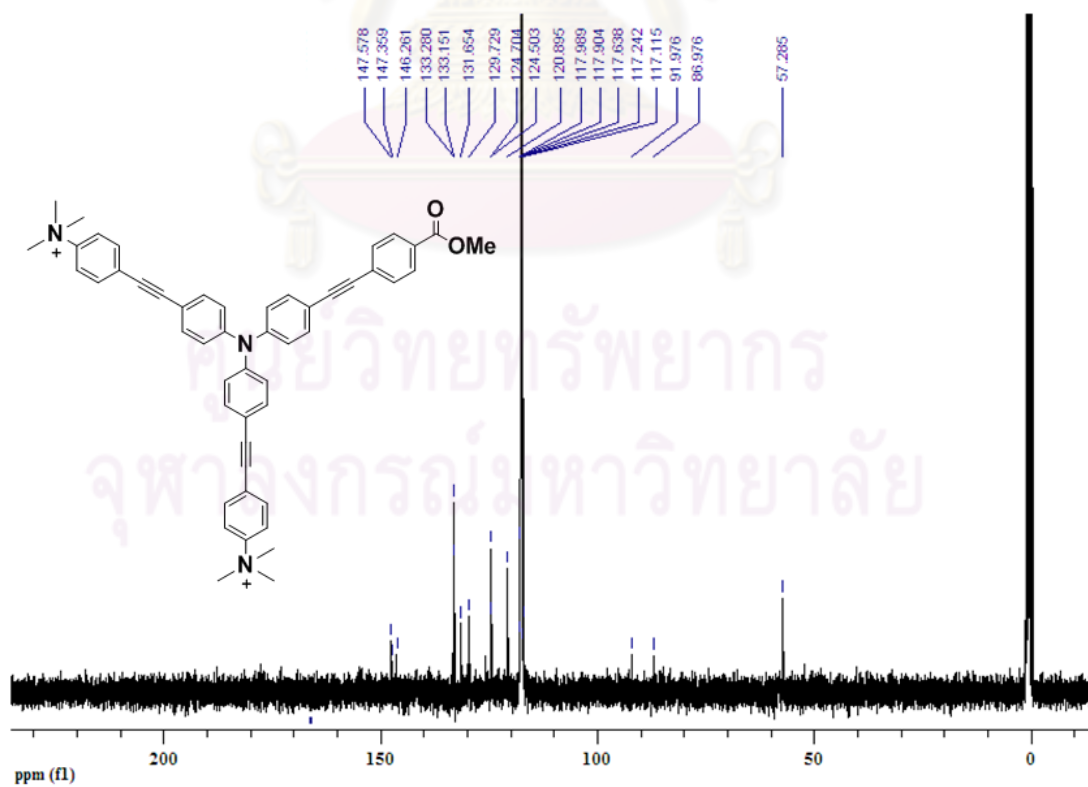


Figure A.64 $^{13}\text{C-NMR}$ (100 MHz) of $\text{C}^0\text{2N}^+$ in CD_3CN .

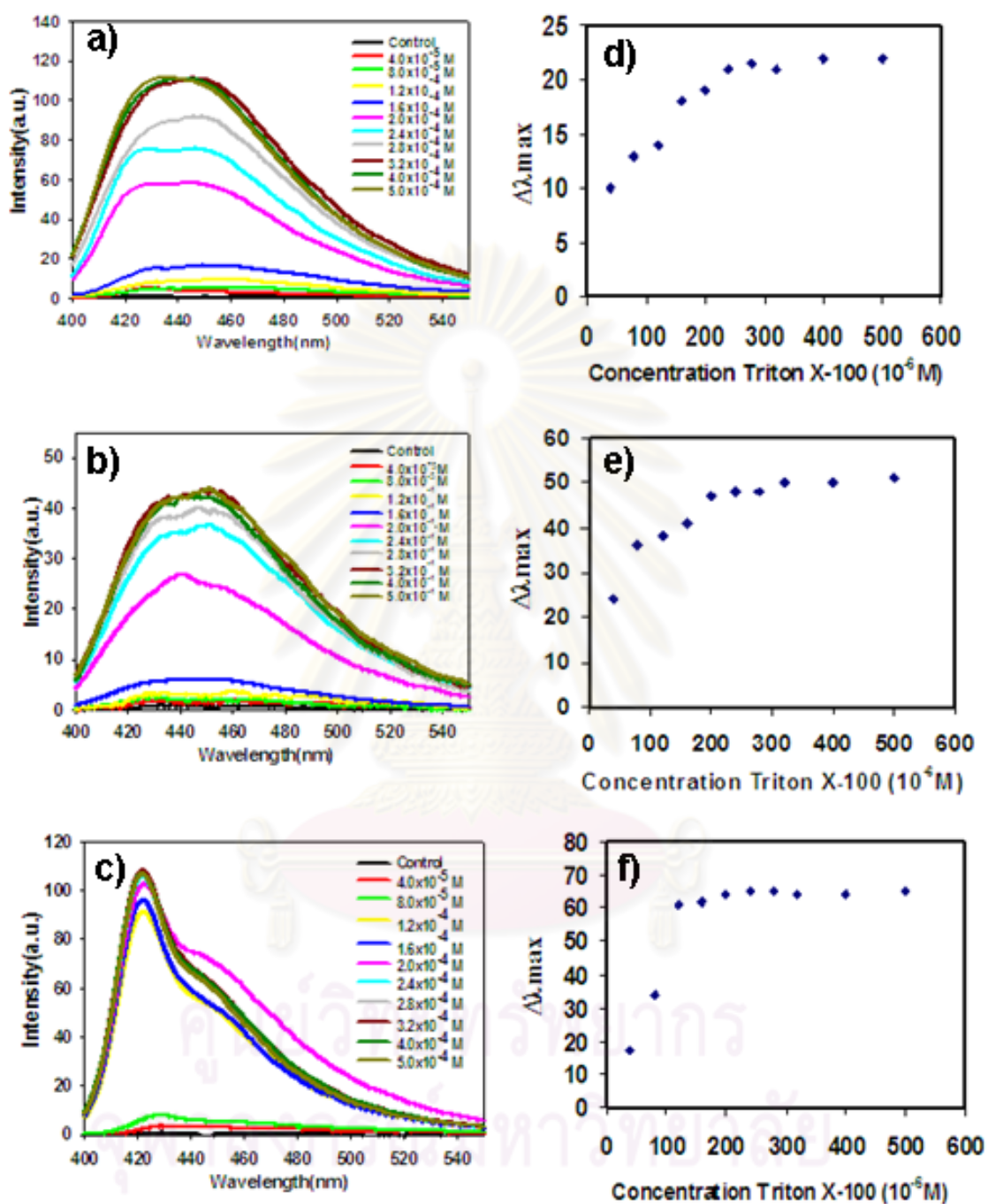


Figure A.65 Emission spectra of fluorophore solutions: a) 3C⁻ (1 μ M) b) 3N⁺ (0.1 μ M) c) 6C⁻ (0.1 μ M) in the presence of increasing concentration of triton X-100. $\Delta\lambda_{\max}$ plots with the concentration of triton X-100 for fluorophores e) 3C⁻ d) 3N⁺ f) 6C⁻.

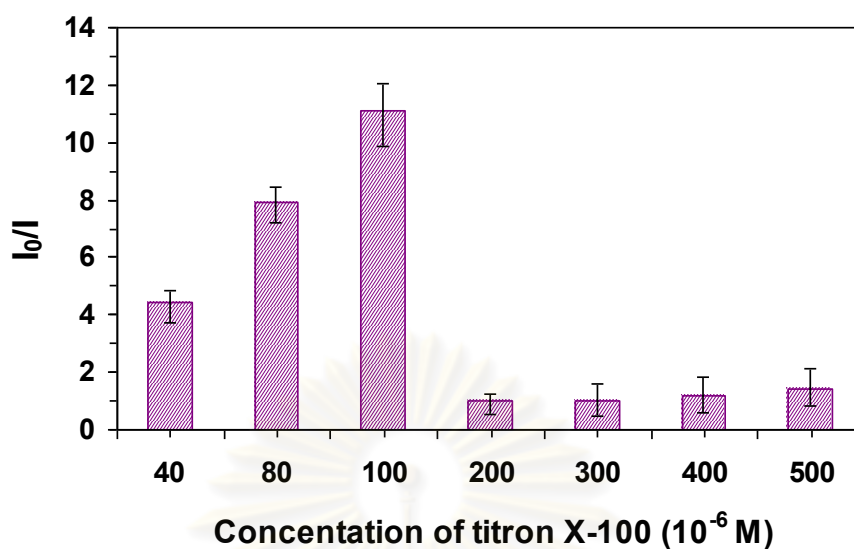
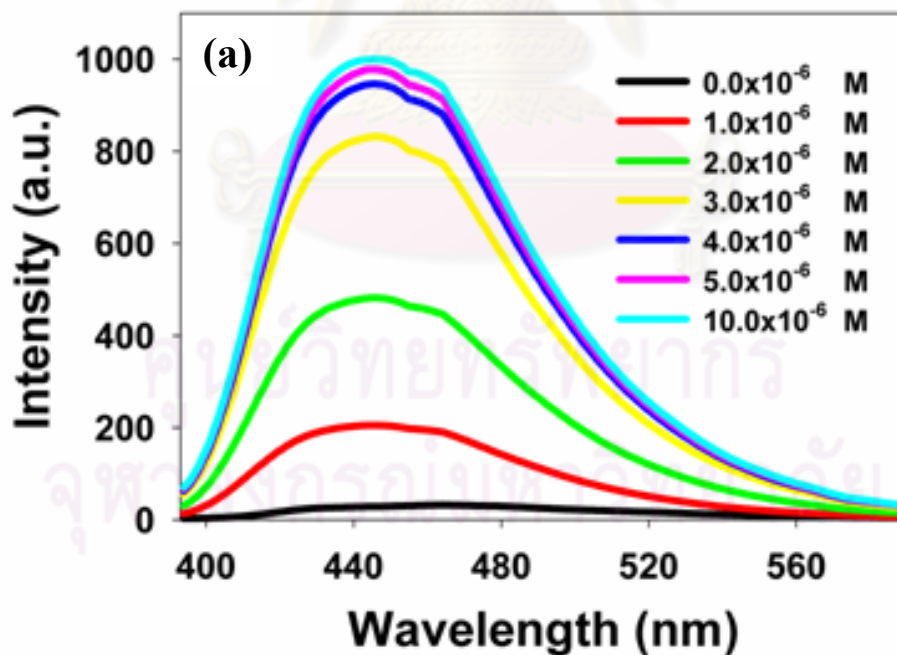


Figure A.66 I_0/I plots of $6C^-$ ($0.1 \mu\text{M}$) with the addition of Hg^{2+} ($40 \mu\text{M}$) in the presence of various concentration of Triton X-100.



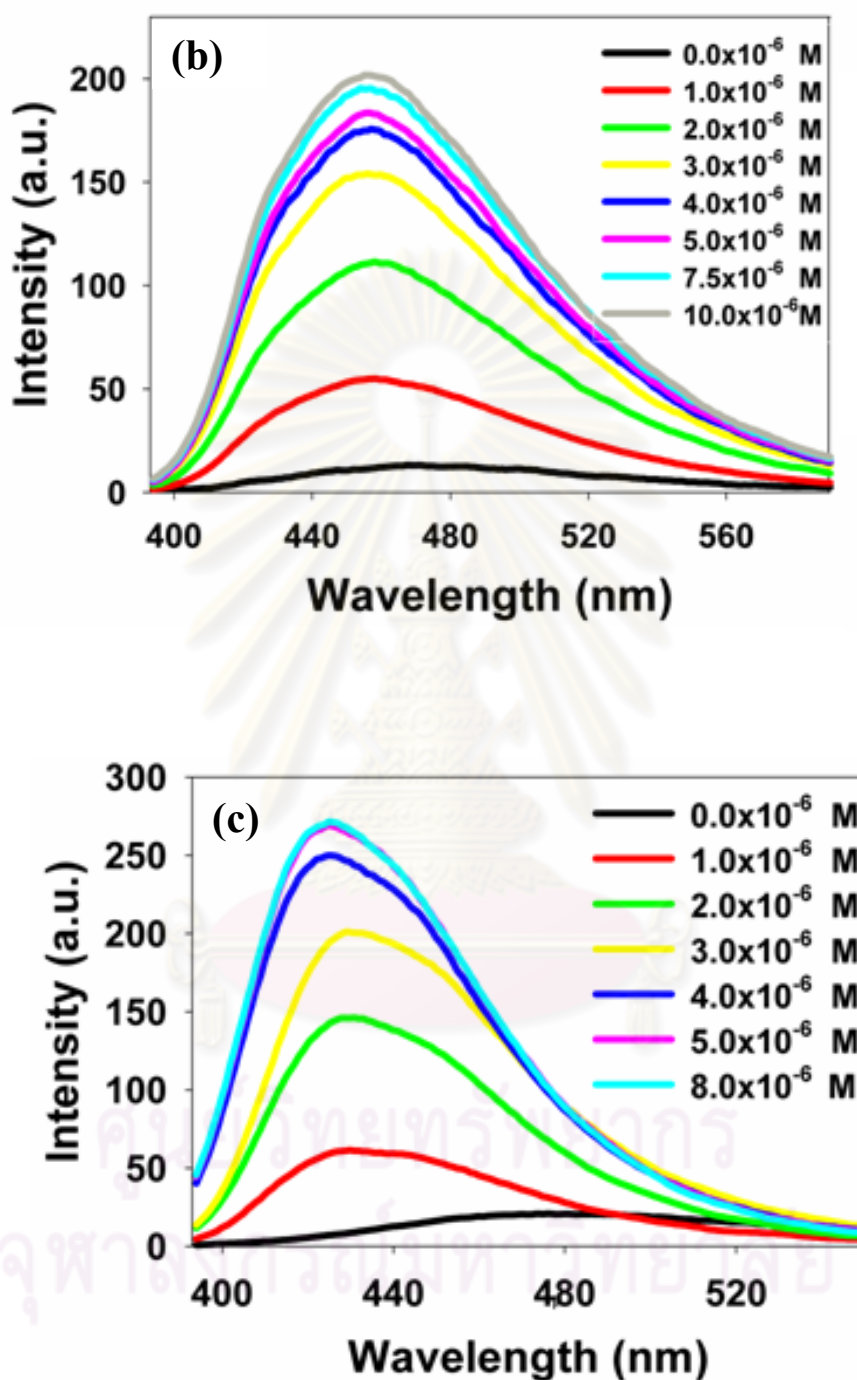


Figure A.67 Emission spectra of (a) 3C^- ($0.2 \mu\text{M}$) (b) C^02N^+ ($0.2 \mu\text{M}$) (c) 3N^+ ($0.2 \mu\text{M}$) upon addition of various concentrations of BSA in 10 mM PBS buffer pH 7.4.

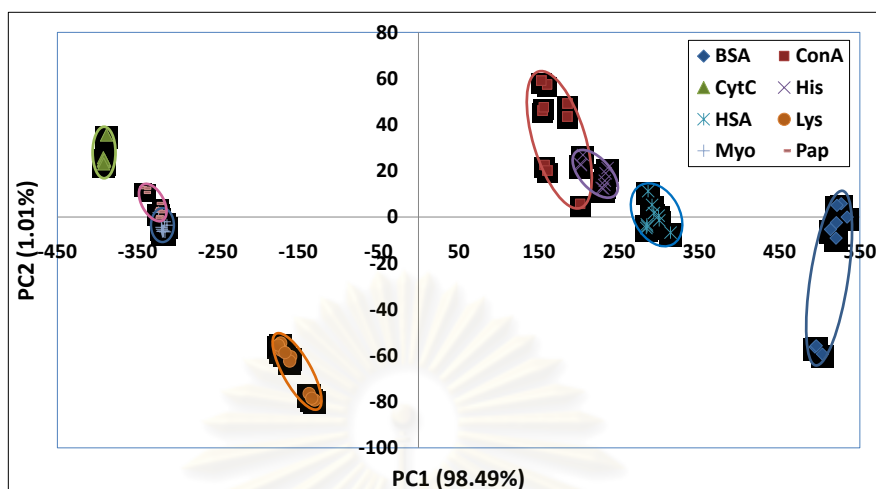


Figure A.68 PCA score plot of ΔI measured at 430 nm obtained from the data set of 5 fluorophores \times 8 protein samples \times 9 replicates.

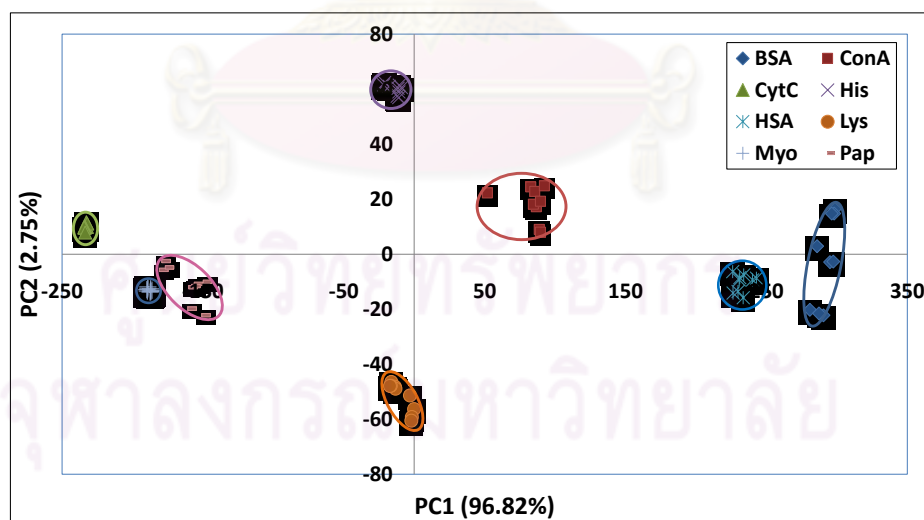


Figure A.69 PCA score plot of ΔI measured at 490 nm obtained from the data set of 5 fluorophores \times 8 protein samples \times 9 replicates.

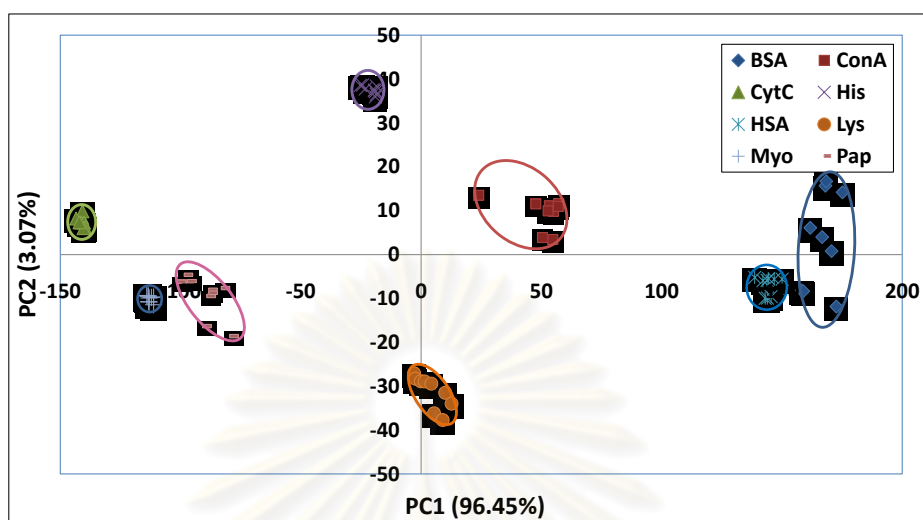


Figure A.70 PCA score plot of ΔI measured at 510 nm obtained from the data set of 5 fluorophores \times 8 protein samples \times 9 replicates.

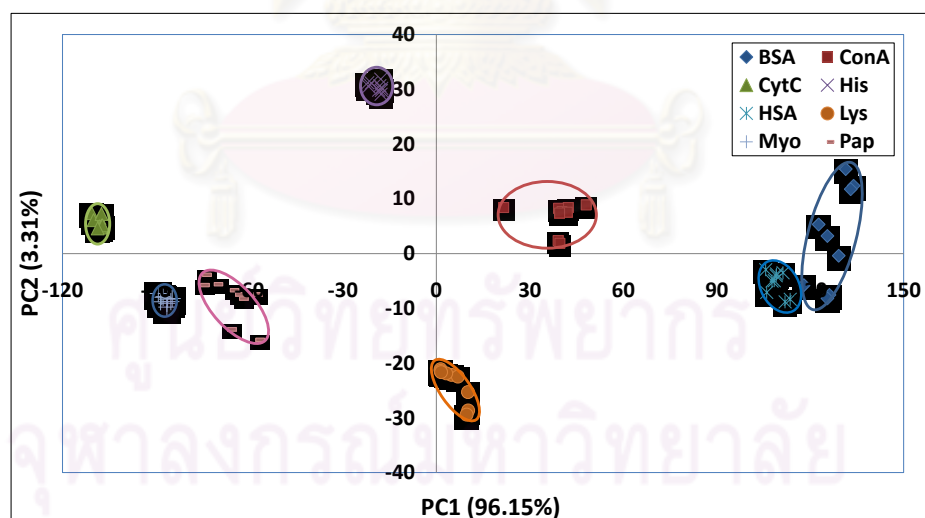


Figure A.71 PCA score plot of ΔI measured at 520 nm obtained from the data set of 5 fluorophores \times 8 protein samples \times 9 replicates.

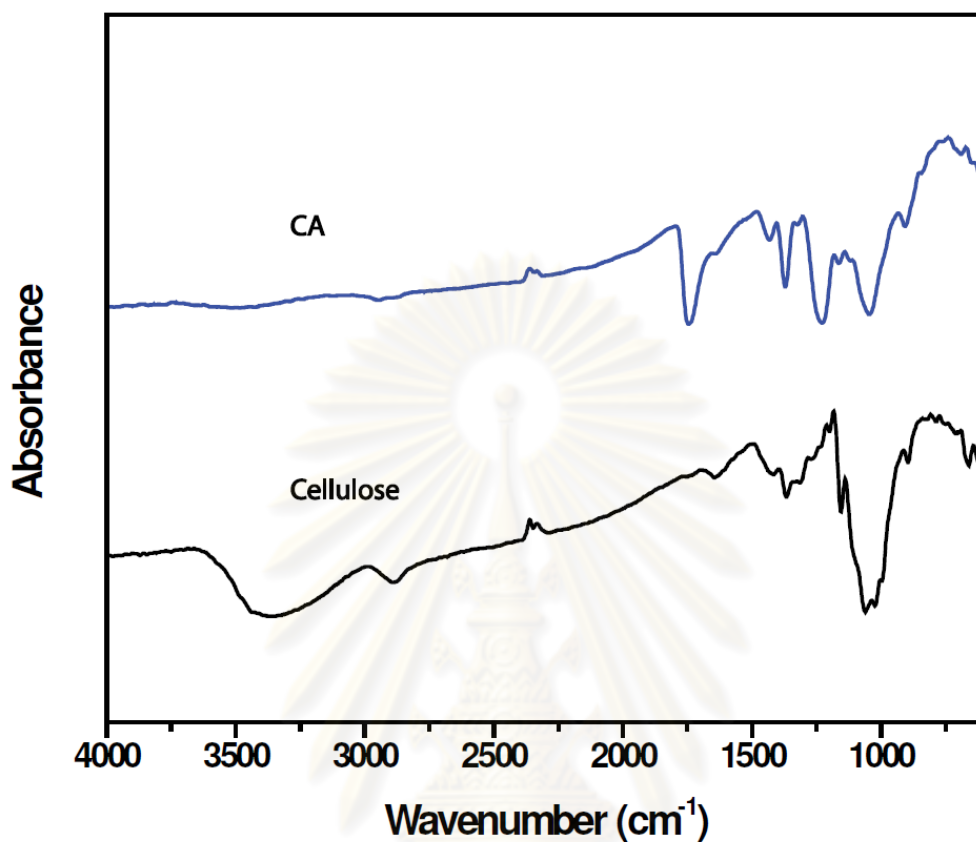


Figure A.72 FT-IR spectra of cellulose acetate (CA) and cellulose fibrous materials (top, before deacytation; bottom, after deacytation). The characteristic adsorption peaks attributed to the vibrations of the acetate group at 1745($\nu_{C=O}$), 1375(ν_{C-CH_3}), and 1235 cm^{-1} (ν_{C-O-C}) disappeared after deacetylation of CA. An adsorption peak at 3500 cm^{-1} (ν_{O-H}) was observed, further indicating successful deacetylation. The FT-IR spectrum obtained after deacytation agrees with that of pure cellulose fibers.

APPENDIX B**REPRINT**

1. **Niamnont, N.**; Siripornnoppakhun, W.; Rashatasakhon, P.; Sukwattanasinitt, M. “A Polyanionic dendritic fluorophore for selective detection of Hg^{2+} in Triton X-100 aqueous media”, *Org. Lett.* **2009**, *11*, 2768-2771.
2. Davis, W. B.; **Niamnont, N.**; Hare, C. D.; Sukwattanasinitt, M.; Cheng, Q. “Nanofibers doped with dendritic fluorophores for protein detection”, *ACS Appl. Mater. Interfaces*, **2010**, *2*, 1798–1803.
3. **Niamnont, N.**; Mungkarndee, R.; Rashatasakhon, P.; Techakriengkrai, I.; Sukwattanasinitt, M. “Protein discrimination by fluorescent sensor array constituted of variously charged dendritic phenylene-ethynylene fluorophores”, *Biosens. Bioelectron.*, **2010**, *26*, 863-867.



ศูนย์วิทยทรัพยากร
จุฬาลงกรณ์มหาวิทยาลัย

A Polyanionic Dendritic Fluorophore for Selective Detection of Hg^{2+} in Triton X-100 Aqueous Media

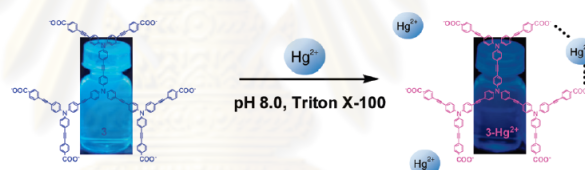
Nakorn Niamnont,[†] Warathip Siripornnoppakhun,[†] Paitoon Rashatasakhon,[†] and Mongkol Sukwattanasinitt^{*,†,‡}

Organic Synthesis Research Unit, Department of Chemistry, Faculty of Science, and Center for Petroleum, Petrochemicals and Advanced Materials, Chulalongkorn University, Bangkok 10330, Thailand

smongkol@chula.ac.th

Received April 29, 2009

ABSTRACT



A series of water-soluble fluorescent dendritic compounds composed of phenylene-ethynylene repeating units and anionic carboxylate or cationic ammonium peripheral groups were synthesized. The first generation fluorescent dendrimer containing nine phenylene-ethynylene units and six carboxylate peripheral groups exhibited a highly selective fluorescence quenching by Hg^{2+} ions. The Stern–Volmer constant (K_{sv}) was $33,700 \text{ M}^{-1}$ in aqueous media in the presence of Triton X-100 surfactant.

Mercury is one of the most toxic environmental pollutants generated from industrial sources. The most abundant ionic form of this element is the mercuric ion (Hg^{2+}), which can be accumulated in the organs of human or animal bodies through the food chain.¹ Inorganic mercury has been reported to produce harmful effects at a concentration of 5 ppb.² Development of highly sensitive and selective Hg^{2+} sensors that can provide direct determinations of the amount of Hg^{2+} in aqueous media is therefore of great interest.³ Chemosensors for Hg^{2+} have been progressively improved using

redox,⁴ chromogenic,⁵ or fluorogenic⁶ changes as the means of detection.

Fluorescence-based methodologies have attracted much interest due to their intrinsic sensitivity and selectivity.⁷ Considerable efforts have been devoted to the design of fluorescent compounds to be used as sensors for mercury. However, their poor solubility in water and low fluorescence quantum yield due to aggregation have limited the satisfactory application of these compounds in aqueous media.⁸

[†] Department of Chemistry, Faculty of Science.

[‡] Center for Petroleum, Petrochemicals and Advanced Materials.

(1) (a) Stern, A. H.; Hudson, R. J. M.; Shade, C. W.; Ekino, S.; Ninomiya, T.; Susa, M.; Harris, H. H.; Pickering, I. J.; George, G. N. *Science* **2004**, *303*, 763–766. (b) Nendza, M.; Herbst, T.; Kussatz, C.; Gies, A. *Chemosphere* **1997**, *35*, 1875–1885.

(2) Boening, D. W. *Chemosphere* **2000**, *40*, 1335–1351.

(3) Darbha, G. K.; Singh, A. K.; Rai, U. S.; Yu, E.; Yu, H.; Ra, P. C. *J. Am. Chem. Soc.* **2008**, *130*, 8038–8043.

(4) Caballero, A.; Martínez, R.; Lloveras, V.; Ratera, I.; Vidal-Gancedo, J.; Wurst, K.; Tárraga, A.; Molina, P.; Veciana, J. *J. Am. Chem. Soc.* **2005**, *127*, 15666–15667.

(5) (a) Zhang, X.; Shiraiishi, Y.; Hirai, T. *Org. Lett.* **2007**, *9*, 5039–5042. (b) Caballero, A.; Espinosa, A.; Tárraga, A.; Molina, P. *J. Org. Chem.* **2008**, *73*, 5489–5497.

(6) (a) Wang, J. B.; Qian, X. H. *Org. Lett.* **2006**, *8*, 3721–3724. (b) Zhao, Y.; Zhong, Z. Q. *Org. Lett.* **2006**, *8*, 4715–4717. (c) Zhao, Y.; Zhong, Z. *J. Am. Chem. Soc.* **2006**, *128*, 9988–9989. (d) Huang, C.-C.; Chang, H.-T. *Anal. Chem.* **2006**, *78*, 8332–8338. (e) Huang, C.-C.; Yang, Z.; Lee, K.-H.; Chang, H.-T. *Angew. Chem., Int. Ed.* **2007**, *46*, 6824–6828. (f) Nolan, E. M.; Lippard, S. J. *Chem. Rev.* **2008**, *108*, 3443–3480. (g) Liu, C. W.; Huang, C. C.; Chang, H. T. *Langmuir* **2008**, *24*, 8346–8350.

(7) (a) De Silva, A. P.; Gunaratne, H. Q. N.; Gunnlaugsson, T.; Huxley, A. J. M.; McCoy, C. P.; Rademacher, J. T.; Rice, T. E. *Chem. Rev.* **1997**, *97*, 1515–1566. (b) Avirah, R. R.; Jyothish, K.; Ramaiah, D. *Org. Lett.* **2007**, *9*, 1133–1136.

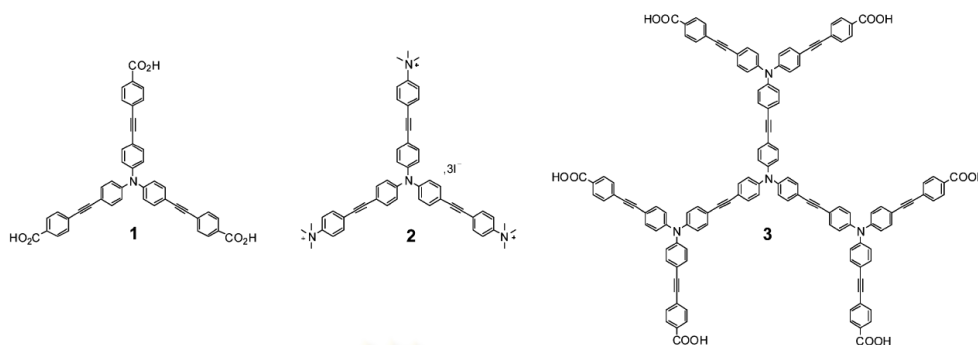


Figure 1. Structures of dendritic molecules **1**, **2**, and **3**.

Several methods have been used to prevent aggregation and increase quantum efficiencies, for example, the use of polyelectrolytes or surfactants.

Conjugated polyelectrolytes have been applied to the detection of metals due to their efficient static quenching properties with quenchers.⁹ In some recent studies, surfactants were also used to enhance the fluorescence quantum yields of hydrophobic conjugated polymers containing hydrophilic side chains.¹⁰ The dominant hydrophobic interactions between surfactants and fluorophores can significantly reduce the aggregation. An application of surfactants for amplification of the quenching effect between the fluorescent polymers and quenchers has also been reported.¹¹

The fluorescent linear polymers poly(phenylene-ethynylenes) substituted by carboxylate groups have been reported to exhibit a quenching effect by Hg^{2+} in aqueous media in the absence and presence of avidin, with Stern–Volmer constant (K_{sv}) values of 10^4 and 10^5 M^{-1} , respectively.¹² Despite offering high sensitivity, the unpredictable secondary and tertiary structures in solution, due to a wide number of repeating fluorophores and random molecular conformations in linear conjugated polymers, can lead to inconsistent quenching effects and inexplicable behaviors.

In comparison with linear polymers, the numbers of fluorophore units in dendrimers can be controlled by a stepwise synthesis. This should reflect in the more predictable fluorescence property and other structure-related behaviors

of dendritic molecules. We thus decided to synthesize dendritic compounds **1–3** (Figure 1) and study their fluorescent sensing applications.

Diphenylacetylene is selected as the repeating fluorescent unit for its known high fluorescence quantum yield and structural rigidity. To make the dendritic compounds water-soluble, carboxyl or quaternary ammonium groups have been installed as the peripheral groups. The compounds were synthesized by a convergent approach as outlined in Scheme 1. The reactive core, 4,4',4''-triiodotriphenylamine **4**, was prepared from the iodination of triphenylamine using benzyltrimethylammonium iododichloride ($\text{BnMe}_3\text{-ICl}_2$).¹³ The peripheral building blocks, methyl 4-ethynyl benzoate **5** and *N,N*-dimethyl-4-ethynylaniline **6**, were obtained through the Sonogashira coupling¹⁴ of trimethylsilylacetylene with the corresponding aryl iodide and a subsequent base-catalyzed desilylation. With the required building blocks in hands, we proceeded with the Sonogashira coupling between **4** and **5** followed by the hydrolysis of triester **7** to afford ionizable fluorophore **1**. Similarly, the reaction between **4** and **6** gave rise to the triamine **8**, which was treated with an excess of MeI to provide the polycationic fluorescent compound **2**. In order to obtain the first generation fluorescent dendrimer **3**, we carried out a reaction of the core **4** with 1 molar equiv of trimethylsilylacetylene to obtain the branch building blocks **9**. The Sonogashira coupling of **9** with **5** followed by desilylation gave the dendron **10**, which was coupled with **4** to afford hexaester **11**. The hydrolysis of **11** eventually afforded first generation fluorescent dendrimer **3** in moderate yield.¹⁵

The effects of surfactants on the photophysical properties of **1–3** were studied. Without the surfactant, compounds **1–3** displayed absorption peaks around 370–375 nm. In the presence of the surfactant Triton X-100, these bands were slightly red-shifted to 379–383 nm. The spectral shifts

(8) Zhu, X.-J.; Fu, S.-T.; Wong, W.-K.; Guo, J.-P.; Wong, W.-Y. *Angew. Chem., Int. Ed.* **2006**, *45*, 3150–3154.

(9) McQuade, D. T.; Pullen, A. E.; Swager, T. M. *Chem. Rev.* **2000**, *100*, 2537. Thomas, S. W.; Joly, G. D.; Swager, T. M. *Chem. Rev.* **2007**, *107*, 1339–1386.

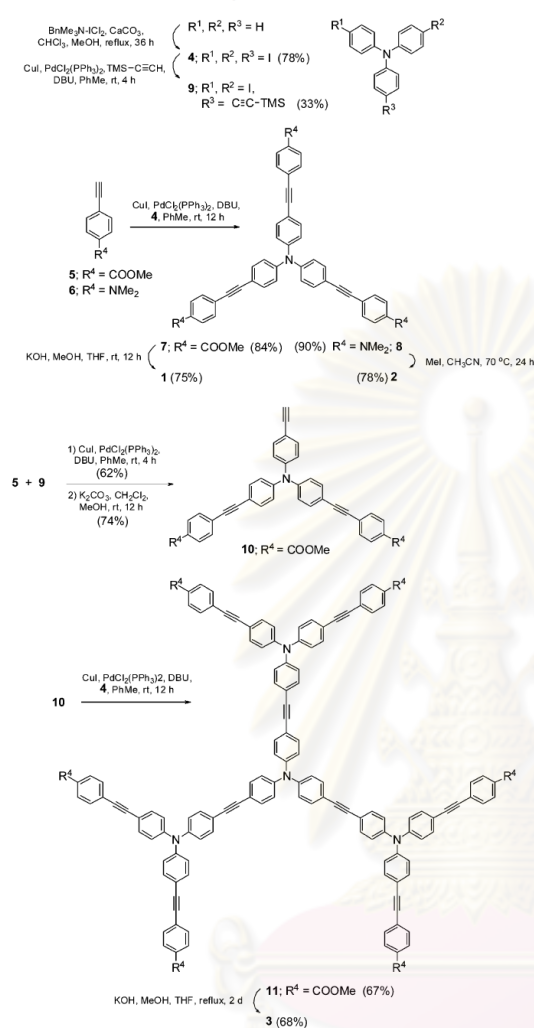
(10) (a) Chen, L. H.; Xu, S.; McBranch, D.; Whitten, D. *J. Am. Chem. Soc.* **2000**, *122*, 9302–9303. (b) Gaylord, B. S.; Heeger, A. J.; Bazan, G. C. *J. Am. Chem. Soc.* **2003**, *125*, 896–900. (c) Burrows, H. D.; Lobo, V. M. M.; Pina, J.; Ramos, M. L.; Seixas de Melo, J.; Valente, A. J. M.; Tapia, M. J.; Pradhan, S.; Scherf, U. *Macromolecules* **2004**, *37*, 7425–7427. (d) Kaur, P.; Yue, H.; Wu, M.; Liu, M.; Treece, J.; Waldeck, D. H.; Xue, C.; Liu, H. *J. Phys. Chem. B* **2007**, *111*, 8589–8596. (e) Pu, K.-Y.; Pan, S. Y.-H.; Liu, B. *J. Phys. Chem. B* **2008**, *112*, 9295–9300.

(11) Dalvi-Malhotra, J.; Chen, L. *J. Phys. Chem. B* **2005**, *109*, 3873–3878.

(12) (a) Kim, I.-B.; Dunkhorst, A.; Gilbert, J.; Bunz, U. H. F. *Macromolecules* **2005**, *38*, 4560–4562. (b) Kim, I.-B.; Bunz, U. H. F. *J. Am. Chem. Soc.* **2006**, *128*, 2818–2819. (c) Kim, I.-B.; Phillips, R.; Bunz, U. H. F. *Macromolecules* **2007**, *40*, 814–817.

(13) Kajigaeshi, S.; Kakinami, T.; Moriwaki, M.; Fujisaki, S.; Maeno, K.; Okamoto, T. *Synthesis* **1988**, 545–546.

(14) (a) Devadoss, C.; Bharathi, P.; Moore, J. S. *J. Am. Chem. Soc.* **1996**, *118*, 9635–9644. (b) Pesak, D.; Moore, J. S. *Macromolecules* **1997**, *30*, 6467–6482. (c) Nantalaksakul, A.; Dasari, R. R.; Ahn, T.-S.; Al-Kaysi, R.; Bardeen, C. J.; Thayumanavan, S. *Org. Lett.* **2006**, *8*, 2981–2984. (d) Zhang, X.; Ren, X.; Xu, Q. H.; Loh, K. P.; Chen, Z. K. *Org. Lett.* **2009**, *11*, 1257–1260.

Scheme 1. Synthesis of **1**, **2**, and **3**

observed in the emission spectra were in the opposite direction and of more significance. The emission peaks of **1**, **2**, and **3** were at 454, 485, and 489 nm in the absence of Triton X-100. The surfactant caused the emission bands to blue-shift by 20, 47, and 68 nm, respectively (Table 1).

The blue shift and increase in fluorescence quantum yields (Φ_F) suggested that the deaggregation of **1–3** was caused by the addition of the surfactants. The enhancement of Φ_F of **3** was greater than that of **1** implied that compound **1**, a smaller molecule, was only partially deaggregated.

We also investigated the fluorogenic behaviors of **1–3** in the presence of metal ions in the +2 oxidation state, such as Cr^{2+} , Fe^{2+} , Co^{2+} , Ni^{2+} , Cu^{2+} , Cd^{2+} , Hg^{2+} , and Pb^{2+} . Without the surfactant, the fluorescence signal of **3** can be quenched

(15) The spectroscopic data (^1H and ^{13}C NMR, MALDI-TOF MS, and ESI-MS spectra) of every compound are available in Supporting Information.

2770

Table 1. Photophysical Properties of **1–3** in 50 mM Phosphate Buffer (pH 8.0) without and with Triton X-100

compd	absorption		fluorescence	
	λ_{max} (nm)	ϵ ($\text{M}^{-1} \text{cm}^{-1}$)	λ_{max} (nm)	Φ_F^a
Without Triton X-100				
1	374	5900	454	0.097
2	370	26823	485	0.14
3	375	63500	489	0.037
With Triton X-100				
1	383	9592	434	0.47
2	382	21310	438	0.46
3	379	49820	421	0.65

^a Quinine sulfate in 0.1 M H_2SO_4 ($\Phi_F = 0.45$) was the reference.

by Hg^{2+} ions (Figure 2a), whereas there are no significant effects on the signals of **1** and **2**. With Triton X-100, the fluorescence signal of **1** was quenched by all metal ions listed above, but the signal of **2** was not affected. On the other hand, the fluorophore **3** still exhibited a selective quenching by Hg^{2+} ions.

A Stern–Volmer plot was made in order to access a quantitative measurement of fluorescence quenching, K_{SV} for the system with Triton X-100 was $33,700 \text{ M}^{-1}$, whereas it was only $5,800 \text{ M}^{-1}$ for the system without Triton X-100 (Figure 3). It is clear that Triton X-100 could amplify this selective quenching effect.

The nonselective quenching of **1** suggested that positively charged metal ions reduce the electrostatic repulsion between

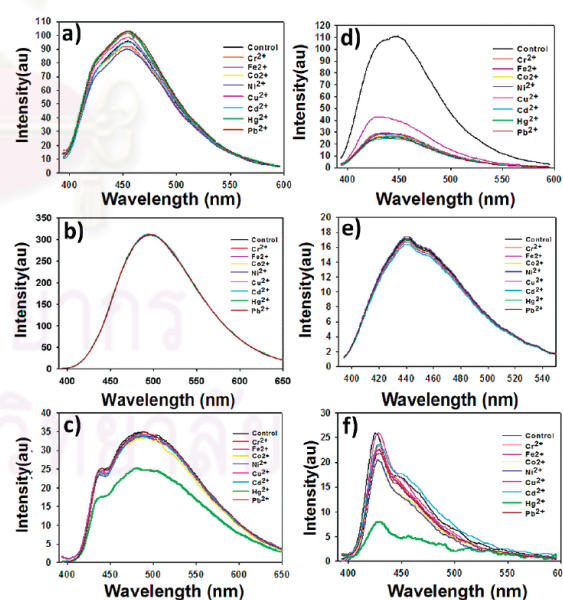


Figure 2. Emission spectra of the solutions of **1–3** ($10 \mu\text{M}$) upon the addition of metal ions ($40 \mu\text{M}$): without Triton X-100 for (a) **1**, (b) **2**, and (c) **3**; with 0.1 mM Triton X-100 for (d) **1** ($1 \mu\text{M}$), (e) **2** ($0.1 \mu\text{M}$), and (f) **3** ($0.1 \mu\text{M}$).

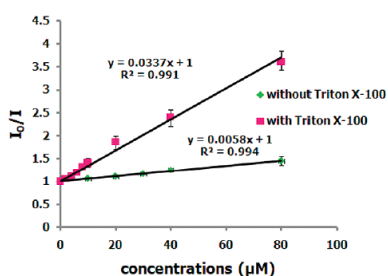


Figure 3. Stern–Volmer plots for fluorescence quenching of **3** (0.1 μM) with and without of Triton X-100 (0.1 mM).

the partially deaggregated negatively charged fluorophores **1**, resulting in the enhancement of self-quenching. Conversely, the charge repulsion among positively charged fluorophore **2**, having a comparable molecular size to **1**, cannot be reduced by the metal ions and therefore exhibits no enhancement of the self-quenching effect.

The selective fluorescence quenching of **3** by Hg^{2+} is more complicated and difficult to rationalize. With the high selectivity for Hg^{2+} , the common metal ion enhanced self-quenching mechanism is unlikely to play the key role. The quenching effect may involve selective formation of $\mathbf{3}\cdot\text{Hg}^{2+}$ complex and efficient energy transfer between the fluorescent units in **3** to this complex at the periphery.¹⁶ To test if the proposed complex could be reversed, a strong chelator, EDTA, was added. The addition of 2.5 molar equiv of EDTA could restore the fluorescent signal of **3** to its original level (Figure 4). The result supports the above hypothesis to some extent.

In summary, a series of diphenylacetylene dendritic compounds containing negatively and positively charged peripheral groups were successfully synthesized through a

(16) (a) Sandanaraj, B. S.; Demont, R.; Aathimankandan, S. V.; Savariar, E. N.; Thayumanavan, S. *J. Am. Chem. Soc.* **2006**, *128*, 10686–10687. (b) Jiwpanich, S.; Sandanaraj, B. S.; Thayumanavan, S. *Chem. Commun.* **2009**, 806–808.

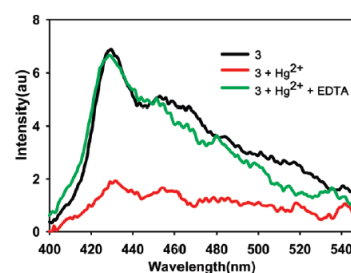


Figure 4. Emission spectra of **3** (0.1 μM) upon the addition of Hg^{2+} (40 μM) and EDTA (100 μM).

convergent approach. We have demonstrated that these diphenylacetylene based dendritic molecules with a charge decorated periphery constitute a new intriguing class of fluorophores useful for sensing applications in aqueous media. The quantum efficiencies of the fluorophores in water were considerably enhanced by the nonionic surfactant Triton X-100. In the presence of Triton X-100, the fluorescent signal of the first generation dendrimer containing a carboxylate periphery could be selectively quenched by Hg^{2+} . A wide linear fluorescence quenching response to Hg^{2+} concentration was observed in the range of 2–80 μM (0.4–16 ppm). Other applications along this line are currently under investigation, and the results will be disclosed in due course.

Acknowledgment. This work is supported by the Thailand Research Fund (TRF) and the 90th Anniversary of Chulalongkorn University Fund (Ratchadaphiseksomphot Endowment Fund). The measurement of fluorescent spectra was performed in the laboratory of Prof. Thawatchai Tuntulani.

Supporting Information Available: Spectroscopic data and detailed experimental procedures. This information is available free of charge via the Internet at <http://pubs.acs.org>.

OL900929G

Nanofibers Doped with Dendritic Fluorophores for Protein Detection

Bryce W. Davis,[†] Nakorn Niamnont,[‡] Christopher D. Hare,[†] Mongkol Sukwattanasinitt,^{*,‡} and Quan Cheng^{*,†}

Department of Chemistry, University of California, Riverside, California 92521, Organic Synthesis Research Unit, Department of Chemistry, Faculty of Science, and Center for Petroleum, Petrochemicals and Advanced Materials, Chulalongkorn University, Bangkok 10330, Thailand

ABSTRACT We report a solid-state, nanofiber-based optical sensor for detecting proteins with an anionic fluorescent dendrimer (AFD). The AFD was encapsulated in cellulose acetate (CA) electrospun nanofibers, which were deacetylated to cellulose to generate secondary porous structures that are desirable for enhancing molecular interactions, and thus better signaling. The protein sensing properties of the fibers were characterized by monitoring the fluorescence response of cytochrome c (cyt c), hemoglobin (Hgb), and bovine serum albumin (BSA) as a function of concentration. Effective quenching was observed for the metalloproteins, cyt c and Hgb. The effect was primarily due to energy transfer of the imbedded fluorescent dendrimers to the protein, as both proteins contain heme portions. Electron transfer, caused through the electrostatic effects in the binding of the anionic dendrimer to the positive patches of globular proteins, could be responsible as well. BSA, on the other hand, triggered a “turn-on” response in fluorescence, suggesting the negatively charged BSA reduces the π - π stacking of the partially dispersed, negatively charged dendritic fluorophores through repulsion forces, which results in an increase in fluorescence. Stern–Volmer constants (K_{sv}) of the electrospun fibers were found to be 3.4×10^5 and $1.7 \times 10^6 \text{ M}^{-1}$ for cyt c and Hgb, respectively. The reusability of the nanofibers is excellent: the nanofibers demonstrated less than 15% change of fluorescence intensity signal in a 5-cycle test.

KEYWORDS: electrospinning • fluorescent dendrimers • protein biosensor • nanofibers

1. INTRODUCTION

The development of solid-state optical biosensors continues to be of major interest within the nanotechnology field because of many practical and potential functions (1). For instance, these solid-state sensors can exhibit advantages of versatility, sensitivity, selectivity, simplified optical setup, and a large dynamic range. However, desirable mechanical, electronic, and optical properties can be difficult to realize at the sensing interface because they require sophisticated synthesis routes and tend to use a broad range of discontinuous objects such as carbon nanotubes, nanorods and wires (2). In the past decade, electrospun polymer nanofibers have proven to contain many of the unique properties desirable for biotech development. Recent work using electrospun nanofibers covers a wide range of applications, including optical sensors and biosensors, filtration membranes, drug delivery devices, and scaffolding for stem cell growth (3–7).

Electrospinning is a polymer processing technique used to create fibers with diameters ranging from a few nanometers to micrometers (8). The electrospinning process works when a flowing polymer solution is subject to a high electric field. When the repulsive electrostatic force overcomes the

surface tension of the polymer solution a stable jet is formed and a membrane-like web of small fibers is emitted onto the ground electrode (9). The use of electrospun nanofibers for chemical sensors using fluorophores has been previously reported. For instance, Samuelson and co-workers have demonstrated that pyrene methanol and hydrolyzed poly[2-(3-thienyl) ethanol butoxy carbonyl-methyl urethane] (H-PURET) can be immobilized to the surface of electrospun membranes for the detection of metal ions (Fe^{3+} and Hg^{2+}), 2,4-dinitrotoluene (DNT), and methyl viologen (MV^{2+}) (10, 11). Tao et al. reported the use of sol–gel chemistry to make porphyrin-doped nanofibrous membranes for the detection of 2,4,6-trinitrotoluene (TNT) vapor (12). A major drawback of these platforms, however, is that they require multiple fabrication steps, resulting in inhomogeneous dispersion of sensing molecules within the membrane and potential fluorescent leakage, and ultimately compromising sensitivity, stability, and reproducibility of the solid-state optical sensors. More recently, Yang et al. demonstrated that secondary porous structures could be added to 9-chloromethylanthracene (9-CMA)-doped cellulose acetate (CA) nanofibers for the detection of MV^{2+} (13). Although Yang’s work provided a simple approach to creating secondary pores within the nanofiber, there is still a need for new fluorescent units that demonstrate distinctive FRET properties and better process characteristics, such as improved retention, all of which are important for generating new protein sensors.

Fluorescent dendrimers are highly effective receptors for fluorescent optical sensors for many different target analytes, such as explosives (TNT and DNT) and biomarkers

* Corresponding author. Tel: (951) 827-2702 (Q.C.). E-mail: quan.cheng@ucr.edu (Q.C.); mongkol.s@chula.ac.th (M.S.).

Received for review April 19, 2010 and accepted June 22, 2010

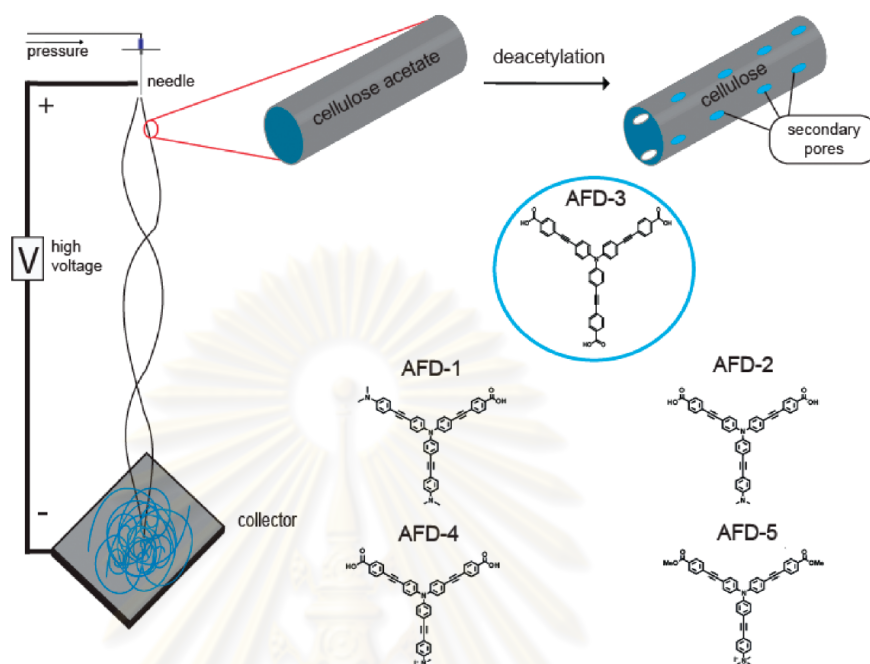
[†] University of California.

[‡] Chulalongkorn University.

DOI: 10.1021/am100345g

© 2010 American Chemical Society

Scheme 1. Schematic Illustration of the Electrospinning Setup, Encapsulation of the Fluorescent Dendrimer, And Deacetylation Process Used in This Study; Five Water-Soluble Fluorescent Dendritic Compounds (AFD-1, AFD-2, AFD-3, AFD-4, and AFD-5) Composed of Phenylene-Ethynylene Repeating Units Are Illustrated^a



^a The circled AFD-3 is the fluorescent dye used to dope the CA nanofibers for detection of metalloproteins.

(14–18). In comparison with molecular fluorophores, the numbers of fluorophore units in dendrimers can be controlled by simple synthetic means. This convergent approach allows for more predictable structure-related and fluorescent properties within the sensor. In this work, a diphenylacetylene dendritic compound containing negatively charged peripheral groups is used as an effective bioreceptor. In the past, Thayumanavan and co-workers have utilized dendritic scaffolding to generate fluorescence-based patterns for both metalloprotein and nonmetalloprotein sensing using solution based detection schemes (19–22). The quenching property of their sensor was reported to be caused by the charge density around the protein, as well as quantity and position of the heme within the metalloproteins. Although the use of fluorescent dendrimers for solution-based protein detection exists (19), there is still a lack of research that uses simple approaches to creating reusable solid-state devices that can respond differentially to a variety of proteins. In this work, we report a novel solid-state fluorescent biosensor, using nanofibers, for quantifying proteins in solution. A straightforward top-down in situ electrospinning approach is utilized along with anionic fluorescent dendrimers (AFD) to fabricate a reusable sensor for the detection of low concentrations of metalloproteins via a fluorescence resonance energy transfer (FRET) principle.

2. EXPERIMENTAL SECTION

All chemicals were of the highest analytical grade, purchased from Sigma-Aldrich (Milwaukee, WI) and used with-

out further purification, unless otherwise stated. Milli-Q (>18 M Ω) water was used in the preparation of all buffer solutions. Steady-state fluorescence measurements were performed on a HORIBA FluoroLog spectrofluorometer using the excitation at 370 nm. Fluorescence image analysis was performed on a Leica TCS SP2/UV confocal microscope using the excitation at 364 nm. The scanning electron microscope (SEM) used is a Phillips XL30-FEG. Fiber analysis was performed using Fourier transform infrared (FTIR) spectroscopy on a Equinox 55/S FTIR spectrometer with a Bruker A590 microscope.

CA is used as the host matrix in our nanofiber fabrication because of its chemical resistance, thermal stability, low nonspecific absorption, and capacity to be easily functionalized with recognition elements (23). To further improve the surface area:volume ratio and overall performance a simple deacetylation treatment was used to create specific secondary structures within our electrospun nanofibers. Park and co-workers have demonstrated that secondary porous structures can be inserted into the backbone of electrospun CA fibers by homogeneous deacetylation treatment of CA to cellulose using a practical processing step while at the same time maintaining the nanofiber's physical properties (24–26). This deacetylation treatment is used in our work to generate evenly distributed secondary pores throughout the nanofiber backbone of cellulose to improve the sensing performance. A schematic illustration of the electrospinning

setup, encapsulation of the fluorescent dendrimer, and deacetylation process is shown in Scheme 1.

Five water-soluble fluorescent dendritic compounds (AFD-1, AFD-2, AFD-3, AFD-4, and AFD-5) composed of phenylene-ethynylene repeating units (Scheme 1) were synthesized according to published procedures and screened in solution for the highest visible fluorescence (see the Supporting Information) (27). These dendrimers commonly demonstrated low visible fluorescent emission, but AFD-3 was found to be an exception that gave visibly high fluorescence. The variability of the fluorescent emission among the dendrimers is due to aggregation, which is caused by small differences in the charge distribution among different AFDs.

The electrospinning solution was prepared by dissolving 17% CA and 0.1% AFD-3 (by weight) in 8:1 (v/v) Acetone/H₂O, and then placed into a plastic syringe. A high-voltage DC power supply (Glassman High Voltage Inc. Series EH) was connected to a 25-gauge blunt nose needle attached to the syringe containing the electrospinning solution. The electrospun fibers were collected on a grounded aluminum plate. The CA/AFD-3 solutions were electrospun at a voltage of 21 kV, a tip-to-collector distance of 10 cm, and a solution flow rate of 1.2 mL/h. All of the electrospinning procedures were carried out at 25 °C with a collection time of approximately 90 s. To create secondary porous structures, we deacetylated the CA fibers in a 50 mM NaOH ethanol solution at 25 °C for 24 h, thoroughly rinsed them with water, and then dried them using N₂. The chemical reaction of CA to cellulose was traced by using FT-IR spectroscopy (see the Supporting Information). The characteristic absorption peaks attributed to the vibrations of the acetate group at 1745($\nu_{C=O}$), 1375(ν_{C-CH_3}), and 1235 cm^{-1} (ν_{C-O-C}) disappeared after deacetylation of CA. An absorption peak at 3500 cm^{-1} (ν_{O-H}) was also observed, indicating successful deacetylation. The FT-IR spectrum obtained after deacetylation agreed with that of pure cellulose fibers.

3. RESULTS AND DISCUSSION

The electrospun fibers exhibited well-defined fibrous morphology without bead formation and good structural stability. An electrospun AFD-3-doped nanofiber nonwoven mat is shown in the SEM image in Figure 1, further illustrating the large surface area:volume ratio formed within the electrospun nonwoven film. The fibers were continuous, uniform, and had a diameter ranging from approximately 400–2000 nm, similar to those reported by Xiang et al. (28). One-dimensional (1D) nanostructures are distributed evenly throughout the electrospun membrane using a simple electrospinning approach. It is assumed that the nanofibers are 3D, because of their inherent porosity created by the deacetylation of CA to cellulose. Consequently, unique secondary porous structures are homogeneously distributed throughout the backbone of the nanofibers creating a larger surface area: volume ratio and in-turn substantially improving sensitivity.

The protein sensing properties of the fibers were characterized by monitoring the quenching behaviors of cyto-

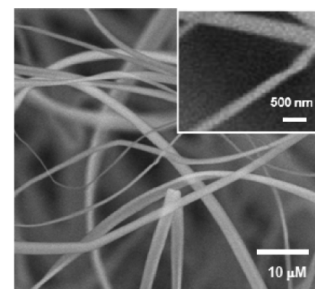


FIGURE 1. SEM image of electrospun AFD-doped deacetylated cellulose fibers (17% CA/0.1% AFD dissolved in 8:1 acetone/water). Inset is a zoomed-in image of the fiber.

chrome c (cyt c), hemoglobin (Hgb), and bovine serum albumin (BSA) as a function of concentration. All proteins were bovine specific, where cyt c is positively charged (pI 10.2–10.7), Hgb is neutral/slightly negative (pI 7.0–7.4), BSA is negatively charged (pI 4.8–4.9), and AFD-3 is negatively charged at physiological pH (29). The fluorescence spectra of the fiber varying with the concentration of cyt c are illustrated in Figure 2a. The fluorescence intensity decreases proportionally with increase in cyt c concentration. Similar behavior was observed with Hgb (Figure 2b). The efficient quenching effects of the metalloproteins, cyt c and Hgb, are primarily due to energy transfer of the imbedded fluorescent dendrimers with the protein as both cyt c and Hgb contain heme portions within the protein. Some of the quenching effect for proteins can be attributed to electron transfer, caused through the electrostatic effects in the binding of the anionic dendrimer to the positive patches of globular proteins. When BSA was used, however, an increase in fluorescence was observed (Figure 2c). The slight increase in local fluorescence of the dendritic fluorophore within the high-surface-area of the nanofibers suggested that the negatively charged BSA proteins reduce the π - π stacking of the partially dispersed negatively charged dendritic fluorophores through repulsion forces, resulting in an increase in fluorescence (30, 31). It is expected that two main factors contribute to protein detection: (1) the charge distribution density on the proteins surface, and (2) the location of the metalloproteins secondary structure. The intricate nature of the interaction of these two factors should result in protein-dependent patterns allowing for good sensing capabilities.

The fluorescence dynamic quenching sensitivity can be quantified through the measurements with the Stern–Volmer equation (32)

$$\frac{I_0}{I} = 1 + K_{SV}[Q] \quad (1)$$

where I_0 and I are the fluorescent intensities in the absence and presence of quencher, respectively; K_{SV} is the Stern–Volmer quenching constant, and $[Q]$ is the concentration of quencher. The quenching data are usually presented as plots

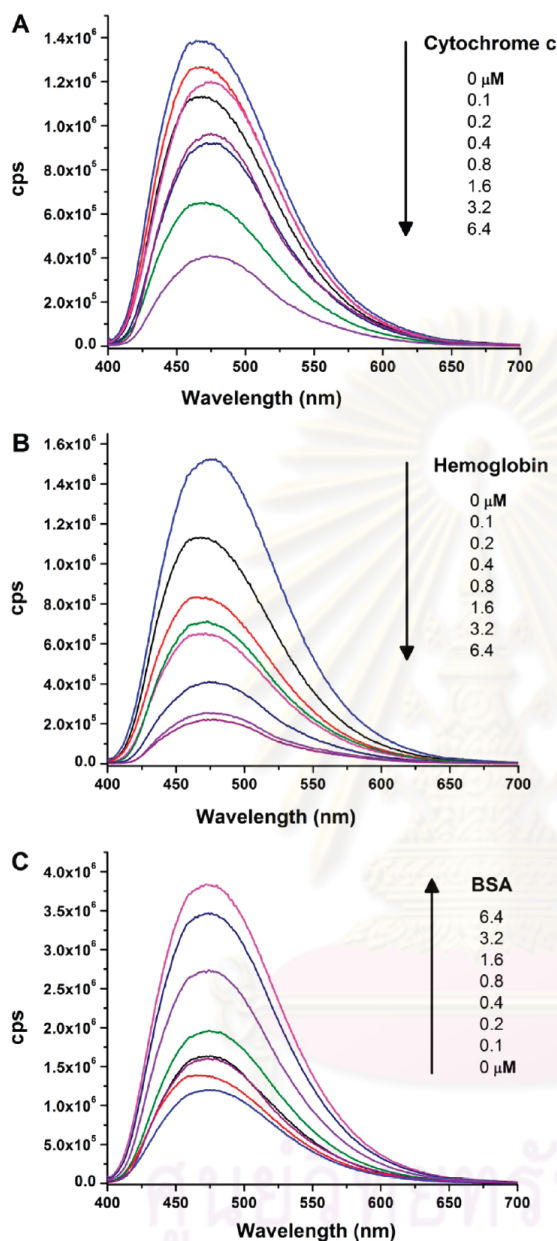


FIGURE 2. Fluorescence emission spectra of the AFD-functionalized nanofibers in response to varied concentrations of (A) cyt c, (B) Hgb, and (C) BSA ($\lambda_{\text{Ex}}/\lambda_{\text{Em}} = 370/475$ nm).

of I_0/I versus $[Q]$ with a slope equal to K_{SV} . The higher the K_{SV} , the lower the concentration of quencher is required to quench the fluorescence and thus the greater detection sensitivity.

The Stern–Volmer analysis of the electrospun sensors for cyt c and Hgb is shown in Figure 3. At concentrations between 100 nM and 6.4 μM , a linear relationship between quencher concentration and I_0/I was obtained, showing homogeneous quencher-accessible sites in the electrospun

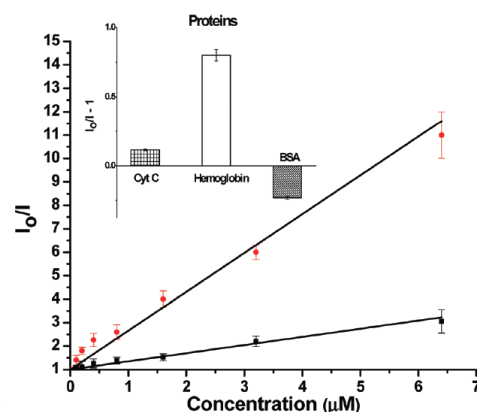


FIGURE 3. Stern–Volmer plots of the nanofibers for cyt c (■) and Hgb (●). Inset: Analyte-dependent pattern for 200 nM of bovine metalloproteins (cyt c, Hgb) and nonmetalloprotein (BSA) in PBS buffer solution (pH 7.4).

fibers under the experimental conditions. The sensitivity, K_{SV} , of the electrospun fibers was found to be 3.4×10^5 and $1.7 \times 10^6 \text{ M}^{-1}$ for cyt c and Hgb, respectively. BSA tested under the same experimental conditions demonstrated a small negative linear relationship. The inset in Figure 3 shows the analyte-dependent pattern from the fluorescence intensity changes at 200 nM. Differential responses for different proteins are demonstrated and therefore illustrated analyte-specific patterns. The results clearly point to an effective approach to the solid-state fabrication of biosensors by embedding selective receptors into electrospun fibers.

The sensitive protein detection was further visualized using a high resolution UV confocal microscope. Figure 4 shows the fluorescence images of the AFD-3-doped cellulose nanofibers before and after incubation with 10 μM cyt c solution for 15 min, further illustrating the remarkable quenching effect of the nanofiber sensors. The fluorescence images before the quenching process indicate the evident fluorescence emission and the uniform dispersion of fluorophores in cellulose, which is beneficial to sensing performance.

The reusability, reproducibility, and stability of the nanofiber material were also investigated. To demonstrate the reusability of the sensor, we immersed the cellulose nanofibers in a 25 μM solution of cyt c for 5 min, and then in a 50 mM NaOH ethanol solution for 15 min followed by rinsing in water and drying in air. The fibers were then reused for sensing the same cyt c solution. Figure 5 demonstrates that the used nanofibers contain similar quenching ability as the pristine fibers. In the tested 5 cycles, the nanofibers exhibited less than 15% loss of fluorescence intensity signal, indicating outstanding reusability. We attribute this to the noncovalent nature of the interaction, which is largely based on the electrostatic interaction between the fluorophore and protein. In fact, that weak binding events and stripping process do not denature the core, which allows for excellent sample recovery. The reproducibility of the sensor is reflected by low batch-to-batch variation of 5.3% for the CA/AFD-3 nanofibers using 3 separate measurements produced on different days. For the stability

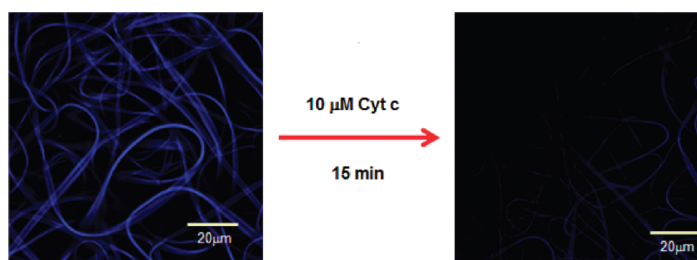


FIGURE 4. Confocal fluorescence images of the electrospun nanofibers before (left) and after (right) incubation in a 10 μM cyt c solution for 15 min.

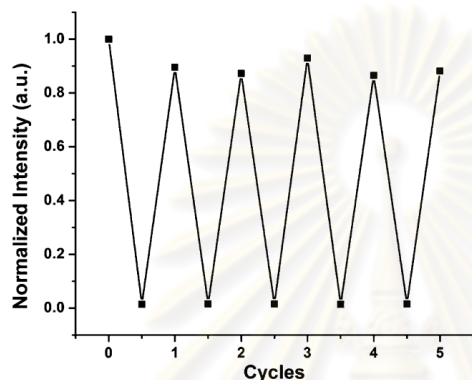


FIGURE 5. Repeated switching of normalized fluorescence emission of the nanofibers for 5 cycles of 25 μM cyt c of quenching/regeneration process. Quenching time: 15 min, regenerated by immersing into 50 mM NaOH ethanol solution for 5 min, PBS buffered solution (pH 7.4) for 5 min and dried with N_2 gas, $\lambda_{\text{ex}}/\lambda_{\text{em}} = 370/475$ nm.

experiments, we tested the buffer solutions before and after each test and no leakage of the fluorophore were found in the aqueous solutions.

4. CONCLUSIONS

In conclusion, a reusable, solid-state fluorescent biosensor was developed using electrospun nanofibers and anionic dendrimers for quantifying proteins in solution via a FRET mechanism. The selectivity and specificity of the sensor is displayed in the specific response each protein has with the fluorescent fibers. The quenching effect is a result of energy/electron transfer processes between iron containing proteins (i.e., cyt c and Hgb) and the fluorescent core. The increase in fluorescence by the BSA is due to the induced decrease in π - π stacking of the AFD-3 fluorophore localized on the surface of the nanofibers. A relatively large quenching sensitivity was obtained for AFD-3-doped cellulose nanofibers with respect to Hgb, which is demonstrated with the Stern–Volmer constants. The electrospun doped fibrous material exhibited large surface area due to small diameter and porosity of the nanofibers. This porosity stems from two factors: the deacetylation of CA to cellulose and the disorderly arrangement of fibers onto the substrate. The ability to homogeneously embed fluorophores into the core of the fiber allows for better reproducibility, reversibility, and

durability of the sensor. Future efforts will focus on exploring a nanofiber sensor array containing different fluorescent dendrimers for the detection and identification of protein targets via distinct fluorescence response patterns.

Acknowledgment. The authors acknowledge financial support from NSF grant CHE-0719224 (Q.C.) and Thailand's National Nanotechnology Center grant NN-B-22-FN9-10-52-06 (M.S.). Images were collected at the Microscopy Core/Center for Plant Cell Biology at the Institute for Integrative Genome Biology at the University of California, Riverside. We thank Jeff Lefler and Craig Graham for the help in the design and construction of the electrospinning setup.

Supporting Information Available: Additional data showing the FTIR spectrum of the deacetylation of the cellulose acetate to cellulose and fluorescence property of dendritic fluorophores in PBS solution (PDF). This material is available free of charge via the Internet at <http://pubs.acs.org>.

REFERENCES AND NOTES

- (1) Ligler, F. S. *Anal. Chem.* **2009**, *81*, 519.
- (2) Dzenis, Y. *Science* **2004**, *304*, 1917.
- (3) Meinel, A. J.; Kubow, K. E.; Klotzsch, E.; Garcia-Fuentes, M.; Smith, M. L.; Vogel, V.; Merkle, H. P.; Meinel, L. *Biomaterials* **2009**, *30*, 3058.
- (4) Luong-Van, E.; Grondahl, L.; Chua, K. N.; Leong, K. W.; Nurcombe, V.; Cool, S. M. *Biomaterials* **2006**, *27*, 2042.
- (5) Long, Y. Y.; Chen, H. B.; Yang, Y.; Wang, H. M.; Yang, Y. F.; Li, N.; Li, K. A.; Pei, J.; Liu, F. *Macromolecules* **2009**, *42*, 6501.
- (6) Patel, A. C.; Li, S. X.; Yuan, J. M.; Wei, Y. *Nano Lett.* **2006**, *6*, 1042.
- (7) Yoon, K.; Kim, K.; Wang, X. F.; Fang, D. F.; Hsiao, B. S.; Chu, B. *Polymer* **2006**, *47*, 2434.
- (8) McKee, M. G.; Layman, J. M.; Cashion, M. P.; Long, T. E. *Science* **2006**, *311*, 353.
- (9) Huang, Z. M.; Zhang, Y. Z.; Kotaki, M.; Ramakrishna, S. *Compos. Sci. Technol.* **2003**, *63*, 2223.
- (10) Wang, X. Y.; Kim, Y. G.; Drew, C.; Ku, B. C.; Kumar, J.; Samuelson, L. A. *Nano Lett.* **2004**, *4*, 331.
- (11) Wang, X.; Drew, C.; Soo-Hyoung, L.; Senecal, K. J.; Kumar, J.; Samuelson, L. A. *Nano Lett.* **2002**, *2*, 1273.
- (12) Tao, S. Y.; Li, G. T.; Yin, J. X. *J. Mater. Chem.* **2007**, *17*, 2730.
- (13) Yang, Y. F.; Fan, X.; Long, Y. Y.; Su, K.; Zou, D. C.; Li, N.; Zhou, J.; Li, K.; Liu, F. *J. Mater. Chem.* **2009**, *19*, 7290.
- (14) Guo, M.; Varnavski, O.; Narayanan, A.; Mongin, O.; Majoral, J. P.; Blanchard-Desce, M.; Goodson, T. *J. Phys. Chem. A* **2009**, *113*, 4763.
- (15) Wang, D. L.; Gong, X.; Heeger, P. S.; Rininsland, F.; Bazan, G. C.; Heeger, A. J. *Proc. Natl. Acad. Sci. U.S.A.* **2002**, *99*, 49.
- (16) Chen, L. H.; McBranch, D. W.; Wang, H. L.; Helgeson, R.; Wudl, F.; Whitten, D. G. *Proc. Natl. Acad. Sci. U.S.A.* **1999**, *96*, 12287.
- (17) Woller, E. K.; Walter, E. D.; Morgan, J. R.; Singel, D. J.; Cloninger, M. J. *J. Am. Chem. Soc.* **2003**, *125*, 8820.
- (18) Klaikherd, A.; Sandanaraj, B. S.; Vutukuri, D. R.; Thayumanavan, S. *J. Am. Chem. Soc.* **2006**, *128*, 9231.

- (19) Jiwpanich, S.; Sandanaraj, B. S.; Thayumanavan, S. *Chem. Commun.* **2009**, 806.
- (20) Savariar, E. N.; Ghosh, S.; Gonzalez, D. C.; Thayumanavan, S. *J. Am. Chem. Soc.* **2008**, *130*, 5416.
- (21) Sandanaraj, B. S.; Demont, R.; Thayumanavan, S. *J. Am. Chem. Soc.* **2007**, *129*, 3506.
- (22) Sandanaraj, B. S.; Demont, R.; Aathimanikandan, S. V.; Savariar, E. N.; Thayumanavan, S. *J. Am. Chem. Soc.* **2006**, *128*, 10686.
- (23) Frey, M. W. *Polym. Rev.* **2008**, *48*, 378.
- (24) Han, S. O.; Son, W. K.; Youk, J. H.; Park, W. H. *J. Appl. Polym. Sci.* **2008**, *107*, 1954.
- (25) Han, S. O.; Youk, J. H.; Min, K. D.; Kang, Y. O.; Park, W. H. *Mater. Lett.* **2008**, *62*, 759.
- (26) Son, W. K.; Youk, J. H.; Park, W. H. *Biomacromolecules* **2004**, *5*, 197.
- (27) Niamnont, N.; Siripornnoppakhun, W.; Rashatasakhon, P.; Sukwattanasinitt, M. *Org. Lett.* **2009**, *11*, 2768.
- (28) Xiang, C. H.; Frey, M. W.; Taylor, A. G.; Rebovich, M. E. *J. Appl. Polym. Sci.* **2007**, *106*, 2363.
- (29) Kim, I. B.; Dunkhorst, A.; Bunz, U. H. F. *Langmuir* **2005**, *21*, 7985.
- (30) Lavigne, J. J.; Broughton, D. L.; Wilson, J. N.; Erdogan, B.; Bunz, U. H. F. *Macromolecules* **2003**, *36*, 7409.
- (31) Turro, N. J.; Lei, X. G.; Ananthapadmanabhan, K. P.; Aronson, M. *Langmuir* **1995**, *11*, 2525.
- (32) Lakowicz, J. R. *Principles of Fluorescence Spectroscopy*, 3rd ed.; Springer: New York, 2006.

AM100345G



ศูนย์วิจัยทรัพยากร
จุฬาลงกรณ์มหาวิทยาลัย



Short communication

Protein discrimination by fluorescent sensor array constituted of variously charged dendritic phenylene–ethynylene fluorophores

Nakorn Niamnont^a, Radeemada Mungkarndee^b, Ittipon Techakriengkrai^c, Paitoon Rashatasakhon^a, Mongkol Sukwattanasinitt^{a,*}^a Organic Synthesis Research Unit, Department of Chemistry, Faculty of Science, Chulalongkorn University, Bangkok 10330, Thailand^b Program in Biotechnology, Faculty of Science, Chulalongkorn University, Phayathai Rd., Bangkok 10330, Thailand^c Department of Food Technology, Faculty of Science, Ramkhamhaeng University, Bangkok 10240, Thailand

ARTICLE INFO

Article history:

Received 29 April 2010

Received in revised form 1 July 2010

Accepted 24 July 2010

Available online 1 August 2010

Keywords:

Dendrimer

Fluorescence

Principal component analysis

Protein identification

Sensor array

ABSTRACT

A protein fluorescent sensor array based on variously charged dendritic fluorophores is developed. The variation of charge is achieved by different combinations of cationic trimethylammonium, anionic carboxylate and non-ionic methyl ester or *N,N*-dimethylamino on the peripheries of the fluorophores. Nine phenylene–ethynylene dendritic fluorophores, seven zeroth generation bearing charges varied from –3 to +3 and two first generation bearing –6 and +6 charges, are synthesized from triiodotriphenylamine through series of Sonogashira coupling. In phosphate buffer saline pH 7.4, five out of these nine compounds fluorogenically response to eight protein analytes distinctively. The data set of fluorescent intensities obtained from 5 fluorophores × 8 proteins × 9 replicated measurements can be statistically sorted into eight clusters corresponding to each protein by principal component analysis (PCA). Factorial discriminant analysis (FDA) cross-validation is applied to locate the optimum detection wavelength and reduce the number of sensing elements from nine to two with 100% discriminating accuracy. The method described should be generally practical for the development of electronic tongue for protein related food analysis and medical diagnosis.

© 2010 Elsevier B.V. All rights reserved.

1. Introduction

To keep pace with growing demands on proteomics, medical diagnosis and pathogenic detections, the development of new protein sensors is of great importance. Currently available biosensors are mostly based on enzyme-linked immunosorbent assay (ELISA) techniques using specific lock and key binding interactions between ligands, usually antibodies, and receptors (Daniels et al., 2004; Ikebukuro et al., 2002; Li et al., 2009). However, the applications of those lock and key binding interactions are limited due to the low stability and reproducibility of antibodies as well as the difficulty in tagging them with fluorescent labels (Kodadek et al., 2004; Haab, 2006; Borrebaeck and Wingren, 2009). For multivalency species such as proteins, the precise design for strong individual interactions is out of the question. The utilization of a sensor array has recently become attractive as it requires selective, rather than specific, binding of various sensing elements to the proteins (McQuade et al., 2000; Albert et al., 2000).

Fluorescence technique has been a detection method of choice due to its high sensitivity and vast potential for selectivity enhancement. Recently, π -conjugated polymers have been developed as highly sensitive signal transducers due to their signal amplifications through energy coupling among their multiple fluorogenic moieties (Kodadek, 2001; Wang et al., 2002; McQuade et al., 2000; Thomas et al., 2007). Polyelectrolyte conjugated polymers with various protein binding abilities have been used to generate patterns for protein discrimination (Fan et al., 2002; Sandanaraj et al., 2006; You et al., 2007; Miranda et al., 2007; Yu et al., 2008; Bunz, 2009; Gonzales et al., 2009).

Complementary binding to protein surfaces has been asserted in the observation of different fluorogenic responses to proteins in an array of tetraphenylporphyrins, consisting of a porphyrin hydrophobic core and hydrophilic amino acid peripheries (Jain and Hamilton, 2000; Baldini et al., 2004; Zhou et al., 2006). Non-conjugated dendrimers containing anthracene core and carboxylate peripheral groups have also been used as a metalloprotein sensor array (Paul et al., 2006; Jiwpanich et al., 2009). Notably, all of the previously reported fluorogenic elements possessed either all positively or all negatively charged groups. We thus see an opportunity to construct a sensor array from fluorophores based on systematic charge variation on dendritic structures which should

* Corresponding author. Tel.: +66 2 2187620; fax: +66 2 2187598.
E-mail address: smongkol@chula.ac.th (M. Sukwattanasinitt).

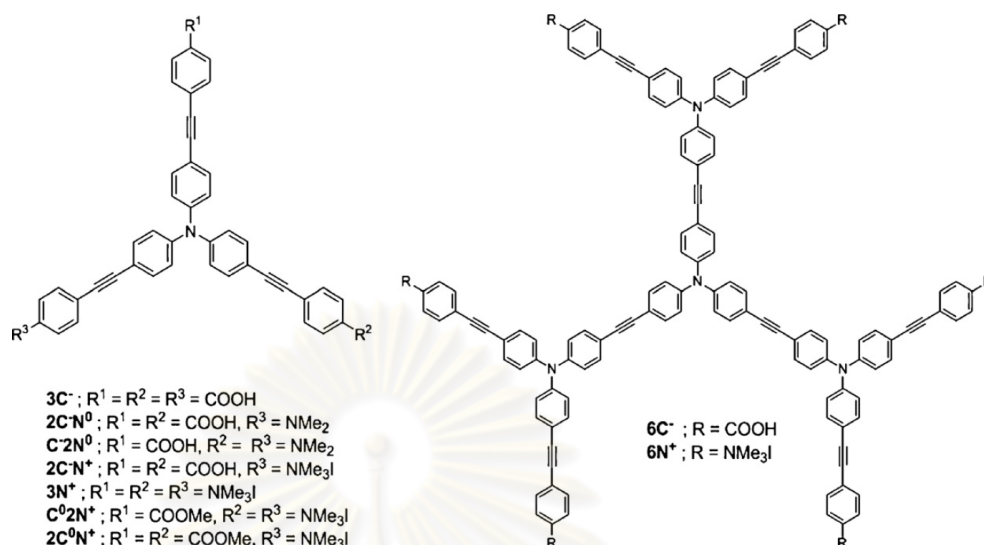


Fig. 1. Structures of variously charged dendritic fluorophores.

offer a unique fine tuning of supramolecular interaction with proteins. To realize this proposition, a series of charge decorated phenylene–ethynylene fluorophores (Fig. 1) were synthesized and examined for their applications in a sensor array for protein discrimination as reported herein.

2. Experimental

2.1. Chemicals and materials

Concanavalin A (ConA, from Jack bean), cytochrome C (CytC, from equine heart), histone (His, from calf thymus, type III-S), human serum albumin (HSA), lysozyme (Lys, from chicken egg white), myoglobin (Myo, from equine heart) and papain (Pap, from papaya latex) were purchased from Sigma. *N,N*-Dimethylaniline, trimethylsilylacetylene, PdCl₂(PPh₃)₂, sodium thiosulfate, benzyltrimethylammonium chloride, potassium hydroxide, potassium carbonate, calcium carbonate and bovine serum albumin (BSA) were purchased from Fluka. Triphenylamine, iodine monochloride, copper (I) iodide, 1,8-diazabicyclo[5.4.0]undec-7-ene (DBU) and quinine sulfate were purchased from Aldrich. 4-Iodobenzoic acid was purchased from Merck. All chemicals were used as received without further purification. Solvents were purified or dried by standard methods prior to use. All reactions were carried out under nitrogen atmosphere unless specified otherwise. Column chromatography was performed on silica gel 60 (70–230 mesh) purchased from Merck.

2.2. General methods

NMR spectra were recorded on Varian Mercury 400 MHz NMR spectrometer using the proton resonance of residual CHCl₃ at 7.26 ppm and the carbon resonance of CDCl₃ at 77 ppm as the references for ¹H and ¹³C NMR spectra, respectively. Mass spectra were recorded on a Bruker Daltonics Microflex MALDI-TOF mass spectrometer using doubly recrystallized α-cyano-4-hydroxy cinnamic acid (CCA) as a matrix. Elemental (C, H, N) analysis was performed on PE 2400 series II (Perkin-Elmer, USA). Absorption spectra were measured by a Varian Cary 50 UV-vis spectropho-

tometer. Fluorescence spectra were recorded on a Varian Cary Eclipse spectrofluorometer. The solutions of all fluorophores were prepared in 10 mM sodium phosphate buffer saline (PBS) pH = 7.4. Concentrations of all fluorophores were adjusted to 5 μM and used as stock solutions. All protein stock solutions were prepared by dilution with PBS until the absorbance at 280 nm (*A*₂₈₀) being 0.4. The protein/fluorophore mixtures were prepared by mixing and PBS dilution to afford the final concentration of fluorophores of 0.2 μM and the protein concentration with *A*₂₈₀ of 0.01.

3. Results and discussion

3.1. Synthesis and photophysical properties of the dendritic fluorophores

Nine dendritic fluorophores structures as shown in Fig. 1 were synthesized from 4,4',4''-triiodotriphenylamine through series of Sonogashira coupling. The variation of charge is achieved by different combinations of cationic trimethylammonium, anionic carboxylate and non-ionic methyl ester or *N,N*-dimethylamino on the peripheries of the fluorophores (Niammont et al., 2009). The key synthetic step involves a statistical coupling with methyl 4-ethynylbenzoate, which provides isolable mono-, di- and tri-substitution products in 84% overall yield (Scheme S1 in the supplement). The abbreviated names of the fluorophores are assigned according to the number and types of the functional groups on their peripheries in which C⁰, C⁻, N⁰ and N⁺ stand for carboxylate ester, carboxylic acid (or carboxylate anion in basic condition), amino and quaternary ammonium groups, respectively. For examples, C⁰2N⁺ possesses one carboxylate ester and two quaternary ammonium groups on its periphery. The synthesis produced seven zeroth generation dendritic fluorophores (3N⁺, C⁰2N⁺, 2C⁰N⁺, 2C⁻N⁺, C⁻2N⁰, 2C⁻N⁰ and 3C⁻) with the electronic charges varied from -3 to +3 and two first generation dendritic fluorophores (6N⁺ and 6C⁻) with -6 and +6 charges (Scheme S2 in the supplement). The detail synthetic procedures and spectroscopic data of all fluorophores are available in the supplementary information.

In aqueous solution, the fluorophores displayed maximum absorption wavelength (*λ*_{max}) ranging from 368 to 392 nm.

The maximum emission wavelength of the fluorophores ranged between 450 and 489 nm (Figures S1–S3 and Table S1 in the supplement). The fluorescent quantum yields (Φ_F) of all fluorophores were relatively low in aqueous media, especially for $2C^-N^0$ and C^-2N^0 which possessed both electron-donating amino and electron-withdrawing carboxyl groups at their peripheries. The low Φ_F due to intramolecular charge transfer from electron-donating and electron-withdrawing group has previously been described (Goodson, 2005; Terenziani et al., 2006; Zhang et al., 2009).

3.2. Fluorescence responses of the fluorophores to proteins

It has been previously reported that simple protein such as bovine serum albumin (BSA) can enhance the fluorescence sig-

nal of many fluorophores in aqueous media by its surfactant-like property (Kim et al., 2005; Tolosa and Bunz, 2009). With several fluorophores exhibiting mediocre Φ_F in hand, we envisaged a good prospect to observe a wide range of fluorescent increases upon protein interactions which is useful for protein discrimination. The BSA was added to a solution of each fluorophore in phosphate buffer saline pH 7.4. As anticipated, the fluorescent intensities of the dendritic fluorophores were enhanced differently upon the addition of BSA (Figures S4 and S5 in the supplement), implying diverse interactions, i.e. hydrophobic, dipole and coulombic, between the fluorophores and the protein.

The large increases in fluorescent intensities and blue-shifting of the signals for $3C^-$, C^02N^+ , and $3N^+$ upon the addition of BSA signify protein-induced deaggregation of the fluorophores. These

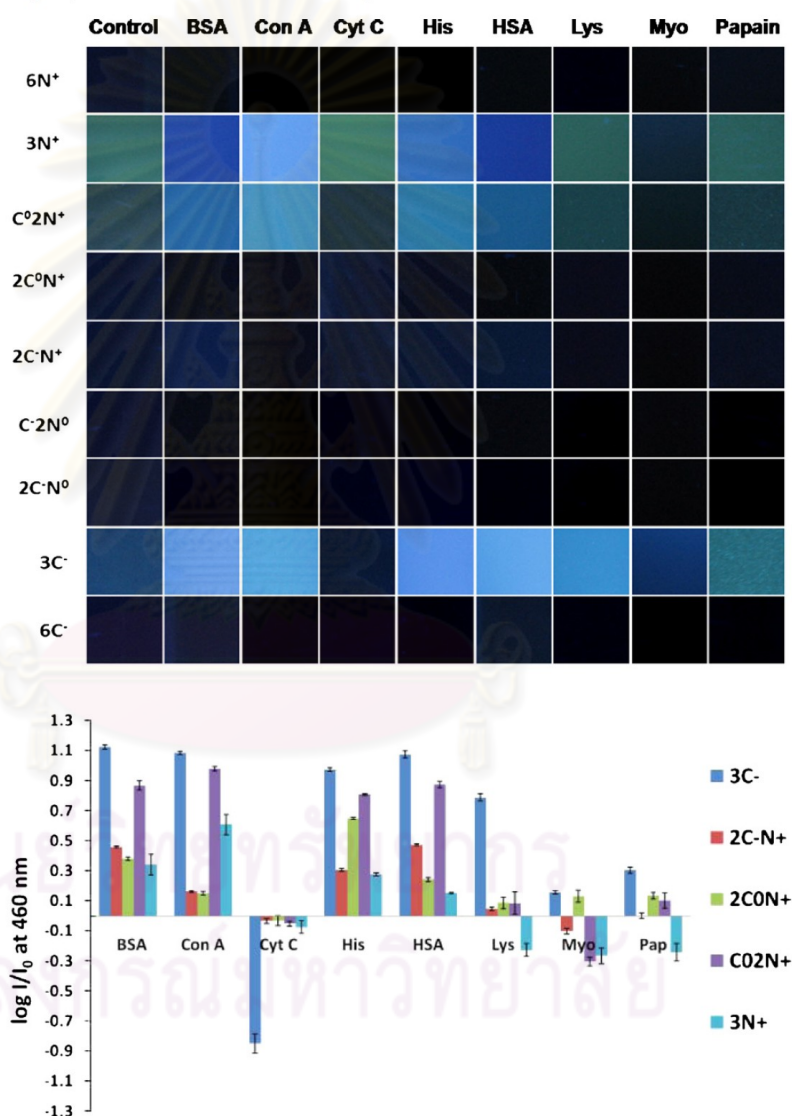


Fig. 2. (a) Cropped photographic image of the fluorophore solutions ($2.0 \mu\text{M}$) in phosphate buffer saline (10 mM , $\text{pH } 7.4$) upon addition of each protein ($A_{280} = 0.1$) under black light. (b) Histogram plot of logarithmic values of relative intensity ($\log I/I_0$) at 460 nm ($\lambda_{\text{ex}} = 375 \text{ nm}$) of fluorophore solutions ($0.20 \mu\text{M}$) in phosphate buffer saline (10 mM , $\text{pH } 7.4$) upon addition of each protein ($A_{280} = 0.01$).

positive preliminary results encouraged us to investigate the fluorescence responses of the nine fluorophores toward a set of eight commercially available proteins selected based on the variation of isoelectric points (pI) ranging from 4.8 to 10.8 as well as molecular weights ranging from 12.3 to 106 kDa. The selected proteins were Bovine Serum Albumin (BSA, pI=4.8, 66.3 kDa), tetrameric Concanavalin A (ConA, pI=5.5, 106 kDa), Cytochrome C (CytC, pI=10.7, 12.3 kDa), Histone (His, pI=10.8, 21.5 kDa), Human Serum Albumin (HSA, pI=5.2, 69.4 kDa), Lysozyme (Lys, pI=11.0, 14.4 kDa), Myoglobin (Myo, pI=7.2, 17.0 kDa), and Papain (Pap, pI=9.6, 23.0 kDa) (Miranda et al., 2007). Upon the addition of these proteins into solutions of the fluorophores, different fluorogenic response patterns were observed. As shown in Fig. 2a, the fluorogenic responses of five fluorophores ($3N^+$, C^02N^+ , $2C^0N^+$, $2C^-N^+$ and $3C^-$) are visually detectable whereas the other four ($6N^+$, C^-2N^0 , $2C^-N^0$ and $6C^-$) respond poorly. Owing to their large hydrophobic cores, the insensitivities of $6N^+$ and $6C^-$ may result from self-associative interaction of the fluorophores which is stronger than the protein–fluorophore interaction. For C^-2N^0 and $2C^-N^0$, their poor responses may be attributed to the intrinsic intramolecular electron transfer, as previously described, that cannot be influenced by the protein-induced deaggregation. We therefore screened out the low responsive fluorophores from the array, leaving only five fluorophores for further investigation with fluorescence spectroscopy.

Fluorescence intensities obtained from nine replicated measurements for each pair of protein and fluorophore were used to construct a histogram plot. After intensive trials, we found that the plot of logarithmic relative intensity ($\log I/I_0$) at 460 nm could provide the most informative pattern for protein discrimination (Fig. 2b). The use of logarithmic values allows a very wide range of data to be concisely and informatively plotted so that the fluorescence quenching (negative values) and enhancement (positive values) can be easily recognized. As shown in Fig. 2b, non-metalloproteins such as BSA, HSA, ConA, and His enhance the fluorescence signals of all fluorophores, presumably by protein-induced deaggregation mechanism (Kim et al., 2005; Tolosa and Bunz, 2009). On the other hands, the metalloproteins containing Fe^{3+} , i.e. Cyt C and Myo quench most of the fluorescence signals, perhaps through either the electron or energy transfer process (Kim et al., 2005; Jiwpanich et al., 2009). Lys and Pap significantly affect only the fluorescent signals of $3C^-$ and $3N^+$ but not the other three fluorophores. Both of these proteins have pI higher than the experimental pH of 7.4 and therefore they should exist mainly in the cationic forms and electrostatically interact with the fluorophores. The fluorescence enhancement for $3C^-$ is likely to operate by a usual protein-induced deaggregation due to a strong coulombic attraction. For the positively charged fluorophore $3N^+$, the opposite fluorescent response occurs probably as an effect of protein–fluorophore charge repulsion.

3.3. Multivariate statistical analyses of the fluorescence responses

Although the histogram plot already showed differentiable patterns of the fluorogenic responses toward each protein analyte, discrimination of these proteins based on this multi-dimensional data set (5 fluorophores \times 8 proteins \times 9 replicates) was further simplified using multivariate statistical analyses. Principal component analysis (PCA), a non-supervised method, and linear discriminant analysis (LDA), a supervised method, have been successfully used in the discrimination of analytes such as metal ions, anions, amino acids, bacterial cells, and cancer cells (Pavlou et al., 2002; Wang et al., 2008; Phillips et al., 2008; Bajaj et al., 2009; De et al., 2009; Tan et al., 2009; Pioggia et al., 2007; Mottram et al., 2007). In this study, we first applied PCA, to transformed our data set of fluorescent intensity differences ($\Delta I = I - I_0$) into

principle component (PC) scores (Poulli et al., 2005; Dufour et al., 2006). Based on the data similarity, a two dimension PCA score plot suitably generated eight clusters of PC scores corresponding to eight types of proteins without knowing which data belong to the same group indicating an encouraging level of protein classification. To quantify the classification accuracy, factorial discriminant analysis (FDA) (Sadecka and Tothova, 2007; Karoui et al., 2007, 2008), a supervised method, was applied on the PC scores to cross-validate the discriminating ability using a leave-one-out technique. After PCA/FDA routines performed on the data at various wavelengths ranging from 430 to 520 nm, the results showed that the data at 500 nm gave the highest classification accuracy of 98.61% (Figures S6–S10 and Table S2 in the supplement). At this wavelength, a total variance of 99.55% can be obtained from the first two

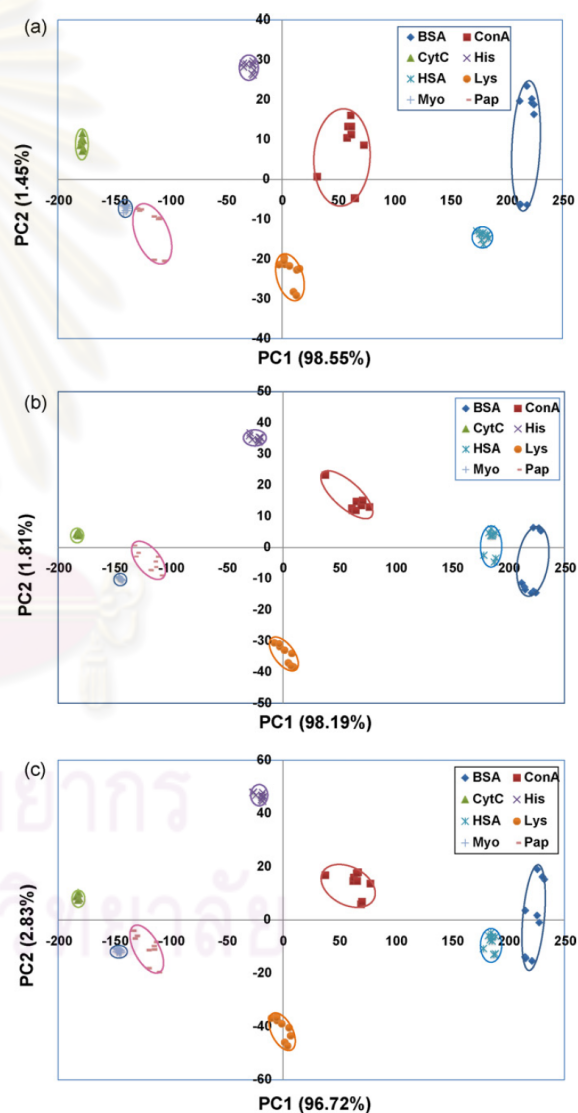


Fig. 3. PCA score plot of ΔI data set at 500 nm obtained from 9 replicates of 8 proteins inducing fluorescence responses of (a) $3N^+$, C^02N^+ , $2C^0N^+$, $2C^-N^+$ and $3C^-$; (b) $3N^+$ and C^02N^+ ; (c) $3N^+$ and $3C^-$.

PCs in which PC1 and PC2 contributed 96.72 and 2.83%, respectively (Fig. 3a).

Since it is not always the case that every variable is significant for the discrimination of the analytes, some of the data may represent noise and can negatively affect the analysis. For a sensor array, if the numbers of sensing elements can be reduced without deterioration of the discriminating performance, its application will be more expedient. In our attempt to reduce the sensing elements, PCA loading plot was used to identify the importance of each individual fluorophore toward each PC. The loading plot obtained from the measurement at 500 nm showed that $3C^-$ was the highest contributor to PC1 while C^02N^+ was the main contributor to PC2 (Figure S11 in the supplement). The PCA score plot of the data obtained from these two selected sensing elements showed that the first two PCs contained 100% of the variance (Fig. 3b). The FDA cross-validation results also revealed 100% classification accuracy for these two sensing elements. In comparison to the five-fluorophore array which provided 99.55% variance for the first two PCs and 98.61% classification accuracy, this two-fluorophore array displayed a better discriminating ability due to the reduction of non-informative and redundant data. It is also important to note that this reduced array can even discriminate between the two proteins with closely related structures, BSA and HSA.

To prove our proposition for the benefits of charge variation on the selection of $3C^-$ and C^02N^+ as the most suitable sensing elements, the PCA was also performed on the data obtained from a reduced array comprising $3C^-$ and $3N^+$, which represent usual fluorophores with all negatively or all positively charged groups. Although the first two PCs obtained from $3C^-$ and $3N^+$ model achieved the same level of total variance of 100%, clusters of two out of eight proteins, Myo and Pap, were located very close to each other (Fig. 3c). The FDA cross-validation on the PC scores also gave only 97.22% classification accuracy which is lower when comparing to the 100% classification accuracy obtained from the $3C^-/C^02N^+$ array. The results highlighted the benefits of the charge variation in the development of high performance protein sensing arrays.

4. Conclusions

A fluorescence sensor array capable of discriminating eight proteins with 100% accuracy has been successfully constructed from just two charged dendritic fluorophores. Statistical Sonogashira cross-coupling were used as a key approach in the synthesis of nine variously charge decorated phenylene-ethynylene fluorophores. Based on the visual fluorogenic responses toward the proteins, these nine fluorophores were screened to five, to be used as sensing elements. Routine PCA and FDA multivariate statistical analyses, of fluorescence intensity data were used systematically to find the optimum detection wavelength and reduce the array of five fluorophores to two. The strategy presented here and the fluorophores themselves should be valuable for the development of electronic tongue for protein related food analysis and medical diagnosis.

Acknowledgment

This study is granted by National Nanotechnology Center, National Science and Technology Development Agency, Thailand (NANOTEC, NSTDA Project NN-B-22-FN9-10-52-06) and the Thailand Research Fund (TRF). This work is part of the Project

for Establishment of Comprehensive Center for Innovative Food, Health Products and Agriculture supported by the Thai Government Stimulus Package 2 (TKK2555, SP2). We would also like to thank Center for Petroleum, Petrochemicals and Advanced Materials, Chulalongkorn University for financial support to students.

Appendix A. Supplementary data

Supplementary data associated with this article can be found, in the online version, at doi:10.1016/j.bios.2010.07.096.

References

- Albert, K.J., Lewis, N.S., Schauer, C.L., Sotzing, G.A., Stitzel, S.E., Vaid, T.P., Walt, D.R., 2000. *Chem. Rev.* 100, 2595–2626.
- Bajaj, A., Miranda, O.R., Kim, I.-B., Phillips, R.L., Jerry, D.J., Bunz, U.H.F., Rotello, V.M., 2009. *Proc. Natl. Acad. Sci. U.S.A.* 106, 10917–10921.
- Baldini, L., Wilson, A.J., Hong, J., Hamilton, A.D., 2004. *J. Am. Chem. Soc.* 126, 5656–5657.
- Borrebaeck, C.A., Wingren, C., 2009. *Proteomics* 72, 928–935.
- Bunz, U.H.F., 2009. *Macromol. Rapid Commun.* 30, 772–805.
- Daniels, M.J., Wang, Y., Lee, M.-Y., Venkataraman, A.R., 2004. *Science* 306, 876–879.
- De, M., Rana, S., Akpinar, H., Miranda, O.R., Arvizo, R.R., Bunz, U.H.F., Rotello, V.M., 2009. *Nat. Chem.* 1, 461–465.
- Dufour, E., Letort, A., Laguet, A., Lebecque, A., Serra, J.N., 2006. *Anal. Chim. Acta* 563, 292–299.
- Fan, C., Plaxco, K.W., Heeger, A.J., 2002. *J. Am. Chem. Soc.* 124, 5642–5643.
- Gonzales, D.C., Savariar, E.N., Thayumanavan, S., 2009. *J. Am. Chem. Soc.* 131, 7708–7716.
- Goodson, T., 2005. *Acc. Chem. Res.* 38, 99.
- Haab, B.B., 2006. *Curr. Opin. Biotechnol.* 17, 415–421.
- Ikebukuro, K., Kohiki, Y., Sode, K., 2002. *Biosens. Bioelectron.* 17, 1075–1080.
- Jain, R.K., Hamilton, A.D., 2000. *Org. Lett.* 2, 1721–1723.
- Jiwpanich, S., Sandanaraj, B.S., Thayumanavan, S., 2009. *Chem. Commun.*, 806–808.
- Karoui, R., Baerdemaeker, J.D., Dufour, E., 2008. *Eur. Food Res. Technol.* 226, 861–870.
- Karoui, R., Dufour, E., Baerdemaeker, J.D., 2007. *Food Chem.* 104, 409–420.
- Kim, I.-B., Dunkhorst, A., Bunz, U.H.F., 2005. *Langmuir* 21, 7985–7989.
- Kodadek, T., 2001. *Chem. Biol.* 8, 105–115.
- Kodadek, T., Reddy, M.M., Olivos, H.J., Bachhawat-Sikder, K., Alluri, P.G., 2004. *Acc. Chem. Res.* 37, 711–718.
- Li, W., Bib, L., Wang, W., Li, Y., Zhou, Y., Wei, H., Jiang, T., Bai, L., Chen, Y., Zhang, Z., Yuan, X., Xiao, J., Zhang, X.-E., 2009. *Biosens. Bioelectron.* 24, 2871–2877.
- McQuade, D.T., Pullen, A.E., Swager, T.M., 2000. *Chem. Rev.* 100, 2537–2574.
- Miranda, O.R., You, C.C., Phillips, R., Kim, I.B., Ghosh, P.S., Bunz, U.H.F., Rotello, V.M., 2007. *J. Am. Chem. Soc.* 129, 9856–9857.
- Mottram, T., Rudnitskaya, A., Legin, A., Fitzpatrick, J.L., Eckersall, P.D., 2007. *Biosens. Bioelectron.* 22, 2689–2693.
- Niamnont, N., Siripornnoppakhun, W., Rashatasakhon, P., Sukwattanasitt, M., 2009. *Org. Lett.* 11, 2768–2771.
- Paul, D., Miyake, H., Shinoda, S., Tsukube, H., 2006. *Chem. Eur. J.* 12, 1328–1338.
- Pavlou, A.K., Magan, N., McNulty, C., Jones, J.M., Sharp, D., Brown, J., Turner, A.P.F., 2002. *Biosens. Bioelectron.* 17, 893–899.
- Phillips, R.L., Miranda, O.R., You, C.-C., Rotello, V.M., Bunz, U.H.F., 2008. *Angew. Chem., Int. Ed.* 47, 2590–2594.
- Pioggia, G., Francesco, F.D., Marchetti, A., Ferro, M., Leardi, R., Ahluwalia, A., 2007. *Biosens. Bioelectron.* 22, 2624–2628.
- Poulli, K.I., Mousdis, G.A., Georgiou, C.A., 2005. *Anal. Chim. Acta* 542, 151–156.
- Sadecka, J., Tothova, J., 2007. *Czech J. Food Sci.* 25, 159–173.
- Sandanaraj, B., Demont, R., Aathimanikandan, S., Savariar, E.N., Thayumanavan, S., 2006. *J. Am. Chem. Soc.* 128, 10686–10687.
- Tan, J., Wang, H.F., Yan, X.P., 2009. *Biosens. Bioelectron.* 24, 3316–3321.
- Terenziani, F., Painelli, A., Katan, C., Charlot, M., Blanchard, D.M., 2006. *J. Am. Chem. Soc.* 128, 15742.
- Thomas, S.W., Joly, G.D., Swager, T.M., 2007. *Chem. Rev.* 107, 1339–1386.
- Tolosa, J., Bunz, U.H.F., 2009. *Chem. Asian J.* 4, 270–276.
- Wang, D., Gong, X., Heeger, P.S., Rininsland, F., Bazan, G.C., Heeger, A.J., 2002. *Proc. Natl. Acad. Sci. U.S.A.* 99, 49–53.
- Wang, Z., Palacios, M.A., Anzenbacher, P., 2008. *Anal. Chem.* 80, 7451–7459.
- You, C.-C., Miranda, O.R., Gider, B., Ghosh, P.S., Kim, I.-B., Erdogan, B., Krovi, S.A., Bunz, U.H.F., Rotello, V.M., 2007. *Nat. Nanotechnol.* 2, 318–323.
- Yu, D., Zhang, Y., Liu, B., 2008. *Macromolecules* 41, 4003–4011.
- Zhang, X., Ren, X., Xu, Q.H., Loh, K.P., Chen, Z.K., 2009. *Org. Lett.* 11, 1257–1260.
- Zhou, H.C., Baldini, L., Hong, J., Wilson, A.J., Hamilton, A.D., 2006. *J. Am. Chem. Soc.* 128, 2421–2425.

VITAE

Mr. Nakorn Niamnont was born on February 13th, 1984 in Ratchaburi, Thailand. He graduated with high school degree from Benchamarachuthit Ratchaburi School, Ratchaburi. He received a Bachelor of Science Program in Chemistry, Department of Chemistry, Faculty of Science, Silpakorn University in 2005. He has been a graduate student in organic chemistry and become a member of Organic Synthesis Research Unit under supervision of Assoc. Prof. Dr. Mongkol Sukwattanasinitt. He had an opportunity to do the research at Department of Chemistry, University of California Riverside, Riverside, California, USA in 2009 (6 months) with Prof. Dr. Quan Jason Cheng and at Department of Chemistry, University of Zurich, Zurich, Switzerland in 2010 (6 months) with Prof. Dr. Jay S. Siegel. He has received scholarship from Institute for the Promotion of Teaching Science and Technology (IPST) for financial support under the Development and Promotion of Science and Technology Talents Project (DPST) since he was studying in Bachelor degree. He graduated with a Ph. D. Degree in Chemistry in academic year 2010.

PUBLICATIONS

1. **Niamnont, N.**; Siripornnoppakhun, W.; Rashatasakhon, P.; Sukwattanasinitt, M. "A Polyanionic dendritic fluorophore for selective detection of Hg²⁺ in Triton X-100 aqueous media", *Org. Lett.* **2009**, *11*, 2768-2771.
2. Davis, W. B.; **Niamnont, N.**; Hare, C. D.; Sukwattanasinitt, M.; Cheng, Q. "Nanofibers doped with dendritic fluorophores for protein detection", *ACS Appl. Mater. Interfaces*, **2010**, *2*, 1798–1803.
3. **Niamnont, N.**; Mungkarndee, R.; Rashatasakhon, P.; Techakriengkrai, I.; Sukwattanasinitt, M. "Protein discrimination by fluorescent sensor array constituted of variously charged dendritic phenyleneethynylene fluorophores", *Biosens. Bioelectron.*, **2010**, *26*, 863-867.